



**HAL**  
open science

# An integrated seismic risk modeling approach including human behavior : Application to Beirut, Lebanon

Rouba Iskandar

► **To cite this version:**

Rouba Iskandar. An integrated seismic risk modeling approach including human behavior : Application to Beirut, Lebanon. Earth Sciences. Université Grenoble Alpes [2020-..], 2022. English. NNT : 2022GRALU022 . tel-04346166

**HAL Id: tel-04346166**

**<https://theses.hal.science/tel-04346166>**

Submitted on 15 Dec 2023

**HAL** is a multi-disciplinary open access archive for the deposit and dissemination of scientific research documents, whether they are published or not. The documents may come from teaching and research institutions in France or abroad, or from public or private research centers.

L'archive ouverte pluridisciplinaire **HAL**, est destinée au dépôt et à la diffusion de documents scientifiques de niveau recherche, publiés ou non, émanant des établissements d'enseignement et de recherche français ou étrangers, des laboratoires publics ou privés.

## THÈSE

Pour obtenir le grade de

### DOCTEUR DE L'UNIVERSITÉ GRENOBLE ALPES

École doctorale : STEP - Sciences de la Terre de l'Environnement et des Planètes

Spécialité : Sciences de la Terre et de l'Univers et de l'Environnement

Unités de recherche : Institut des Sciences de la Terre, Laboratoire d'Informatique de Grenoble et Pacte

## Modélisation intégrée du risque sismique incluant le comportement humain

## An integrated seismic risk modeling approach including human behavior

Présentée par :

**Rouba ISKANDAR**

#### Direction de thèse :

**Cécile CORNOU**

DIRECTRICE DE RECHERCHE IRD, Université Grenoble Alpes

Directrice de thèse

**Julie DUGDALE**

PROFESSEUR DES UNIVERSITES, Université Grenoble Alpes

Co-directrice de thèse

**Elise BECK**

MAITRE DE CONFERENCES HDR, Université Grenoble Alpes

Co-directrice de thèse

#### Rapporteurs :

**Etienne BERTRAND**

DIRECTEUR DE RECHERCHE, Université Gustave Eiffel

**Alexis DROGOUL**

DIRECTEUR DE RECHERCHE, IRD délégation Ile-de-France

#### Thèse soutenue publiquement le 13 juillet 2022, devant le jury composé de :

**Etienne BERTRAND**

DIRECTEUR DE RECHERCHE, Université Gustave Eiffel

Rapporteur

**Alexis DROGOUL**

DIRECTEUR DE RECHERCHE, IRD délégation Ile-de-France

Rapporteur

**Didier GEORGES**

PROFESSEUR DES UNIVERSITES, Grenoble INP

Président

**Edwige DUBOS-PAILLARD**

PROFESSEUR DES UNIVERSITES, Université Paris

Examinatrice

**Mona FAWAZ**

PROFESSEUR, American University of Beirut

Examinatrice

**Cécile CORNOU**

DIRECTRICE DE RECHERCHE, IRD délégation Sud-Est

Directrice de thèse

**Elise BECK**

MAITRE DE CONFERENCES HDR, Université Grenoble Alpes

Co-directrice de thèse

**Julie DUGDALE**

PROFESSEUR DES UNIVERSITES, Université Grenoble Alpes

Co-directrice de thèse

#### Invités :

**Jocelyne ADJIZIAN-GERARD**

PROFESSEUR, Université Saint Joseph de Beyrouth

**Pierre-Yves BARD**

INGENIEUR GENERAL DES PONTS, EAUX ET FORETS, IFSTTAR

**Jacques HARB**

PROFESSEUR, Notre Dame University





# REMERCIEMENTS

Je tiens à exprimer ma reconnaissance à Etienne Bertrand et Alexis Drogoul d'avoir accepté de relire cette thèse et d'en être rapporteurs. Vos remarques et votre intérêt pour mon travail ont été très précieux pour moi. Je tiens à remercier chaleureusement les membres du jury Didier Georges, Edwige Dubos Paillard et Mona Fawaz pour avoir accepté avec enthousiasme d'être examinateurs. Merci pour votre temps et pour vos retours très pertinents sur mon travail.

Faire une thèse, ce n'est pas facile; faire une thèse interdisciplinaire, c'est encore un défi plus important.

Pour moi, ceci n'aurait pas été possible sans le soutien continu de mes trois directrices de thèse Cécile Cornou, Elise Beck et Julie Dugdale. Merci pour votre confiance dès le premier jour, merci de m'avoir introduit chacune dans sa discipline; mais aussi de m'avoir montré comment un travail interdisciplinaire peut être mené dans une belle ambiance. Je tiens aussi à vous remercier pour l'immense liberté que vous m'avez accordée, tout en étant présentes dès que j'en avais besoin. Travailler avec vous a été un immense plaisir, et j'en suis reconnaissante pour toujours.

Je tiens à remercier aussi les membres de mon comité de thèse Pierre Yves Bard, Bertrand Guillier, Rémy Bossu et Frédéric Amblard, de m'avoir suivie tout au long de la route. Merci pour l'intérêt que vous avez eu pour ma thèse et pour vos conseils, toujours bienveillants. Un grand merci aussi à Stéphane Cartier, qui a aussi passionnément suivi ce travail et avec qui j'ai pu avoir de nombreuses discussions stimulantes sur les risques au Liban.

Merci au CDP Risk pour avoir financé cette thèse, et qui à travers l'organisation de différentes animations, séminaires et journées m'a donné plusieurs opportunités de présenter mon travail et de recevoir des retours constructifs pour l'améliorer. Un grand merci aussi aux doctorants du CDP Risk, les Riskuers pour votre sympathie. Avec vous je sentais que j'appartenais à une communauté, et que je n'étais pas la seule à essayer de me retrouver parmi les mille et une définitions des termes risques, vulnérabilité et résilience.

Un merci profond aux membres du projet AUF PCSI, Jocelyne Gérard, Nada Saliba, Rita Zaarour, Kamel Allaw et Jacques Harb qui ont contribué à l'aboutissement de ce travail. Merci aussi aux personnes avec qui j'ai étroitement travaillé : Bilal Al Tfaily, Christelle Salameh Antonin Méjean, et Kevin Chapuis. Ça a été un plaisir de travailler avec vous, et sans vous ce travail ne serait pas aussi abouti.

Durant ma thèse, j'ai eu la grande chance d'être accueillie au sein de l'équipe Risques d'ISTerre, l'équipe Environnement de Pacte et l'équipe Steamer du LIG. Merci aux membres des trois équipes de m'avoir accueillie, et pour vos conseils et encouragements continus.

Je remercie particulièrement mes collègues doctorants, post-doctorants, ingénieurs et stagiaires, vous étiez plus que des collègues, vous êtes des amis. Merci pour votre sympathie et votre soutien, et pour les agréables moments passés ensemble au bureau mais aussi au resto, en randonnée et au ski. Un grand merci à mes amis qui m'ont soutenue et supportée tout le long de ces années et surtout ces derniers mois particulièrement stressants. Un merci particulier à Pier, Eliane, Grace et Manon d'avoir relu certains chapitres de ma thèse, même ceux qui faisaient plus de 40 pages.

Pendant ma thèse j'ai eu la chance de rencontrer des personnes formidables qui sont devenues de vraies sources d'inspiration aussi bien que sur le plan professionnel que personnel. La période de ma thèse a également été marquée par de multiples crises dans mon pays, une pandémie mondiale et des périodes de deuil difficilement vécues. Néanmoins, le soutien sans faille et permanent de ma maman Nadia, mon papa Youssef, ma sœur Rita et mon frère Rabih, m'a aidé à surmonter les périodes les plus difficiles. Rien de ce que je fais ne sera jamais suffisant pour vous exprimer mon extrême gratitude pour votre amour inconditionnel.



# RÉSUMÉ

De nombreuses observations faites lors de séismes précédents ont mis en évidence l'influence du comportement humain sur le risque sismique (L'Aquila 2009 ; Great East Japan 2011 ; Lorca 2011). Les actions, ou même l'inaction, des individus peuvent avoir des effets néfastes sur les conséquences sociales d'un séisme. Pourtant, les méthodologies d'évaluation des risques sismiques prennent rarement en compte le comportement humain. Cette thèse explore comment la modélisation des comportements humains et de la mobilité dans un environnement post-séisme peut contribuer à la définition d'indices de risque sismique dynamiques qui intègrent le comportement humain.

Nous adoptons une approche interdisciplinaire, fusionnant les sciences de la terre, les sciences sociales et l'informatique, pour modéliser le risque sismique en tenant compte de ses aspects physiques et sociaux. Plus précisément, nous développons un modèle à base d'agents pour la simulation de l'évacuation des piétons en cas de séisme (PEERS). PEERS intègre des composantes physiques réalistes liées aux dommages causés aux bâtiments et aux débris qui en résultent. La composante sociale est prise en compte en intégrant les réponses comportementales, représentées par les décisions d'évacuation et de mobilité et les interactions entre individus qui aboutissent à la formation de groupes.

Nous choisissons Beyrouth, au Liban, comme zone d'étude et recréons un environnement virtuel de crise sismique. Nous définissons deux scénarios sismiques : le premier correspond à l'accélération maximale au sol (PGA) réglementaire de 0,3 g et le second à une PGA de 0,5 g. Nous construisons une base de données de bâtiments pour Beyrouth, puis nous estimons les dommages aux bâtiments pour les scénarios sismiques définis à l'aide de réseaux neuronaux artificiels. Pour estimer les débris induits par les dommages, nous développons une approche pour prédire la distribution des débris autour d'un bâtiment en fonction de son niveau de dommage. Nous définissons des espaces ouverts, c'est-à-dire des zones éloignées des bâtiments où les individus sont en sécurité, et nous identifions les contraintes dans l'environnement urbain qui pourraient affecter la mobilité des piétons. De plus, nous recréons une population synthétique d'individus et de ménages qui reproduit les données disponibles sur la population de Beyrouth. Enfin, nous calibrons les réponses comportementales dans PEERS sur la base des données d'enquête de l'explosion du 4 août 2020 dans le port de Beyrouth.

Nous effectuons plusieurs simulations d'évacuation en cas de tremblement de terre dans cet environnement virtuel et nous examinons la sécurité des personnes à la suite d'un tremblement de terre, la sécurité étant définie comme le fait de se trouver dans un espace ouvert. Nous étudions la capacité des espaces ouverts de Beyrouth à fournir un abri à la population immédiatement après un tremblement de terre. Nous étudions également les effets d'environnements physiques et sociaux plus complexes sur l'arrivée de la population dans des zones sûres.

Nous constatons qu'à Beyrouth, la distribution des espaces ouverts en termes de taille et d'emplacement ne peut assurer la sécurité de toute la population, même dans des conditions idéales avec des contraintes sociales et physiques minimales. En outre, nous constatons que les débris et les comportements humains retardent tous les deux de manière significative les temps d'arrivée aux espaces ouverts. Cependant, le comportement humain retarde les arrivées de deux fois par rapport au retard causé uniquement par la présence de débris.

Une approche similaire peut être adoptée pour identifier et classer les composants physiques et sociaux d'un indice de risque sismique dynamique.



# ABSTRACT

Numerous observations from previous earthquakes highlighted the influence of human behavior on seismic risk (L'Aquila 2009; Great East Japan 2011; Lorca 2011). Individuals' actions, or even inaction, may have detrimental effects on the social consequences of an earthquake. Yet, seismic risk assessment methodologies rarely take into account human behavior. This thesis explores how modeling human behaviors and mobility in a post-earthquake environment can contribute to the definition of dynamic seismic risk indices that integrate human behavior.

We adopt an interdisciplinary approach, merging earth, social and computer sciences, to model seismic risk while accounting for both its physical and social aspects. Specifically, we develop an agent-based model for the simulation of pedestrian earthquake evacuation (PEERS). PEERS integrates realistic physical components related to building damages and resulting debris. The social component is taken into account by integrating behavioral responses, represented by the evacuation and mobility decisions and the interactions between individuals that result in the formation of groups.

We choose Beirut, Lebanon as a study area and recreate a virtual seismic crisis environment. We define two seismic scenarios: the first one corresponding to the regulatory Peak Ground Acceleration (PGA) of 0.3 g and the second one corresponding to a PGA of 0.5 g. We construct a building database for Beirut, and then estimate the building damages for the defined seismic scenarios using Artificial Neural Networks. To estimate the damage-induced debris, we develop an approach to predict the distribution of debris around a building according to its damage level. We define open spaces, i.e. areas away from buildings where individuals are safe, and identify the constraints in the urban environment that might affect pedestrians' mobility. Moreover, we recreate a synthetic population of individuals and households that replicates the available data on Beirut's population. Finally, we calibrate the behavioral responses in PEERS based on survey data from the August 4, 2020 explosion at the port of Beirut.

We run several earthquake evacuation simulations in this virtual environment, and look at people's safety in the aftermath of an earthquake, with safety defined as being in an open space. We investigate the capacity of the open spaces in Beirut for providing shelter for the population in the immediate aftermath of an earthquake. We also investigate the effects of more complex physical and social environments on the population's arrivals to safe areas.

We find that in Beirut, the distribution of open spaces in terms of size and location cannot ensure the safety of all of the population, even in ideal conditions with minimal social and physical constraints. Furthermore, we find that debris and human behaviors both significantly delay the arrival times to open spaces. Yet, the human behavior delays the arrivals by two times compared to the delay caused only by the presence of debris.

A similar approach can be adopted to identify and rank physical and social components of a dynamic seismic risk index.



# Content

<b>Chapter 1: Introduction</b> .....	21
<b>Chapter 2: Context</b> .....	25
2.1. INTRODUCTION .....	25
2.2. KEY CONCEPTS AND TERMS.....	25
2.2.1. International frameworks and evolution of the disaster research field.....	26
2.2.2. Definition of general terms.....	26
2.2.3. Vulnerability definition .....	27
2.2.4. Risk definition .....	28
2.2.5. Summary.....	29
2.3. SEISMIC RISK ASSESSMENT .....	29
2.3.1. Classical seismic risk assessment approaches .....	30
2.3.2. Integrated seismic risk assessment approaches .....	33
2.3.3. Summary.....	36
2.4. HUMAN BEHAVIORS IN RESPONSE TO EARTHQUAKES.....	37
2.4.1. Theories about human behaviors in emergency .....	37
2.4.2. Observed behaviors and contextual factors .....	39
2.4.3. Summary.....	42
2.5. APPROACHES FOR MODELING HUMAN BEHAVIORS IN EARTHQUAKES .....	43
2.5.1. EPES .....	44
2.5.2. SOLACE.....	45
2.5.3. IdealCity .....	45
2.5.4. Summary.....	46
2.6. STUDY AREA: BEIRUT, LEBANON.....	46
2.6.1. Seismic hazard context in Lebanon .....	47
2.6.2. Beirut: geological, urbanization and seismic risk contexts.....	48
2.6.3. Beirut’s social vulnerability context.....	55
2.7. CONCLUSION.....	56
<b>Chapter 3: Pedestrian Evacuation in Earthquake Risk Simulations</b> .....	57
3.1. INTRODUCTION .....	57
3.2. CITY MODEL.....	58
3.2.1. Model of the urban environment .....	58
3.2.2. Model of the residents and their social ties.....	59
3.3. EARTHQUAKE DAMAGE MODEL.....	60
3.3.1. Seismic scenario .....	60
3.3.2. Building damages .....	61
3.3.3. Generation of debris .....	61
3.3.4. Casualty estimation.....	62
3.4. HUMAN BEHAVIOR AND MOBILITY MODEL.....	62
3.4.1. Ideal behaviors.....	63
3.4.2. Realistic behaviors.....	63
3.4.3. Decision-making- Individual level .....	64
3.4.4. Decision-making related to group behavior.....	66
3.4.5. Model of pedestrians’ mobility.....	68

3.5.	ARCHITECTURE OF THE MODEL .....	71
3.5.1.	UML class diagram of PEERS .....	71
3.5.2.	Activity diagram of a person agent in PEERS.....	73
3.6.	VALIDATION OF THE CONCEPTUAL MODEL .....	74
3.7.	IMPLEMENTATION.....	75
3.7.1.	Creation of the model’s species.....	76
3.7.2.	Behaviors of the person agents .....	79
3.8.	CONCLUSION.....	82
<b>Chapter 4:</b>	<b>Estimation of seismic damages and resulting debris in Beirut.....</b>	<b>85</b>
4.1.	INTRODUCTION .....	85
4.2.	ESTIMATION OF SEISMIC DAMAGES AT THE BUILDING SCALE IN BEIRUT (LEBANON).....	85
4.2.1.	Introduction.....	85
4.2.2.	Method for estimating seismic damages building by building.....	87
4.2.3.	Generation of a 3D building model in Beirut and estimation of the seismic damages	92
4.2.4.	Conclusion .....	107
4.3.	DEBRIS ESTIMATION .....	108
4.3.1.	Estimation of the debris volume corresponding to the damage level of the building	109
4.3.2.	Estimation of the debris footprints around a building .....	111
4.3.3.	Validation of the approach.....	112
4.3.4.	Application to Beirut .....	113
4.3.5.	Summary.....	114
4.4.	ASSIGNMENT OF CASUALTY RATES TO BUILDINGS AND DEBRIS ZONES .....	115
4.5.	CONCLUSION.....	116
<b>Chapter 5:</b>	<b>Mixed approaches for the generation of spatial, social and behavioral data in Beirut .....</b>	<b>117</b>
5.1.	INTRODUCTION .....	117
5.2.	DELIMITATION OF OPEN SPACES IN BEIRUT .....	117
5.2.1.	Open spaces in Beirut .....	117
5.2.2.	Processing and results.....	118
5.2.3.	Summary.....	120
5.3.	DELIMITATION OF NATURAL AND URBAN CONTSTRAINTS ON PEDESTRIAN MOBILITY IN BEIRUT.....	120
5.3.1.	Derivation of the terrain’s slope from the DTM.....	121
5.3.2.	Delimitation of barriers.....	121
5.4.	ESTIMATION OF THE POPULATION’S SIZE AND DISTRIBUTION: SYNTHETIC POPULATION.....	122
5.4.1.	Challenges in the collection of accurate population data in Lebanon and proposed approach	123
5.4.2.	Identification of the buildings’ function .....	123
5.4.3.	Estimation of the number of residential apartments in Beirut .....	126
5.4.4.	Methodology for the generation of a synthetic population of households and individuals in Beirut .....	128
5.4.5.	Application: generation of a synthetic population for Beirut .....	130
5.4.6.	Summary.....	134

5.5. COLLECTION OF HUMAN BEHAVIORS IN RESPONSE TO THE AUGUST 4, 2020, EXPLOSION AT THE PORT OF BEIRUT .....	134
5.5.1. Motivation behind the collection of behavioral responses to the Beirut port explosion .....	134
5.5.2. Questionnaire on the behavioral response to the Beirut port explosion .....	136
5.5.3. Analysis of the survey responses .....	137
5.5.4. Summary.....	145
5.6. CONCLUSION.....	146
<b>Chapter 6: Simulation of pedestrian earthquake evacuation in Beirut.....</b>	<b>149</b>
6.1. INTRODUCTION .....	149
6.2. SIMULATIONS IN PEERS .....	149
6.2.1. Technical configuration .....	149
6.2.2. Simulation outputs .....	150
6.3. MODEL VERIFICATION .....	151
6.3.1. Verification of the agent’s navigation towards a target and around obstacles.....	152
6.3.2. Verification of the modification of the agent’s speed due to the slope and the debris .....	153
6.3.3. Verification of the spatial distribution of agents for day and night scenarios .....	154
6.3.4. Verification of the agent’s evacuation decision and the assignment of the evacuation delay .....	154
6.3.5. Verification of group behavior: homogenization of the attributes of the agents that belong to the same group .....	155
6.4. LARGE-SCALE SIMULATIONS .....	157
6.4.1. The headless bash script .....	157
6.4.2. Cluster configuration: hardware specifications and limitations.....	157
6.5. DESIGN OF THE EXPERIMENT PLAN .....	159
6.6. PRE-PROCESSING OF THE SIMULATIONS RESULTS .....	161
6.6.1. Variability between different runs of the same scenario .....	162
6.6.2. Casualties estimated in the simulations with PEERS .....	164
6.7. ANALYSIS OF THE SIMULATIONS RESULTS.....	166
6.7.1. The capacity of the open spaces in Beirut for immediate disaster shelter .....	167
6.7.2. Analysis of the effects of more complex physical and the social contexts.....	174
6.8. DISCUSSION.....	182
<b>Chapter 7: Conclusion and future work.....</b>	<b>187</b>
7.1. CONCLUSION.....	187
7.2. LIMITATIONS AND FUTURE WORK.....	189
7.3. CONCLUDING REMARKS AND LONG-TERM PERSPECTIVES.....	191
<b>References.....</b>	<b>193</b>
<b>Appendix A.....</b>	<b>209</b>
<b>Appendix B.....</b>	<b>210</b>
<b>Appendix C.....</b>	<b>211</b>
<b>Appendix D.....</b>	<b>214</b>
<b>Appendix E.....</b>	<b>215</b>
<b>Appendix F.....</b>	<b>218</b>
<b>Appendix G.....</b>	<b>219</b>



# List of Figures

Figure 1-1: Examples of human behaviors observed during the 2015 Nepal earthquake in an open market area. In general, people gather in the open space away from buildings. Particular observations: (a) Falling debris (red arrow) while a person is next to a building (red circle), (b) person running back towards buildings in a danger zone (red circle), (c) group of people –man with children- evacuating to an open space together. The full video can be found at <a href="https://www.youtube.com/watch?v=6HqcduyK_Lw&amp;ab_channel=DebeshUtube">https://www.youtube.com/watch?v=6HqcduyK_Lw&amp;ab_channel=DebeshUtube</a> .....	22
Figure 1-2: Thesis structure.....	24
Figure 2-1 : Map of the economic losses in Istanbul. Source: (Erdik, 2017) adapted from (Silva et al., 2012).....	31
Figure 2-2: Map of the estimated losses for regulatory accelerations in France. Loss here refers to the mean losses in the building stock. Source: Riedel and Guéguen (2018).....	32
Figure 2-3: Map of the average annual economic losses across Europe. Source: Crowley et al. (2021).....	32
Figure 2-4: Application of the EDRI to 10 cities worldwide. Source:Davidson (1997).....	34
Figure 2-5: Application of the USRi to the city of Medellín, Colombia. (a) Physical risk index by county, (b) Aggravating coefficients by county, (c) USRi results by county. Source: Salgado-Gálvez et al. (2016).....	35
Figure 2-6: Integrated seismic risk modeling for Portugal at the county level, performed using GEM’s IRMT. (a) Map of the physical risk, quantified in terms of the Average Annual Loss, (b) Map of the social vulnerability index, computed in the IRMT, (c) Integrated seismic risk computed in the IRMT. Source: Burton and Silva (2014).....	36
Figure 2-7: Regional tectonic setting. (a) Map of the Levant fault system. (b) Zoomed view on the active faults in Lebanon. Source: (Daeron et al., 2007).....	48
Figure 2-8: Satellite view of Beirut. The red line delimits the limits of Municipal Beirut. (Sources: Beirut boundary: OpenstreetMap; basemap: Google Satellite).....	48
Figure 2-9: Location of Municipal Beirut and Greater Beirut. Modified from Faour and Mhawej, 2014. ....	49
Figure 2-10: Geological map of Beirut with layouts of Beirut faults (continuous lines) and limits of Beirut (dashed lines). Source: (Brax et al., 2014) modified from (Dubertret, 1945).....	50
Figure 2-11: A view of Beirut's skyline from the southeast to the northeast. Source: (Kanafani, 2016).....	50
Figure 2-12: Phases of Beirut's urban growth. Source: Yassin (2012).....	51
Figure 2-13: Heterogeneity of the urban fabric in Beirut (Achrafieh district) highlighted by a traditional masonry house in the first plan, residential buildings in the second plan and “modern” skyscrapers in the third plan. Source: unknown.....	53
Figure 2-14: Interpolated map of the damage increment in Beirut and a part of its eastern suburbs for an earthquake of PGA=0.25 g. The damages are shown in terms of incremental damage between soil and rock to highlight the effects of the soil conditions on the buildings damages. White zones in the middle of Beirut correspond to areas with missing building data. Source: Salameh et al. (2017).....	54
Figure 2-15: Demographic characteristics of the population in Beirut. (a) Gender distribution, (b) Age distribution. Data from: (CAS, 2020).....	55
Figure 3-1: Temporal context of the behavioral responses to an earthquake. Source: Bañgate, 2019 modified from Alexander, 1990.....	57
Figure 3-2: Multi-model framework in PEERS.....	58
Figure 3-3: Illustration of an urban environment in PEERS.....	58
Figure 3-4: Model of the residents and their social ties in PEERS.....	60
Figure 3-5: Illustration of the evacuation decision-making in PEERS.....	65
Figure 3-6: Target destination choice in PEERS according to the person’s attributes.....	66
Figure 3-7: Illustration of the designation of the group leader in PEERS: (a) when the head of the household is in the group, (b) when the head of the household is not in the group.....	67
Figure 3-8: Example of the evaluation of the group's evacuation decision.....	68
Figure 3-9: Example of the evaluation of group's target destination choice.....	68

Figure 3-10 : Delimitation of the free space by subtracting the obstacles from the spatial extents of the study area. The obstacles are the buildings (in grey) and the barriers (in yellow).....	69
Figure 3-11: Illustration of the forces applied on a pedestrian in the SFM. An attraction force is applied from the pedestrian towards its destination, while repulsive forces are applied on the pedestrian from the other pedestrians who are nearby as well as obstacles (wall) (Source: Prédhumeau, 2021).....	70
Figure 3-12: Variation of the speed reduction factor, $\gamma$ , according to the slope of the terrain.....	71
Figure 3-13: Simplified UML class diagram of PEERS.....	72
Figure 3-14: Simplified activity diagram of a person agent in PEERS when realistic behaviors are considered.....	74
Figure 3-15: First version of PEERS defined in the framework of the AUF-PCSI project. This first version represented a night scenario with ideal behaviors for an earthquake of 0.3 g [Beirut, June 2019].....	75
Figure 3-16: Pseudo-code of the definition of the free space geometry in PEERS.....	77
Figure 3-17: Pseudocode of the spatial distribution of the person agents for a day scenario.....	78
Figure 3-18: Pseudocode of the assignment of attributes related to the knowledge of open spaces and the desire to join someone.....	78
Figure 3-19: Pseudocode of the evaluation of the evacuation decision and the assignment of the evacuation delay.....	79
Figure 3-20: Pseudocode of the evacuation behavior of a person agent.....	79
Figure 3-21: Pseudocode of the simulation of the indoor casualties in PEERS.....	80
Figure 3-22: Pseudocode of the simulation of the outdoor casualties in PEERS.....	80
Figure 3-23 : Illustration of the movement around an obstacle by a person agent. The obstacle is represented by the grey rectangle. The person agent moves directly towards its target unless it detects an obstacle. When an obstacle is detected, the agent moves along the boundary of the obstacle. ....	82
Figure 3-24: Overview of the inputs needed for the simulations in PEERS with the dedicated chapters in this manuscript.....	83
Figure 4-1 : Site transfer functions for the site ATKH05 from the Kik-Net database computed from the results of the nonlinear site response analysis under 60 different seismic loadings. The site transfer function for the linear site response is plotted in black and the non-linear site responses are indicated in color according to the surface PGA.....	88
Figure 4-2 : Synaptic weight proportions for the inputs of ANN7 for building classes 1, 2 and 3. ....	91
Figure 4-3 : Interpolated maps of $f_{soil}$ and $A_{0HV}$ in Beirut derived from the ambient vibration measurements performed in Salloum et al. (2014), Salameh et al. (2017) and Brax et al. (2018).....	93
Figure 4-4: Buildings in Beirut surveyed in the framework of the LIBRIS project (Salameh, 2016) ..	93
Figure 4-5 : Distribution of the surveyed buildings according to (a) their number of floors and (b) construction year.....	94
Figure 4-6: Distribution of the typology of the buildings surveyed in the framework of the LIBRIS project (Salameh et al., 2016).....	94
Figure 4-7: Buildings footprints retrieved from OSM.....	95
Figure 4-8 : Geolocalisation incompatibilities between the LIBRIS buildings (purple) and the OSM buildings (orange).....	96
Figure 4-9: Spatial distribution of the 947 geolocalized LIBRIS buildings (LIB-STAT).....	96
Figure 4-10 : Distribution of the buildings' number of floors (a), construction year (b) and class (c) in the subset of 947 extracted from LIBRIS for the statistical analysis (LIB-STAT).....	97
Figure 4-11: Preview of one of the Pleiades 1-B panchromatic satellite images taken over Beirut ....	98
Figure 4-12: Digital elevation models.....	98
Figure 4-13: Beirut elevation models derived from processing high-resolution satellite images.....	99
Figure 4-14 : Comparison of the DFM building heights to the building height retrieved from OSM or LIBRIS.....	99
Figure 4-15: DSM elevations at the location of 9 high-rise buildings in Beirut. The building's name is indicated on the top the corresponding figure and the corresponding building's footprint is highlighted in red.....	100
Figure 4-16 : Boxplot distribution of the building heights according to the number of floors in the LIB-STAT dataset. Outliers are represented by black crosses.....	101

Figure 4-17 : Linear regression of the number of floors of the LIB-STAT dataset according to the building heights retrieved from the DFM.....	102
Figure 4-18 : Estimation errors in the linear regression between the number of floors and the building heights: (a) the predicted number of floors vs the actual number of floors, (b) the residuals between the predicted and actual value of the number of floors, according to the actual number of floors .....	102
Figure 4-19 : Prediction of the construction period from the building's number of floors and X and Y coordinates using a classification tree. (a) Predictor importance estimates, (b) Comparison of the distribution of the predicted and true construction periods classes .....	103
Figure 4-20 : Distribution of the predicted (a) number of floors, (b) construction year and (c) typology for the buildings in the OSM database .....	104
Figure 4-21 : Distribution of the buildings' damage states for the seismic scenarios 1 and 2, for the 3 buildings configurations obtained by considering: the mean predicted number of floors (N), the mean predicted number of floors -3 (N - 3) and the mean predicted number floors + 3 (N + 3).....	105
Figure 4-22: Beirut damages maps for scenarios 1 and 2 for buildings with the average predicted number of floors (N), predicted number of floors +3 (N+3) and predicted number of floors - 3 (N-3). The damages were computed building by building, but for presentation purposes they were averaged on a radius of 100 m.....	107
Figure 4-23: Models for the estimation of the spatial distribution of debris from the literature. Sources: (a) Nishino et al., 2012, (b) Ravari et al., 2016, (c) Argyroudis et al., 2015 .....	109
Figure 4-24 : Debris generation from the building's construction elements .....	110
Figure 4-25 : Percentage of total debris volume generated depending on the mean damage for each building type.....	111
Figure 4-26 : Front and top views of truncated pyramid shaped debris .....	111
Figure 4-27 : Comparison of the debris width estimated following the developed methodology to the typical formulas found in the literature .....	113
Figure 4-28 : Distribution of the debris width according to the building height and the mean damage. (a) Seismic scenario with PGA = 0.3 g, (b) Seismic scenario with PGA = 0.5 g.....	113
Figure 4-29 : Distribution of the debris height according to the building height and the mean damage. (a) Seismic scenario with PGA = 0.3 g, (b) Seismic scenario with PGA = 0.5 g.....	114
Figure 4-30: Debris zone for a building for a scenario PGA = 0.3 g and a scenario of PGA = 0.5 g. ....	114
Figure 4-31: Spatial distribution of the debris' heights in Beirut for a seismic scenario of PGA = 0.5 g. ....	115
Figure 4-32: Interpolated indoor and outdoor HAZUS casualty rates according to the building mean damage for building types URML, C1 and C3. C1 and C3 buildings have the same indoor casualty rates. ....	116
Figure 5-1: Public open spaces in Beirut identified by the BUL. Source: <a href="https://beiruturbanlab.com/en/Details/619/vacancy-as-opportunity-re-activating-public-life-in-beirut">https://beiruturbanlab.com/en/Details/619/vacancy-as-opportunity-re-activating-public-life-in-beirut</a> .....	118
Figure 5-2 : Examples of unbuilt spaces in Beirut considered unsafe for the gathering of populations in the case of an earthquake. (a) Saint Dimitrios Cemetery in Achrafieh, Beirut. Photo by: Katrice Dustin, retrieved from: <a href="https://www.travel-almanac.com/blogs/psychological-sightseeing/st-demetrius-marmitr">https://www.travel-almanac.com/blogs/psychological-sightseeing/st-demetrius-marmitr</a> . (b) Container area at the port of Beirut. Photo by: Rami Rizk, retrieved from: <a href="https://www.lebanoninapicture.com/pictures/port-of-beirut-lebanon-beirut-port-dji-drones-quadcopte">https://www.lebanoninapicture.com/pictures/port-of-beirut-lebanon-beirut-port-dji-drones-quadcopte</a> . ....	119
Figure 5-3 : Map showing the open spaces that are always accessible (green polygons) or can be locked (red polygons) in Beirut identified based on the proposed definition. Beirut buildings footprint is extracted from OpenStreet Map (last accessed: 26/02/2021) .....	120
Figure 5-4: Slope of the terrain in Beirut .....	121
Figure 5-5: Stretch of the highway 51M in Salim Salam, Beirut with walls on the side of the road. Phototaphy by: Jean ISENMANN.....	122
Figure 5-6: Barriers in Beirut digitized on the highway 51M .....	122
Figure 5-7: Map showing the buildings in Beirut retrieved from the Beirut Built Environment Database (BUL). Buildings function are indicated in colored polygons. ....	125
Figure 5-8 : Beirut buildings retrieved from OSM (black contour) overlaying the buildings from the Beirut Built Environment Database (red and turquoise). ....	125

Figure 5-9 : Map showing the OSM buildings classified as: residential, hospital and work .....	126
Figure 5-10 : Schematic representation of the methodology used to generate individuals in Beirut and aggregate them into households .....	130
Figure 5-11 : Distribution of synthetic and original residents according to sex and age groups.....	132
Figure 5-12 : Distribution of households' characteristics in both the synthetic and the original populations .....	133
Figure 5-13: Map of the damages caused by the explosion at the port of Beirut (edited from Municipality of Beirut and UN Habitat, 2020) .....	135
Figure 5-14: Maps of the reported felt intensities of the Beirut port explosion, according to: (a) the USGS DYFI and (b) the CSEM's Lastquake .....	136
Figure 5-15 : Distribution of the number of the respondents per municipality in Lebanon (source: Méjean, 2021).....	139
Figure 5-16: Distribution of the respondents in Beirut per district (adapted from Méjean, 2021).....	139
Figure 5-17 : Overview of the inputs and outputs of PEERS and their dedicated chapters in this manuscript .....	147
Figure 6-1: Simulation interface in GAMA showing, (a) the simulation's parameters, (b) the graphical display of the agents and (c) the monitors of the population's and open spaces' states.....	151
Figure 6-2: Chart displaying the evolution of the agents' states over time in GAMA's simulation interface. The purple line shows the number of agents indoor, the yellow line shows the number of moving agents, i.e. those who have not arrived, and the green line shows the number of safe agents in open spaces.....	151
Figure 6-3: Snapshots from GAMA showing an agent (in purple) moving towards an open space (in green) while avoiding obstacles represented by buildings (in gray) and barriers (in red). A black circle is added around the agent to facilitate its traceability .....	152
Figure 6-4: Snapshot from the agents' attribute table in GAMA. The columns (left to right) show the identifier of the agent, its age, its natural speed in m/s (i.e. preferred speed that depends on the person's age), the slope in degrees at the location of the agent, the modified speed resulting from the effect of the slope, and whether or not the person is in danger, i.e. in a debris zone. The final column shows the final speed of the agent that depends on whether the person is in a debris zone or not and on the height of the debris in the zone.....	153
Figure 6-5: Snapshots from GAMA displaying the population distribution in PEERS at the initialization of the simulation for night and day scenarios. Buildings are displayed in 3D with a transparency factor in order to see the agents inside. The buildings have different colors according to their function. (a) Night scenario, (b) Close-up view for the night scenario, (c) Day scenario, (d) Close-up view for the day scenario.....	154
Figure 6-6 : Snapshots from the agent and building attribute tables, showing the evaluation of the evacuation decision of an agent. (a) Agents' attribute table and (b) buildings' attribute table .....	155
Figure 6-7: Snapshots from GAMA showing (a) the attributes a group (group3), and the attributes of the group's members related to the designation of (b) the group's leader (in red), (c) the group's evacuation decision and delay (in blue), (d) the group's speed (in green) and (e) the group's target location (in yellow).....	156
Figure 6-8: Command line used to launch simulations with GAMA in headless mode .....	157
Figure 6-9: Time taken (in min) to execute each cycle of the large-scale PEERS simulation on the ISTerre cluster. The number of active agents is also plotted for reference .....	159
Figure 6-10 : Average cycle duration for each of the simulated scenarios .....	162
Figure 6-11: Number of people in open space 8 at each simulation cycle in runs 1 to 5 of Scenario 6 .....	163
Figure 6-12 : Total number of people in open spaces in the 5 runs of Scenario 6 .....	163
Figure 6-13 : Relative variation in the number of people in open spaces in the different runs of Scenario 6 with respect to run 1. The horizontal axis is in logarithmic scale .....	164
Figure 6-14: Injuries resulting from the simulations results.....	165
Figure 6-15: Fatality rates derived in the framework of the USGS PAGER for selected countries using an empirical model. Source: Jaiswal and Wald, 2010.....	166

Figure 6-16: Evolution of the percentage of the population: indoor (purple), not arrived (orange), safe (green) and arrived to a saturated open space (yellow) from the start of the earthquake to 15 minutes after its occurrence .....	168
Figure 6-17: Distribution of the population's states at the end of the simulation in Scenario 1 .....	168
Figure 6-18: Times of arrivals to unsaturated open spaces in Scenario 1 .....	169
Figure 6-19: Distribution of the open spaces' occupancy rates in Scenario 1 .....	169
Figure 6-20: Occupancy rates of the open spaces in Beirut at the end of the simulation in Scenario 1 .....	170
Figure 6-21 : Comparison of the simulation outputs between Scenario 1 and Scenario 2. (a) Distribution of the population's states at the end of the simulation, (b) Arrival times to open spaces .....	171
Figure 6-22: Distribution of the population's states at the end of the simulation in Scenario 3 compared to Scenario 2 .....	172
Figure 6-23: Occupancy rates of open spaces in Scenario 3 .....	172
Figure 6-24 : Changes in the occupancy of the open spaces between Scenario 3 and Scenario 2. Close up on locked open spaces: (a) Sanayeh Garden, (b) Horsh Beirut and Hippodrome, (c) Sioufi Garden, (d) Beirut port.....	173
Figure 6-25: Comparison of (a) the distribution of the population's states at the end of the simulation and (b) the open space arrival times, in Scenarios 2 (PGA=0.3 g) and 4 (PGA=0.5 g) .....	175
Figure 6-26: Changes in the number of people in open spaces and outside saturated open spaces between Scenario 4 and Scenario 2 .....	175
Figure 6-27: Comparison of the distribution of the population's states at the end of the simulation in Scenarios 2 (ideal behaviors) and 5 (realistic behaviors) .....	177
Figure 6-28: Comparison between the open spaces arrival times in Scenario 5 and Scenario 2.....	177
Figure 6-29: Average evacuation delays and travel times in Scenarios 2 and 5 .....	178
Figure 6-30: Effect of the group behavior on the evacuation delay and the speed .....	178
Figure 6-31: Comparison of the distribution of the population's states at the end of the simulation in Scenario 5 (night scenario) and Scenario 6 (day scenario) .....	180
Figure 6-32: Distribution of the target destinations of the people who were still moving at the end of the simulation in Scenario 6 .....	180
Figure 6-33: Comparison of the arrival times to open spaces between Scenario 5 and Scenario 6 ....	181
Figure 6-34: Tweet from a Turkish citizen just after the 26 September 2019 earthquake (M 5.8) in Istanbul, highlighting the insufficiency of open spaces. Retrieved from: <a href="https://twitter.com/canokar/status/1177187759645216768">https://twitter.com/canokar/status/1177187759645216768</a> .....	183
Figure 6-35 : Increase in arrival times caused by the debris in different seismic scenarios compared to the case with no earthquake.....	183
Figure 6-36 : Damage and debris during the August 24, 2016 Amatrice, Italy earthquake. Source: (Baňgate, 2019) .....	184
Figure 6-37: Rescue of people trapped in debris during in the aftermath of the August 24, 2016 Amatrice earthquake. Photograph by: Alessandra Tarantino/AP.....	184
Figure 6-38: Relative effects of the debris (PGA 0.5 g) and realistic human behaviors on the increase of the average time taken to reach an open space, compared to a scenario of PGA 0.3 g and with ideal behaviors .....	185



## List of Tables

Table 2-1 : Definition of key terms according to the Terminology on Disaster Risk Reduction (United Nations, 2015) .....	27
Table 2-2 : Selected definitions of the term ‘risk’ in the field of natural hazards .....	28
Table 2-3 : Behaviors adopted during an earthquake. The studied earthquakes are given in brackets .	39
Table 2-4 : Behaviors adopted immediately after the earthquake. The studied earthquakes are mentioned between brackets .....	40
Table 2-5: Complexity level included in the most advanced ABMs for the simulation of pedestrians’ earthquake evacuation .....	46
Table 2-6 : Evolution of the quality of the construction materials and height limitations throughout the urban evolution of Beirut. Source: Salameh (2016).....	54
Table 3-1: Damage states included in PEERS and their direct correspondence with the damage grades defined in the European Macroseismic scale EMS-98. (Adapted from: Lagomarsino and Giovinazzi, 2006, and Grünthal, 1998).....	61
Table 3-2 : Preferred moving speeds for individuals in the child, adult and elderly categories as defined in Bañgate et al., 2018, 2019 .....	70
Table 3-3: GIS data requirements of PEERS .....	77
Table 3-4: Assignment of the agent’s target location according to its target destination.....	80
Table 3-5: Implementation of the rules that control an agent’s movement in PEERS.....	81
Table 4-1 : For each building class, range of fundamental building resonance frequency ( $f_{struct}$ ), yielding ( $d_y$ ), ultimate ( $d_u$ ), maximum ( $d_{max}$ ) displacement and mean damage ( $\mu DS$ ).....	89
Table 4-2 : Summary of the input variables and the performance of the 9 ANNs trained to estimate the mean damages of building classes 1, 2 and 3. ANN1 is composed of the same input variables as in Salameh et al. 2017. The underlined input variables from ANN2 to ANN9 represent the variables that were changed with respect to ANN1. The values of $R^2$ highlighted in bold represent the maximum $R^2$ attained for each building class. ....	91
Table 4-3 : Distribution of the DFM values and the quality of the DSM over high-rise buildings in Beirut .....	100
Table 4-4 : The 4 different classification trees trained and their corresponding performance in terms of validation accuracy .....	103
Table 4-5 : Distribution of the buildings damage states for the two earthquake scenarios .....	105
Table 4-6 : Percentage of debris weight from damaged structural elements (source: HAZUS, FEMA 2012).....	110
Table 4-7 : Mean indoor and outdoor fatality rates in Beirut for seismic scenarios of PGA 0.3 g and 0.5 g. The standard deviation (std) is indicated in brackets .....	116
Table 5-1 : Tags in OpenStreetMap considered to refer to non-residential use of buildings .....	124
Table 5-2 : Distribution of apartment surfaces for low-rise and high-rise buildings in the LIBRIS buildings database .....	127
Table 5-3 : Data on the distribution of residents and households provided by the LFHLCS.....	129
Table 5-4 : Extracts from the users’ testimonies on the Lastquake app with their corresponding locations and approximate distance from the explosion site (source: CSEM-EMSC) .....	136
Table 5-5 : Demographic characteristics, spatial and social contexts of the participants of the survey (N=481) .....	138
Table 5-6: Distribution of respondents’ answers to questions related to the felt experience during the explosion and knowledge of safe areas. N is the number of respondents .....	140
Table 5-7: Indoor respondents’ reactions to the explosion. N indicates the number of answers .....	141
Table 5-8 : Results of the bi-variate analysis of the evacuation behavior. ....	142
Table 5-9 : Results of the multivariate binary logistic regression analysis between the evacuation behavior and the building damage, age and gender.....	143
Table 5-10 : Distribution of the behaviors adopted outdoors. N denotes the number of respondents. ....	143
Table 5-11: Destination reached in the aftermath of the explosion. N denotes the number of respondents .....	144
Table 5-12 : Mean of transports used for travels. N denotes the number of respondents .....	144

Table 5-13 : Bi-variate analysis of mean of transport used and the city where the respondents were located when the explosion occurred. Blue and red colors indicated under- and over-represented elements respectively ..... 145

Table 6-1: Hardware specifications of the nodes on the ISTERre cluster used for running PEERS .... 158

Table 6-2 : Research questions and parameters of the experiments in PEERS. The cell indicating the parameter of interest in each scenario is highlighted in green ..... 160

# Chapter 1: Introduction

## THESIS MOTIVATION AND PROBLEM STATEMENT

Earthquakes have always affected human lives. While today, earthquakes are understood as a natural phenomenon caused by a sudden slip on a fault (Elnashai and Di Sarno, 2008), in early cultures, earthquakes, just like other disasters, were viewed as divine punishment for human sins (Agnew, 2002).

Perhaps the first time an earthquake's origin was attributed to a natural phenomenon, and its consequences to the context of the affected area, was in the 1755 Lisbon, Portugal earthquake (Dynes, 2003). This earthquake caused massive destruction in the city and killed more than 10 000 people (Dynes, 2003). The Lisbon earthquake sparked a dialogue between French intellectuals of the era about the origins of disasters. In a correspondence to Voltaire, Jean-Jacques Rousseau wrote:

*“Without departing from your subject of Lisbon, admit, for example, that nature did not construct twenty-thousand houses of six or seven stories there, and that if the inhabitants of this great city had been more equally spread out and more lightly lodged, the damage would have been much less and perhaps of no account.”*(Masters and Kelly, 1992; Rousseau, 1756)

Here, Rousseau's statement highlights that the disastrous consequences of the Lisbon earthquake did not only depend of natural phenomenon, but rather on human settlements and building practices. Here, Rousseau attempts to define what is commonly referred to today as building vulnerability (the building's height), exposure (the number of buildings and people exposed to the earthquake), and prevention measures (avoiding dense population concentration in hazardous areas).

Furthermore, Rousseau then stresses the detrimental consequences that individual responses can have on fatalities:

*“How many unfortunate people have perished in this disaster because of one wanting to take his clothes, another his papers, another his money?”* (Masters and Kelly, 1992; Rousseau, 1756)

According to Rousseau, fatalities were not only due to building damages but that people's actions exacerbated the earthquake consequences. Instead of taking protective measures, people tried to retrieve material objects. Lisbon's vulnerability was not only physical, it was also related to the social structure and the culture, i.e. people's sensitivity to status, which made them discount the physical danger in order to retrieve material status markers (Dynes, 1999).

In recent times, the importance of human behavior on fatalities has been highlighted in several earthquake events. For example, in the 2011 Great East Japan earthquake (Magnitude 9.1) and tsunami, the highest numbers of casualties were among those who had a delayed evacuation after the tsunami warning was issued (Sawai, 2012). Similar observations were also reported for moderate magnitude earthquakes. The analysis of the death toll of the L'Aquila, Italy earthquake in 2009 (Magnitude 6.3) showed that women had higher fatality rates than men, because women were less likely to flee from buildings (Alexander and Magni, 2013).

Classical earthquake risk assessment methods in the engineering community often focus on estimating the damages to the built-environment. In these studies, earthquake risk is defined by the hazard, i.e. the earthquake activity in the region and the predicted ground motion for various earthquake scenarios; the exposure, i.e. the building inventory and its occupancy; and the vulnerability [physical], i.e. the characteristics of the building stock that make it more or less likely to suffer from damage (Lin et al., 2015). In contrast, the social sciences community often defines vulnerability [social] in terms of the capacity of individuals and groups to cope with, resist and recover from hazards (e.g. Blaikie et al., 1994). In the last 20 years, some studies developed integrated approaches that include both the physical and societal factors in urban seismic risk assessment (e.g. Carreño et al., 2012; Davidson, 1997). The societal factors included social, economic, political and emergency management conditions; however, the human behavior was not taken into account in these approaches.

Human behavior during crisis is still rarely included in urban seismic risk assessment. Yet, the actions taken by individuals during and immediately after an earthquake highly affect their exposure (Rojo et al., 2017) (Figure 1-1). In an urban area where the environment is modified by an earthquake, the interactions between the individuals and their surroundings are a key element in determining their safety (Quagliarini et al., 2016). Additionally, the availability of and access to open spaces, i.e. areas open to the public that serve as immediate safe evacuation destinations, have a key role in increasing an urban area's ability to adapt and cope with the effects of an earthquake (Shrestha et al., 2018; Villagra et al., 2014).



(a)



(b)



(c)

Figure 1-1: Examples of human behaviors observed during the 2015 Nepal earthquake in an open market area. In general, people gather in the open space away from buildings. Particular observations: (a) Falling debris (red arrow) while a person is next to a building (red circle), (b) person running back towards buildings in a danger zone (red circle), (c) group of people –man with children- evacuating to an open space together. The full video can be found at [https://www.youtube.com/watch?v=6HqcdyK\\_Lw&ab\\_channel=DebeshUtube](https://www.youtube.com/watch?v=6HqcdyK_Lw&ab_channel=DebeshUtube)

This thesis addresses the need for including human behaviors in seismic risk simulations, with a long-term goal being the definition of dynamic risk indices that include these behaviors. This thesis proposes a first step towards this goal, by studying the impact of behaviors on the safety of people in an urban environment modified by an earthquake. The underlying general question is:

## **To what extent does human behavior affect seismic risk?**

Nevertheless, this question can not be answered in an absolute manner. The responses of individuals depend on the context in which they find themselves, particularly the cultural context (Palm, 1998). Consequently, this thesis focuses on a particular urban area: Beirut, Lebanon. Beirut is prone to near-fault large magnitude earthquakes with a significant hazard variability due to geological conditions and heavy constraints on the physical and social vulnerabilities (Beck et al., 2018; Salameh et al., 2017).

This thesis looks at people's safety in the aftermath of an earthquake and analyzes the constraining factors. Here, safety is defined as being in an open space, i.e. an area away from buildings and debris.

This thesis aims to address the following scientific issues:

- (i) Does Beirut's urban form, particularly its open spaces, have the capacity to provide shelters for the residents in the immediate aftermath of an earthquake?
- (ii) How do more complex physical and social contexts, such as the extent of debris, the human behavior and the spatial distribution of the population during day and night, increase the challenges to the population's safety?

Incorporating the dynamics of human behavior into seismic risk assessment studies necessitates an interdisciplinary approach that captures all facets of a crisis. In this thesis, we propose a holistic modeling approach aiming to recreate a virtual playground that replicates the dynamics of a seismic crisis at the microscopic scale. To be relevant and realistic, such modeling requires a precise estimation of buildings and debris at the building level and models of human behaviors calibrated to the social context of the study area.

This requires close interaction between:

- Earth sciences: by estimating building seismic damage at the building scale and the resulting debris;
- Social sciences: by the analysis of human behavior and mobility in relation to social, environmental and cultural factors;
- Computer sciences: through modeling a seismic crisis using agent-based modeling and simulations.

## **STRUCTURE OF THE THESIS**

This thesis is composed of 7 chapters, which present the steps taken to achieve the objectives. The structure of the thesis is illustrated in Figure 1-2.

**Chapter 2** presents the context of this thesis. The first part of this chapter, the state of the art, gives a detailed motivation of the thesis, and the research gaps it intends to fill. The state of the art focuses on key definitions and terms in the disaster research field, seismic risk assessment, human behaviors in earthquakes and approaches for modeling human behaviors in earthquakes. The second part focuses on the study area, Beirut. This part gives an overview of the seismic context in Lebanon, the urbanization, and the findings from previous works on the seismic risk and social vulnerability in Beirut.

**Chapter 3** focuses on PEERS (Pedestrians' Earthquake Evacuation in Earthquake Risk simulations), the agent-based model developed in this thesis for the simulation of pedestrian earthquake evacuation. This chapter starts by presenting the conceptual model and its constituent sub-models: the city model, the earthquake damage model and the human behavior and mobility model. This is followed by the formalization of PEERS and its validation. Furthermore, the implementation of PEERS is also included in this chapter.

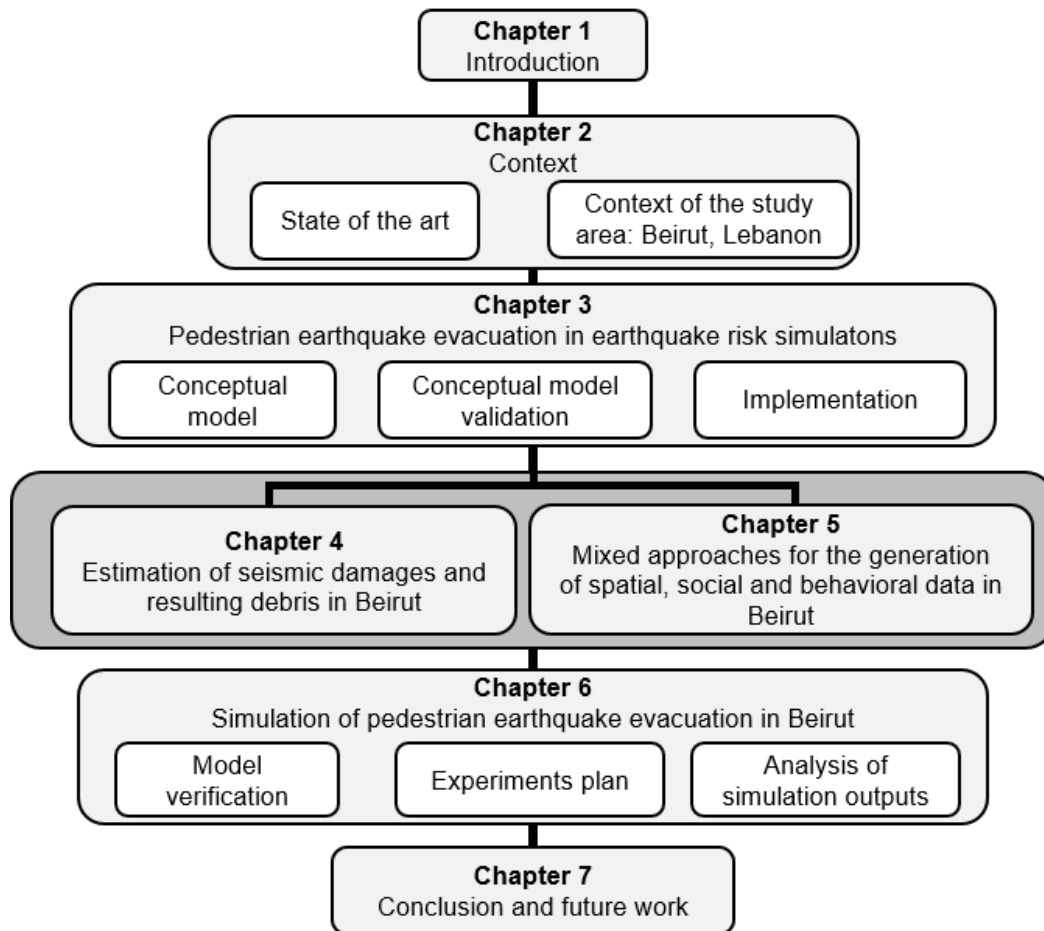


Figure 1-2: Thesis structure

**Chapter 4** focuses on the estimation of seismic damages and resulting debris in Beirut. This chapter presents the approach developed for the estimation of seismic damages at the building level, followed by the generation of a 3D buildings model in Beirut and the estimation of its seismic damages. The second part of this chapter presents the approach for the estimation of damage-induced debris around buildings. This chapter is concluded by the assignment of casualty rates to buildings and debris zones.

**Chapter 5** presents the approaches for the generation of additional spatial data (open spaces and mobility constraints) related to the urban form of Beirut. The chapter also covers the generation of a population exposure model, in which the size of the population and its spatial distribution are estimated, before generating a synthetic population for Beirut. Finally, this chapter presents the survey on the behavioral responses in the aftermath of the Beirut port explosions from which data were extracted for the development and calibration of human behaviors in PEERS.

**Chapter 6** presents the simulation of pedestrian earthquake evacuation in Beirut. The chapter gives an overview of the general configuration and outputs of the simulations before presenting the verification of the implemented model through simulations at a small spatial scale. Then it describes the technical challenges behind the simulations at the scale of the city, followed by the definition of the plan of experiments done with PEERS. Finally, the outputs of the simulations are analyzed to answer questions (i) and (ii) formulated previously.

**Chapter 7** concludes with the main learnings and contributions of this thesis. Finally, limitations and future works, as well as long-term perspectives are presented.

# Chapter 2: Context

## 2.1. INTRODUCTION

Earthquakes are high-impact natural hazards characterized by their rapid onset. Although the occurrence of earthquakes can not be prevented, a significant reduction in earthquake disasters losses could be achieved through improving infrastructure resilience, emergency preparedness, and response systems (UNISDR, 2015). A fine understanding and characterization of seismic risk are necessary for these measures to be efficient.

Various disciplines have analyzed earthquakes from different perspectives. Some Earth and Engineering scientists have developed earthquake risk assessment studies, based on the characterization of the earthquake hazard and the assessment of the exposed assets' vulnerability (e.g. Erdik, 2017). Among the Social science community, some have addressed the impacts of social economic and political factors on a communities' ability to resist, cope and recover from earthquakes (e.g. Alizadeh et al., 2018; Armaş, 2008).

Despite evidence that individuals' behaviors affect their exposure and injury during an earthquake (Alexander and Magni, 2013; Rojo et al., 2017; Shapira et al., 2015), human behavior is still rarely included in seismic risk assessments. This is mainly due to the difficulty in quantifying behaviors into tangible measures that can be integrated into these quantitative methodologies.

Moreover, despite several global efforts to promote the development of interdisciplinary disaster research (Gall et al., 2015), earthquake risk analysis is still very fragmented between disciplines.

This thesis proposes an integrated seismic risk modeling approach applied to the case of Beirut, Lebanon. The context of the thesis is presented in this chapter. The first part of this chapter presents the state of the art on the key concepts and terms used in the disaster research field (section 2.2), the seismic risk assessment methodologies (section 2.3), human behaviors in response to earthquakes (section 2.4) and the approaches for modeling human behaviors in earthquakes (section 2.5). The second part of this chapter (section 2.6) focuses on the context of the study area: Beirut, and presents its seismic hazard and urbanization contexts and the findings from previous works on the seismic risk and social vulnerability in Beirut.

## 2.2. KEY CONCEPTS AND TERMS

The concept of risk is addressed in many different fields such as safety engineering, health, security, finance or transportation (Althaus, 2005; Aven, 2016). Although most fields seem to agree that risk is the possibility of occurrence of an event that holds negative or undesirable consequences for the exposed elements, the interpretation of the term is different depending on the angle from which risk is analyzed.

This review covers only the definitions of the key concepts and terms in the disaster research field. Multiple disciplines defined simultaneously, but separately, the same terms and notions, which resulted in the same term being defined in various ways (Thywissen, 2006).

Several efforts were undertaken in an attempt to elucidate the confusion in the terminologies. The first efforts were carried out by the UNDRO (United Nations Disaster Relief Organization), which distinguished the term hazard from risk in its glossary (UNDRO, 1980). However, these definitions were not widely accepted and researchers have been compelled to provide their own definitions of terms, such as 'hazard', 'risk' and 'vulnerability' (Birkmann, 2013).

As we believe that a shared language is a crucial stepping-stone for the realization of an integrated approach for risk assessment, the following sections present the framing of the terms used in this study. First, the evolution of the disaster research field in line with the frameworks of international organizations is presented. Then, the adopted definitions are presented, starting with general, less ambiguous terms, followed by the definitions of the more debated terms of vulnerability and risk.

### **2.2.1. International frameworks and evolution of the disaster research field**

International organizations (such as the United Nations) had a major influence on the orientation of the research in the disaster field.

While the early studies in the disaster research field focused mainly on the hazard component, the report of the UNDRO in 1980 was one of the first documents at the international level that highlighted the importance of addressing vulnerability “*Through vulnerability analysis it becomes possible to make rational decisions on how best the effects of potentially disastrous natural events can be mitigated...*”. (UNDRO, 1980, p.iii).

The United Nations (UN) designated the 1990s as the “International decade of Natural Disaster Reduction” (IDNDR) which had the objectives to reduce by a concerted international efforts human losses, material losses and social and economic perturbations caused by natural disasters. With the IDNDR, the research in risks and disasters has gained popularity, and different studies dealing with hazards, vulnerability and risk have emerged (Carreño et al., 2007).

The Hyogo Framework for Action (HFA) (2005-2015) introduced by the UN emphasized the importance of addressing vulnerability to reinforce the resilience of nations by reducing disaster risk. Vulnerability was defined in a multidimensional aspect, including physical, social economic and environmental vulnerabilities. The HFA also stressed the development of indices and indicators at national or subnational levels to help decision-makers to assess the possible impacts of disasters on their community (United Nations, 2005). As a result, theoretical concepts about vulnerability and risk were often paired with analytical approaches that formulated the theories into quantifiable measures via the use of indices. Indices were used to describe inherent characteristics of systems (Tate, 2012).

In 2015 (and until 2030), the Sendai framework for disaster risk reduction followed the lead of the HFA. The goal of the Sendai framework is to reduce disaster risk through the implementation of integrated and inclusive measures to prevent and reduce hazard exposure and vulnerability to disaster and to increase preparedness for response and recovery. One of the priorities of the Sendai framework is to understand disaster risk in its all dimensions: vulnerability, capacity, exposure of persons and assets, hazards characteristics and the environment.

Despite the global organizations’ aim to provide holistic, multidimensional definitions, the research disciplines in disaster risk did not uniformly follow the same trends, which is a major obstacle for communication in a multidisciplinary environment.

The terms used in this study, were mostly defined based on definitions by the UN. Nevertheless, subtle modifications to the terms risk and vulnerability were proposed. This is further detailed in the following sections.

### **2.2.2. Definition of general terms**

The glossary of the United Nation’s International Strategy for Disaster Reduction (UN/ISDR) provides general definitions to terms commonly used in the field. This glossary was first introduced in 2004 and updated in 2009 and 2015. In this study, we have adopted the latest definitions of the UN/ISDR (United Nations, 2015) for the terms of: disaster, crisis (or emergency), emergency management, natural hazard and exposure. The corresponding definitions are presented in Table 2-1.

Table 2-1 : Definition of key terms according to the Terminology on Disaster Risk Reduction (United Nations, 2015)

Term	Definition
Disaster	<i>“A serious disruption of the functioning of a community or a society due to hazardous events interacting with conditions of vulnerability and exposure, leading to widespread human, material, economic and environmental losses and impacts.”</i>
Crisis / Emergency	<i>“A crisis or emergency is a threatening condition that requires urgent action”.</i>
Emergency management	<i>“The organization and management of resources and responsibilities for addressing all aspects of emergencies and effectively responding to a hazardous event or disaster.”</i>
Natural hazard	<i>“Natural process or phenomenon that may cause loss of life, injury or other health impacts, property damage, loss of livelihoods and services, social and economic disruption, or environmental damage.”</i>
Exposure	<i>“People, property, systems, or other elements present in hazard zones that are thereby subject to potential losses.”</i>

### 2.2.3. Vulnerability definition

Vulnerability studies have seen an emergence in the last four decades in many research disciplines. However, each discipline gave its own definition of vulnerability and framed it depending on its object of interest. Despite these thematic differences, in general, there seems to be an agreement that the impact of a given hazard (with its specific magnitude, duration, spatial extension) depends on the vulnerability of the exposed elements. There exists more than 30 definitions of the term vulnerability (Marre, 2013). As a thorough analysis of the term is outside the scope of this work, in the following, selected definitions are presented to illustrate the different connotations of “vulnerability” according to the perspective from which it was defined.

Natural and engineering sciences have given the following definitions:

- *The degree of loss to a given element at risk or set of such elements resulting from the occurrence of a natural phenomenon of a given magnitude and expressed on a scale from 0 (no damage) to 1 (total loss) or in per cent of the new replacement value in the case of damage to property.”* (Buckle et al., 2000)
- *“[Seismic] vulnerability represents the amount of damage that could be present in a building as a consequence of the occurrence of an [earthquake] of certain intensity.”*(Preciado et al., 2015)

We can see in the previous definitions that vulnerability has a quantitative dimension, related to the damages of the built environment, as a function of the magnitude of an event. In contrast, in the social sciences community, human-centric definitions of vulnerability were proposed. We cite for instance:

- *“The characteristics of a person or a group in terms of their capacity to anticipate, cope with, resist, and recover from the impact of a natural hazard.”* (Blaikie et al., 1994)
- *“The characteristics of a person or a group in terms of their capacity to anticipate, cope with, resist and recover from the impact of a natural or man-made disaster noting that vulnerability is made up of many political-institutional, economic and socio-cultural factors.”* (Schneiderbauer and Ehrlich, 2004)

These definitions, in contrast to the first two, are qualitative, relating to how individuals or groups cope, adapt and recover in response to a hazard. However, they only capture the characteristics of the social “system” isolated from its physical environment. More comprehensive definitions have defined the vulnerability of systems and communities, we cite for instance:

- “Vulnerability is the degree to which a system, subsystem, or system component is likely to experience harm due to exposure to hazard, either a perturbation or stress/stressor.” (Billie L. Turner et al., 2003)
- “The conditions determined by physical, social, economic, and environmental factors or processes, which increase the susceptibility of a community to the impact of hazards.” (United Nations, 2015)

While the definitions of vulnerability presented previously can be qualified as static (i.e. they refer to internal characteristics of objects/individuals/systems that make them more or less susceptible to suffer from harm) the literature also provides dynamic definitions of vulnerability. These definitions refer to the evolution of the environment and the way people respond to the changes in their environment, which may aggravate or reduce the impacts of a hazard. We cite for instance:

- “[Urban] vulnerability to natural hazards such as earthquakes is a function of human behavior. It describes the degree to which socioeconomic systems and physical assets in urban areas are either susceptible or resilient to the impact of natural hazards. [...]. V [Urban vulnerability] is continuously modified by human actions and therefore it varies over space and time. V cannot be assessed in absolute terms; the performance of the urban place should be assessed with reference to specific spatial and temporal scales.” (Rashed and Weeks, 2002)
- “... disasters are better viewed as a result of the complex interaction between a potentially damaging physical event (e.g. floods, droughts, fire, earthquakes and storms) and the vulnerability of a society, its infrastructure, economy and environment, which are determined by human behaviour.” (Birkmann, 2006)

In this thesis, human behaviors are an essential component of the analysis. However, none of the discussed definitions is generic enough to describe both the physical behaviors (the dynamic behaviors of buildings in response to an earthquake) and the social behaviors (the behaviors of individuals) at the same time.

Therefore we propose a modified version of the definition of United Nations (2015) in which we emphasize on the system’s (physical and social) response:

*“The conditions determined by physical, social, economic and environmental factors or processes, which influence the response of a system and increase its susceptibility to the impact of hazards”.*

#### 2.2.4. Risk definition

In the field of natural hazards, most studies have defined risk as the probability of occurrence of negative consequences due to a natural phenomenon (Table 2-2). In some studies, risk is defined as the “probability of loss”, we cite for instance the definitions of Alexander (2000) and Crichton (1999), while in others, it is defined as the expected losses, without mentioning probabilities (ADRC, 2005; Coburn et al., 1994). In all cases, the definition of risk seems to have a mathematical connotation, which is sometimes explicitly formulated. Risk has been formalized as a function of its components, hazard exposure and vulnerability (ADRC, 2005; Hori et al., 2002). Nevertheless, some definitions of vulnerability encompass the exposure too, and therefore risk is defined by the hazard and the vulnerability only (Garatwa and Bollin, 2002; UN/ISDR, 2004).

Table 2-2 : Selected definitions of the term ‘risk’ in the field of natural hazards

Source	Definition
Coburn et al., 1994	“The term risk refers to the expected losses from a given hazard to a given element at risk, over a specified future time period”
Crichton, 1999	“‘Risk’ is the probability of a loss, and this depends on three elements, hazard, vulnerability, and exposure. If any of these three elements increases or decreases, then the risk increases or decreases respectively.”

Alexander, 2000	<i>“Risk can be defined as the likelihood, or more formally the probability that a particular level of loss will be sustained by a given series of elements as a result of a given level of hazard. The elements at risk consist of populations, communities, the built environment, the natural environment, economic activities and services, which are under threat of disaster in a given area.”</i>
Hori et al., 2002	<i>“The risk associated with flood disaster for any region is a product of both the region’s exposure to the hazard (natural event) and the vulnerability of objects (society) to the hazard. It suggests that three main factors contribute to a region’s flood disaster risk: hazard, exposure, and vulnerability.”</i>
Garatwa and Bollin, 2002	<i>“The following formula is used to calculate disaster risk: Disaster Risk = Hazard × Vulnerability. In this equation risk is the product of the two factors, hazard and vulnerability. Therefore, it is clear that a risk exists only if there is vulnerability to the hazard posed by a natural event.”</i>
UN/ISDR, 2004	<i>“The probability of harmful consequences, or expected loss of lives, people injured, property, livelihoods, economic activity disrupted (or environment damaged) resulting from interactions between natural or human induced hazards and vulnerable conditions. Risk is conventionally expressed by the equation: Risk = Hazard × Vulnerability.”</i>
ADRC, 2005	<i>“In general, ‘risk’ is defined as the expectation value of losses (deaths, injuries, property, etc.) that would be caused by a hazard. Disaster risk can be seen as a function of the hazard, exposure and vulnerability as follows: Disaster Risk = function (Hazard, Exposure, Vulnerability).”</i>

Risk has also been defined as a function of the human response, we cite for instance:

- *“The combination of the probability of a hazardous event and its consequences which result from interaction(s) between natural or man-made hazard(s), vulnerability, exposure and capacity. [...] It is important to consider the social contexts in which risks occur and that people therefore do not necessarily share the same perceptions of risk and their underlying risk factors.”* (United Nations, 2015)
- *“The risk associated with environmental hazards depends not only on physical conditions and events but also on human actions, conditions (vulnerability factors, etc.), decisions and culture. The seriousness of the consequences of any disaster will depend also on how many people choose, or feel they have no choice but, to live and work in areas at higher risky.”* (International Council for Science, 2008)

These definitions are closer to our research interest; however they are quite lengthy and ambiguous. Therefore, as for the term vulnerability, we have defined risk as:

*“Risk is the product of interactions between the hazard, exposed people and property, their conditions and how they behave when faced with a hazard”.*

### 2.2.5. Summary

In this section, we have seen that several research fields have taken interest in disaster studies. However, the terminology is not uniformly defined, especially for the term vulnerability, which holds different dimensions depending on the research interest. In order to be able to communicate in a multidisciplinary environment, we have based our definitions on the generic terminology proposed by UN/ISDR. However, as our work focuses on the behavioral dimensions that affect the risk, we have proposed some definitions to the terms vulnerability and risk in order to highlight the effects of behaviors.

In the following section, we focus on seismic risk, by first presenting how seismic risk is traditionally assessed in the field of seismology and earthquake engineering and then presenting multidisciplinary approaches that have included the social dimension in seismic risk assessments.

## 2.3. SEISMIC RISK ASSESSMENT

Several methodologies have been developed to estimate seismic risk, usually quantified in terms of the probable losses due to earthquakes. The main objectives of these methods are to inform the engineers

on the level of earthquake hazard so they can adapt the building codes, and to inform decision-makers on how this hazard could translate into potential social, infrastructure and economic losses in their community (Calvi et al., 2006). A prompt assessment of seismic risk can also contribute to the improvement of relief efforts as it can identify the areas with the highest expected damages and casualties, and direct the emergency rescue teams accordingly (So and Spence, 2013).

Seismic risk assessment approaches have emerged in the engineering community and they are often focused on buildings and physical elements exposed to the earthquake hazard. In this study, we denote engineering-based approaches as “classical approaches”. However in the past 20 years we have seen a rise of integrated approaches that include social vulnerability into the assessment, which we denote here as “integrated approaches”.

In the following sections, the classical and integrated seismic risk assessment approaches are described with practical examples on their applications.

### 2.3.1. Classical seismic risk assessment approaches

In classical seismic risk assessment, seismic risk is often defined as the probable consequences of an earthquake given the predisposition of the exposed elements. If we consider the definitions adopted in Barbat et al. (2006):

*“Risk:  $Rie|_T$ , can be defined as the probability of loss or as the loss average in an exposed element  $e$  as a consequence of the occurrence of an event with intensity larger than or equal to  $i$  during an exposition period  $T$ .*

*Hazard:  $Hi|_T$ , can be understood as the probability or as the average expected rate of occurrence of an event with an intensity greater than or equal to  $i$  during an exposition period  $T$ .*

*Vulnerability:  $Ve$ , is the intrinsic predisposition of the exposed element  $e$  to be affected or of being susceptible to suffer a loss as a result of the occurrence of an event with intensity  $i$ .*

*Starting from these definitions, risk is defined as a function  $f$  of the convolution between hazard  $Hi$  and vulnerability  $Ve$  during an exposition period  $T$ :*

$$Rie|_T = f(Hi \otimes Ve)|_T$$

*where the symbol  $\otimes$  stands for convolution.”*

Similar definitions have been adopted in seismic risk assessments (e.g. Erdik, 2017; Lantada et al., 2010; Salameh, 2016) where the focus of the studies was only on the vulnerability of the built-environment. In this perspective, it is the damages that create the disruptions; the consequences of an earthquake are defined by the level of failure of man-made systems. The consequences are quantified using several metrics. For instance, a seismic risk assessment study can estimate the structural and non-structural damages to buildings, the economic losses due to the costs of damage repairs, and the injuries and loss of life of the building occupants and passers-by (Crowley et al., 2021). Usually, the results of these studies are communicated in terms of average expected annual losses (economic and social losses) (Crowley et al., 2021; FEMA et al., 2017).

The approaches followed for earthquake hazard assessment can take the form of (1) a deterministic, or scenario-based approach, in which the hazard is defined for a plausible earthquake scenario; or (2) a probabilistic approach, where the seismicity of the region is analyzed based on a probabilistic seismic hazard assessment (PSHA) (McGuire, 2008) to obtain the probability of exceedance of a certain hazard level in a given time period (Lantada et al., 2010).

The vulnerability of structures can be characterized using (1) qualitative descriptors, such as low, medium high, etc. or A, B, C, etc. which is often used in macro seismic scales (Grünthal, 1998); (2) physical vulnerability indices, such as the vulnerability index proposed in the RISK-UE project (Cherif et al., 2017), which can take values between 0 and 1 depending on the characteristics of the building; and (3) capacity curves, which describe the elasto-plastic behavior of a structure, depending on its typology, height and the paraseismic code to which it was designed (e.g. Lagomarsino and Giovinazzi, 2006).

The expected physical damage can be obtained using vulnerability functions, fragility curves and damage probability matrices (Lantada et al., 2010). From the damages, a cost of repair, replacement or demolition can be incurred. As for the social losses, depending on the number of occupants in the building (the time of the day) and the use of the building (thus occupancy class), the number of injured, dead and homeless can be estimated (FEMA, 2012)

Several methodologies, tools and software have been developed for seismic risk modeling and loss estimation. The differences in these tools can be seen in the approach adopted for modeling the hazard (probabilistic or deterministic) and the vulnerability (empirical or analytical). Another difference also arises in the geographical area of application of the software. For instance HAZUS (developed by the Federal Emergency Management Agency (FEMA)) is developed for the US, however it is applicable worldwide; CAPRA, developed by the World Bank, the Inter-American Development Bank and UN/ISDR is applicable for Central America, and OpenQuake, developed by the Global Earthquake Model (GEM) has a global domain of application (Makhoul and Argyroudis, 2018).

These tools have been applied at the city-scale, such as scenario-based risk assessment of Istanbul (Silva et al., 2012), displayed in Figure 2-1; at the country scale, such as the intensity-based probabilistic approach adopted for the estimation of the direct seismic losses in France (Riedel and Guéguen, 2018) displayed in Figure 2-2, and the probabilistic seismic risk assessment at the scale of Europe (Crowley et al., 2021) displayed in Figure 2-3.

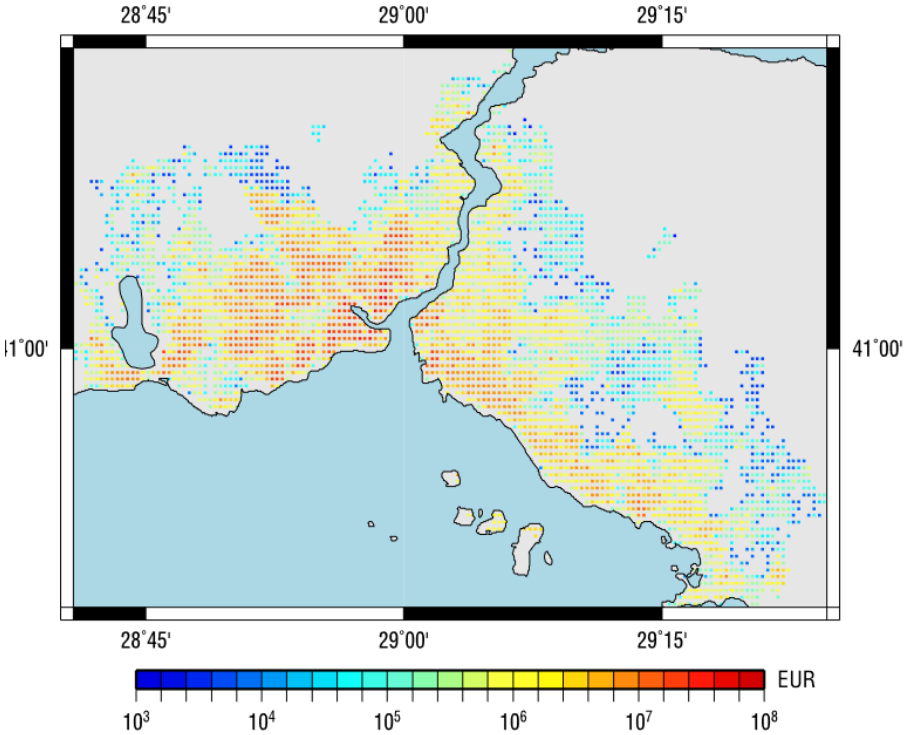


Figure 2-1 : Map of the economic losses in Istanbul. Source: (Erdik, 2017) adapted from (Silva et al., 2012)

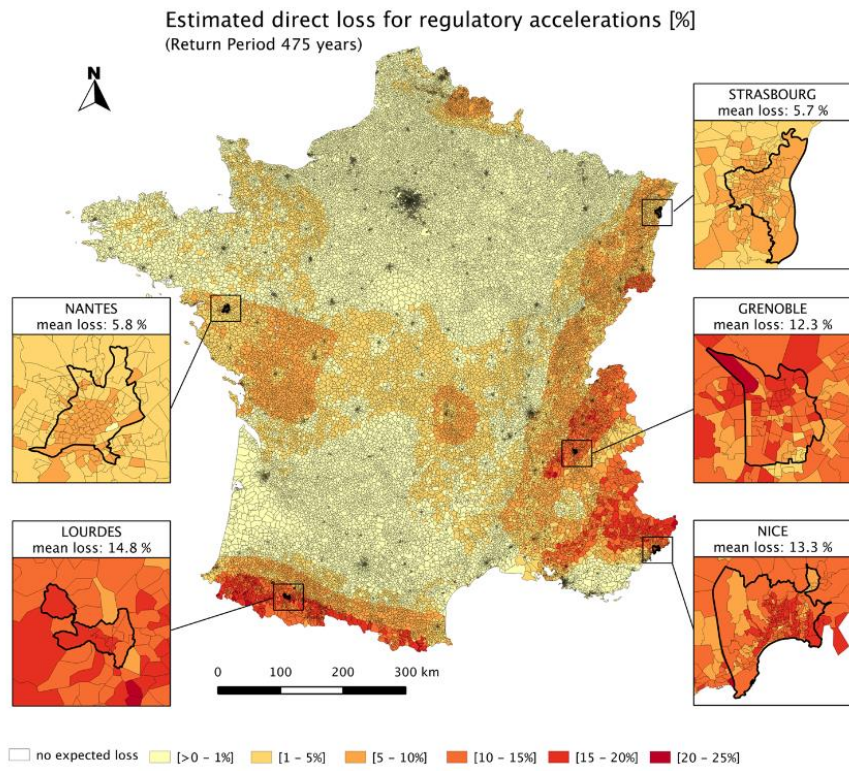


Figure 2-2: Map of the estimated losses for regulatory accelerations in France. Loss here refers to the mean losses in the building stock. Source: Riedel and Guéguen (2018)

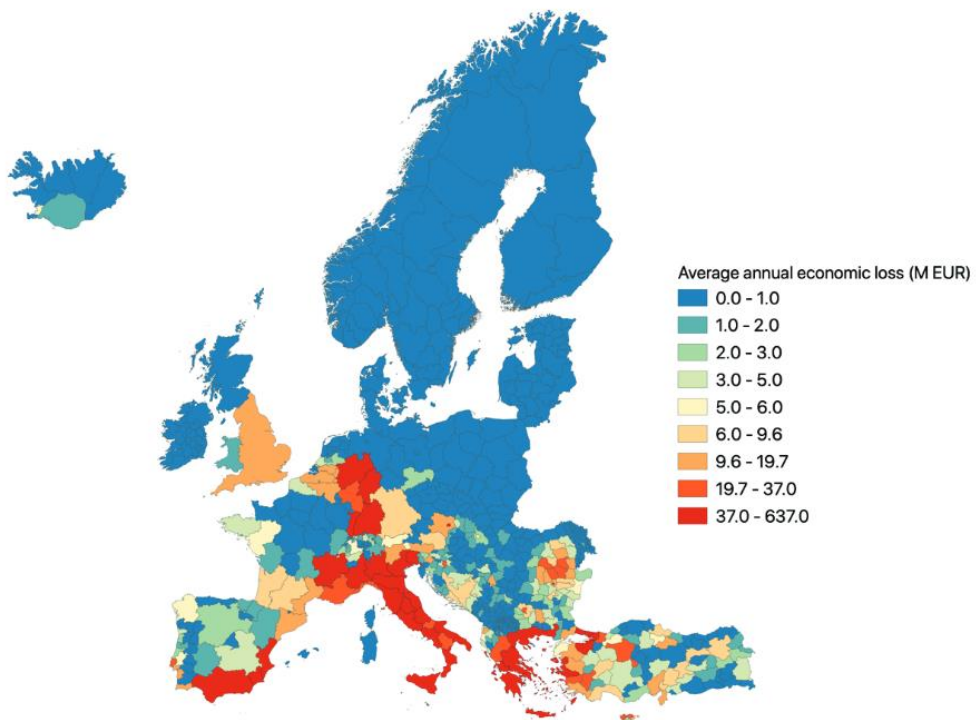


Figure 2-3: Map of the average annual economic losses across Europe. Source: Crowley et al. (2021)

### **2.3.2. Integrated seismic risk assessment approaches**

With the progress made in the disaster research field and the rise of integrated definitions of risk and vulnerability that include the underlying societal factors, the dependence of seismic risk on societal factors has progressively gained traction in the natural hazards community.

The first integrated approach for seismic risk assessment was in the framework of the Earthquake Disaster Risk Index (EDRI) (Davidson, 1997), in which the social vulnerability, the economic and political contexts, as well the emergency response and recovery capacities were included in the risk definition. Some approaches developed integrated the seismic risk assessment methodologies focusing on social losses, namely on the estimation of the casualties taking into account social vulnerability factors (Lin et al., 2015; Shapira et al., 2016). Nevertheless, the most noteworthy integrated approaches in the geosciences community were through the development of integrated seismic risk indices, which will be presented in the following sub-sections.

#### **2.3.2.1. Earthquake Disaster Risk Index (EDRI) (Davidson, 1997)**

The EDRI (Davidson, 1997) is one of the pioneering integrated seismic risk indices. The aim of the EDRI is to synthesize knowledge of urban earthquake disaster risk into a concise, easily accessible summary. The EDRI was built to allow direct comparison of the relative overall earthquake disaster risk of cities worldwide, while describing the relative contributions of different factors to the overall risk. Therefore, the EDRI is a relative index that can be used for comparing two or more cities, rather than giving an absolute measure of disaster risk.

Earthquake disaster risk is defined as the convolution between the hazard, described by its probability and severity; the exposure of the physical structures, the population and the economy; the vulnerability, which encompasses the physical, social and economic aspects; the political context; and finally the emergency response and recovery capacities.

After selecting the indicators that represent each of these components, they are normalized, weighted and aggregated to form the index. In order to illustrate the application of the EDRI, a map of the EDRI in 10 cities worldwide is shown in Figure 2-4. On this map, we can see that the highest value for the EDRI is Tokyo (54), while the lowest EDRI is St. Louis (36). We can also see, for instance, that San Francisco and Santiago have the same EDRI value although the hazard factor in San Francisco is significantly less important than in Santiago. However, the high importance of emergency response and the recovery factor and vulnerability in Santiago, makes it reach the same disaster risk level as San Francisco.

The development of the EDRI was definitely a leap forward in the integration of societal factors in seismic risk assessment; however, the usefulness of this index is limited. Although the comparison of the components of disaster risk between cities worldwide contributes to improving the understanding of the importance of each and every component of the disaster risk, from an operational point of view, it does not improve the seismic risk mitigation and emergency preparation at a local level.

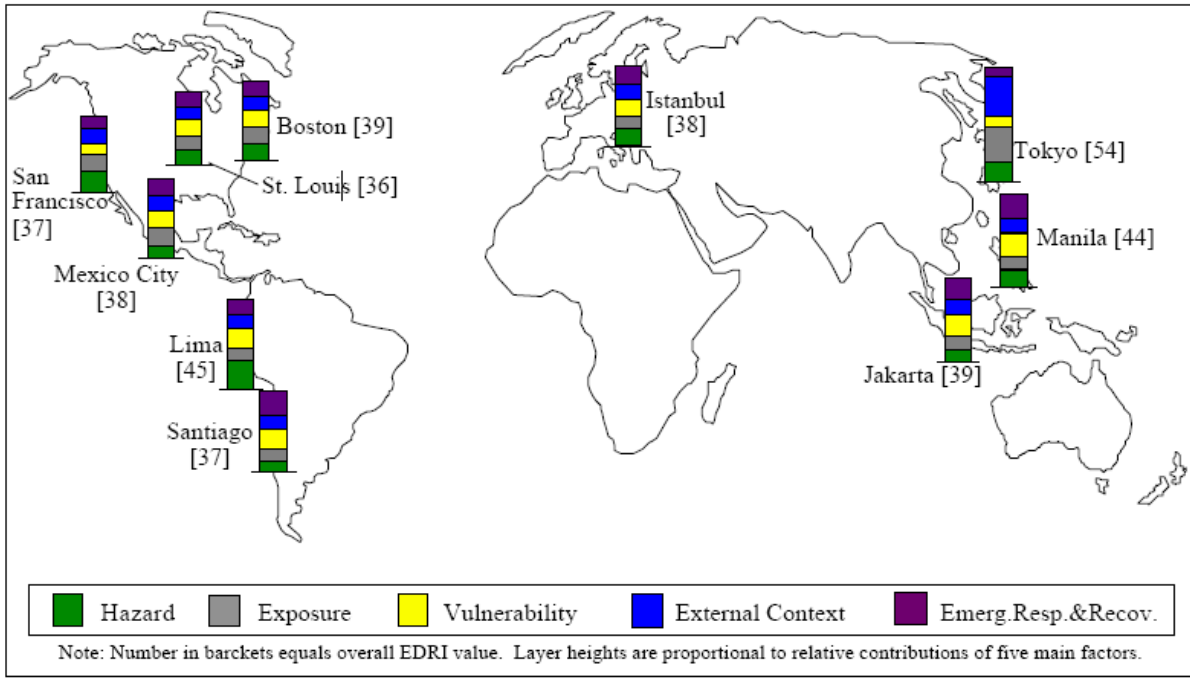


Figure 2-4: Application of the EDRI to 10 cities worldwide. Source: Davidson (1997)

### 2.3.2.2. Urban Seismic Risk Index (Carreño et al., 2007)

The Urban Seismic Risk Index (USRI) developed by Carreño et al. (2007) was based on the holistic seismic risk estimation approach proposed by Cardona and Hurtado (2000). The USRI offers a holistic view of seismic risk by integrating the physical damages of buildings and infrastructures with society's fragility and lack of resilience, which are incorporated as aggravation factors of the physical effects. The goal of the USRI is to measure the seismic risk in an urban area from an integrated perspective. The analysis is done at the level of the territorial division in the urban area. Therefore, the USRI can contribute to the identification of the disparities between the different localities in the urban area and highlight the main risk drivers in order to improve its management.

In the USRI, the physical risk is first computed and then multiplied by an aggravating factor calculated as the combination of indicators of socio-economic fragility and lack of resilience. Thus, the total risk is expressed as:

$$R_T = R_F \times (1 + F) \quad (2.1)$$

where  $R_T$  is the total risk index,  $R_F$  is the physical risk index and  $F$  is the aggravating factor.

The indicators for physical risk represent, among others, the damaged area, the number of dead and injured, which are calculated using classical seismic risk estimation approaches. The aggravating factors represent the social, economic and emergency management conditions. For instance, population density, the number of hospital beds and the percentage of public space (i.e. open space) were proposed as indicators in Carreño et al. (2007).

The USRI was applied to numerous cities worldwide. We can cite for instance the application to Bogotá (Colombia) and Barcelona (Spain) (Carreño et al., 2007), Metro Manila (Philippines) (Fernandez et al., 2006), Mumbai (Khazai and Bendimerad, 2011). It should also be noted that USRI was integrated in the loss modeling software CAPRA and was used to perform the holistic seismic risk assessment of Medellín (Colombia) (Salgado-Gálvez et al., 2016) displayed in Figure 2-5.

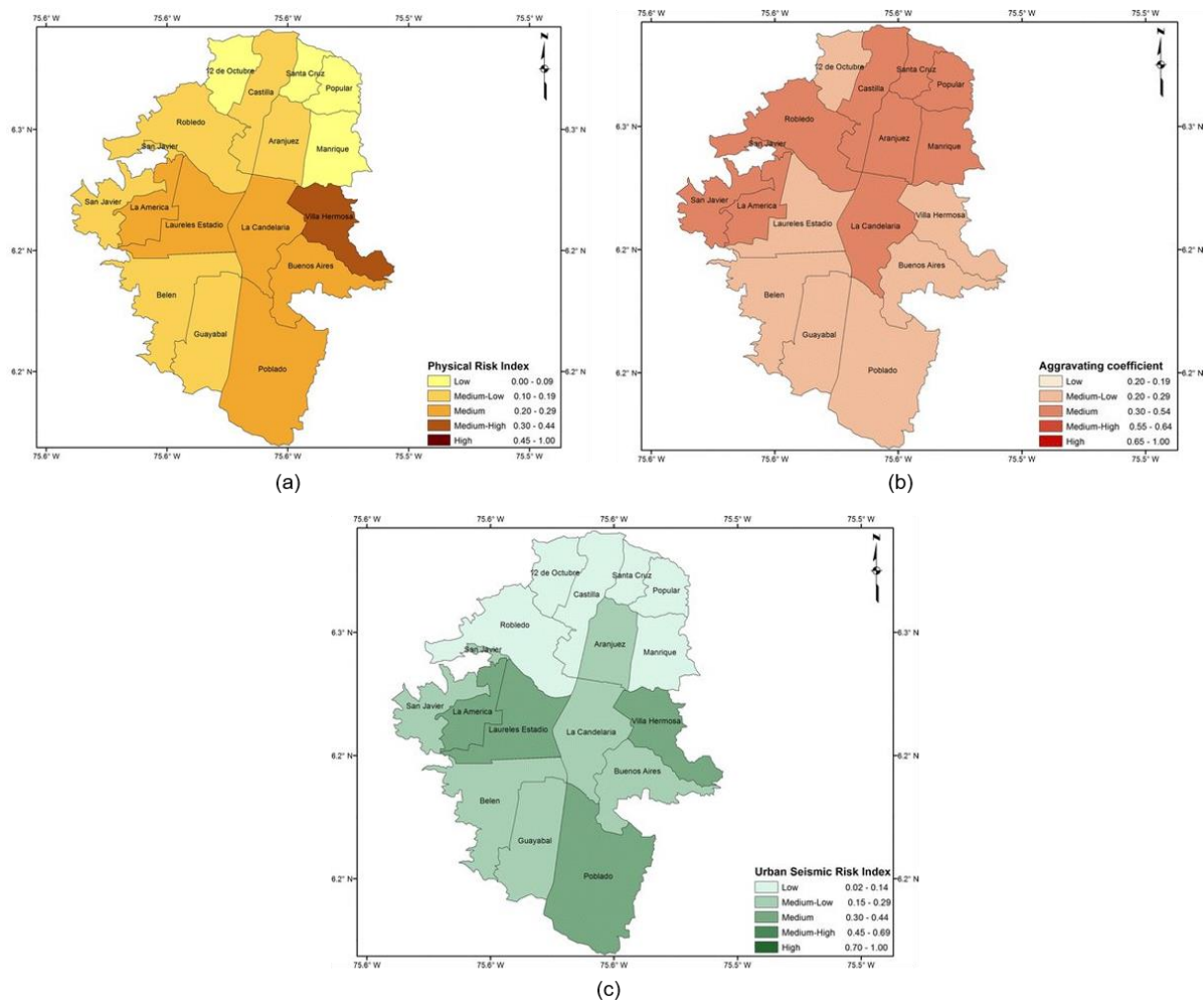


Figure 2-5: Application of the USRi to the city of Medellín, Colombia. (a) Physical risk index by county, (b) Aggravating coefficients by county, (c) USRi results by county. Source: Salgado-Gálvez et al. (2016)

Although the USRi gained a lot of popularity and was used for several applications, its implementation in CAPRA, developed for Central America, limits its global visibility.

### 2.3.2.3. GEM's Integrated Risk Modeling Toolkit (Khazai et al., 2014)

The most notable integration of social vulnerability in the assessment of seismic risk was the development of GEM's Integrated Risk Modeling Toolkit (IRMT) (Khazai et al., 2014). The IRMT was designed to facilitate the integration of socio-economic indicators with measures of physical risk and to perform an integrated risk assessment.

The IRMT can be accessed as a plugin in the QGIS software or from GEM's Openquake platform. GEM provides data related to socio-economic indicators, compiled from statistical databases worldwide. Nevertheless, the user is given the option to integrate data from other sources. The IRMT can construct a social vulnerability index, which can be combined with classical risk measures provided by the OpenQuake platform. The integration of physical and social vulnerability measures in the same index follows the same approach as in the USRi (Carreño et al., 2007).

The test-application of the IRMT for the integrated seismic risk assessment of Portugal is shown in Figure 2-6. Additionally, in 2020 GEM launched its Global Model for Earthquake Social Vulnerability and Resilience (SVR), and provided global maps for social, economic and recovery indices, which can be consulted on this page: <https://www.globalquakemodel.org/gem>.

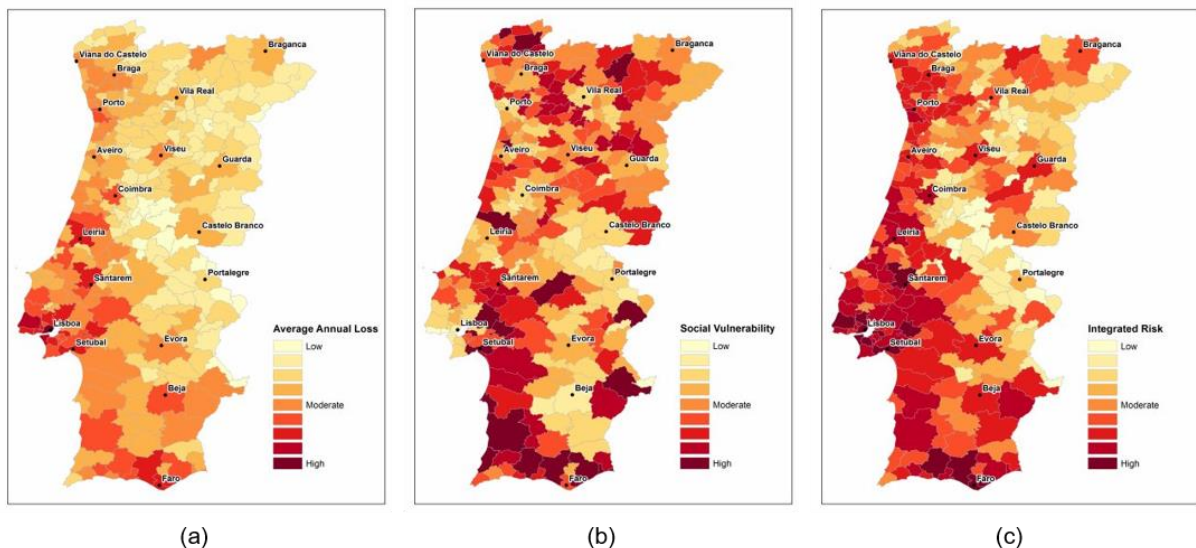


Figure 2-6: Integrated seismic risk modeling for Portugal at the county level, performed using GEM’s IRMT. (a) Map of the physical risk, quantified in terms of the Average Annual Loss, (b) Map of the social vulnerability index, computed in the IRMT, (c) Integrated seismic risk computed in the IRMT. Source: Burton and Silva (2014)

The integration of the social vulnerability indices and the ability to perform integrated seismic risk assessment within the OpenQuake platform, which has a global-domain of application, promotes and confirms the wide-scale acceptability of social determinants of risk by the geosciences community.

Although these approaches manage to include societal factors into seismic risk assessment we find that they have several limitations, as discussed below.

### 2.3.3. Summary

In the previous sections we have presented the most notable methodologies developed for integrated seismic risk assessment. Although these indices include the physical and social components of risk, we find that these indices fail to capture the seismic risk in a holistic way, mainly for three reasons:

- From an ontological perspective, considering the societal conditions as “aggravating factors” puts the physical elements of the urban area in the center of the analysis, while the society’s capacity to cope, adapt and overcome the effects of a hazard is considered as secondary aspect. Therefore, although these approaches claim to be integrated, they are still very “object” centered, and fail to capture the interplay between the natural and social environments;
- From an analytical perspective, it is not clear how these indices take into account the correlation between physical and social indicators. If we take for example the correlation between the socio-economic level of the population and the quality of building in which they live, people with low socio-economic level are more likely to live in poorly built structures. Consequently, they are more prone to damage during an earthquake (high physical risk). Therefore, the multiplication of the physical risk by an aggravating factor that includes the socio-economic level of the population is likely to overestimate the total risk, since different indicators showcasing related notions are included in the estimation twice;
- On a final and more important note, in these indices, the seismic risk is assessed in static, pre-crisis conditions, without taking into account the dynamics of the crisis. Nevertheless, the behaviors that individuals adopt, i.e. fleeing from buildings and going in the streets, staying in buildings and hiding under furniture, have been demonstrated to impact their level of exposure (Rojo et al., 2017). Therefore, the adopted behaviors can aggravate or reduce the exposure and consequently the risk. In addition, indicators of emergency management conditions, such as open spaces capacities, which can be used to shelter population, do not take into account the accessibility to these spaces. They do not include how close or far the population is from these

spaces and what is their actual post-earthquake capacity, knowing that urban spaces may be affected by debris from building damages.

Consequently, we consider that true integrated approaches should simultaneously: capture the characteristics of the social and physical environments, recreate the responses of the buildings to earthquakes and consider the responses of individuals. Additionally, the interactions between the individuals and the post-seismic physical environments should be included as well in the analysis. While the dynamic responses of buildings has been widely analyzed in the earthquake-engineering community, the research on human behaviors in earthquakes is still an exploratory field.

In the next part of this review, we present the theories and observations on human behaviors in earthquakes. This is followed by a review on the approaches for modeling human behaviors in earthquakes.

## **2.4.HUMAN BEHAVIORS IN RESPONSE TO EARTHQUAKES**

When faced with a dangerous situation, the instinctive human response is to ensure survival and self-preservation (Mobbs et al., 2015). The traditional views on individual responses to threat, consider that when faced with a threat, the typical behavioral responses can be described as freeze, fight, flight, fright or faint. The individual response is assumed to be guided by fear or purely egoistic motives (Bracha, 2004; Schmidt et al., 2008).

However, the egoistic point-of-view is not sufficient alone to describe the complexity of human behaviors. Collective and altruistic actions have been observed in several studies (Cocking et al., 2012; Ma, 2017). Human interactions are governed by social and cultural norms reflecting social structures, institutions and relationships in which people are embedded (Bianchi and Squazzoni, 2015; Burns et al., 2018; Misyak et al., 2014).

Through evolution, people have developed social and collective mechanisms to respond to threats (Gavrilets, 2015). When in a group, people might be less anxious and therefore have a reduced risk of panic (Moussaïd and Trauernicht, 2016). Additionally, being in a group reduces a person's cognitive effort needed to face a threat because group members share their cognitive resources to work towards the same goal, which is ensuring survival. Moreover, people have different situational awareness due to their varying sensitivity levels and personalities (Slovic and Weber, 2002). Consequently, the notion of safety and the strategies deployed to deal with stressors may differ from one person to another. Furthermore, a person might have limited physical or mental abilities (decreased sensory awareness, disability, reduced mobility) which could hamper his/her survival. In that sense, a group of people with a mixture of personality traits and physical and cognitive abilities can increase the chances of survival in disasters because individuals in a group can follow, lead, mimic or help others when facing a threat (Ein-Dor, 2014).

In this section, we present the social theories about human behaviors in emergencies, as well as observations documented in post-seismic surveys that highlight the highly-contextual nature of human response to earthquakes.

### **2.4.1. Theories about human behaviors in emergency**

Several social theories have been formulated to explain the complex behaviors people adopt during emergencies. A comprehensive review on the social theories is presented in Bañgate (2019). In the following subsections, we present the most relevant theories, namely panic theory, theories on collective behavior, and social attachment theory.

#### **2.4.1.1. Panic theory**

According to panic theory, the social response in an emergency is irrational and chaotic (Chertkoff and Kushigian, 1999). In this context, panic refers to a hysterical flight behavior that is completely groundless and irrational, occurring with a total disregard for others (Mawson, 2005). Social bonds are dissolved and each individual strives for survival, which results in competitive behaviors within crowds

(Drury et al., 2008; Strauss, 1944). Panic has been used to explain observations of stampedes during mass evacuations that have resulted in deaths and injuries (Helbing et al., 2000; Khan and Noji, 2016; Ngai et al., 2009; Riboldi, 2014).

While some experts discard this theory and consider mass panic to be an unfounded myth that does not accurately represent human behaviors in emergency (Cocking et al., 2009; Heide, 2004), others support it, but only under certain conditions. According to Verdière et al. (2014) panic, as a fear behavior, is not always adopted, and if adopted it only lasts for a specific duration. According to Ma et al. (2011), there are three factors necessary for panic: a belief of an impending threat, being in a confined space, and importantly, feeling that there is no escape.

#### **2.4.1.2. Collective behaviors in emergencies: Emergent Norm theory, Social Identity theory**

Normative theory states that the norms that exist in everyday life are maintained in emergencies (Aguirre et al., 2011; Johnson, 1988, 1987). Therefore, social order and organization are maintained even in a crisis. Example of these norms include caring for children, aiding old people, helping the disabled, and following traffic rules. In this theory, human behavior is assumed to be predictable even in disasters, as people adopt the recommended behaviors prescribed in guidelines and evacuation plans. However, the weakness of normative theory can be highlighted by its inability to represent the illogical behaviors observed during crises. For instance, when evacuating from a building, people usually exit from a familiar door (mostly the one they used to enter the building), instead of following the recommended behavior of heading to the nearest exit (Rai & Wong, 2009). Similarly, in cases of evacuation from a burning aircraft, it has been observed that instead of evacuating right away, people try to retrieve their luggage which therefore delays their evacuation (Flight Safety Foundation, 2004).

On the other hand, the Emergent Norm theory argues that an emergency overrides existing norms and forces people to establish new norms that will guide their behaviors (Turner and Killian, 1987). Due to the urgent nature of a crisis, collective actions, i.e. group behaviors, develop as a result of the emergence of new behavioral norms. In that sense, the responses to disasters are primarily group decisions shaped by existing social bonds, rather than primitive emotional and behavioral reactions to environmental stressors (Solberg et al., 2008).

In the same context, the social identity theory (Drury et al., 2009a, 2009b) suggests that bonds between strangers in unfamiliar places may develop in emergencies due to the shared identity resulting from the common fate of those in an emergency (Drury, 2018). This theory can explain observations of crowd solidarity and support for strangers who are also affected by the emergency.

The theories presented in this section are mainly focused on collective behaviors, rather than processes behind individual decision-making. Although they are useful for explaining behaviors observed in crowds and groups they fail to describe the motives behind each person's decisions.

#### **2.4.1.3. Social attachment theory**

Social attachment theory states that, in emergencies, individuals seek the proximity of familiar people and places, even if it would mean staying in or approaching dangerous situations (Mawson, 2005). This is because the presence of familiar persons and places induce a calming effect, whereas their absence might create more stress than the physical danger itself. Consequently, behaviors such as movement to familiar exits, reluctance to flee from home, or heading towards home, reuniting with familiar people and surroundings can be explained with this theory (Mawson, 2005).

However, the influence of the presence of significant others during emergencies has shown mixed findings. For example, when studying behaviors of hurricane survivors, it was observed that the presence of children was associated with evacuation, whereas the presence of elderly resulted in less chance of evacuation (Dash, 2002; Gladwin and Peacock, 1997). However, in other studies, no significant between evacuation and the presence of senior people was shown (Heath et al., 2001).

In summary, although theories about human behaviors provide substantial understanding of human behaviors in emergencies, they fail to capture the elements of context needed to understand the variability of behaviors observed at an individual level. Studies in the literature linked the actions people adopt during and in the immediate aftermath of an earthquake to several elements of context, namely:

- (1) the seismic context, i.e. the earthquake characteristics, such as the felt seismic intensity and the building damage;
- (2) individual characteristics, such as the person's age, gender and previous earthquake experience;
- (3) the social, cultural and environmental context, namely the individual's location, whether they are alone or with other people and the influence of cultural adaptations.

In the following, we explore the state of the art on the contextual factors that influence individual behaviors in earthquakes.

#### 2.4.2. Observed behaviors and contextual factors

Individual responses to earthquakes that occurred in Italy, the US, New Zealand, Japan and Mexico were collected using post-seismic surveys (Goltz et al., 2020b, 2020a, 1992; Goltz and Bourque, 2017; Jon et al., 2016; Lindell et al., 2016; Ohta and Ohashi, 1985; Prati et al., 2013, 2012; Santos-Reyes and Gouzeva, 2020). In these surveys, the behaviors are usually categorized in behaviors adopted during the shaking, and behaviors adopted in the immediate aftermath, i.e. after the shaking stopped. A comparison of the main findings on the predominant individual behaviors and their distribution among the respondents are summarized in Table 2-3 and Table 2-4.

Table 2-3 : Behaviors adopted during an earthquake. The studied earthquakes are given in brackets

	<b>Earthquake Maximum Intensity</b>	<b>Evacuating Immediately</b>	<b>Taking Cover</b>	<b>Freezing in Place</b>	<b>Reaching/ Protecting Others</b>
Prati et al. 2012* (Umbria-Marche, Italy, 1997)	IX	38%	12%	22%	4%
Prati et al. 2013 (Emilia-Romagna, Italy, 2012)	VIII	36%	30%	33%	No data available
Goltz and Bourque 2017 (Whittier Narrows, USA, 1987)	VIII	6%	39%	35%	6%
Goltz and Bourque 2017 (Loma Prieta, USA, 1989)	IX	8%	25%	37%	11%
Goltz and Bourque 2017 (Northridge, USA, 1994)	IX	8%	27%	39%	17%
Lindell et al. 2016 (Christchurch, New Zealand, 2011)	IX	11%	17%	38%	10%
Lindell et al. 2016 (Tohoku, Japan, 2011)	IX	28%	7%	32%	10%
Santos-Reyes and Gouzeva 2020 (Mexico City, Mexico, 2017)	VIII	53%	14%	2%	17%

\* In this survey, the respondents cited all the behaviors they adopted. Therefore, the choices between behaviors were not exclusive

Table 2-4 : Behaviors adopted immediately after the earthquake. The studied earthquakes are mentioned between brackets

	<b>Earthquake Maximum Intensity</b>	<b>Evacuating</b>	<b>Returning to house</b>	<b>Reuniting with family members</b>	<b>Continuing previous activities</b>
Prati et al. 2012* (Umbria-Marche, Italy, 1997)	IX	93%	59%	51%	4%
Jon et al. 2016 (Christchurch, New Zealand, 2011)	IX	Going to a public shelter (1%) Going somewhere else (20%)	28%	12%	13%
Jon et al. 2016 (Tohoku, Japan, 2011)	IX	Going to a public shelter (12%) Going somewhere else (11%)	29%	11%	6%
Jon et al. 2016 (Cook Strait, New Zealand, 2013)	VI	Going to a public shelter (12%) Going somewhere else (8%)	10%	10%	54%
Jon et al. 2016 (Lake Grassmere, New Zealand, 2013)	VI	Going to a public shelter (1%) Going somewhere else (13%)	22%	9%	42%
Santos-Reyes and Gouveza 2020 (Mexico City, Mexico, 2017)	VIII	16%	8%	54%	4%

\* In this survey, the respondents cited all the behaviors they adopted. Therefore, the choices between behaviors were not exclusive.

The different studies seem to agree on the predominant behaviors during earthquakes: evacuating, taking cover, freezing in place and protecting others. However, the frequency of each adopted behavior varies from one earthquake to another, despite very close reported maximum intensities (from VIII to IX). For instance, in Table 2-3, the percentage of the survey respondents that reported evacuating immediately ranges from below 10% in Goltz and Bourque (2017) and exceeds 50% in Santos-Reyes and Gouveza (2020). On the other hand, the behaviors adopted in the minutes following the shaking were found to be mainly: evacuating, returning home, reuniting with family members or continuing previous activities. Similarly, the percentage of the population who adopted each action varied from one study to another.

The analysis of the contextual factors that affect human behaviors in earthquakes is presented in the following subsections with a focus on the seismic context, the individual characteristics and the environmental, social and cultural contexts.

#### 2.4.2.1. Seismic context

Seismic intensity has been reported to influence an individual's immediate reaction in several studies. It has been observed that during an earthquake, people freeze for a few seconds when they first experience an earthquake before undertaking any further action (Bernardini et al., 2019; Goltz et al.,

2020b; Lambie et al., 2017; Zhou et al., 2018). During this time, people attempt to understand the situation, looking for signals from the environment or from other people, also referred to as milling behavior (Wood et al., 2018). The time people took to undertake actions was observed to decrease with increasing intensity (Bernardini et al., 2019). For instance, in Zhou et al. (2018), the average delay was reported to be 22 s at intensity (Modified Mercalli Intensity MMI scale) IV, which decreased to 1.8 s at intensity VIII until no delay was observed at intensity IX.

In their analysis of DYFI<sup>1</sup> data from eight countries, Goltz et al. (2020a) observed that at low intensities (between MMI I-V) people did not take any action during the earthquake. However, higher felt intensities were found to be correlated with undertaking protective behaviors (Jon et al., 2016; Lindell et al., 2016),

Moreover, behaviors were also found to be related to building damage, where the experience of building damage was linked to higher probabilities of fleeing (Goltz and Bourque, 2017; Prati et al., 2012). However, the link between building damage and the cultural context was highlighted in Goltz et al. (2020a). For earthquakes in Pakistan, China, Nepal and Mexico the experience of building damage resulted in significantly greater probabilities of evacuating from buildings, whereas in Napa, Oklahoma and Japan, flight from buildings was rare even when damage was experienced.

Despite these differences, the findings are more or less consistent: a higher seismic intensity (or damage) results in a higher propensity for behavioral adaptations. The findings on the influence of the individual characteristics on behaviors are presented in the next section.

#### **2.4.2.2. Individual characteristics**

The behaviors that people adopt in reaction to earthquakes were found to be related to several demographic variables such as: age, gender and previous earthquake experience. However mixed findings were highlighted in different studies.

Regarding age, adults were found to be more likely to stay in place, especially if they were surrounded by other adults (not children nor the elderly) (Goltz and Bourque, 2017). Younger age (18 and less) was found to be associated with taking cover, while older people (65 years old and more) were reported to be more likely to continue normal activities, protect property and less likely to protect others or take cover (Lindell et al., 2016). The effects of age on behaviors were associated to movement and mobility, as older people were found to be unable to move during severe shakings, while babies and infants also did not move due to their incapacity of interpreting the emergency of the situation and adapting accordingly (Murakami and Durkin, 1988).

The analysis of the influence of gender on the behavior adopted in the aftermath of an earthquake yielded mixed results. Men were found to be more likely to evacuate buildings (Goltz and Bourque, 2017; Prati et al., 2013, 2012). In some studies, women were found to be more prone to taking cover, reaching for and protecting others (Goltz and Bourque, 2017). However, in other studies both women and men had similar probabilities of doing these behaviors (Santos-Reyes and Gouzeva, 2020). In Jon et al. (2016), gender was uncorrelated with the actions undertaken in the immediate aftermath actions. However, women were consistently found to be injured more often than men in the immediate aftermath of an earthquake (Horspool et al., 2020; Peek-Asa, 1998; Taylan Susan, 2015). This finding was attributed to the role of women as caregivers, which make them hurry to provide assistance to children or others people for whom they are responsible (Horspool et al., 2020).

Studies on the behaviors in New Zealand and Japan found that earthquake experience, earthquake information, and emergency preparedness were significantly positively related to the recommended protective action (take cover) and negatively related to the discouraged protective action (evacuate immediately) (Lindell et al., 2016; Ohta and Ohashi, 1985). However, discrepancies were noted on the effects of previous earthquake experience; it was reported that having experienced earthquakes might

---

<sup>1</sup> "Did You Feel it?" (DYFI) is a program of the U.S. Geological Survey for collecting information from people who felt an earthquake. More information can be found at: <https://earthquake.usgs.gov/data/dyfi/background.php>

give people a false sense of earthquake security and decrease the motivation for undertaking protective actions (Lindell and Perry, 2003).

Overall the influence of individual characteristics on behaviors is not conclusive. This is also the case of the environmental, social and cultural contexts as detailed next.

### **2.4.2.3. Environmental, social and cultural contexts**

The familiarity with the building the individual was in during the earthquake was found to be associated with the behavioral response. People who were in a familiar environment, such as being at home, were found more likely to take cover indoor (Prati et al., 2012). Conversely, when people were unfamiliar with their environment, they were more likely to flee outside (Goltz and Bourque, 2017). These observations were explained by the sense of safety a person feels when in a familiar environment (Prati et al., 2012). However, contrary observations were reported in Santos-Reyes and Gouzeva (2020), as people who were at home were more likely to escape than those who were at work.

Behaviors were also found to be related to the social context the individuals were in when the earthquake occurred. Individuals who were not alone, particularly in the presence of dependent people such as children or elderly, were less likely to freeze (stay in place) when the earthquake occurred and more likely to take cover, or reach and protect others (Goltz and Bourque, 2017; Jon et al., 2016; Lindell et al., 2016; Prati et al., 2012). These observations could be explained by the social roles individuals occupy, especially with respect to household members. If a person is a caretaker or responsible for someone, the person maintains this responsibility in the event of an earthquake (Lambie et al., 2017).

Culture was found to have a crucial role on shaping the individual responses to earthquakes, as it determines how the risk is perceived (Alexander, 2012). The cultural context may reduce or increase the awareness of risk, and limit the range of acceptable responses (Wildavsky and Dake, 1990). For instance, the cultural differences between the U.S. and Japan, represented by the belief over the control of one's destiny, were found to have significant effects on the individuals' behavioral responses to earthquakes (Palm, 1998). Additionally, certain populations may develop an "earthquake culture", a term used to describe how the earthquake experience shapes the way people live with earthquakes (Ibrion, 2018). The earthquake culture was found to be related to earthquake-resistant construction practices (Javier Ortega et al., 2017) in addition to improved institutional preparedness and response (Mileti et al., 2002).

### **2.4.3. Summary**

During an earthquake, the most common behaviors are evacuating, taking cover, freezing in place and reaching and protecting others. When the shaking ends, some people resume their previous activities, while others are likely to evacuate from buildings, return to their houses, or look for their relatives and reunite with them.

Although several theories exist to explain the human responses to earthquakes, these theories are not sufficient to capture the behavioral differences observed at the individual-level.

These differences were found to be related to several factors, such as the person's age, gender and previous earthquake experience, and the intensity of the earthquake. However, no universal rules can be defined as some findings were contradictory between different studies. The differences in the observations could be related to the cultural context, which was found to influence risk perception and response.

Therefore, in order to model the human response to an earthquake in a society of interest, the best approach would be to analyze, within the same culture, the behaviors adopted during events that are relatively similar to the event modeled.

## 2.5. APPROACHES FOR MODELING HUMAN BEHAVIORS IN EARTHQUAKES

Modeling human behaviors in an earthquake, especially evacuation behavior, is critical for the improving emergency management plans. Indeed, evacuation simulations can help determining the fastest routes, or the nearest safe areas for people to seek shelter, in order to make evacuations faster and safer. The simulations results can help identify and anticipate the possible challenges (Gaire et al., 2018). Modeling pedestrian evacuation is particularly important for emergency evacuation because traveling by car in the aftermath of an earthquake can be compromised by the presence of debris on the roads, whereas pedestrians have more flexibility in their path choice (Bolton, 2007).

Pedestrian evacuation, defined as travel on foot either by walking or running from dangerous areas to safe areas, can be modeled through different approaches, such as fluid-dynamic models, cellular automata and agent-based models (Zheng et al., 2009). In fluid-dynamic models, pedestrian crowds are assimilated to behave like fluids or gases, based on several analogies between fluid dynamics and medium to high density crowds (Helbing et al., 2002; Hughes, 2003). In fluid-dynamic models, the crowd is modeled as one entity, the fluid, and the pedestrians are modeled as particles in this fluid. Although this approach is suitable for dense crowds, it is not applicable for individual behaviors and mobility.

Cellular automata models are made of a collection of cells on a regular grid, in which the state of each cell can evolve at each time step according to a set of rules and based on the states of the neighboring cells (Wolfram, 1983). Cellular automata have been applied to model evacuation behaviors, especially in building evacuations (evacuation from a floor). For instance, cellular automata were used for simulating an evacuation from a room during an earthquake and to estimate the resulting casualties (Li et al., 2018). Cellular automata are more adapted than fluid-dynamics for modeling individual behaviors of pedestrians; however, their limitation is the homogeneous nature and size of cells used to discretize the space (Battezzorre et al., 2021).

Agent-based models (ABMs) are computational models that model a system as a collection of autonomous entities, called agents that are defined in terms of their attributes and behaviors (Ferber and Weiss, 1999). Agents are able to operate without direct human intervention and are capable of perceiving and responding to their environment (Wooldridge and Jennings, 1995). ABMs have proven to be a powerful tool for modeling and understanding phenomena in several fields such as economics, health care and social sciences (Kravari and Bassiliades, 2015). ABMs have been widely used in the simulation of emergency evacuations (Daudé et al., 2019; Manley, 2012; Pan et al., 2007; Zia et al., 2013). This is particularly due to the ABMs' ability to represent the heterogeneity of social agents at the individual level and the emergent phenomena that result from the interactions among individuals, and between the individuals and their environment (Bonabeau, 2002). An important advantage of ABMs is also their capability to include individual-decision making and social behaviors of individuals and groups (Cimellaro et al., 2017).

Although the use of agent-based modeling is not common in the earthquake engineering community, the important role of ABMs for the improvement of earthquake emergency management plans has been emphasized (Hori, 2011). The literature is not very rich in ABMs for the simulation of individual behaviors in earthquakes scenarios. Most of the models focused on modeling indoor room or building evacuations (Cimellaro et al., 2017; Li et al., 2018; Xiao et al., 2016). Only few studies have developed ABMs for modeling pedestrians' earthquake evacuation at the urban scale (outdoor mobility). In general, these models include the building damages, the debris generated from the building damages, and usually individuals have at least one behavior: going to a safe area or to an emergency shelter.

We have considered that in order for a model to be useful for improving emergency management it has to show some level of realism, by this we mean:

- integrating realistic human behaviors;
- integrating realistic estimates of the seismic consequences on the urban environment: the building damages and debris;

- estimating the earthquake casualties: the injuries and fatalities;
- analyzing the capacities of the urban resources needed for emergency management.

The models do not necessarily have to fulfill all of these criteria, but at least some level of realism is desirable. Most of the models found in the literature did not show enough realism. In Hashemi and Alesheikh (2013), pedestrian evacuation was modeled in an urban area after an earthquake. However, the model did not integrate any realistic behaviors as all agents move on the road network and go to a safe area. Beck et al. (2014) included realistic human behaviors derived from a questionnaire, and modeled social interactions such as leader followers-dynamics. However, the model did not integrate realistic estimations of buildings damages and debris. Torrens (2014) developed a model that included a highly-realistic graphical representation of the agents. Nevertheless, the model was poor on the calibration of human behaviors, damages and debris. Lu et al. (2019) developed a pedestrian evacuation model with a realistic estimation of the extent of debris around buildings and their influence on pedestrians' speed. However, the model did not include any realistic behaviors and was applied only on a small spatial scale.

In contrast, some advanced models in the literature have shown good levels of realism. They are: EPES (D'Orazio et al., 2014; Quagliarini et al., 2016; Zlateski et al., 2020), SOLACE (Bañgate, 2019; Bañgate et al., 2018, 2017) and IdealCity (Battezzozze et al., 2021), which are presented separately in the following sections.

### **2.5.1. EPES**

Earthquake Pedestrian Evacuation Simulation (EPES) (D'Orazio et al., 2014) models pedestrians' evacuation in an urban area based on behaviors derived from the analysis of earthquake evacuation videos.

In EPES, agents have a pre-movement phase, in which they are assumed to exchange information about the event and decide if they want to evacuate or not. The probability of evacuation of each agent is related to the earthquake's macroseismic intensity. Evacuation is assumed to take place at intensities greater than 5 (MMI), with an increasing probability of evacuation with increasing seismic intensities.

Regarding the agents that evacuate, they choose their paths in a way to go towards safe areas while avoiding collisions with obstacles and other people. Furthermore, groups of agents can form and therefore share bonds that maintain the group's cohesion. These groups also attract agents that are travelling individually.

In EPES, the probable damage grade of each building is calculated as a function of the macroseismic intensity and the building's vulnerability by adopting the damage probability matrix approach. Although the debris formation rules were roughly estimated in the first version of the model, the authors refined their ruin formation algorithm (Quagliarini et al., 2016; Santarelli et al., 2018), which was included in a recent application of EPES (Zlateski et al., 2020). Furthermore, the evaluation of the urban area's shelter capacity in post-earthquake environment was also recently implemented (Zlateski et al., 2020). However, EPES does not integrate the injuries and fatalities that might result from the interactions between the individuals and their environment.

EPES was implemented as a Java simulation tool using a single-thread execution. It was applied to the historical city-center of Coimbra, Portugal, where only 1200 person agents were simulated (Zlateski et al., 2020). The authors justified that the limited area and number of agents that were simulated were due to their limited computational resources.

To summarize, EPES integrates realistic simulations of building damages and ruin formation. Regarding behaviors, although linking the evacuation probability to the seismic intensity is a good idea, it could be improved by calibrating the probabilities using realistic estimates rather than hypothesis. Moreover, EPES assumes that all pedestrians who evacuate go to a safe area, which does not correspond to observations of people going to unsafe areas such as one's home. Finally, casualty estimations could be added to the model to make it more realistic.

### 2.5.2. SOLACE

SOLACE (Bañgate, 2019; Bañgate et al., 2018, 2017) is a model for simulating human behaviors in an earthquake that is explicitly based on the social attachment theory. In SOLACE, social interactions are modeled at the microscopic level by integrating the agents' perception and attachment bonds.

Social agents in SOLACE have cognitive abilities, implemented with the Belief-Desire-Intention (BDI) approach (Rao and Georgeff, 1995). When the earthquake occurs, agents can choose to perform one or many actions, such as searching for information and seeking shelter under furniture. Then, depending on the actions chosen, evacuation from buildings may take place or not. If the agent decides to evacuate, it leaves the building after a certain amount of time, which depends on the different pre-evacuation actions undertaken by the agent.

The agents' motion in the urban environment is guided by the perception and the strength of bonds. Agents have target locations, which can be either roads or safe areas; however, if they perceive an attachment figure, such as a family member, a colleague or a friend, they change their heading and move towards this attachment figure before continuing towards their target.

SOLACE also represents the crisis environment using geographic data, and models different seismic intensity levels and the resulting building damage and ruins. SOLACE also includes casualties resulting from an earthquake. However, the algorithms for the estimation of the buildings damages, debris and casualties are not calibrated with physics-based rules commonly used in seismic risk assessment methodologies, but rather with hypothetical estimates.

SOLACE was implemented in the GAMA platform (Taillandier et al., 2018). Although some simulations in SOLACE covered the whole extent of the city of Grenoble, France (composed of 69 administrative divisions, or IRIS), the majority of the simulations were performed on small (2 IRIS) or moderate (6 IRIS) spatial scales due to the hardware limitations and the excessive resources needed to run the simulations at the full spatial scale (Bañgate, 2019). The simulations have focused on the number of people arriving to safe areas and the time taken to arrive to safe areas under different scenarios. However, the capacities of the safe areas were not investigated.

Overall, SOLACE includes very sophisticated and realistic decision-making and navigation algorithms. However, it should be calibrated with realistic damages, debris and casualties estimation approaches to be accepted by the earthquake-engineering community.

### 2.5.3. IdealCity

IdealCity (Battagazzorre et al., 2021) is a hybrid model for human behaviors during earthquake evacuation at an urban scale. It is composed of a module for buildings damage assessment coupled with an ABM for the simulation of pedestrians' evacuation. IdealCity includes also the transportation network, used for the navigation of ambulances.

In IdealCity, the building damage assessment module provides calibrated estimates of building damages for a seismic event, the resulting debris and their impact on roads. Additionally, IdealCity models different injury states of individuals based on statistical distributions associated to the damage state of the buildings and the agent's proximity to debris.

The human behaviors implemented in IdealCity are the following: all the agents start exiting from buildings when the earthquake occurs. When outside of a building, an agent can decide to stay within the vicinity of the building go to an emergency shelter or to a hospital. The choice of destination depends on the agent's injury level and on the damage state of the building. Seriously injured individuals stay in place and wait to be rescued by ambulance.

When running simulations using IdealCity, the occupancy rates of emergency shelters and hospitals are continuously updated. If individuals reach a saturated target destination (shelter or hospital), they are redirected to the closest target destination of the same type that still can accept people. Due to this option, IdealCity offers quantitative measures that can be used by decision-makers for resource planning.

IdealCity was implemented in the 3D game engine Unity<sup>2</sup> and was tested on the city of Turin in Italy for different scenarios. Although these simulations included around 600,000 agents, they ran in near-real time on a standard PC. Nevertheless, the efficient simulation times could be due to the simplified agents behaviors because in the current version of IdealCity the complexity of group dynamics or leader-follower behaviors are not integrated.

In summary, IdealCity’s ability to simulate hundreds of thousands of social agents and run in nearly real-time represents a technological advancement for ABMs. Moreover, the post-seismic urban modifications are also well calibrated. Furthermore, the model has an operational output due to the tracking available resources. However, the model could be refined to include more realistic human behaviors, preferably calibrated to the context of the case-study.

#### 2.5.4. Summary

Several approaches exist for modeling human behaviors in earthquake. ABMs’ ability to recreate interactions between heterogeneous agents at the micro-scale, make them suitable for integrated seismic risk modeling including human behavior.

The review of the most-advanced ABMs for the simulation of pedestrian evacuation in earthquake scenarios is summarized in Table 2-5.

Table 2-5: Complexity level included in the most advanced ABMs for the simulation of pedestrians’ earthquake evacuation

Model	Human behavior	Buildings damages and debris	Casualty estimation	Focus on the urban resources
EPES	Based on the analysis of video recordings	Realistic	Not included	Yes, capacities of emergency shelters
SOLACE	Based on social attachment theory	Included but not realistic	Included but not realistic	No
IdealCity	Not calibrated	Realistic	Realistic	Yes, capacity of hospitals and emergency shelters

Several limitations were found in the reviewed models, either on the integration of realistic human behaviors, or on the estimations of the earthquake damages, debris and casualties. However, the main limitation faced by the highly-complex ABMs is the difficulty to simulate large spatial areas with a high number of agents capable of performing complex behaviors. EPES was only used on a relatively small historical city center and the spatial scale for the simulations in SOLACE had to be reduced due to the extensive computational resources needed to simulate the whole city of Grenoble. IdealCity showed promising capabilities for the simulation at the city-scale with an impressive number of agents. Nevertheless, it should be tested with more complex behaviors to validate the efficiency of the simulations.

In this study, we aim to develop an ABM for modeling seismic crisis occurring in an urban area, while taking into account human behaviors, calibrated to the context of the study area. The model also integrates realistic estimates of debris, damages and casualties, and focuses on the capacities of the urban open spaces. The study area chosen for the application of the methodological framework is the city of Beirut, the capital of Lebanon. The study area is presented in the next section.

## 2.6. STUDY AREA: BEIRUT, LEBANON

Beirut was chosen as the study area due its interesting context. Beirut is surrounded by a system of faults that have historically caused devastating earthquakes. Although Beirut did not witness any major earthquakes in the last couple of decades, the dense urbanization and the recent and partial and recent

<sup>2</sup> <https://unity.com/fr>

implementation of the seismic building code (decrees number 14293 (2005) and 7964 (2012)) considerably increase the seismic risk in the city.

Moreover, this thesis is a part of a bigger framework of previous and on-going collaborations between French and Lebanese research institutions. Particularly, a previous French-Lebanese multidisciplinary project, the ANR-LIBRIS project (2010-2014), analyzed several aspects of the seismic risk in Beirut through the investigation of soil, buildings and social responses to earthquakes. The data derived from ANR-LIBRIS constitute the building blocks of this thesis; nevertheless, missing and incomplete data were further elaborated in this study.

Furthermore, this thesis is part of an ongoing project with Lebanese institutions in the framework of the AUF-PCSI<sup>3</sup> (2019-2022) around modeling human behaviors in earthquakes and the mobility constraints of pedestrians in Beirut.

In the following sections, we will describe the seismic context in Lebanon, the urbanization history of Beirut, along with findings from previous works on seismic risk and social vulnerability in Beirut.

### **2.6.1. Seismic hazard context in Lebanon**

Lebanon is a Middle Eastern country situated on the 1200 km long Levant Fault System that stretches from the Gulf of Aqaba to Turkey (Figure 2-7). In Lebanon, the Levant Fault splits into 4 main ramifications: the three left-lateral strike slip faults: the Yammouneh, Roum and Serghaya-Rachaya faults, and the recently discovered Mount-Lebanon Thrust (Daeron et al., 2007; Elias et al., 2007; Huijer et al., 2016; Walley, 1988). Lebanon and its surroundings have been struck by several strong earthquakes that have caused massive destruction and a high number of fatalities (Khair et al., 2000). The most devastating earthquake in Lebanon was the 551 A.D. earthquake (moment magnitude,  $M_w \sim 7.5$ ) attributed to a rupture on the Mount-Lebanon Thrust (Elias et al., 2007). The rupture of the Yammouneh fault in 1202 has also been documented to have caused wide-scale destruction in the Mediterranean region (Daeron et al., 2007; Ellenblum et al., 1998). The double-shock of the 16 March 1956 ( $M_w=6.1$ ,  $M_w=6.3$ ), was attributed to a rupture on the Roum Fault (Nemer and Meghraoui, 2006) and was the most recent high-magnitude earthquake to affect Lebanon. It killed 136 people, destroyed 6000 houses and damaged 17000 others (Harajli et al., 2002).

Given the slip rates of the faults in Lebanon and the time since the occurrence of major seismic events, it has been estimated that large destructive earthquakes, similar to the historical ones, are likely to occur in the coming century in Lebanon (Daeron et al., 2007).

The seismic hazard in Lebanon has been the subject of several probabilistic seismic hazard assessment studies (Arango and Lubkowski, 2012; Harajli et al., 2002; Huijer et al., 2016, 2011). In the most recent study, which took into account the relatively new discovery of the Mount Lebanon Thrust, the seismic hazard in Lebanon was qualified as moderate to high, with a 10% probability that the Peak Ground Acceleration (PGA) exceeds 0.2 to 0.3g in 50 years. The Mount Lebanon Thrust was found to have a high impact on the hazard of the coastal cities (such as Beirut, Saida and Tripoli). It was also suggested that the local building code should raise the reference PGA for the design of structures to 0.3 g (from the value of 0.25 g prescribed in the code) in the coastal area, including Beirut (Huijer et al., 2016).

Despite the high seismic hazard in Beirut, the urban landscape has few to no green spaces, with buildings constructed in disregard of the earthquake risk. This observation was explained by the absence of seismic disasters in the city's recent, albeit eventful, history (Pico and Amat, 2006). The seismic risk in Beirut in addition to the local geological and urbanization contexts are presented in the next section.

---

<sup>3</sup> Agence Universitaire de la Francophonie- Projets de Coopération Scientifiques Inter universitaires - PCSI

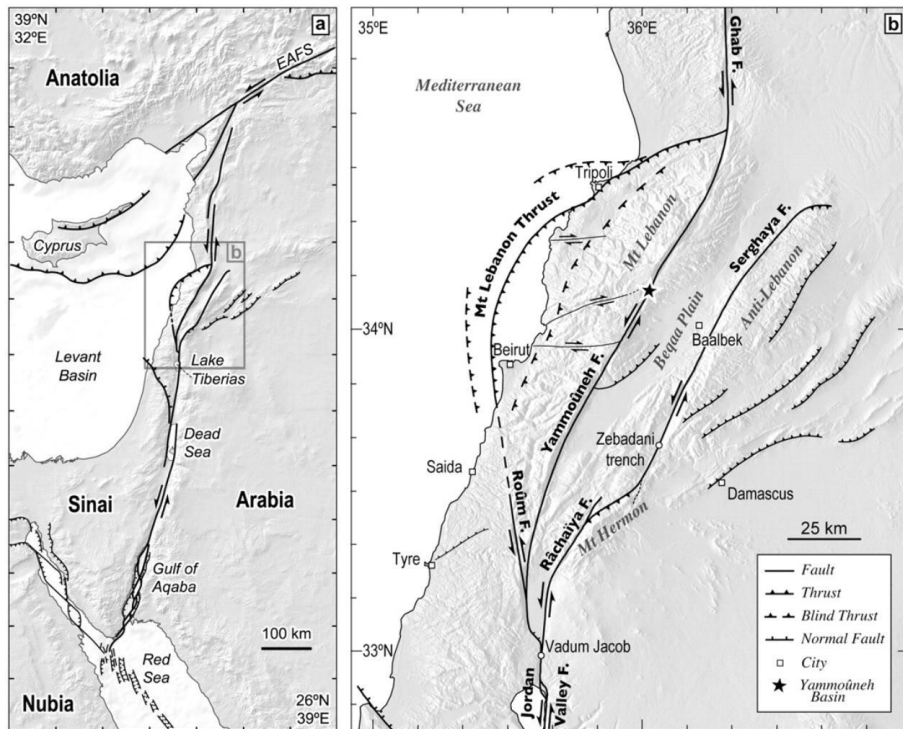


Figure 2-7: Regional tectonic setting. (a) Map of the Levant fault system. (b) Zoomed view on the active faults in Lebanon. Source: (Daeron et al., 2007)

### 2.6.2. Beirut: geological, urbanization and seismic risk contexts

Beirut is a coastal city at high seismic hazard. The definition of Beirut's borders remains somewhat confusing due to the necessary distinction between Municipal Beirut and Greater Beirut areas. Municipal Beirut refers to the municipality of Beirut, which also has the status of a governorate (Figure 2-8). Greater Beirut designates Municipal Beirut and its surrounding suburbs as it can be seen in Figure 2-9. The borders of Greater Beirut are roughly estimated as it does not refer to an actual administrative unit (Yassin, 2012).



Figure 2-8: Satellite view of Beirut. The red line delimits the limits of Municipal Beirut. (Sources: Beirut boundary: OpenstreetMap; basemap: Google Satellite)



Figure 2-9: Location of Municipal Beirut and Greater Beirut. Modified from Faour and Mhawej, 2014.

In this study, we have focused on Municipal Beirut, which we will simply refer to as Beirut in this manuscript. Beirut has a surface area of nearly 20 km<sup>2</sup>.

In the following subsections, we will present the geological, urban and seismic risk context in Beirut.

### 2.6.2.1. Geological context

The complex tectonic setting of Lebanon has resulted in a complex geology in the country and in Beirut specifically (Clark and BouDagher-Fadel, 2020). On the geologic map of Beirut, displayed in Figure 2-10, it appears that Beirut features an irregular relief, characterized by a Miocene hill in Ashrafiieh in the East and a Cenomanian hill in Ras Beirut in the West. These hills are mostly made of marly limestone. A sandy Quaternary cover extends from the lower parts of the hills towards the south east of Beirut.

This heterogeneity of the geology in Beirut has a direct consequence on seismic ground motion, recorded at the surface of the soil. This is due to the important role of the site effects (soft soils, topography, etc.) that can amplify seismic waves (e.g. Kawase, 2003; Sanchez-Sesma, 1987). The ground motion amplification due to site effects and soil resonance properties in Beirut were assessed through ambient noise recordings performed in the framework of the ANR-LIBRIS (Brax et al., 2018; Salameh et al., 2017; Salloum et al., 2014).

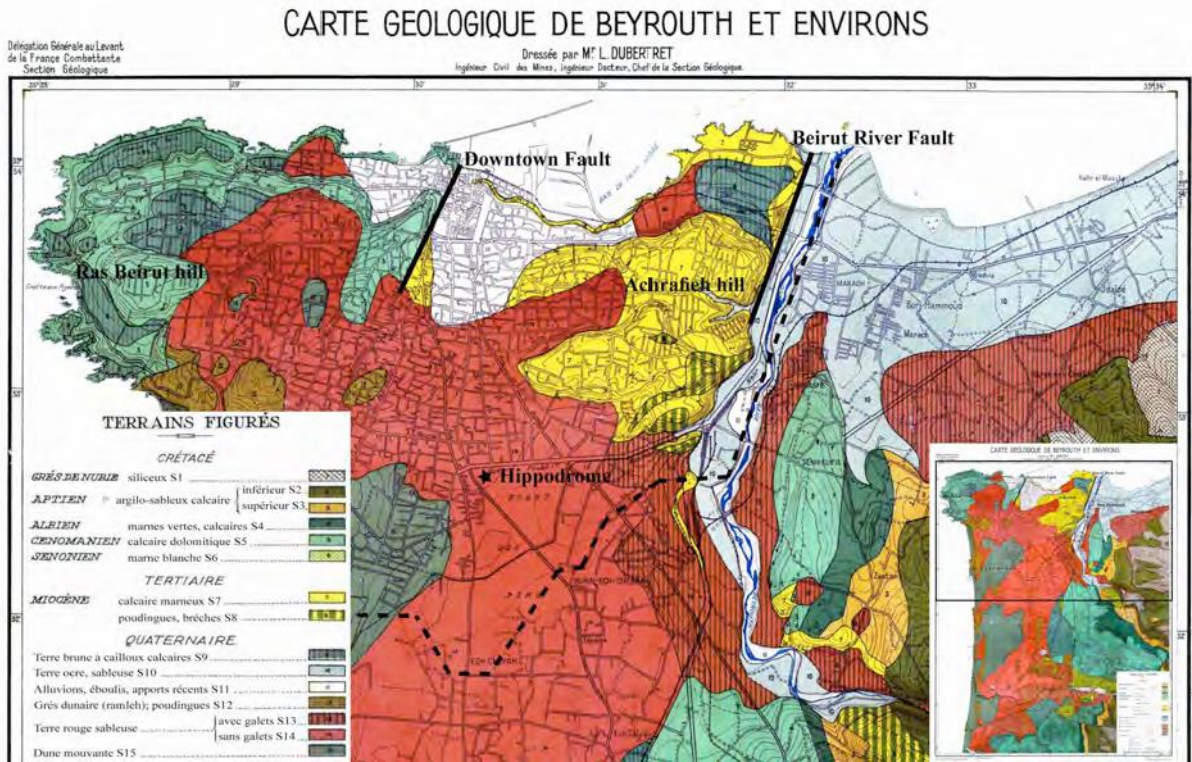


Figure 2-10: Geological map of Beirut with layouts of Beirut faults (continuous lines) and limits of Beirut (dashed lines).  
Source: (Brax et al., 2014) modified from (Dubertret, 1945)

### 2.6.2.2. Urbanization context

Beirut nowadays has a very dense and heterogeneous urbanization (Figure 2-11). The urban scene in Beirut is a result of a fragmented history of external occupations, and a modern era marked by a destruction/reconstruction pattern that emerged after the civil war (1975-1990). In this section, the growth of Beirut is presented from a historical perspective to illustrate how the different phases in history shaped the urban form, and directly affected the city's physical vulnerability and seismic risk. The historical time-line is given by Yassin (2012).



Figure 2-11: A view of Beirut's skyline from the southeast to the northeast. Source: (Kanafani, 2016)

The pre-modern golden period of Beirut (called Berytus back then) was during the Roman times, around the first century AD, with a peak in prosperity witnessed in the 4<sup>th</sup> century AD, before it was wiped out due to the 551 earthquake. Little is known about the history of Beirut between the 7<sup>th</sup> and the 12<sup>th</sup> centuries, except that in around 1100 AD the Crusaders took control of the city, which was under Islamic control at that time, and fortified it with walls and a castle. The Memluks re-controlled Beirut in 1291 AD, but during their reign the city did not see much prosperity (1291 - 1516). The Ottomans took over Beirut in 1516, which resulted in a slow growth until the 1840s, however still, at that time Beirut's economic and political significance was rather limited.

According to Yassin (2012), starting from the second half of the 19<sup>th</sup> century, Beirut played a “magnet” role, hosting most of Lebanon's cultural and economic activities. The attractiveness of Beirut resulted in several waves of newcomers, either migrants from peripheral areas of Lebanon, or refugees from neighboring countries.

Beirut's growth from 1850 went through five urban transformation phases (Figure 2-12), each influenced by an interplay of global and local events, summarized below.

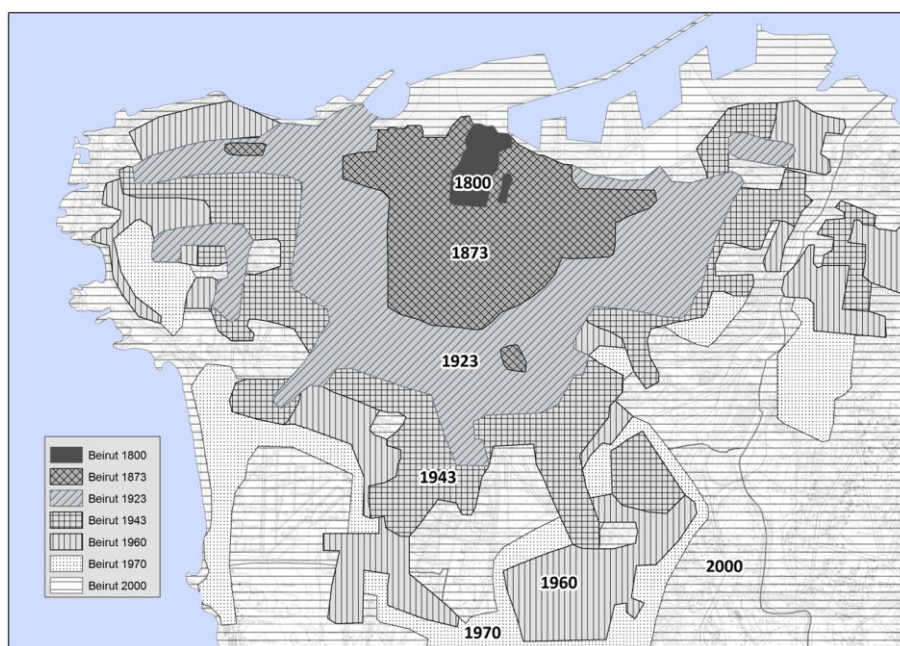


Figure 2-12: Phases of Beirut's urban growth. Source: Yassin (2012)

*Phase 1: 1850–1920: the growth of cosmopolitan Beirut as a gateway to the Levant*

The change in the administrative policies of the Ottoman Empire gave the provinces more roles in governing their affairs. These changes resulted in a flourishing trade from inland Syria towards Europe through the port of Beirut. Beirut became the gateway to the Levant.

This period witnessed the first expansion of Beirut beyond its medieval walls. It was estimated that between 1841 and 1876 the city's surface area increased 15 times (Davie, 2006). By the early 20th century, Beirut had expanded even further from the medieval walls. The growth pattern in this phase followed a semi-circular pattern around the old town with more affluent residents migrating to the suburbs.

*Phase 2: 1920–1958: French mandate and early independence*

After the end of the First World War, Lebanon was under the French mandate. The infrastructures and constructions in Beirut continued to grow in this period. Concrete became commonly used for the constructions instead of sandstone (Salameh, 2016).

The same trends promoting Beirut as a service and commerce center continued in the first post-independence presidential terms (1943-1952 and 1952-1958). However, a “laissez-faire” approach was

adopted towards the management of the economic and social spheres, including the urban planning. Beirut grew further in the east, northeast and south.

This phase also was marked by the arrivals of various displaced populations such as Armenians and Palestinians who settled at the edge of Beirut's municipal borders.

*Phase 3: 1958–1975: rapid urbanization, urban sprawl and the misery belt*

From the late 1950s until the mid 1970s, Beirut proclaimed its role as a Middle Eastern hub of service economy with more than two-thirds of the economic activity of Lebanon, and most governmental and educational institutions in Beirut. Beirut was becoming a city-state that accommodated half of the country's population. A rapid-rate migration from Lebanon's rural areas to the city resulted in a massive suburbanization all around the capital in order to accommodate the population's growth.

This phase also witnessed the sprawl of unregulated settlements in Beirut, especially in the east and the south of the city, which accommodated refugees and the Lebanese working class. These settlements were referred to as the "misery belt", employed to describe their degraded environmental and sanitary conditions, in addition to the high population density and poverty.

*Phase 4: 1975–1990: violent urbanization and civil war*

The Lebanese civil war emerged in 1975 with unprecedented violence creating a segregation in the urban space: the city was divided into a "Christian-controlled" East and a "Muslim-controlled" West, with physical barriers demarcating the separation line. This division lasted until the end of the war in 1990. The period was marked by heavy damages and destruction to buildings and infrastructure.

*Phase 5: 1991–now: post-war urban reconstruction and neoliberal peace*

After the war ended, the physical barriers separating the East from the West were removed. Beirut's population was able to move freely in the city. The plan for the post-war reconstruction was influenced by a "neoliberal peace model", which assumed that the sustainment of peace and prosperity would be linked to the liberal world system and economic growth. This plan focused on the reconstruction of the old center. It was transformed from a commercial and business center, based on local and regional trade, to an exclusive residential, commercial and financial center (Davie, 1993).

The reconstruction of the city center initiated Beirut's most recent urban renewal, which boomed from the mid-1990s until 2010 (Kanafani, 2016). The city witnessed a pattern of land sale/purchase, demolition, agglomeration of small adjacent plots for the construction of (mostly) high-end residential blocks. These practices were regulated by construction laws that authorized the increase in the exploitation ratio of plots, the increase of buildings heights and the agglomeration of adjacent land parcels (Kanafani, 2016). As a result, old houses were demolished to give place to giant towers, increasing further the heterogeneity of the urban fabric (Figure 2-13).

The building code for seismic regulation was first introduced in 2005, specifying the horizontal seismic acceleration for the design of buildings (the PGA) at 0.2 g. This code exempted the constructions of less than 10 m height from any seismic requirements. Another decree was issued in 2012, increasing the reference acceleration for the design to 0.25 g. Nevertheless, the application of the issued codes was very limited and the construction practices were still poorly supervised (Salameh, 2016).

The urbanization history of Beirut has a direct impact on its physical vulnerability and seismic risk. This is further explained in the next section.



*Figure 2-13: Heterogeneity of the urban fabric in Beirut (Achrafieh district) highlighted by a traditional masonry house in the first plan, residential buildings in the second plan and “modern” skyscrapers in the third plan. Source: unknown*

### **2.6.2.3. Seismic risk context and first attempt to evaluate it**

The construction materials and building practices in Beirut were directly influenced by the city’s history. However, one of the major challenges to the evaluation of the physical vulnerability in Beirut is the lack of complete and accessible data about the built environment.

In order to overcome this limitation, field investigations were done in the framework of the ANR-LIBRIS project. Due to political and security constraints during the time of the study, the buildings investigations were restricted to the eastern and western areas of Beirut, leaving a data void in the middle of the city. Nevertheless, the constructions periods and number of floors were collected for 7692 buildings.

To assess the vulnerability of the building stock, the quality of the construction materials and the limitations on the building and story heights were evaluated throughout the different phases of the urban evolution (Table 2-6) (Salameh, 2016). Then, according to the building heights and the construction period, the vulnerability of each building - related to the construction material - was qualified. The buildings were categorized as masonry (28% of the building stock), non-designed reinforced concrete (66% of the building stock) and reinforced concrete with low ductility (6% of the building stock).

Once the buildings’ vulnerability was assessed, the seismic risk in Beirut was evaluated by estimating the damages to the buildings for different seismic scenarios (Salameh et al., 2017). Figure 2-14 shows one of the damage increment maps for a scenario of  $PGA= 0.25\text{ g}$ . The damage increment refers to the difference in damage between soil and rock conditions, and outlines the importance of site effects on the damage distribution in Beirut. Due to the lack of information about the buildings in the central area of Beirut, the seismic risk could not be estimated for the whole city. Therefore, a first step towards the assessment of the seismic risk at the scale of Beirut would be to collect a complete building database with the information on the building’s vulnerability.

In addition to the building’s physical vulnerability, the social vulnerability of Beirut residents’ was also assessed in previous studies.

Table 2-6 : Evolution of the quality of the construction materials and height limitations throughout the urban evolution of Beirut. Source: Salameh (2016)

Construction Period	Construction Material					Height	
	Type construction material	Assumed quality of cement	Assumed quality of Sand	Assumed quality of Steel	Water/Cement dosage	Height limitation	Average Height per floor
Prior 1950, French mandate (Ruppert 1969)	Sandstone or Mixed : Sandstone/ Reif. Concrete	Good	Good		Manual	26 m	Approx. 5 m for ground floor, 4 m per floor
1950-1970, after WWII (Ruppert 1969)	Reinforced Concrete	Good	Good		Manual	1954: Suppression in certain cases of height limitation. Beginning of column floor	Approx. 3m25
1970-1975	Reinforced Concrete	Good	Good		Automatic	1970: Exemption of limitation for "big group structures"	Approx. 3m25
1975-1980	Reinforced Concrete	Probably Bad	Probably Bad		Automatic		Approx. 3m25
1980-1990	Reinforced Concrete	Probably Bad	Probably Bad	Often Bad, Problems at import	Automatic	1990-1997 : Possibility of increasing one floor ("Floor el-Murr")	Approx. 3m25
1990-2005	Reinforced Concrete	Good	Medium	Good	Automatic		Approx. 3m25
Post 2005	Reinforced Concrete	Good	Medium	Good	Automatic	Lebanese Seismic Code application	Approx. 3m25

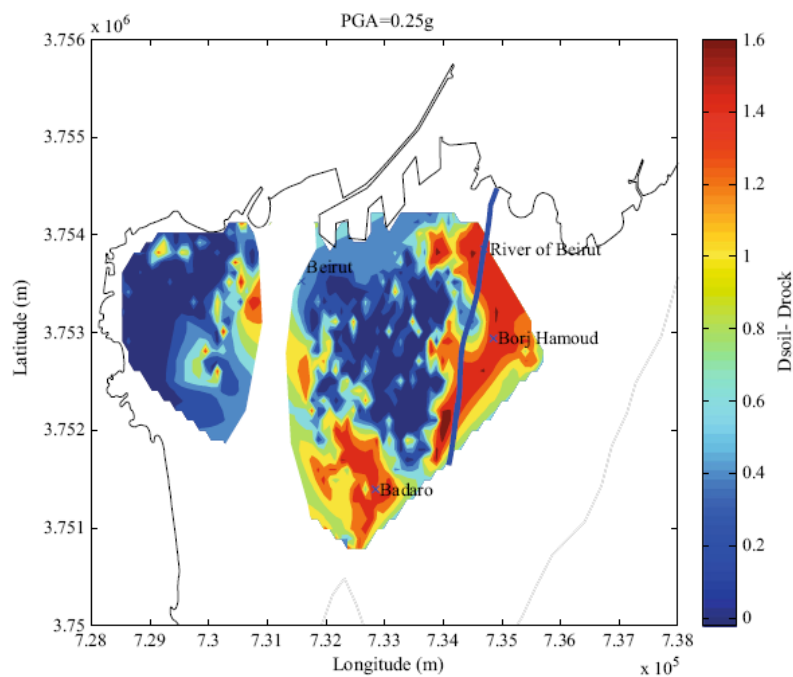


Figure 2-14: Interpolated map of the damage increment in Beirut and a part of its eastern suburbs for an earthquake of  $PGA=0.25\text{ g}$ . The damages are shown in terms of incremental damage between soil and rock to highlight the effects of the soil conditions on the buildings damages. White zones in the middle of Beirut correspond to areas with missing building data. Source: Salameh et al. (2017).

### 2.6.3. Beirut's social vulnerability context

Very few information exist about the population in Beirut (Verdeil and Dewailly, 2019). The last census conducted in Lebanon dates from 1932, and despite estimation efforts based on extrapolation of household surveys, accurate data about the residents of Lebanon is still a big challenge due to difficulties in accounting for the immigration of the Lebanese population and the installation of foreign nationals in Lebanon (Verdeil et al., 2006).

The latest household survey undertaken by the Central Administration of Statistics in Lebanon (CAS) (CAS, 2020) estimated the population of Beirut at around 342 000 residents, distributed in 100 000 households. Regarding gender, it was estimated that the 54% of the population are women, while 46% are men. The age groups were distributed as follows: 19% less than 14 years old, 15% between 15 and 24 years old, 23% between 25 and 39 years, 27% between 40 and 64, while 16% of the population is aged above 65 (Figure 2-15).

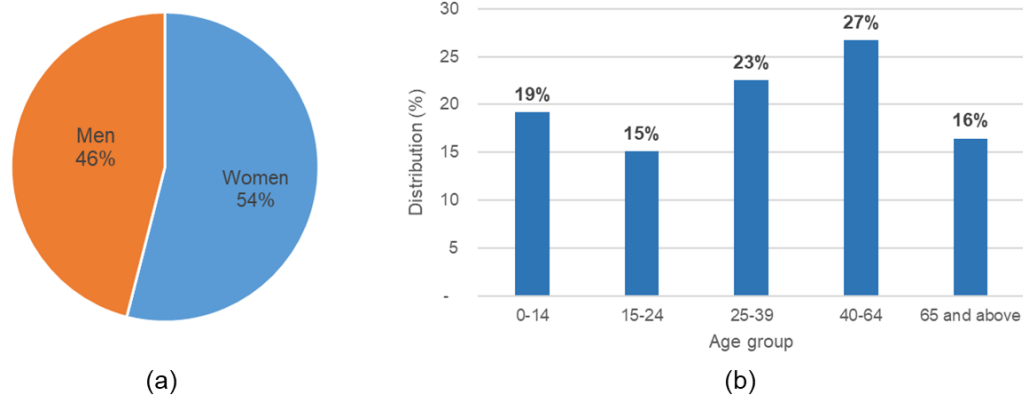


Figure 2-15: Demographic characteristics of the population in Beirut. (a) Gender distribution, (b) Age distribution. Data from: (CAS, 2020)

The social vulnerability of Beirut's residents was evaluated in previous studies through a survey that questioned the population's perception and knowledge about the seismic hazard, their behaviors in previous earthquakes and their protection strategies for future earthquakes. This survey was administrated to the residents of the Sanayeh and Sioufi districts in Beirut (176 respondents) (Beck et al., 2018), and to the residents of Bourj Hamoud (31 respondents), a suburban area outside of Municipal Beirut (Cartier et al., 2017).

The study of Beck et al. (2018) revealed that more than half of the survey respondents were aware of the seismic hazard. When asked about the origins of an earthquake, 67% believed that an earthquake's origin is tectonic, while more than quarter of the sample (26.7%) related it to a divine dimension. The factors that exacerbate the social vulnerability of individuals were found to be the age (the older are more vulnerable than the younger) and educational attainment (the higher the educational level, the lower the person's vulnerability).

Concerning behaviors adopted in previous earthquakes, 137 respondents had previously experienced earthquakes in Beirut, however only 24% of them adopted mobility behaviors (tried to go somewhere). Nevertheless, stronger felt tremors were related to a higher propensity for mobility.

The results of this survey should be treated with caution as it only focused on 2 districts of Beirut and might not be representative of the total Beirut population. Additionally, the relatively small size of the sample makes it difficult to generalize behavioral responses to earthquakes in Beirut.

## 2.7. CONCLUSION

In this chapter, we have seen that disaster studies are a common interest in both earth-sciences and social sciences disciplines. However, each discipline proposes its own interpretation of terms such as vulnerability or risk, depending on whether the interest is on the physical system or the social system. One of the challenges of communicating effectively in an inter-disciplinary environment is the myriad of definitions available to define each term. An effort to promote interdisciplinary studies was undertaken by the United Nations that proposed a glossary in which the terms were defined in a generic way, without losing the meaning behind the term. However, the definitions of vulnerability and risk in this glossary did not sufficiently highlight the importance of behaviors on vulnerability and risk. Consequently, we have proposed modified definitions for these two terms.

When it comes to seismic risk studies, although in the last 25 years few approaches have been developed for including factors related to the social vulnerability and the emergency management into classical seismic risk assessment studies, the proposed “integrated” approaches were centered on the physical systems, and considered the social factors as aggravating effects. Additionally, the effectiveness of these studies is somewhat limited since they do not consider dynamic effects, such as human behaviors that may increase or decrease exposure to hazards, or the difficulties of access to safety shelters or hospitals due to streets blocked by debris.

Human responses to earthquakes are indeed complex. Several factors affect how a person might respond to the sudden onset of an earthquake and these factors are highly context-dependent. The response depends on whether the person is alone or with a family member; at home or at work; Japanese or Mexican. The cultural context is particularly important as it can determine the way risk is perceived, what is thought to be the appropriate behavior and even gender roles and responsibilities.

Agent-based models (ABMs), in which each entity is modeled as an agent that has its own characteristics and behaviors, can facilitate the integration of human responses in seismic risk studies. ABMs for the simulation of dynamic earthquake crisis in urban environments have been developed; however, they had varying levels of realism and often limitations.

In this study, we develop an ABM for modeling seismic crisis occurring in an urban area, while integrating realistic human behaviors, calibrated to the context of the study area. The model also integrates realistic estimates of debris, damages and casualties. Although, the long-term goal of the model is to contribute to the definition of dynamic risk indices including human behaviors; in this thesis, we focus on people’s safety in the aftermath of an earthquake and the capacities of the urban open spaces.

Beirut is chosen as a study area, due its interesting context. Beirut is characterized by a moderate to high seismic hazard. The local geology makes the city prone to site effects, which further amplify the seismic ground motion. Moreover, the dense and heterogeneous urbanization, the physical and social vulnerabilities further exacerbate the seismic risk in the city. Previous works have provided elementary data for the seismic risk assessment Beirut; however, due to the difficulty of data collection in Lebanon the datasets were not complete.

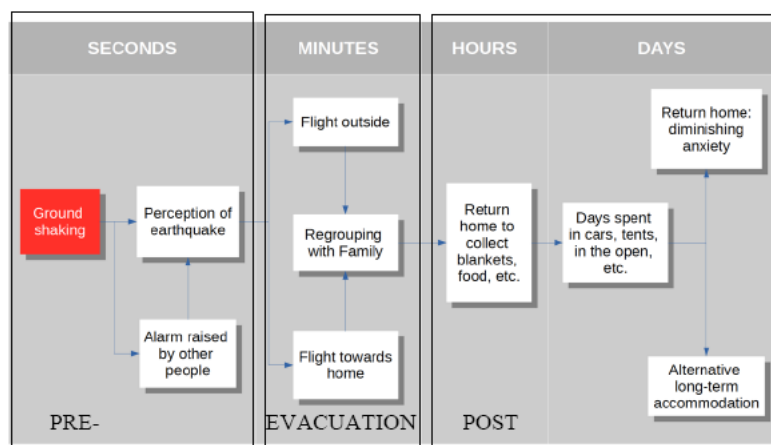
Having defined the context of the study, next chapter will present the ABM developed for the dynamic simulation of seismic crises in Beirut.

# Chapter 3: Pedestrian Evacuation in Earthquake Risk Simulations

## 3.1. INTRODUCTION

This chapter presents PEERS (Pedestrians' Evacuation in Earthquake Risk Simulations), an interdisciplinary ABM for the simulation of a seismic event occurring in an urban area, Beirut specifically, while integrating the behavioral responses of individuals to the earthquake. The behavioral adaptations of an individual vary according to the temporal context (Alexander, 1990). We can see in Figure 3-1 that the ground shaking usually lasts only for a few seconds (or tens of seconds depending on the earthquake magnitude). It takes a person a few additional seconds to perceive the earthquake, or alternatively be alarmed about it from other people. This stage is called the pre-evacuation stage, in which the critical decision to evacuate is made. Once the evacuation takes place, the person adopts mobility behaviors to reach a place of interest (flight outside, regrouping with family and flight towards home), which usually takes place within minutes from the occurrence of the earthquake. The return to home, i.e. the post-evacuation stage, takes place usually after hours, once the threat of aftershocks has subsided and the buildings' inspection showed no visible serious structural damage. However, in the cases where the damages are severe or the building is totally collapsed, the individual seeks alternative long-term accommodation options.

In PEERS, we focus on the pre-evacuation and evacuation stages, as in these stages, the most critical decisions that can impact a person's safety are taken. Therefore, we simulate the evacuation behavior of individuals and their mobility in the urban area. In this context, we define evacuation as the action of exiting a building, and mobility as the movement of a person outdoors from one location to another. We focus on the first few minutes after the earthquake, since during this period, the information about the nature of the event and its consequences are still unknown to both the individuals experiencing it, and to the decision-makers in charge of coordinating the emergency response. Consequently, if inserted in an operational context, the simulations can offer a concrete approach to anticipate as realistically as possible the consequences of an earthquake occurring in the city and prepare the emergency response. Therefore, the simulations in PEERS start at the time of occurrence of the earthquake, and last until 15 minutes after the earthquake (real time).



Modified from Alexander, 1990

Figure 3-1: Temporal context of the behavioral responses to an earthquake. Source: Bañgate, 2019 modified from Alexander, 1990

PEERS, like any model, represents a simplification of reality (Box, 1976; de Leeuw, 1988). PEERS is based on a multi-model framework, recreating the interaction of three simple, but empirically and theoretically grounded models (Figure 3-2). PEERS combines a city model representing the spatial environment and the population, along with an earthquake model that represents the consequences of an

earthquake (damages, debris, casualties) in the urban environment. PEERS also integrates a human behavior and mobility model. This model recreates complex human behaviors, as well as pedestrians' mobility and constraints in an urban environment.

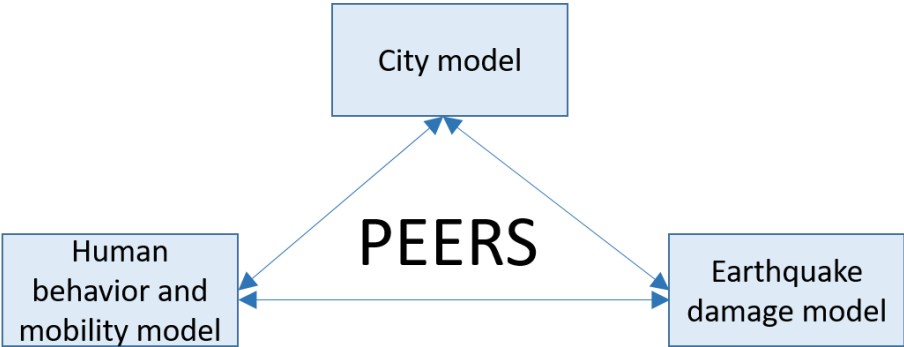


Figure 3-2: Multi-model framework in PEERS

In the following sections, the structuring models of PEERS are presented from the conceptual point of view. Then we present the formalization and validation of the conceptual model, before describing the implementation of PEERS in a simulation platform. The derivation of the data used for the calibration and simulations in PEERS is presented in Chapter 4 and Chapter 5.

**3.2.CITY MODEL**

The city model in PEERS aims to recreate as closely as possible the urban and social conditions in Beirut. The city model is composed of a geospatial model of the urban environment, coupled with a model of the residents and their social ties, which are presented in the following sub-sections.

**3.2.1. Model of the urban environment**

In PEERS, a realistic 3D model represents the urban form of Beirut. The representation of Beirut's urban environment is facilitated by the use of Geographic Information Systems (GIS), which represents each component of the spatial environment by a layer, as illustrated in Figure 3-3.



Figure 3-3: Illustration of an urban environment in PEERS

The city model includes the features of the urban environment that are relevant for the simulation of an earthquake in an urban environment, along with the human behaviors and mobility, namely:

(1) The boundary:

The boundary represents the limits of Municipal Beirut, therefore defining the spatial extent of the study area.

(2) The buildings:

The buildings of Beirut were included in the model of the urban environment for several purposes:

- a. Buildings are the urban assets that can be damaged when an earthquake occurs.
- b. Buildings have different uses depending on their functions, which are relevant for the population's spatial distribution at different times of the day. In PEERS, the buildings' functions are classified into 3 categories: residential, work and hospital.
- c. Residential buildings and hospitals can also be mobility destinations (this is discussed in section 3.4.2).
- d. Buildings also represent obstacles for the mobility of pedestrians as people should avoid buildings and move around them when navigating in the urban area.

(3) The open spaces:

By definition, urban open spaces are the undeveloped (free from built structures) sites in human settlements that can be freely accessed by the public (Gong et al., 2017; Villagra et al., 2014). In the event of an earthquake, people need a safe refuge space for taking shelter, which can be provided by the urban open spaces (Godschalk, 2003; Shrestha et al., 2018).

Therefore, we have represented the open spaces in Beirut in the urban environment model. However, in Beirut, some open spaces may be secured by gates and barriers and when the gates are locked these open spaces become inaccessible to the population, thus morphing from what should be considered a safe space into an obstacle for pedestrian mobility. The possibility of an open space being locked is also taken into consideration in PEERS. Additionally, we have considered that depending on its surface, each open space has a maximum number of people that it can accommodate in safe conditions. Therefore, although a person might arrive to an open space, if this open space has already reached its full capacity, the person will not be able to enter in this open space due to its overcrowded conditions.

(4) The slope:

The slope of the terrain was included in the model as it affects pedestrian movements: people exert an increased effort to travel an uphill slope and should move slowly to ensure their safety in steep downhill slopes, resulting in the reduction of their speed in both directions (Campbell et al., 2019).

(5) The barriers:

The barriers represent the obstacles that obstruct pedestrians' mobility. The barriers can be natural features of the terrain, such as cliffs or water bodies (rivers, lakes, etc.) or features of anthropic origins such as highways, bridges and tunnels.

### **3.2.2. Model of the residents and their social ties**

Effective emergency planning and response in the event of an earthquake requires having a good knowledge of the size and spatial distribution of the exposed population. Quantifying the dispersal of individuals in an urban environment is a complex problem as the population is not static: the population's size and spatial distribution shift dramatically between day and night as people migrate from residential units to places of work and commerce (McPherson and Brown, 2004). For simplification purposes, and due to the complexity of assessing the population's migration flow from and to Beirut during the day, PEERS integrates the residents of Beirut only, who are assumed to stay within the boundaries of the city during the simulation.

In addition to its size and spatial distribution, the PEERS' population is also characterized by social attributes related to the population's age, gender and household composition. These attributes were included because they are relevant to the decision-making (presented in section 3.4.2) and to the mobility of individuals (presented in section 3.4.5).

The model of the residents and their social ties is illustrated in Figure 3-4. Each person is characterized by an age (from 0 to 100) and a gender (Male or Female). Additionally, the social ties between the residents are represented by organizing the population into households. A household is composed of members who share the same living space and who have social ties. Each person is considered to belong to a household (one household only). Households may have different sizes; however, only one household member is designated as the head of the household, i.e., the person who has more decision-making power than others in the household and more control over the household's resources (Posel, 2001). The notion of the head of the household was introduced in PEERS due its prevalent use in household surveys in Lebanon (CAS, 2020). As the building stock in Beirut is composed mostly of apartment buildings and not individual houses, each household (and therefore its members) is considered to live in an apartment (one apartment only) in a residential building (one building only).

The dynamic spatial distribution of the residential population is accounted for by locating the population in residential units during the night. This is because we make the assumption that people don't have any work or outdoors activities at night-time. During the day, people may have different activities: work/ school/ leisure activities, and therefore some people will be at home whilst others will be in non-residential buildings or outdoors. A probabilistic approach was therefore used to distribute the population during the day.

The generation of the residents of Beirut and their grouping into households was handled by a synthetic population generation model, which is presented in Chapter 5.

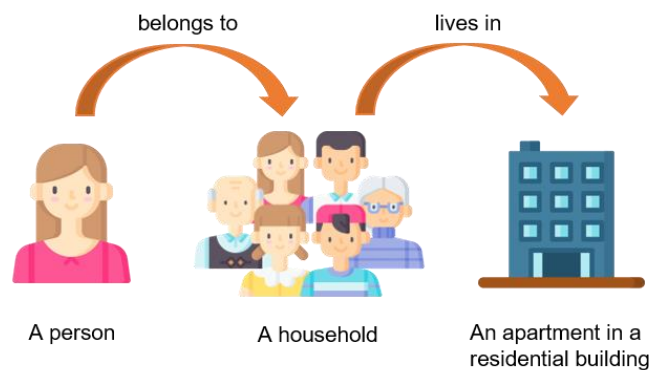


Figure 3-4: Model of the residents and their social ties in PEERS

### 3.3.EARTHQUAKE DAMAGE MODEL

The earthquake damage model represents the ground shaking and the effects that it has on the buildings. Namely, buildings could be damaged when an earthquake occurs, and debris might result from the building damages. Additionally, casualties may occur because of the damages in the environment. Therefore, the building's damage assessment is a fundamental element for modeling the impacts of an earthquake on the urban environment. The damage assessment is handled by a separate module. This module is presented in Chapter 4.

In PEERS the earthquake is represented by key indicators that describe the seismic scenario and its effects on the urban features and the population: the building damages, the generation of debris and the estimation of the casualties.

#### 3.3.1. Seismic scenario

The seismic scenario in PEERS is defined by:

- The strength of the shaking: Although a PGA-PGV (Peak Ground Velocity) couple is used to estimate the building damages (Chapter 4), for simplification purposes the strength of the shaking in PEERS is represented only by the PGA at outcropping rock, the maximum recorded acceleration during an earthquake (Douglas, 2003). We chose the PGA to represent the strength of the shaking since it is a commonly used metric in earthquake engineering for the design of earthquake-resistant buildings.
- The earthquake’s duration: which represents the duration of the ground shaking. The duration of the earthquake was included in PEERS because we considered that in an earthquake casualties occur due to falling objects and debris, which only happen while the ground is shaking. A duration of 20 s was assumed for earthquakes in PEERS.

### 3.3.2. Building damages

When an earthquake occurs, the buildings exposed to shaking may suffer from damages. A variability between the buildings damages in an urban area may be observed due to the spatial variability of the soil properties, as well as the variability of the building’s vulnerability. These considerations were taken into account in the damage assessment module, which is explained in Chapter 4. In PEERS, the buildings’ damages was included by representing the damage state of each building. The damage states were classified according to Lagomarsino and Giovinazzi, 2006, which offer a direct correspondence with the damage grades defined in the European Macroseismic Scale EMS-98 (Grünthal, 1998) as presented in Table 3-1.

Table 3-1: Damage states included in PEERS and their direct correspondence with the damage grades defined in the European Macroseismic scale EMS-98. (Adapted from: Lagomarsino and Giovinazzi, 2006, and Grünthal, 1998)

Damage state	EMS-98 Damage grade	Description for masonry buildings	Description for reinforced concrete buildings
None	-	No damage	No damage
Slight	Grade 1	Hair-line cracks in very few walls. Only small pieces of plaster fall. Fall of loose stones from upper parts of buildings in very few cases.	Fine cracks in plaster over the frames or in walls at the base. Fine cracks in partitions and infills
Moderate	Grade 2	Cracks in many walls. Fall of fairly large pieces of plaster. Partial collapse of chimneys.	Cracks in columns and beams of frames and in structural walls. Cracks in partition and infill walls; fall of brittle cladding and plaster. Falling mortar from the joints of wall panels.
Extensive	Grade 3	Large and extensive cracks in most walls. Roof tiles detach. Chimneys fracture at the roof line; failure of individual non-structural elements (partitions, gable walls).	Cracks in columns and beam column joints of frames at the base and at joints of coupled walls. Spalling of concrete cover, buckling of reinforced rods. Large cracks in partition and infill walls, failure of individual infill panels.
Complete	Grade 4	Serious failure of walls; partial structural failure of roofs and floors.	Large cracks in structural elements with compression failure of concrete and fracture of rebars; bond failure of beam reinforced bars; tilting of columns. Collapse of a few columns or of a single upper floor
	Grade 5	Total or near total collapse	Collapse of ground floor or parts (e. g. wings) of buildings.

### 3.3.3. Generation of debris

Most of the buildings in Beirut are built of masonry or reinforced concrete frames with masonry in-fills. When damaged by an earthquake, the structural and non-structural components of these types of buildings might fall and form debris around them (Lu et al., 2019). Numerous studies of previous earthquakes have documented casualties induced by falling debris. For instance, in the 1994 Northridge earthquake, most of the hospital-admitted injuries were caused by falling objects (Peek-Asa, 1998). In

addition, the fallen debris can hinder pedestrians' mobility. Pedestrians are forced to reduce their speed when moving in a debris area (Bernardini et al., 2016), and the higher the debris, the more difficult it is for people to climb over (Osaragi et al., 2017). Therefore, the debris formed by the building damages were considered in PEERS to accurately represent the constraints that affect pedestrians' mobility and to estimate the resulting casualties.

In PEERS, the debris are represented by debris zones, i.e. areas around buildings formed by the deposition of the debris generated from the building earthquakes damages. Although the simulations start at the time of occurrence of the earthquake, the dynamic generation of debris was not simulated. Instead, the spatial extents and the height of the debris -that depend on the damage state of each building - were assumed to be constant from the start of the simulation until its end.

### **3.3.4. Casualty estimation**

Building damage was identified by several existing studies as the most important factor causing casualties in earthquakes (Noji et al., 1990; Spence et al., 2003; Wald et al., 2011). The HAZUS loss estimation manual of the Federal Emergency Management Agency (FEMA, 2012) provides for each building type, at each damage state, the probabilities of causing casualties to the people who are indoors and outdoors.

Because of these specifications, we have followed the approach of the HAZUS to estimate the casualties. We have considered that buildings can cause casualties to people who are inside the buildings during the earthquake. Therefore, each building in PEERS has indoor casualty rates. For outdoor scenarios, we considered that it is the debris from the building damage that cause the injuries to people. Therefore, the building's outdoor casualty probabilities are assigned to the debris zones.

Although casualties from earthquakes are classified by HAZUS into 4 main severity levels, only three injury severity levels were considered in PEERS:

- Injury severity 2, which refers to a person having a moderate injury, requiring him/her to go to hospital in order to be treated. Although in a crisis, some people with this level of injury may continue their activities instead of going to a hospital, for the sake of simplicity, we consider that they seek medical attention.
- Injury severity 3, which refers to a person having a severe injury and consequently immobile, which would impose on the person to stay in place and wait for emergency medical assistance.
- Injury severity 4 (fatal injury) refers to a person being killed, and consequently the person is considered dead.

Injury severity 1, related to injuries that require basic medical aid was not included in PEERS since it does not result in any behavioral changes such as severe mobility constraints nor an urgent need to go to a hospital.

In order to estimate the casualties in PEERS, we considered that during ground shaking, a person who is in a building or in a debris zone might become injured. The injury can be moderate (casualty severity 2), severe (casualty severity 3) or fatal (casualty severity 4), and it depends on the casualty rates of the building (or debris zone) that the person is in.

## **3.4.HUMAN BEHAVIOR AND MOBILITY MODEL**

The guidelines for protective behaviors to adopt when an earthquake occurs vary from one country to another. The behavioral instructions are usually adapted to each country's building standards. While in the USA, Japan and New Zealand the recommended policy is the "drop cover and hold on" (DCHO), in Mexico and Nepal the official instruction is to "flee outside the building" and go to an open space (McBride et al., 2022; Rapaport and Ashkenazi, 2020). The nations that recommend to DCHO are usually developed countries where buildings are designed to resist earthquakes (Goltz et al., 2020a).

As Lebanon is a developing country that recently implemented the paraseismic building code (decree 7964 in 2012), we assumed that most of the buildings in Beirut are not earthquake resistant. Therefore, in this work, we considered that the most adapted policy for behaviors in Lebanon would be to immediately evacuate from buildings and to go to the nearest open space.

However, as evidenced by the documented observations from previous earthquakes presented in the previous chapter (section 2.4.2), people who are in buildings during an earthquake do not always evacuate, and when they do, they do not necessarily go to open spaces.

Consequently in PEERS, we have chosen to either simulate “ideal” behaviors - in which all the people adopt the official guidelines- or to simulate “realistic” behaviors. In the latter case, people can decide whether they want to evacuate or not, and in the case a person evacuates, he/she can have a different target destination that depends on his/her motivations and other contextual factors. The realistic behaviors implemented were derived from a targeted literature review on human behaviors in earthquakes, and were adjusted to the local context using detailed survey results (see Chapter 5).

Finally, we modeled the motion of pedestrians and the constraints that affect their mobility in the urban environment. These different behaviors are now presented in details.

### **3.4.1. Ideal behaviors**

When simulating ideal behaviors, we assumed that people have perfect knowledge of where the open spaces are located. When an earthquake occurs, each person goes to the nearest open space. People do not act in groups, as each person behaves autonomously regardless of his/her age. If a person is indoors when the earthquake occurs, he/she evacuates from the building. However, a delay in the evacuation can occur because a person may take time to perceive the shaking or take additional time to go down the stairs and arrive to the building’s exit door. Consequently, we assumed that a person might have a random delay between 0 to 100 s before leaving the building he/she is in from the time of occurrence of the earthquake.

People who are in buildings and debris zones might become injured. People who have fatal (severity 4) and severe injuries (severity 3) do not perform any actions after they are injured, i.e. they stay at the same place. Those who are not injured and those who have moderate injuries (severity 2) start moving towards the nearest open space, while avoiding obstacles, debris and other people.

When a person arrives to an open space, he/she can not enter the open space if the latter is locked, i.e. its gate is closed. In the case where the open space is locked, we assumed that communication will happen between people and those who know which open spaces are unlocked will share this information with others. Therefore, the people who arrived to the locked open space will change destination and go to the nearest open space that is unlocked.

When a person arrives to an unlocked open space, if the open space has not reached its full capacity, the person enters the open space and is considered safe. However, if the person arrives to a saturated open space, we assumed that this person will prefer to stay around the crowd gathered in the open space rather than traveling again towards another open space. Therefore, the person stays outside the saturated open space. This hypothesis is based on the theory of social attachment (Mawson, 2005), which claims that in response to threats and disasters, people seek the proximity of familiar people and places for the calming effect it brings them, even if this results in approaching or remaining in an unsafe situation.

### **3.4.2. Realistic behaviors**

When realistic behaviors are considered, people can decide on the behaviors they want to adopt in the aftermath of an earthquake.

Decision-making in ABM can be implemented through several approaches. A summary of the most frequently used decision-making models can be found in An (2012). We can cite for instance, the psychosocial and cognitive models in which agents make decisions based on their own cognition, memory and intentions. Empirical models are another type of decision-making model, in which behavioral rules are derived from data and observations. In cases where inadequate data or theory exist,

decision-making can be modeled by assumption-based rules, in which the modelers make assumptions on the agents' behaviors and the factors that influence them (An, 2012).

In PEERS, decision-making is a data-and-assumption-based approach: human behaviors in PEERS are derived from observations made on previous earthquakes and reports in the literature. These behaviors were calibrated to the case of Lebanon by an online survey about the individuals' responses to sudden onset disasters in Lebanon (presented in Chapter 5). Nonetheless, when the required data for the model could not be extracted from the survey results, assumptions based on observations, previous works and hypothesis were made.

Since the model focuses on pedestrian mobility, evacuation is the only dynamic behavior modeled for individuals who are indoors. Although other indoor behaviors such as collecting belongings and looking for information are not directly modeled, they are considered as pre-evacuation behaviors and are accounted for by the time delay before evacuation. Therefore, people who are indoors during the earthquake, may choose to evacuate or not, and in case of evacuation, the maximum evacuation delay is increased to 180 s (3 minutes) (compared to 100 s in the ideal case).

We assumed that all the people who are outdoors adopt mobility behaviors. In other words, we do not model freezing behavior where a person is immobile. We considered that while a person might freeze for a few seconds, he/she will start moving shortly afterwards. Therefore, when a person is outdoors in PEERS he/she decides on his/her target destination. The target destination represents the first destination the person heads to after experiencing an earthquake. A person can follow the recommended behavior and go to the nearest open space. However, he/she might choose to join a family member and thus go to his/her home to look for relatives. A person might also need to go to a hospital if he/she is injured. Finally, a person can go to an undefined location, a location that does not fit in any of the previous categories such as the doorstep of a building or any outdoor location in the city; usually this location is not so far from the person's location at the time of the earthquake. Therefore, each person who is outdoors chooses one of these destinations, and navigates towards it.

A person who arrives to a home, a hospital or an undefined location, is not considered to be safe as the person's exposure to threats from aftershocks is high if he/she is close to buildings. A person is considered only to be safe if he/she has entered an open space; and as for ideal behavior, a person can only enter an open space if the latter is unlocked and unsaturated. Otherwise, the person either goes to an unlocked open space (if the open space is locked) or waits outside the saturated open space (if the open space is saturated).

Additionally, as several observations have reported, in emergencies families tend to group and evacuate together (Chu et al., 2011), PEERS integrates group behaviors driven by the social bonds between the household members. Therefore, if people from the same household are together (in the same building, or at a close distance outdoors), they form a group, share the same decisions for the both the evacuation decision and the choice of target destination and navigate together.

In the following sections, we present the decision-making process in PEERS at both the individual level and for group behaviors.

### **3.4.3. Decision-making- Individual level**

When realistic behaviors are considered, people in PEERS decide: (1) if they want to evacuate if they are indoor, and (2) their target destination in case of mobility.

#### **3.4.3.1. Evacuation decision for people who are indoor at the occurrence of an earthquake**

An approach based on binary logistic regression was adopted to evaluate a person's probability of evacuation if he/she in a building during an earthquake. Binary logistic regressions can assess the simultaneous impact of multiple variables on the outcome of a binary dependent variable, i.e. the evacuation decision. The equation of the logistic regression model is as follows:

$$\ln\left(\frac{p_{i,evac}}{1 - p_{i,evac}}\right) = \beta_0 + \sum_{k=1}^n \beta_k X_k \quad (3.1)$$

where  $p_{i,evac}$  is the evacuation probability of a person,  $i$ ,  $\beta_0$  is the model's constant,  $X_k$  are the explanatory variables,  $\beta_k$  are the variables' coefficients and  $k$  is the total number of categories in the explanatory variables.

In PEERS, the person's evacuation probability of evacuation depends on the perceived building's damage state, and the person's age and gender as illustrated in Figure 3-5. The detailed regression analysis for the calculation of the individual evacuation probability is presented in Chapter 5.

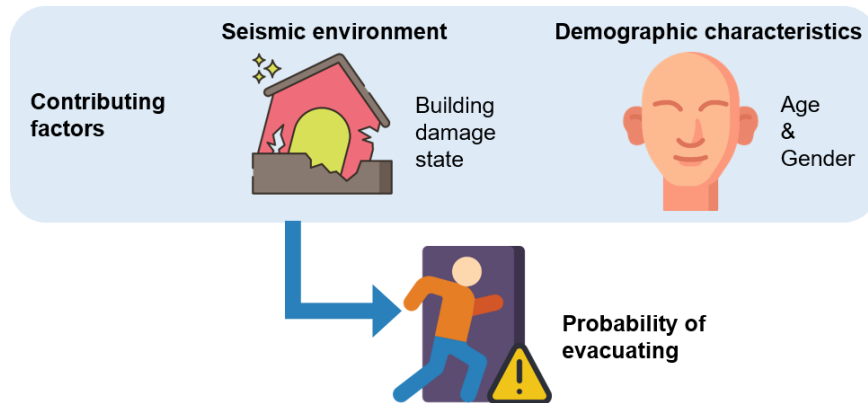


Figure 3-5: Illustration of the evacuation decision-making in PEERS

### 3.4.3.2. Target destination choice for people who adopt mobility behaviors

As it is detailed in Chapter 5, the survey revealed that in outdoor situations, the most common behaviors in the immediate aftermath of a sudden onset event in Lebanon are meeting up with family members, going to a safe area, going to a hospital and going to an undefined location. However, the factors that influence the choice of target destination could not be directly inferred from the survey since it did not contain a close-ended question asking the respondents to choose among one of these options when specifying their mobility destination.

In order to fill this gap in the data, it was assumed that the target destination of each person depends on his/her characteristics, namely: whether or not the person knows where the open spaces are located, whether or not the person wants to join a family member and whether or not the person is injured.

The assumptions made on the decision-making behind the choice of target destination are presented in Figure 3-6. We assumed that:

- If a person knows the location of open spaces, the target destination is the nearest open space.
- If a person is not at home and wants to join someone, the target destination is the home building.
- If a person has a moderate injury (severity 2), the target destination is the nearest hospital.
- If a person does not know the location of open spaces, does not want to join a family member, and is not injured, the person would go an undefined location.

However, if a person has more than one of these characteristics, we assumed that the probability of following the recommended behavior (going to open space) decreases in the favor of altruistic (going home to check-up on family members) and self-preservation behaviors (going to a hospital to treat injuries). Altruistic and self-preservation behaviors were given the same level of priority whenever a person had to choose between these two options. We considered that:

- If a person knows the location of open spaces and wants to join someone, the person has a 70% probability of going home and a 30% probability of going to an open space.

- Similarly, if a person knows the location of open spaces and has a moderate injury, the probability of going to a hospital is 70%, while the probability of going to an open space is 30%.
- If a person wants to join someone but also has a moderate injury, the person has a 50% probability of going to a hospital and a 50% probability of going home.
- Finally, if a person knows the location of open spaces, wants to join someone and has a moderate injury, the probability of going to an open space is reduced to 20%, while the probabilities of going home and to a hospital are of 40% each.

These parameters were based on assumptions due to the lack of data; nevertheless, if in the future more data become available they can be easily changed depending on the new findings.

Person's characteristics			Probability of choosing each target destination			
Knows the location of open spaces	Wants to join a household member	Has a moderate injury	Home	Hospital	Undefined location	
✓	&	✗	100%	0	0	0
✗	&	✓	0	100%	0	0
✗	&	✗	0	0	100%	0
✓	&	✓	30%	70%	0	0
✓	&	✗	30%	0	70%	0
✗	&	✓	0	50%	50%	0
✓	&	✓	20%	40%	40%	0
✗	&	✗	0	0	0	100%

Figure 3-6: Target destination choice in PEERS according to the person's attributes

A person's probabilities of knowing the location of open spaces and joining someone were derived from the survey results. The probability of having a moderate injury depends on the person's location during the earthquake, whether the person is in a building or a debris zone during the earthquake, and therefore is computed during the simulation.

### 3.4.4. Decision-making related to group behavior

In PEERS, when people from the same household are at a close distance, they form a group, share common decisions and navigate together. A group can be formed indoors whenever people from the same household are in the same building. In outdoor scenarios, people from the same household group together whenever they are within 50 meters from each other; this is the perception distance between family members (Bañgate et al., 2018).

As found in the literature, groups are typically characterized by a leader-follower dynamic: each group is characterized by a leader, a person who is in charge of the decision-making and is followed by the other group members (Kuligowski, 2011). Therefore, in PEERS, each group has a leader who is followed by the other group members in both the evacuation decision and the choice of mobility destination. The group leader is evaluated when the group is formed and every time the group members change. The evaluation of the group leader is illustrated in Figure 3-7, and can be explained as follows:

- If the head of the household is in the group, he/she is the group leader.
- If the head of the household is not in the group, the person with the highest leadership score is

assigned as the group leader.

The leadership score is a metric, that takes values between 0 to 1, introduced to classify people according to their level of influence on others during emergencies. The leadership score is calculated for each person using equation (3.2):

$$leadership\ score = \frac{open\ space\ knowledge + \left(\frac{age}{100}\right)}{2} \quad (3.2)$$

The leadership score is the average of the open space knowledge (1 if the person knows the location of open spaces, 0 otherwise), and the person’s age normalized over 100, the maximum age that a person can have in PEERS. The open space knowledge was considered as a leadership indicator as it has been found in previous emergencies that people with a better knowledge of emergency egress routes often lead other evacuees towards safe destinations (Chu and Law, 2013). The choice of the age as a leadership indicator come from observations that in Lebanese families, the relational structure is mostly vertical (Kazarian, 2005). Older members, such as parents or older siblings often assume leading roles with respect to other family members.

Person in the group				
Is the head of the household	✓	✗	✗	✗
Is the group leader	✓	✗	✗	✗

(a)

Person in the group		
Is the head of the household	✗	✗
Age	70	75
Knows location of open spaces	✓	✗
Leadership score	0.85	0.37
Is the group leader	✓	✗

(b)

Figure 3-7: Illustration of the designation of the group leader in PEERS: (a) when the head of the household is in the group, (b) when the head of the household is not in the group

Hence, if the group is indoors during the earthquake, the group’s decision to evacuate will be the same as the leader’s. If we consider the example illustrated in Figure 3-8, we can see that the group has two members with different individual evacuation decisions (i.e. their decision if they were alone). However, as the leader’s decision is to evacuate, the other person follows the leader’s decision and evacuates as well.

In the case where a group evacuates, all group members evacuate at the same time (Mikami and Ikeda, 1985), they therefore wait for the group member who has the longest evacuation delay.

Person in the group		
Is the group leader		
Individual evacuation decision	 To evacuate	 Not to evacuate
Evacuation decision	 To evacuate	 To evacuate

Figure 3-8: Example of the evaluation of the group's evacuation decision

Similarly, the individual target destinations of the group members are changed to the target destination of the group's leader. We can see in the example in Figure 3-9, that despite the group members having different individual target destinations, all the group members follow the leader's decision and go to an open space.

Person in the group				
Is the group leader				
Individual target destination	 Open space	 Open space	 Hospital	 Undefined location
Target destination	 Open space	 Open space	 Open space	 Open space

Figure 3-9: Example of the evaluation of group's target destination choice

To ensure the group navigates in a cohesive manner towards the leader's target destination the leader is set to navigate towards his/her target destination while the other group members follow the leader by navigating towards the leader's position at each step. Additionally, the group's cohesion is also maintained by imposing the same speed for all group members, set to the speed of the slowest group member (Proulx, 1995).

The mobility of pedestrians, their speed and the different constraints that affect it is further explained in the following section.

### 3.4.5. Model of pedestrians' mobility

In PEERS, we assumed that all mobility behaviors will take place on foot in the immediate aftermath of an earthquake. Although, this is a high simplification of the reality, this simplification was assumed for two main reasons:

- Ideally, people should only move on foot after an earthquake, as roads should be reserved for the access of emergency crews to damaged areas (ECPFE and OASP, 2002).
- Modeling a person's choice of transportation and the navigation of vehicles in the urban area significantly increases the complexity of the model, which was not the priority in this thesis.

Nevertheless, we are aware that in Beirut, the mobility of pedestrians is compromised by the poor management of pedestrians' pathways. Many streets lack sidewalks, and where they exist they are often broken or obstructed by diagonally parked cars and motorbikes (Myntti and Mabsout, 2014). However, these constraints are difficult to assess at the city scale, as they are dynamic (number of cars parked on a sidewalk) or require site investigations (presence of sidewalks and their conditions). For simplification purposes, we considered that in emergency evacuation, pedestrians' mobility is not restricted to the sidewalks. Pedestrians can move freely in the urban space, however, several constraints affect their route options and speed, namely the presence of obstacles, the slope of terrain and the presence of debris in the aftermath of the earthquake. In the following, we present how we delimited the space where pedestrians can move, how the pedestrians move towards their target, and the factors that influence their speed.

### 3.4.5.1. Delimitation of the free space

A pedestrian's path might be obstructed by obstacles. The obstacles can be either buildings or barriers. Therefore, pedestrians can only move in the space that is free from obstacles. In order to represent the obstruction of pedestrian's path by obstacles we restricted the pedestrian's movement to the space in the city that is free from obstacles: the free space. The free space was delimited by performing GIS data modeling: the layers that represent mobility obstacles (buildings and barriers) were subtracted from the boundary layer as illustrated in Figure 3-10.

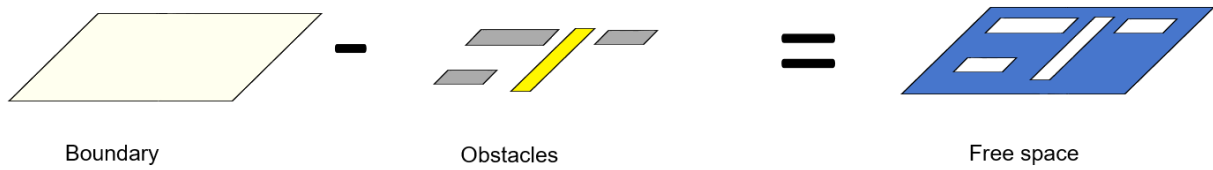


Figure 3-10 : Delimitation of the free space by subtracting the obstacles from the spatial extents of the study area. The obstacles are the buildings (in grey) and the barriers (in yellow)

### 3.4.5.2. Motion of a person in the free space

The pedestrian's motion in PEERS is based on the social force model (SFM) (Helbing and Molnar, 1995). This model uses the physical forces of Newtonian dynamics to model the motion and local interactions between the agents. In the SFM, three forces describe the internal motivations of pedestrians to perform certain actions, as illustrated in Figure 3-11. An attraction force  $F_p^{des}$ , represents the desire of a person to move towards his/her destination. A repulsive force, the "social force",  $F_{pq}^{soc}$  is applied from the other pedestrians in order to avoid collisions between pedestrians when they are too close. Similarly, a repulsion force  $F_{pb}^{repuls}$  is applied from the static obstacles so that the pedestrians avoid them.

The resulting force applied on a pedestrian p,  $\vec{F}_p(t)$ , is defined as follows:

$$\vec{F}_p(t) = \vec{F}_p^{des}(t) + \sum_{q \neq p}^{N_{ped}} \vec{F}_{pq}^{soc}(t) + \sum_b \vec{F}_{pb}^{repuls}(t) \quad (3.3)$$

where q represents a pedestrian from the  $N_{ped}$  nearby and b represents a static obstacle. More details on each term of this equation can be found in (Helbing and Molnar, 1995).

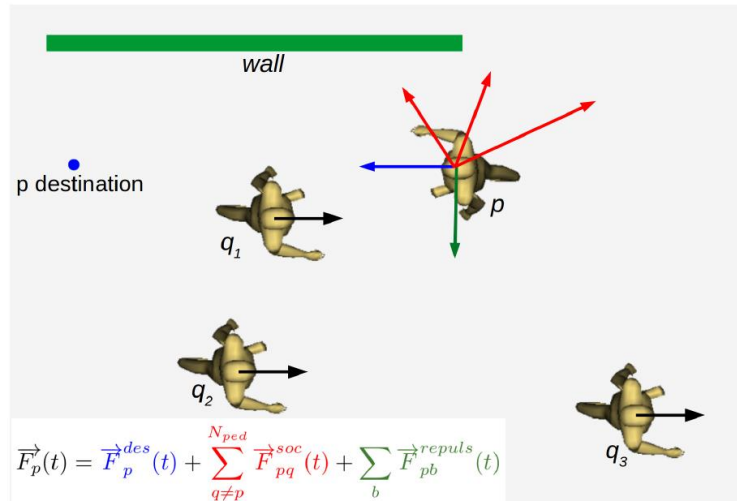


Figure 3-11: Illustration of the forces applied on a pedestrian in the SFM. An attraction force is applied from the pedestrian towards its destination, while repulsive forces are applied on the pedestrian from the other pedestrians who are nearby as well as obstacles (wall) (Source: Prédhumeau, 2021)

Each person in PEERS has an attraction force towards his/her target. The person avoids collisions with other people, and keeps a safe distance from buildings and debris zones. The avoidance of people, obstacles and debris zones is modeled as repulsive forces on the person. The sum of these forces calculates the direction at which the pedestrian will move. The step size the person takes depends on his/her speed which is discussed in the next section.

### 3.4.5.3. Speed

Each person has a preferred speed of movement that depends on the his/her age as defined in Bañgate et al.(2018, 2019). People were classified into three categories depending on their age: people aged less than 14 years old were assigned to the children category, people between 15 and 59 years old were considered adults and people who are 60 or more were considered to be in the elderly category. In PEERS, no differentiation was made between walking and running: the model considers both displacement modes and assigns to each category of agents a range of possible preferred speeds, varying from the minimum walking speed to the maximum running speed of individuals belonging to this category (Table 3-2). Finally, the preferred speed was assigned to each person following a normal distribution with ranges depending on which category he/she falls into.

Table 3-2 : Preferred moving speeds for individuals in the child, adult and elderly categories as defined in Bañgate et al., 2018, 2019

Category	Age	Preferred speed (m/s)
Child	<14	0.56 - 2.23
Adult	15-59	0.9 - 3.83
Elderly	60+	0.7 - 1.11

However, the speed of a person can be affected by environmental factors namely the slope of the terrain and the presence of debris along his/her path.

In PEERS, when a person is moving uphill or downhill, his/her speed is reduced by a factor  $\gamma$  that depends on the slope's value.  $\gamma$  is calculated using equation (3.4), given by (Tobler, 1993), where  $\theta$  is the slope angle relative to the horizontal plane (in degrees). The values taken by  $\gamma$  according to the slope is shown in Figure 3-12. We can see that for a slope of around  $10^\circ$ , the speed is reduced by 50%, and when the slope is  $35^\circ$ , the person moves at 10% of his/her speed.

$$\gamma = e^{-3.5 (|\tan \theta + 0.05| - 0.05)} \quad (3.4)$$

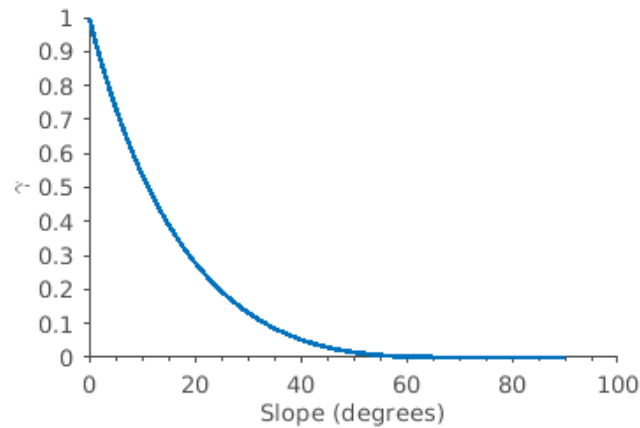


Figure 3-12: Variation of the speed reduction factor,  $\gamma$ , according to the slope of the terrain

In addition to the slope of the terrain, the presence of debris further constrains the pedestrian's mobility: when a person is in a debris zone, he/she is moving on unsteady objects, therefore the person needs to adjust his/her speed to manage this instability.

The effect of the debris on a person's speed in PEERS was adapted from Osaragi et al., 2017:

- If the debris' height is less than 1 m, the person's speed is reduced by 50%;
- If the debris are more than 1 m high, the person has to climb over the debris, and therefore his/her speed is reduced to 0.16 m/s.

Therefore in PEERS, each person has a preferred speed. At each step the person evaluates the value of the slope and whether or not he/she is in a debris zone, and adjusts his/her speed accordingly. In the case of group behaviors, at each step, every person in the group evaluates his/her speed, but only the speed of the slowest group member will be assigned to all the group members.

After defining the conceptual model, PEERS was formalized and the architecture of the model is detailed in the following section.

### 3.5. ARCHITECTURE OF THE MODEL

The previous sections have focused on describing the definition of three sub-models of PEERS (city, earthquake damage, human behavior and mobility) as well as their interactions. This section describes the architecture of PEERS, the model that integrates the 3 sub-models, and its formalization in the UML (Unified Modelling Language) class diagram (Fowler and Scott, 2002). The UML class diagram, represents the classes of the model, their attributes (characteristics) as well as their methods (behaviors). Additionally, in this section we present the activity diagram of a person agent in PEERS. An activity diagram represents the flow from one activity to another, as well as the constraints and conditions behind the algorithm.

#### 3.5.1. UML class diagram of PEERS

Figure 3-13 shows the UML class diagram of PEERS. PEERS has a multi-level architecture, represented by a world class that contains 4 high-level classes: *person*, *obstacle*, *debris\_zone* and *open\_space*. The classes *building* and *barrier* represent different types of obstacles. Finally, the *people\_in\_group* class represents a special type of person: a person who belongs to a group; and the *group* class represents a group of people. A brief presentation of each class with its attributes and methods is given in the following:

- The class *world*, defines the environment that contains the other classes of the model. The *world's* attribute *shape* represents the extent of the environment, and therefore the limits of Beirut. The

*world* also defines the *free\_space* geometry, which represents the space in the environment that is free from obstacles. Additionally, the topography of the environment is represented by the attribute *slope* that indicates the slope of the terrain.

In addition to its spatial attributes, the *world* defines the scenario considerations of the simulation. The earthquake scenario is defined by specifying the duration of the earthquake, its PGA and the time of day when it occurs. The *world* also defines considerations related to the behaviors of the individuals: whether the individuals follow the ideal guidelines or behave realistically, whether the open spaces that have locked gates or not.

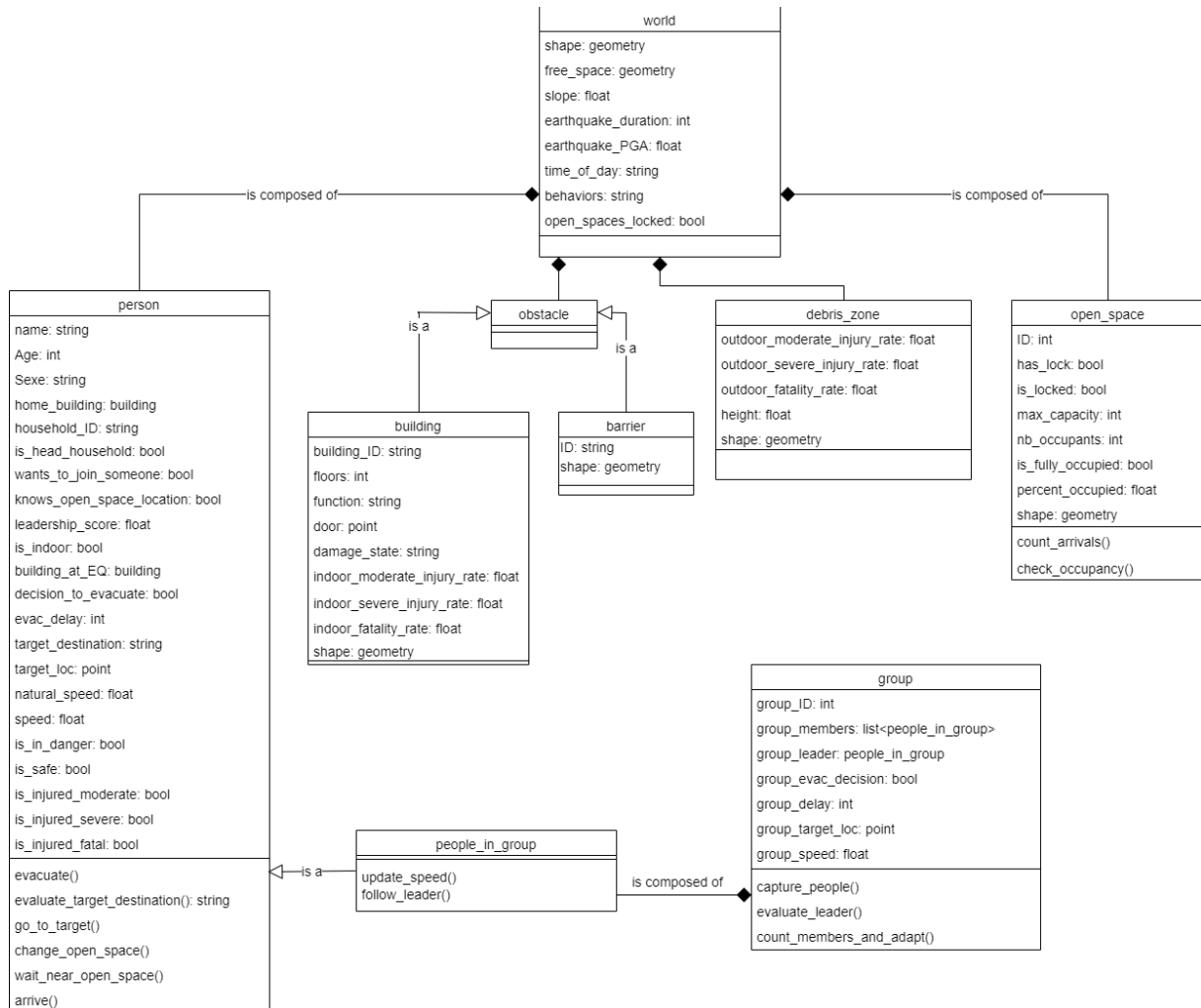


Figure 3-13: Simplified UML class diagram of PEERS

- The *person* class represents the residents of Beirut, each characterized by an age and a gender. Each *person* has a *home\_building* and a *household\_ID*. The *household\_ID* defines the household to which each person belongs, therefore, people from the same household share the same *household\_ID*.

A boolean *is\_head\_household* is added to the *person* class, to represent if a person is the head of the household. Additionally, the booleans *wants\_to\_join\_someone* and *knows\_open\_space\_location* represent respectively if a person wants to join a household member and if the person knows the location of open spaces.

The *person*'s attribute *target\_destination* designates the type of the destination the person wants to go to, which can be an open space, a building (hospital or home), or an undefined location. On the other hand, the precise location that a person wants to go to is designated by the point attribute *target\_loc*.

The *person* class also has attributes related to the situation of the person, such as the *is\_in\_danger* boolean that takes a *true* value when the person is in a debris zone, and the *is\_safe* boolean that takes a *true* value when a person is in an open space. Additionally, the injury level of the person is indicated by booleans that represent if the person has a moderate, severe or a fatal injury.

The *person* class has methods that represent the actions taken by a person, such as evacuating, evaluating a target destination, going to a target, changing target open space, waiting near an open space and arriving to a destination.

- The *obstacle* class represents the obstacles that block the mobility of pedestrians and that should be avoided when he/she is moving. The obstacle can be either a *barrier* or a *building*. The *building* class has a *function* attribute that defines the use of the building. For implementation purposes, we have added a point attribute *door* to designate a location on the building's façade that serves as an exit point for people who evacuate from buildings, and a target location for the people whose target destination is a building. Finally, buildings also have attributes related to their damage level: their *damage\_state*, as well as the injury rates of a person in the building during the earthquake.
- The *debris\_zone* class represents the debris around a building, it has attributes related to the *height* of the debris and the injury rates of a person in the debris zone during the earthquake.
- The *open\_space* class, represents the open spaces. The open space's attribute *has\_lock* indicates if the open space has a gate, and the open space's attribute *is\_locked* indicates if the gate is locked or not. Each open space has an attribute that indicates its maximum capacity. The open space class has methods to count the number of arrivals and update the *nb\_occupants* attribute, which indicates the number of people in the open space. Additionally, the method *check\_occupancy()* updates the *percent\_occupied()* attribute of the open space, which designates the ratio of the open space's number of occupants to its maximum capacity. Finally, the boolean *is\_fully\_occupied* indicates if the open space is saturated or not.
- The *group* class represents the groups formed by the people from the same household when realistic behaviors are considered. The group's method *capture\_people()* adds people to the group, and updates the list of group members contained in the attribute *group\_members*. The method *evaluate\_leader()* assigns the *group\_leader*. Finally the method *count\_members\_and\_adapt()* updates the attributes related to the group's evacuation decision, evacuation delay, target location and speed.
- The class *people\_in\_group* designates the people who are in a group. This class inherits from the class *person*: each *people\_in\_group* object is also a *person*. However, in addition to the attributes and methods of the *person* class, the *people\_in\_group* has two additional methods. The *update\_speed()* method changes the speed of the *people\_in\_group* to the speed of the slowest group member, and the *follow\_leader()* method that updates the target location of the *people\_in\_group* who are not group leaders, to the position of the leader.

### 3.5.2. Activity diagram of a person agent in PEERS

Figure 3-14 shows the activity diagram of a person agent in PEERS when realistic behaviors are considered. The activity diagram when ideal behaviors are considered can be found in Appendix A.

In order to facilitate the readability of the activity diagram, the following are not represented:

- the decision changes caused by group behavior;
- the interruption of a person agent's activity if the agent has a fatal or severe injury (severity 3 and 4).

At the start of the simulation, if the agent is indoor it evaluates its evacuation decision. If the agent decides not to evacuate, it stays indoor and does not execute any further actions. In the case where the agent decides to evacuate, an evacuation delay time is assigned to the agent as a random number between 0 and 180; the agent waits until its evacuation time arrives and then exits the building.

The target destination is evaluated for the person agents who are outdoor at the start of the simulation, as well as the agents who evacuated from buildings. After the target destination is evaluated, the agent moves toward its target and keeps moving until reaching this target. The agent’s activity is terminated when it arrives to its target. However, if the agent’s target is an open space, two conditions have to be satisfied before ensuring the person’s arrival and termination of activity. (1) The open space has to be unlocked; otherwise the agent changes its target open space to the nearest open space that is unlocked; and (2) the open space needs to be non-saturated, otherwise the person waits outside the open space.

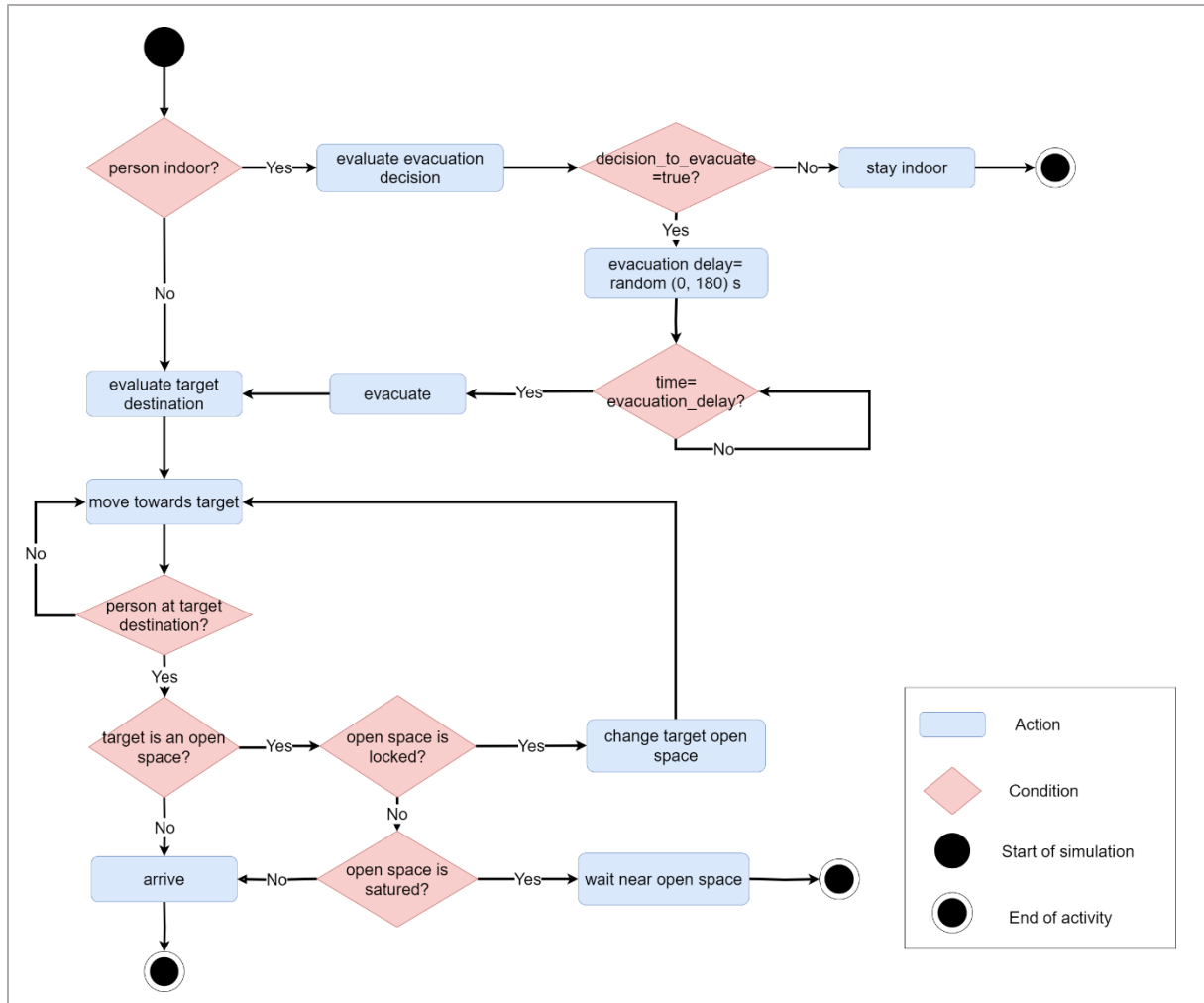


Figure 3-14: Simplified activity diagram of a person agent in PEERS when realistic behaviors are considered

### 3.6. VALIDATION OF THE CONCEPTUAL MODEL

PEERS was developed in the framework of this thesis, which was supervised by a multidisciplinary team of researchers in social sciences, computer sciences and earth sciences. The supervisors’ compound expertise in the simulation of earthquakes, the simulation of crowds in crisis, and the analysis of the drivers of human behaviors and social vulnerability, was a first validation of the model.

PEERS also benefited from a strong collaboration with researchers in social sciences and earthquake engineering in Lebanon in the framework of the project “Modélisation du comportement humain en cas de crise sismique: les freins à la Mobilité” funded by the AUF-PCSI<sup>4</sup>. The first project meeting took place in June 2019 in Beirut, in which a collaborative approach was adopted for the identification of the mobility constraints for pedestrians in Beirut and the definition of the first conceptual version of PEERS

<sup>4</sup> Agence Universitaire de la Francophonie- Projets de Coopération Scientifiques Inter universitaires - PCSI

(Figure 3-15). PEERS was also presented in international conferences in different fields. The first simulations performed in PEERS were presented in a paper for the 17<sup>th</sup> World Conference in Earthquake Engineering (Iskandar et al. 2020), and were validated by the earthquake engineering community. The theoretical framework of PEERS, mainly the model for realistic behaviors and decision making, was presented in a peer-reviewed paper for the 18<sup>th</sup> International Conference on Information Systems for Crisis Response and Management (Iskandar et al. 2021), for the validation by the crisis simulation community.

Finally, PEERS was presented to the multidisciplinary community of researchers involved in the Cross-Disciplinary Project Risk@UGA. Overall, the model received encouraging feedback, especially on the articulation between the different disciplines involved in PEERS.

PEERS could not be validated by stakeholders in Beirut, due to unstable political and institutional contexts in Lebanon during our study.

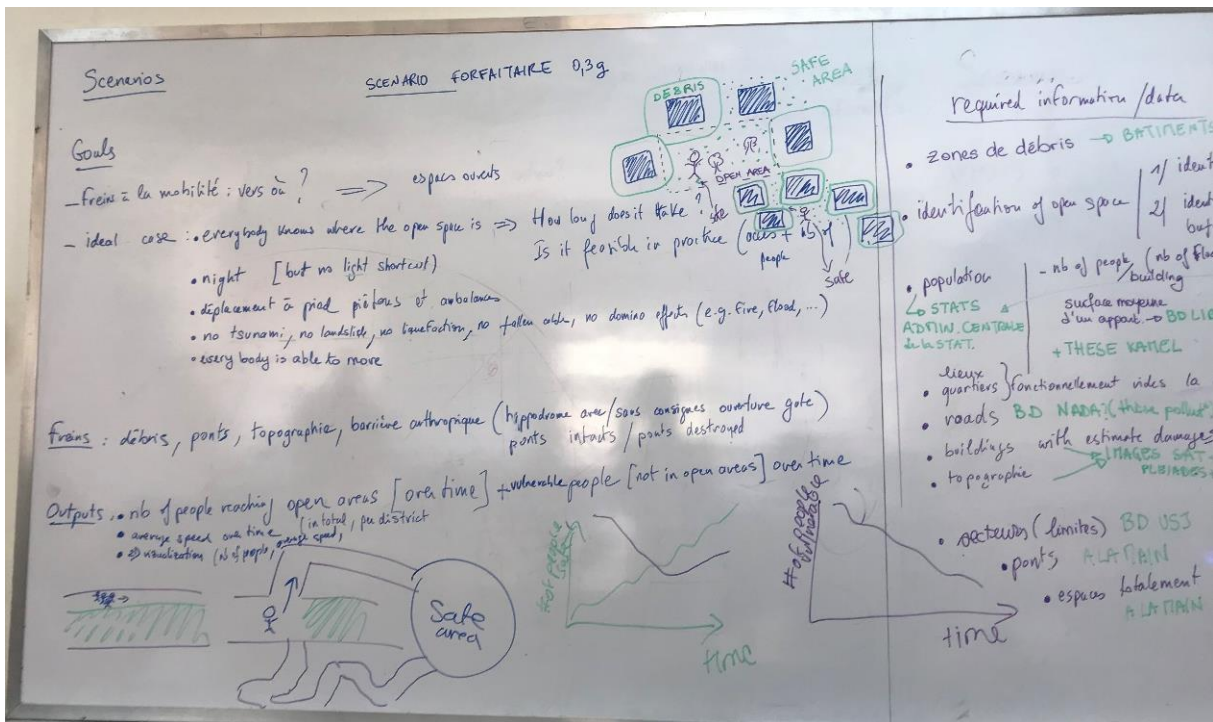


Figure 3-15: First version of PEERS defined in the framework of the AUF-PCSI project. This first version represented a night scenario with ideal behaviors for an earthquake of 0.3 g [Beirut, June 2019]

### 3.7.IMPLEMENTATION

After defining the conceptual model of PEERS it was implemented in a simulation platform to perform dynamic simulations of pedestrians' evacuation and mobility in a seismic event. The GAMA Platform<sup>5</sup> (Taillandier et al., 2018) was chosen for the implementation of PEERS due to its (1) ability of integrating and manipulating geospatial data, (2) capacity to handle large-scale simulations, needed to run simulations at the city-scale (3) intuitive modeling language (GAML), which makes it accessible to non-computer scientists and (4) open source framework, which facilitates the reproduction and the communication of the model. In GAML, a species is the equivalent to a class in UML, whereas an agent represents an instance of the species (an object of the class).

The implementation of PEERS in GAML was organized as follows: the built-in *global* species was defined in the first part of the model, which represents the *world* class in the UML. This section also controls the creation of the other species (the other classes in the UML diagram), along with the

<sup>5</sup> <http://gama-platform.org/>

definition of the model's global variables. Therefore, the *global* species can be seen as a public species that initializes the simulation and defines its behaviors.

After the definition of the *global* species, each species was implemented individually, by declaring and defining its attributes, methods and displays (how it is represented in the simulation's graphical interface).

The experiment section was then implemented. This defines how the simulations of the model will be run. In this section, the simulation's parameters were defined, i.e. the variables of the simulation that can be changed by the user, and the simulation's outputs, i.e. what is displayed during the simulation and what is exported. The simulations in PEERS are detailed in Chapter 6; nevertheless, we present few notions about the simulations here:

- The parameters in PEERS are the earthquake PGA, the time of day (day or night), the behaviors (realistic or ideal), and whether or not the open spaces that have gates are locked.
- When a simulation is launched in PEERS, the model's species are initialized depending on the parameter values chosen by the user. Once initialized, the dynamic simulations can be run.
- A cycle in GAML represents a time step, which is defined as 1 second. Therefore, at each time step, the methods of the species are executed. Since we simulated 15 minutes, the simulations were scheduled to automatically stop after 900 cycles.

The following sections describe the creation of the model's species. Then we focus on the implementation of the dynamic aspects of the *person* agent: the evaluation of the evacuation decision and delay, the choice of target destination and the movement of the agents. .

### 3.7.1. Creation of the model's species

GAMA's ability of integrating geospatial data facilitated the creation of the non-human species in PEERS directly from GIS files. As the population's attributes and initial location depend on the simulated scenario, the population's fixed attributes were initialized from a csv file, and the remaining attributes were assigned in a probabilistic approach in GAMA.

#### 3.7.1.1. GIS-based creation of non-human agents

In PEERS, the spatial extents of the model were defined from the GIS polygon layer (shapefile) corresponding to the boundary of the city. Practically, the *shape* of the *global* species was set as the geometry of the polygon in the GIS layer.

Similarly, the non-human agents were directly created from their corresponding shapefiles. When creating agents from a shapefile, an agent is created for each polygon in the layer, and the shape of the agent is directly assigned as the geometry of the polygon. Additionally, the attributes of the agents were directly initialized from the layers' attributes. We should note that as PEERS does not handle the estimation of the buildings damages, the buildings and debris shapefiles were prepared beforehand for each desired seismic scenario. Then, depending on the simulated seismic scenario, its corresponding shapefiles are imported into the simulation.

In order to introduce the slope of the environment in PEERS, a grid species was created in GAMA. The size and value (slope) of each cell in the grid were initialized from a GIS raster layer.

The GIS data needed to initialize the species of GAMA and their attributes are summarized in Table 3-3.

The *free\_space* geometry, which defines the space where agents can move in PEERS, was dynamically created in GAMA as shown in Figure 3-16. It was first initialized as the *shape* of the *global* species, and as each *obstacle* (*building* or *barrier*) was created, the *shape* of the *obstacle* was subtracted from the *free\_space*.

```

free_space = shape(global)
for each obstacle created
    free_space = free_space - shape (obstacle)
end

```

Figure 3-16: Pseudo-code of the definition of the free space geometry in PEERS

Table 3-3: GIS data requirements of PEERS

Species	GIS Layer	GIS Layer type	Attributes		
			Description	Name in PEERS	Name in GIS layer
<i>global</i>	Boundary	Polygon	Spatial extents	<i>shape</i>	-
<i>building</i>	Buildings	Polygon	Shape	<i>shape</i>	-
			ID	<i>building_ID</i>	BatiID
			Number of floors	<i>floors</i>	NombreEtag
			Function	<i>function</i>	TYPE
			Damage state	<i>damage_state</i>	damage_sta
			Probability of causing moderate injury	<i>indoor_moderate_injury_rate</i>	ind_inj_2
			Probability of causing severe injury	<i>indoor_severe_injury_rate</i>	ind_inj_3
<i>debris_zone</i>	Debris zones	Polygon	Shape	<i>shape</i>	-
			Height	<i>height</i>	h_debris
			Probability of causing moderate injury	<i>outdoor_moderate_injury_rate</i>	outd_inj_2
			Probability of causing severe injury	<i>outdoor_severe_injury_rate</i>	outd_inj_3
<i>open_space</i>	Open spaces	Polygon	Shape	<i>shape</i>	-
			ID	<i>ID</i>	ID
			Capacity	<i>max_capacity</i>	Capacity
			Possibility of being locked	<i>has_lock</i>	Has_lock
<i>barrier</i>	Barriers	Polygon	Shape	<i>shape</i>	-
<i>grid</i>	Slope	Raster	Slope of the terrain	<i>slope</i>	[pixel value]

### 3.7.1.2. Use of probabilities for the creation of person agents

Person agents in PEERS have constant values for attributes that do not depend on the simulated scenario. These values are for socio-demographic attributes and the distribution in households, namely: the agent's age, gender, whether he/she is the head of the household, and the agent's household and home building IDs. On the other hand, the agents have attribute values that are not deterministic, namely each agent has:

- a probability of being at work, at home, or outdoors, for a day scenario;
- a probability of knowing where the open spaces are located;
- a probability of wanting to join someone.

In order to integrate the randomness in the agents' attribute values, these were initialized directly in GAMA at each simulation. Therefore, for each simulation of a day scenario or realistic behaviors, the initial location of an agent, its open space knowledge and desire to join someone were assigned in a probabilistic approach.

The *person* agents were created from a csv file that contains the constant values for attributes. For each agent created, the agent's *home\_building* was assigned as the *building* whose ID that matches the agent's building ID.

After creating the agents, each agent's location was assigned depending on the time of the day. For a night-time scenario, each *person* was set to be indoors and at home: the agent's location was initialized as any location in his/her home building.

For a day scenario the pseudo-code for the agents' distribution is given in Figure 3-17. The probability of being at home, at work or outdoors was defined by a global list *pop\_distribution*. The choice of the place for each agent was assigned by picking randomly one of the three proposed modalities, with a chance of picking each modality as defined by the *pop\_distribution* list.

```

pop_distribution=[probability of being at home, probability of being at work, probability of being outdoor]
If day scenario
  for each person created
    place = random choice between home, work or outdoor
    the chances of choosing each modality are assigned by pop_distribution
  end
end

```

Figure 3-17: Pseudocode of the spatial distribution of the person agents for a day scenario

The initial locations of the agents were distributed as follows: each agent at work was located in a random building whose function is “work” or “hospital” (non-residential buildings), and each agent outdoors was located at a random point in the free space. After distributing the agents, each agent's preferred speed (attribute *natural\_speed*) was initialized as a random number between the minimum and maximum speeds of the agent's age category.

When realistic behaviors were considered, the *person*'s knowledge of the location of open spaces was initialized with the percentage of the population that knows the location of open spaces. We used the *flip()* operator in GAMA, which returns a true value with a probability equal to this percentage. Similarly the person's desire to join someone was initialized for the *person* agents which are not at home with the percentage of the population who want to join someone (Figure 3-18). Finally, the *leadership\_score* of each person agent was calculated according to its age, and whether or not it knows the location of open spaces following equation (3.2).

```

If realistic behaviors
  for each person
    knows_open_space_location = flip (probability of knowing the location of open spaces)
    if not at home
      wants_to_join_someone= flip (probability of wanting to join someone)
    end
  end
end

```

Figure 3-18: Pseudocode of the assignment of attributes related to the knowledge of open spaces and the desire to join someone

### 3.7.2. Behaviors of the person agents

In this section, we present the implementation of the main behaviors of the *person* agents in PEERS: the agent's evacuation, the evaluation of its injury level, its target destination choice and its movement in the free space.

#### 3.7.2.1. Agent's evacuation decision and behavior

The evacuation decision of each agent indoor is evaluated at the initialization of the simulation as shown in Figure 3-19.

If the behaviors are ideal, the *decision\_to\_evacuate* is set to *true* for all the agents. The evacuation delay is assigned as a random number between 0 and 100.

If the behaviors are realistic, the probability of evacuating is calculated for each agent as a function of the building's damage state, and the person's age and gender, following equation (4.2). The *decision\_to\_evacuate* is then evaluated with the flip() operator, with a probability of being *true* equal to the calculated probability. If the agent decides to evacuate, the evacuation delay is assigned as a random number between 0 and 180.

```
for each person indoor
  If ideal behaviors
    decision_to_evacuate=true
    evac_delay= random (0, 100)
  end

  If realistic behaviors
    calculate probability of evacuation depending on age, gender and building's damage state
    decision_to_evacuate= flip (probability of evacuation)
    If decision_to_evacuate=true
      evac_delay= random (0, 180)
    end
  end
end
end
```

Figure 3-19: Pseudocode of the evaluation of the evacuation decision and the assignment of the evacuation delay

The evacuation behavior was implemented as shown in Figure 3-20: each person who is indoors and wants to evacuate, waits for the simulated time to be equal to its evacuation delay, then the agent changes its location to the door of the building and its value for the *is\_indoor* attribute turns to *false*.

```
for each person indoor
  If decision_to_evacuate= true
    If simulated_time= evac_delay
      location= door of building
      is_indoor=false
    end
  end
end
end
```

Figure 3-20: Pseudocode of the evacuation behavior of a person agent

#### 3.7.2.2. Evaluation of the agent's injury level

Each agent who is indoors during the earthquake has a probability of having either a moderate or a severe or a fatal injury, depending on the building (*building\_at\_EQ* attribute). As agents can only exit buildings in PEERS, at the initialization step all the agents who might be indoors during the simulation are already in buildings. Therefore, the injury state of the agents who are indoors is evaluated only once, at the initialization of the simulation, as described in Figure 3-21.

```

at time=0
for each person indoor
  is_injured_fatal=flip(building's fatality rate)
  if is_injured_fatal=false
    is_injured_severe=flip(building's severe injury rate)
    if is_injured_severe=false
      is_injured_moderate=flip(building's moderate injury rate)
    end
  end
end
end

```

Figure 3-21: Pseudocode of the simulation of the indoor casualties in PEERS

Similarly, each agent who is outdoors and has a debris zone that overlaps its location has a probability of having either a moderate, severe, or fatal injury during the earthquake. However, as the agents move outdoors, the number of agents in debris zones varies from one time step to another. Therefore, the probability of an agent who is in a debris zone to be injured is evaluated at each simulation step while the simulated time is less than the earthquake duration (Figure 3-22).

```

While time<= earthquake duration
  for each person in debris zone
    is_injured_fatal=flip(debris zone's fatality rate)
    if is_injured_fatal=false
      is_injured_severe=flip(debris zone's severe injury rate)
      if is_injured_severe=false
        is_injured_moderate=flip(debris zone's moderate injury rate)
      end
    end
  end
end
end

```

Figure 3-22: Pseudocode of the simulation of the outdoor casualties in PEERS

### 3.7.2.3. Choice of target location

Each *person* agent who is outdoors in PEERS has a target destination ('open space', 'home', 'hospital' or 'undefined location') and a target location, which is the exact location where a *person* wants to go. The target destination is evaluated at the initialization of the simulation for the agents that are created outdoors, and when an agent that was created indoors evacuates.

For a simulation with ideal behaviors, the target destination of each person is assigned as 'open space'. For realistic behaviors, the agent's target destination is evaluated as described in Figure 3-6, depending on whether or not the person: knows the location of open spaces, wants to join someone, or has moderate injury.

Depending on the target destination of each agent, its target location is assigned as presented in Table 3-4. The nearest open space and hospital are calculated based on straight-line distances. The undefined location is chosen as a point in the free space within 100 m from the agent's location.

Table 3-4: Assignment of the agent's target location according to its target destination

Target destination	Target location
Open space	Any point in the nearest open space
Home	Door of the person's home building
Hospital	Door of the nearest hospital building
Undefined location	Any point in the free space (in a radius of 100 m)

Once the target location of a person is defined, the agent moves towards its target. The movement of a person agent in PEERS is described in the next section.

### 3.7.2.4. Movement of an agent in PEERS

Agents who are outdoors and who do not have severe or fatal injuries move in the free space until they reach their target location. At each time step, the agents move in a given direction  $\vec{v}$  with a step size ( $s$ ). The rules that control the direction and the step size of an agent at every time step were implemented in separate actions (methods) in GAMA, as shown in Table 3-5 and described as follows:

- the agent desires to go towards to its target. The *follow\_goal* action computes the desire force from the agent to its target;
- it was assumed that person agents keep 1 m between each others when moving. Therefore, the *separate\_from\_others* action applies the repulsion forces from the person agents at less than 1 m;
- it was assumed that an agent keeps a distance of 2 m from obstacles. The *avoid\_obstacles* action applies the repulsion forces from the obstacles at less than 2 m;
- the agent also keeps a 2 m distance from debris zones. The *avoid\_debris* action computes the repulsion forces from the debris zones at less than 2 m.

$\vec{v}$  is computed from the addition of all these forces. The step size of the agent is then computed by multiplying the *natural\_speed* of the agent by the slope reduction factor  $\gamma$  and modifying it according to the height of the debris zone, if the agent is in a debris zone.

Table 3-5: Implementation of the rules that control an agent's movement in PEERS

Action	Description	Implementation
<i>follow_goal</i>	computes the desire force from the agent's location (p) to its target location (g)	$\vec{v} = \overrightarrow{pg}$
<i>separate_from_others</i>	detects the other <i>person</i> agents at less than 1 m, and applies a repulsive force from the location of each detected <i>person</i> (q)	For each person detected $\vec{v} = \vec{v} - \overrightarrow{pq}$ end
<i>avoid_obstacles</i>	detects the <i>obstacle</i> agents at less than 2 m, and applies a repulsive force from the location of each detected <i>obstacle</i> (b)	For each obstacle detected $\vec{v} = \vec{v} - \overrightarrow{pb}$ end
<i>avoid_debris</i>	detects the <i>debris_zone</i> agents at less than 2 m, and applies a repulsive force from the location of each detected <i>debris_zone</i> (d)	For each detected debris zone $\vec{v} = \vec{v} - \overrightarrow{pd}$ end
<i>evaluate_speed</i>	calculates the step size ( $s$ ) of the agent according to its natural speed, the reduction factor ( $\gamma$ ) of the slope ( $\theta$ ), and the presence in a <i>debris_zone</i>	$\gamma = e^{-3.5 ( \tan \theta + 0.05  - 0.05)}$ $s = \text{natural\_speed} \times \gamma$ If agent in debris zone If height debris < 1 $s = s \times 0.5$ else $s = 0.16$ end end

From the calculated direction and step size, the next location of the agent is calculated. However, before moving, the agent verifies if its next location is in the free space, i.e. within the boundaries of the model and not in an obstacle.

If the next location is in the free space, the person moves to this new location. However, if the next location falls within an obstacle, we added an additional force to oblige the agent to move around the obstacle, by following the obstacle's boundary. Therefore, the agent's next location is computed as a point at a distance equal to the agent's step size, along the direction of the obstacle's wall (boundary).

On the other hand, if the next location is not in the free space and not in an obstacle, this means that the calculated location was outside the boundary of the model. Therefore, the agent's location is changed to the closest point to its location in the free space.

The movement of an agent is illustrated in Figure 3-23. The flowchart of the motion in the free space can be found in Appendix B.

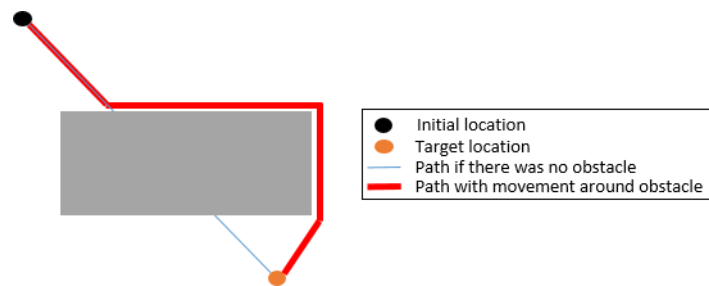


Figure 3-23 : Illustration of the movement around an obstacle by a person agent. The obstacle is represented by the grey rectangle. The person agent moves directly towards its target unless it detects an obstacle. When an obstacle is detected, the agent moves along the boundary of the obstacle.

### 3.8.CONCLUSION

This chapter presented PEERS, a model for the simulation of pedestrians' evacuation in an urban area in the immediate aftermath of an earthquake. PEERS simulates the environmental changes caused by the earthquake: the damages to buildings, the fallen debris resulting from the building damages, and the behavioral adaptations of the individuals, i.e. people's immediate reactions to the sudden onset of an earthquake, as well as their mobility in the city.

PEERS was conceptualized in a multi-model approach, relying on a city model, an earthquake damage model and a human behavior and mobility model. Each sub-model was presented in detail in this chapter, as well as the interactions between the components of each model. The conceptual framework of PEERS was then formalized in the UML language, which served as a blueprint for the implementation of PEERS in GAMA.

Nevertheless, PEERS is a data-rich model that needs to be calibrated by GIS data representing the different components of the urban space and how they are affected by the earthquake. PEERS also needs population data that represents the socio-demographic characteristics of the population and the composition of households. Moreover, PEERS needs to be calibrated with data related to the driving factors behind the behaviors adopted by the population.

Next chapters will focus on the preparation of the data needed for PEERS (Figure 3-24). Namely, Chapter 4 will cover the preparation of the GIS data related to the buildings (and building damages) and the corresponding debris. Then Chapter 5 will cover the mixed approaches and methods for the preparation of additional GIS data as well social and behavioral data.

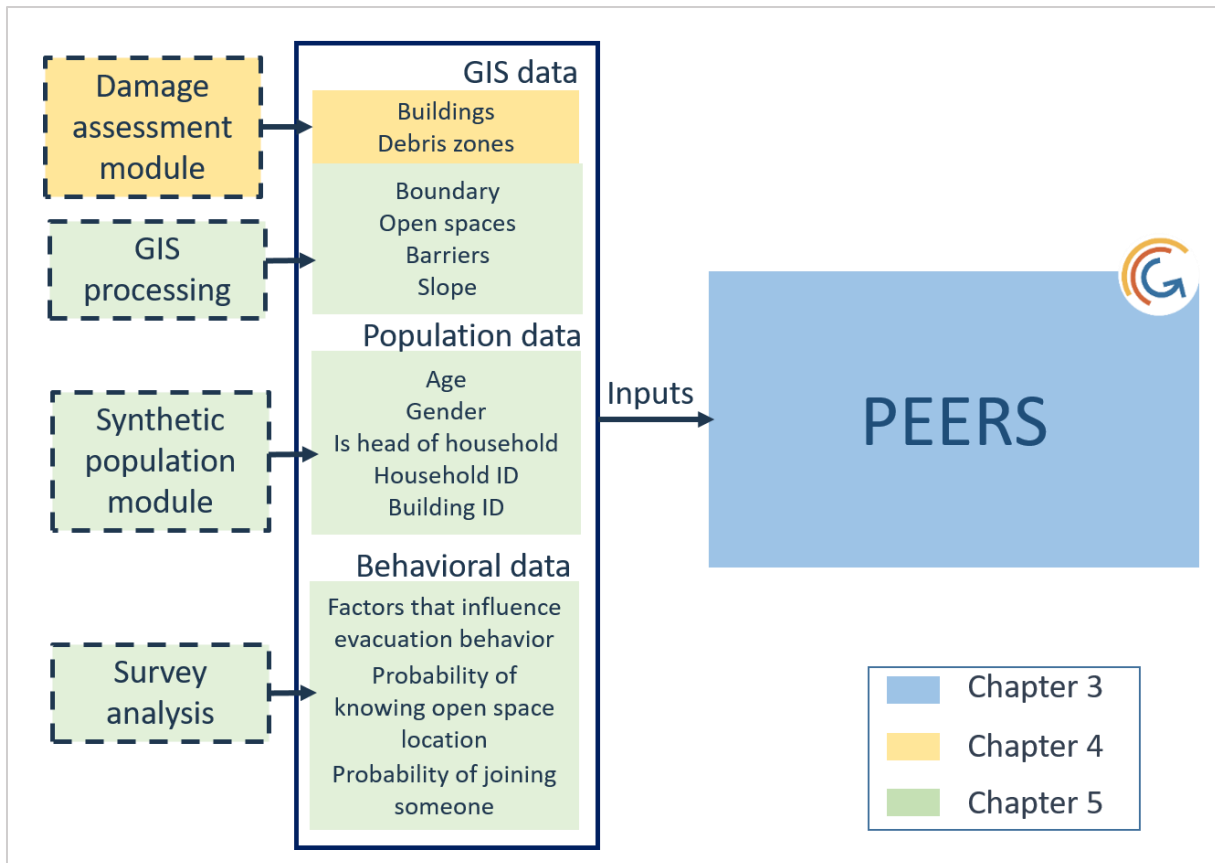


Figure 3-24: Overview of the inputs needed for the simulations in PEERS with the dedicated chapters in this manuscript



# Chapter 4: Estimation of seismic damages and resulting debris in Beirut

## 4.1. INTRODUCTION

Integrated seismic risk modeling requires a realistic assessment of the seismic damages in the urban area. This assessment should capture the spatial variability of the soil and building properties. Additionally, it should take into account the site effects resulting from the local soil conditions and the interplay between the soil and building earthquake responses. Salameh et al. (2017) proposed an approach for the prediction of seismic damages at the building scale, while taking into account the vibrational properties of soil and buildings. This approach is based on Artificial Neural Networks (ANN) that were trained on numerical simulations of soil and building responses. This approach was applied to predict damages in Beirut. Nevertheless, due to the incomplete building database, the assessment could not be done for the whole city.

Moreover, the debris resulting from building damages should also be estimated due to the direct effects of debris on the social environment: falling debris can injure people, and piles of debris obstruct pedestrians' mobility. However, the methodologies found in the literature for estimation of debris extents around buildings only consider cases of complete building collapse and do not account for other damage severity levels.

In this chapter we present the approach that we adopted for the estimation of seismic damages in Beirut, which was applied on a new and complete building database. Then we present the developed methodology for the estimation of debris. Finally, the assignment of casualty rates to buildings and debris is presented.

## 4.2. ESTIMATION OF SEISMIC DAMAGES AT THE BUILDING SCALE IN BEIRUT (LEBANON)

The following sections are part of a paper entitled "Estimating urban seismic damages in Beirut at a fine spatial scale in the context of the lack of comprehensive data" in preparation to be submitted to Natural Hazards. Below is the list of authors grouped by affiliation:

- *ISTerre, LIG, Pacte, University Grenoble Alps, Grenoble, France*: R. Iskandar, B. AL-Tfaily, C. Salameh, P.-Y. Bard, B. Guillier, C. Cornou, P. Lacroix, E. Beck and J. Dugdale;
- *Saint Joseph University, Beirut, Lebanon*: J. Gerard,;
- *Notre Dame University, Zouk, Lebanon*: J. Harb.

### 4.2.1. Introduction

Earthquakes are one of the most devastating natural hazards that cause great loss of life and livelihood especially in dense urban areas located near seismic faults (e.g. Bam, 2003; Haiti, 2010; Christchurch, 2015) (Elnashai and Di Sarno, 2008). Earthquake risk assessment and mitigation was promoted at an international scale in 1990 under the UN-IDNDR (International Decade for Natural Disaster Reduction) by the RADIUS project (Okasaki, 2000). Since then, a large number of methodologies for earthquake risk assessment have been developed, such as HAZUS (Federal Emergency Management Agency (FEMA), 2012), RISK-UE (Mouroux and Le Brun, 2006) and CAPRA (Marulanda et al., 2013). Seismic risk is usually evaluated in terms of the physical damages from probable earthquake shaking and related economic and social losses. The approaches for seismic damage assessment can be divided into two main categories. (1) Macroseismic methods, i.e. empirical methods, such as the EMS-98 method (Grünthal, 1998), that rely on indices derived from post-seismic observations relating building damages to macroseismic intensities. (2) Mechanical methods, such as the Capacity Spectrum Method (CSM) (Chopra and Goel, 1999; Freeman et al., 2004), which are analytical methods based on the building's

capacity curve that represents fundamental building characteristics (the building's stiffness and its ductility capacity). In CSM method, the site and seismic excitation are represented by the response spectrum, which describes the distribution of the spectral acceleration as a function of the spectral displacement imposed by the earthquake. The intersection point of the capacity curve and the response spectrum, denoted the performance point, indicates the maximum displacement of the structure. The expected damages are then quantified by comparing the performance point to the ductility parameters of the structure. The facility and applicability of the CSM made it very popular and it has been adopted in various seismic risk assessment methodologies, such as HAZUS and Risk-UE.

However, one of the limitations of the CSM is that the response spectra used in this methodology are typically generic spectra, which rely on soil classifications based on time-averaged shear wave velocities (usually to a depth of 30 m), that has been found to sometimes fail in representing the actual site amplification (Puglia et al., 2011). Although some methodologies, such as HAZUS, take into account site effects by applying a constant amplification factor that depends on the soil class, this amplification factor remains generic and does not represent accurately the site amplification at the location of the building (Pitilakis et al., 2004).

Additionally, despite repeated observations highlighting the aggravation of building damages due to site effects, and especially to the coincidence of resonance frequency between soils and buildings – also called double-resonance effects - (e.g. Mexico 1985, Mexico 2017; Mayoral et al., 2019; Takewaki, 1998), most seismic damages assessment approaches fail to explicitly take into account site effects.

Recently, Salameh et al. (2017) proposed a seismic damage assessment approach that takes into account the effect of the spectral coincidence between soils and buildings. Another particularity of this approach is that it can be used to estimate damages on a large urban scale, with a micro-resolution of the damage at the building level.

This approach was developed by simulating the structural displacement of buildings having various mechanical characteristics and typologies for different levels of ground motion. To do so, a comprehensive data set of seismic signals, soil profiles and single degree of freedom (SDOF) oscillators was used. These simulations were performed for both linear, and non-linear site responses. From the structural displacement, a building damage index was inferred based on the EMS98 damage levels, on a 0–4 scale as in the RISK-UE project. The same simulations were performed for buildings located on rock (no site effects), which allowed to compute a rock damage index, used to calculate the damage increment between soil and rock conditions. Artificial Neural Networks (ANN) were then trained to predict the damage index (and damage increment) from easily accessible indicators of signal, soil and buildings properties. The best predictors for buildings damages were found to be the Peak Ground Acceleration (PGA) on outcropping rock, the ratio between structure and site ( $f_{struct}/f_{soil}$ ) frequencies and the H/V amplitude ( $A_{OHV}$ ), which is a proxy for the impedance of contrast, the latter being more challenging to determine since it requires obtaining the bedrock's shear wave velocity. The trained ANNs constitute therefore a simple and robust tool to estimate building damages while combining both the spectral content of the ground motion and the dynamic behaviors of the buildings and soils. These ANN could be easily applied at a large scale if the required inputs are available.

The ANN were tested and applied to the city of Beirut, in Lebanon, which allowed to establish damage index and damage increment maps for different levels of seismic shaking. However, one of the limitations of the approach comes from the building data set being incomplete, which only allowed to compute the damages on the eastern and the north-western parts of the city, leaving a void in the central area of Beirut. Another limitation comes from the quantification of the damages in terms of the damage index and damage increment, as it is not a standard metric for the evaluation of buildings damages.

In the present paper, we propose improvements to the model of Salameh et al. (2017) by (i) modeling the non-linear soil behavior using an equivalent-linear (EL) site response analysis instead of a full nonlinear approach -since the EL approach requires less input parameters and performs faster calculations-; (ii) quantifying the building damage using the mean damage defined in Lagomarsino and Giovinazzi (2006) instead of the damage index, and (iii) training a new set of ANNs to predict the mean damage using different combinations of damage predictors, in the aim of improving the performance of the ANN. The newly-trained ANNs are applied to Beirut, where a new 3D building model is derived

using volunteered geographic information, satellite images and machine learning tools, with the aim to predict buildings damage maps at the scale of the city for different seismic scenarios.

The paper is organized in two main sections: the first section focuses on the approach adopted to estimate the mean damages, from numerical simulations to training the ANN. The second section covers the application on Beirut, namely the acquisition of the new building database and the damage assessment results.

#### **4.2.2. Method for estimating seismic damages building by building**

##### **4.2.2.1. Simulation of the non-linear site response**

Several observations after large earthquake have outlined that under strong ground shaking, the soil's behavior becomes nonlinear as it manifests by the shift of the soil's resonance frequency to lower frequencies and the reduction of the soil's amplification (Beresnev and Wen, 1996). The soil's nonlinear behavior is a result of the reduction of the soil's shear modulus and the increase in damping that occur when the soil undergoes high deformation levels (Finn, 1991). The soil's nonlinear behavior has also been demonstrated by laboratory tests on different types of soils, which resulted in laws that can be applied for the simulation of the soil's nonlinear behavior (Hardin and Drnevich, 1972a, 1972b). These laws, called degradation curves, relate the loss in shear modulus and the increase in damping to the level of shear strain in the soil. The dynamic soil response can be simulated by fully nonlinear models, such as NOAH (Bonilla, 2001), in which the dynamic equation of motion is integrated in the time-domain at small incremental steps. On the other hand, the computation of the nonlinear soil response can be simplified by an Equivalent Linear (EL) site response analysis, in which the nonlinear soil behavior is simulated by a linear elastic model, with dynamic values of the shear modulus and damping updated iteratively to correspond to the level of strain achieved by the soil according to given degradation curves. Although the EL site response analysis is an approximation of the actual nonlinear response of the soil, this approach has proved to be computationally efficient, capable of providing reasonable results for many practical problems and is widely used by the earthquake-engineering community (Assimaki et al., 2011; Kaklamanos et al., 2015; Kim et al., 2016).

As the EL approach is less computationally demanding than the full nonlinear method, we have simulated the EL site response of the 887 1-D multi-layered soil profiles for 60 synthetic base rock accelerations ranging from 0.02 to 8.6 m/s<sup>2</sup> and 141 elasto-plastic single degree of freedom (SDOF) oscillators representing different building typologies as used in Salameh et al. (2017). The distribution of the dataset's characteristics can be found in Appendix C. The simulations were performed in SHAKE (Schnabel et al., 1972) which computes the response to vertically propagating plane shear waves of a layered soil profile overlying a uniform half-space. In SHAKE, the soil profile is defined in terms of each sublayer's shear wave velocity, damping ratio, shear modulus and damping degradation curves, total unit weight and thickness. The degradation curves of Darendeli (2001) were used as they are generic curves composed of simple equations, which makes them easy to adapt to any soil type. Nevertheless, the application of Darendeli's relationships requires values of plasticity index and overconsolidation ratios, parameters that are not provided in the soil database. Due to the absence of these site-specific information in the synthetic soil profiles, all the soils were assumed to be dry sand, which yields to values of both plasticity index and overconsolidation ratio equal to 0. The assumption of dry sand is at first order well suited to the study case of Beirut according to the known surface geology (Dubertret, 1945). It should be noted that this assumption leads to an exaggeration of the soil's nonlinearity.

The non-linear surface ground motion synthetics were analyzed by calculating the site's transfer function (TF) as the ratio of the Fourier amplitude spectrum of the surface ground motion to that of a reference outcropping rock (Borcherdt, 1970). The TF provides frequency-dependent amplification of the bedrock input motion by the soil deposit (Kramer, 1996). The typical shape of the TF displays many peaks, the peak at lowest frequency occurring at the site's fundamental resonance frequency. When soils behave nonlinearly under strong ground seismic excitation, the fundamental resonance frequency is decreased together with amplification and de-amplification of the surface ground motion at frequencies

below and beyond the fundamental resonance frequency, respectively (Bonilla, 2005; Frankel, 2002; Regnier et al., 2013). Figure 4-1 shows the TFs of one of the sites in the dataset (site AKTH05 from the KiK-Net database) computed for the EL soil response for various bedrock accelerations. The TF corresponding to a linear soil response is also shown for reference. We can see that the site response in the EL case depends on the PGA reached at the top of the soil column (surface PGA): while the TFs are relatively close to the linear TF for low-to moderate surface PGA ( $< 2 \text{ m/s}^2$ ), the fundamental resonance frequency is decreasing for larger surface PGA by about 20% for the largest surface PGA (from 9 Hz in the linear case to 7 Hz in the non-linear case). The seismic amplification is reduced as well at the fundamental resonance frequency (by around 10% for the largest surface PGA) and at high frequencies, reaching up to a 40% reduction of the amplification at 20 Hz, while slighter amplification is observed at low frequency.

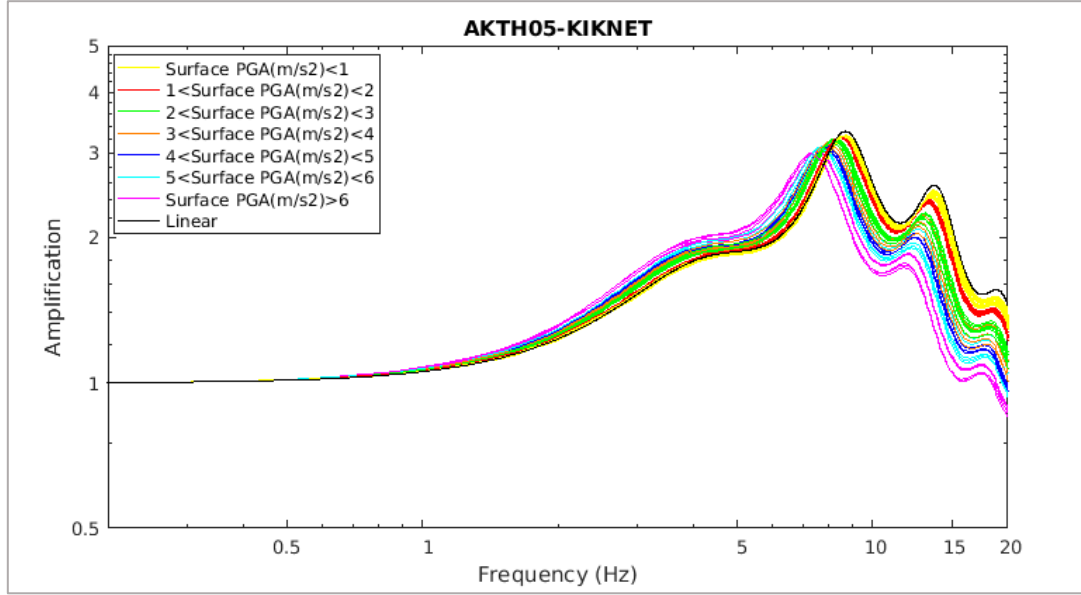


Figure 4-1 : Site transfer functions for the site AKTH05 from the Kik-Net database computed from the results of the nonlinear site response analysis under 60 different seismic loadings. The site transfer function for the linear site response is plotted in black and the non-linear site responses are indicated in color according to the surface PGA.

#### 4.2.2.2. Computation of the building mean damage

The structural displacement was simulated by computing the relative displacement of the damped elastoplastic SDOF oscillators (without including soil-structure interactions for simplification) by solving the dynamic equation of motion using the step-by-step Newmark method:

$$m \times \ddot{d} + c \times \dot{d} + k \times d = -m \times a_{S,i} \quad (4.1)$$

where  $d$  (m) is the displacement of the elastoplastic oscillator,  $\dot{d}$  (m/s) is its velocity, and  $\ddot{d}$  ( $\text{m/s}^2$ ) its acceleration.  $m$  (kg) is its mass,  $c$  is the viscous damping taken equal to 5%,  $k$  is its rigidity and  $a_{S,i}$  ( $\text{m/s}^2$ ) is the surface acceleration at the base of the oscillator (top of soil column) obtained from the equivalent linear calculations.

The building mean damage was then estimated following the mechanical model proposed by Lagomarsino and Giovinazzi (2006). In this approach, four structural displacement thresholds,  $S_{d,k}$  ( $k=1\dots4$ ), were specified according to the yielding ( $d_y$ ) and ultimate ( $d_u$ ) displacements of the building, which allowed to define four damage states  $D_{S,k}$  ( $k=1\dots4$ ) as follows:

$$\begin{aligned} S_{d,1} &= 0.7 d_y ; D_{S1} = \text{Slight damage} \\ S_{d,2} &= 1.5 d_y ; D_{S2} = \text{Moderate damage} \\ S_{d,3} &= 0.5(d_y + d_u) ; D_{S3} = \text{Extensive damage} \end{aligned}$$

$$S_{d,4} = d_u; D_{S4} = \text{Complete damage}$$

In a second step, the probability that a damage reaches or exceeds a certain damage state  $D_{Sk}$ , is expressed as a function of the maximum displacement  $d_{max}$  reached by the oscillator and the displacement thresholds  $S_{d,k}$ , using a lognormal cumulative probability function as follows:

$$P[D_{Sk}|d_{max}] = \Phi \left[ \frac{1}{\beta} \ln \left( \frac{d_{max}}{S_{d,k}} \right) \right] \quad (k = 1, 2, 3, 4) \quad (4.2)$$

$$\beta = 0.4 \ln \mu \quad (4.3)$$

$$\mu = \frac{d_u}{d_y} \quad (4.4)$$

where  $\Phi$  is the normal cumulative function,  $\beta$  is the normalized standard deviation of the natural logarithm of the displacement threshold, defined as a function of  $\mu$ , the ductility capacity of the building.

Finally, the mean damage ( $\mu_{DS}$ ) is computed as:

$$\mu_{DS} = \sum_{k=1}^4 k P_{Sk} \quad (4.5)$$

Where  $P_{Sk}$  is the probability of reaching each damage limit state, derived from the cumulative distribution as follows:

$$P_{S4} = P[D_{S4}|d_{max}] \quad (4.6)$$

$$P_{Sk} = P[D_{Sk}|d_{max}] - P[D_{S_{k+1}}|d_{max}] \quad (k = 1, 2, 3) \quad (4.7)$$

$$P_{S0} = 1 - P[D_{S1}|d_{max}] \quad (4.8)$$

Table 4-1 shows the range of displacements attained by the oscillators, and the corresponding mean damage ranges. The mean damages range between values around 0 (No damage) and reach a value of 4, corresponding to complete damage.

Table 4-1 : For each building class, range of fundamental building resonance frequency ( $f_{struct}$ ), yielding ( $d_y$ ), ultimate ( $d_u$ ), maximum ( $d_{max}$ ) displacement and mean damage ( $\mu_{DS}$ ).

Building class	$f_{struct}$ range (Hz)	$d_y$ range (m)	$d_u$ range (m)	$d_{max}$ range (m)	$\mu_{DS}$ range
Class 1	2 - 6.7	0.0015- 0.0107	0.0070 - 0.0387	$1.2477 \times 10^{-5}$ - 0.5	0 - 4
Class 2	0.77 - 1.85	0.015 - 0.0407	0.0451 - 0.1227	$3.8239 \times 10^{-5}$ - 0.9023	0 - 4
Class 3	1.1 - 2.33	0.0108 -0.0709	0.0324 - 0.2125	$4.3947 \times 10^{-5}$ - 0.7237	0 - 4

#### 4.2.2.3. Training Artificial Neural Networks for the prediction of mean damage

The ANN approach is a statistical learning algorithm inspired by biological neural networks. Its main characteristic is investigating, without any a priori knowledge, the relationship between input and output variables (McCulloch and Pitts, 1943; Minsky and Papert, 1969). The use of ANNs has emerged in the geophysical field particularly between 1989 and 1994 (Poulton, 2001) and has since become a popular tool in solving complex geophysical problems. Following Salameh et al.(2017), we have used ANNs to identify the relationship between the mean damage and indicators related to soil, building and input earthquake signal characteristics. While keeping the same neural network architecture and activation functions, the main changes compared to Salameh et al.(2017) were the choice of the mean damage as the output variable and testing different combinations of input variables as predictors of the mean damage. Moreover, similar to Salameh et al.(2017), the ductility capacity of the buildings was not

considered to be an input variable in the ANNs; instead, an independent neural network was created for each building typology, namely for masonry buildings (Class 1), non-designed reinforced concrete buildings (Class 2) and DCL reinforced concrete buildings (Class 3).

Feedforward neural networks with a supervised learning paradigm were created using the MATLAB® Neural Network Toolbox™ in the following architecture:

- i) an input layer containing the explanatory variables, made of 3 to 5 neurons, depending on the number of explanatory variables considered;
- ii) a single hidden layer, containing 10 neurons;
- iii) an output layer with 1 neuron, containing the variable we aim to estimate, the mean damage herein.

The activation functions were the tangential sigmoid activation function in the hidden layer and the linear sigmoid in the output layer. For the choice of damage indicators, in addition to variables retained by Salameh et al. (2017) - i.e. PGA,  $A_{0HV}$  as the amplitude of the H/V peak at the fundamental resonance frequency serving as a proxy to site amplification in the linear case and the ratio between the fundamental resonance frequency of the building ( $f_{struct}$ ) and the soil ( $f_{soil}$ ),  $f_{struct}/f_{soil}$  - we have also considered  $f_{struct}$  and  $f_{soil}$  separately instead of the frequency ratio. Finally, the Peak Ground Velocity (PGV) on outcropping rock was also considered as a proxy of the seismic signal, as several studies have found the PGV to be a better proxy for macroseismic intensity than the PGA (Kästli and Fäh, 2006; Wald et al., 1999a). 9 different combinations of these variables were formed, in a way that each combination included at least one proxy for each of the signal, site and structure. Each one of the 9 artificial neural networks was trained for building classes 1, 2 and 3 and the ANN's performance was assessed by the coefficient of determination  $R^2$  (from 0 to 1), which shows how well the independent variables (the input variables) can predict the variation in the dependent variable (the mean damage).

The ANNs' input variables and performances are summarized in Table 4-2. We can see that all the neural networks performed comparably well in estimating the mean damages, as demonstrated by the high  $R^2$  values ranging from 0.8845 to 0.9602.

By comparing the  $R^2$  values in ANN1 and ANN2, the PGV seems to perform better than the PGA in explaining the buildings' mean damages, especially for Class 2 buildings. The same applies for the improvement between ANN3 and ANN4, as well as between ANN5 and ANN6. On the other hand, the consideration of both PGA and PGV simultaneously as proxies of the seismic signal (ANN7, ANN8 and ANN9), improved the prediction of the mean damages. In ANN3, the consideration of  $f_{soil}$  and  $f_{struct}$  separately did not lead to the improvement in the  $R^2$  values in any of the classes with respect to ANN1. However, in ANN5, the separation of  $f_{struct}$  and  $f_{soil}$  without removing  $A_{0HV}$  improved the performance for Class 1 but worsened it for the other building classes. By comparing ANN7 and ANN8, where the only difference is the replacement of  $A_{0HV}$  in ANN7 by  $f_{soil}$  in ANN8, we can see that  $A_{0HV}$  performed better in explaining the damages than  $f_{soil}$ , when  $f_{struct}/f_{soil}$  was considered as well. Finally, the consideration of all the variables separately in ANN9, improved the prediction of the mean damages for Class 1 compared to ANN7 while the ANN's performance declined for Classes 2 and 3.

Finally, while the best performance for Class 1 is achieved in ANN9, ANN7 ensures the best performance for Classes 2 and 3 buildings and was retained as the optimal neural network for the prediction of the building mean damage.

Table 4-2 : Summary of the input variables and the performance of the 9 ANNs trained to estimate the mean damages of building classes 1, 2 and 3. ANN1 is composed of the same input variables as in Salameh et al. 2017. The underlined input variables from ANN2 to ANN9 represent the variables that were changed with respect to ANN1. The values of  $R^2$  highlighted in bold represent the maximum  $R^2$  attained for each building class.

ANN	Nb. of input variables	Input variables	Coefficient of determination $R^2$		
			Class 1	Class 2	Class 3
ANN1	3	PGA; $A_{0HV}$ ; $f_{struct}/f_{soil}$	0.8778	0.9153	0.8597
ANN2	3	<u>PGV</u> ; $A_{0HV}$ ; $f_{struct}/f_{soil}$	0.8793	0.9579	0.8735
ANN3	3	PGA; <u><math>f_{soil}</math></u> ; <u><math>f_{struct}</math></u>	0.8724	0.9038	0.8466
ANN4	3	<u>PGV</u> ; <u><math>f_{soil}</math></u> ; <u><math>f_{struct}</math></u>	0.8817	0.9514	0.8662
ANN5	4	PGA; $A_{0HV}$ ; <u><math>f_{soil}</math></u> ; <u><math>f_{struct}</math></u>	0.8855	0.9111	0.8551
ANN6	4	<u>PGV</u> ; $A_{0HV}$ ; <u><math>f_{soil}</math></u> ; <u><math>f_{struct}</math></u>	0.8866	0.9551	0.8785
ANN7	4	PGA; <u>PGV</u> ; $A_{0HV}$ ; $f_{struct}/f_{soil}$	0.8957	<b>0.9602</b>	<b>0.8845</b>
ANN8	4	PGA; <u>PGV</u> ; <u><math>f_{soil}</math></u> ; $f_{struct}/f_{soil}$	0.8836	0.9549	0.8752
ANN9	5	PGA; <u>PGV</u> ; $A_{0HV}$ ; <u><math>f_{soil}</math></u> ; <u><math>f_{struct}</math></u>	<b>0.8981</b>	0.9594	0.8804

After identifying the optimal neural network, we investigated the input variables' synaptic weights, i.e. relative importance of each input variable in ANN7 in the prediction of the buildings' mean damages. We can see in Figure 4-2 that for Class 1 buildings, the PGV has the highest synaptic weight (37.7%), followed by  $f_{struct}/f_{soil}$  (29.1%). For Class 2 buildings,  $f_{struct}/f_{soil}$  has a higher synaptic weight (38.1%) than the PGV (34.2%), however for Class 3 buildings  $f_{struct}/f_{soil}$  is the predominant indicator with a synaptic weight (68.7%), while all the other variables have significantly lower weights. From the synaptic weights distribution, it can be concluded that it is  $f_{struct}/f_{soil}$  and the PGV that mostly control the buildings mean damages, followed by the PGA and finally the  $A_{0HV}$ .

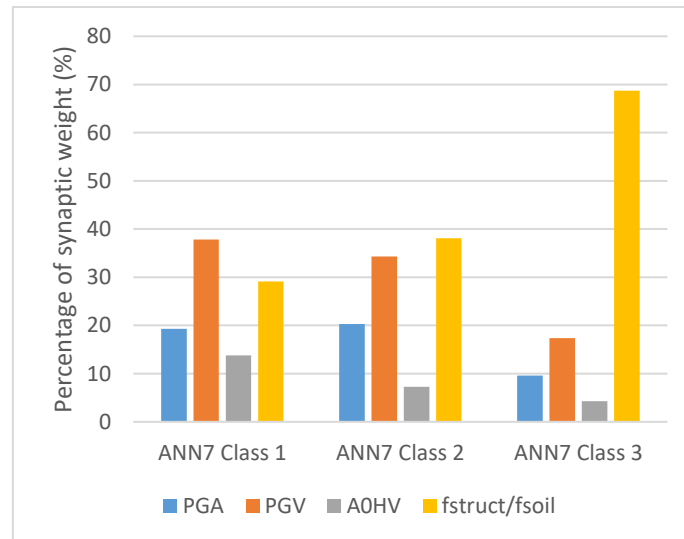


Figure 4-2 : Synaptic weight proportions for the inputs of ANN7 for building classes 1, 2 and 3.

#### 4.2.2.4. Summary

Artificial neural networks were trained on the prediction of buildings mean damages resulting from extensive simulations of the site and buildings responses to synthetic input motion on a comprehensive dataset of soil profiles and SDOF oscillators. Several proxies for structure, soil and signal properties were tested to find the optimal predictors of the mean damage. It was found that the PGV is a better

proxy for the input ground motion than the PGA. However better performances were achieved by considering both the PGA and the PGV simultaneously. The frequency ratio  $f_{\text{struct}}/f_{\text{soil}}$  explained better the damage for reinforced concrete buildings (Classes 2 and 3), while considering  $f_{\text{struct}}$  and  $f_{\text{soil}}$  separately improved the prediction of mean damages in masonry buildings (Class 1).  $A_{0\text{HV}}$  performed better than  $f_{\text{soil}}$  in the damage prediction when considered with  $f_{\text{struct}}/f_{\text{soil}}$ . Nevertheless, the best performances were reached when considering: PGA, PGV,  $A_{0\text{HV}}$  and  $f_{\text{struct}}/f_{\text{soil}}$  as input variables in the ANNs. The corresponding ANNs for each building class were retained for the estimation of the buildings mean damages in Beirut.

#### **4.2.3. Generation of a 3D building model in Beirut and estimation of the seismic damages**

The estimation of the seismic damages in Beirut using the trained ANN requires spatial inputs related to the soil and building resonance frequencies as well as the building typology. Salameh et al. (2017) estimated the damages at the scale of Beirut, using data on soils and buildings in Beirut provided by the ANR-LIBRIS project (2010-2014), a collaborative project between French and Lebanese research institutes. However, one of the limitations of the damages estimated by Salameh et al. (2017) was due to the incomplete building inventory in Beirut; which only allowed the computation of the damages on the eastern and the north-western parts of the city, leaving a void in the central area of Beirut where the damages could not be estimated.

In order to extrapolate the building damages throughout the city, we have relied on the existing building database, satellite images and volunteered geographic information to generate a 3D building model in Beirut and related seismic vulnerability. The use of satellite images and/or open-accessible geospatial data have been found to be highly relevant for setting up seismic exposure models (Geiß et al., 2017; Gomez-Zapata et al., 2022; Krayem et al., 2021; Nievas et al., 2022). The building mean damages were then estimated for the generated buildings model. The following sections are organized as follow: section 4.2.3.1 covers the description of the existing soils and buildings database in Beirut, section 4.2.3.2 presents the approach for the generation of the 3D building model and 4.2.3.3 presents the results of the application of the ANNs on the new building database.

##### **4.2.3.1. Existing Beirut's soil and buildings database**

###### **4.2.3.1.1. Fundamental soil resonance frequency map**

In the framework of the ANR-LIBRIS project, soils investigations campaigns were carried out in Beirut and part of its suburbs. This project allowed to investigate 827 sites using seismic noise recordings (Brax et al., 2018; Salameh et al., 2017; Salloum et al., 2014). The soil fundamental resonance frequency ( $f_{\text{soil}}$ ) could be obtained from these recordings using the HVSR (horizontal to vertical spectral ratio) approach (Nakamura, 1989). From these measurements, interpolated maps of both the  $f_{\text{soil}}$  and  $A_{0\text{HV}}$  were derived for the surveyed area and are displayed in Figure 4-3. The high resonance frequencies (above 10 Hz) and low  $A_{0\text{HV}}$  (around 1) observed in the east and west of Beirut suggest the presence of rock sites in these areas. On the other hand, the presence of soil deposits can be observed in areas with low resonance frequencies (between 1 and 3 Hz), namely in the northern and the southern sides of Beirut.

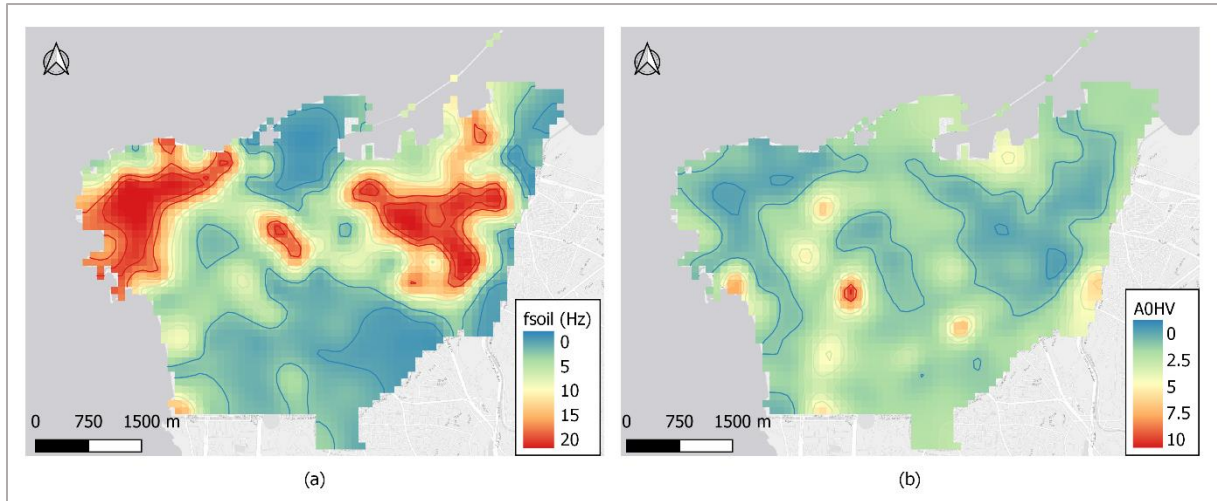


Figure 4-3 : Interpolated maps of  $f_{soil}$  and  $A_{OHV}$  in Beirut derived from the ambient vibration measurements performed in Salloum et al. (2014), Salameh et al. (2017) and Brax et al. (2018)

#### 4.2.3.1.2. Building inventory

As part of the ANR-LIBRIS project, the Saint Joseph University (USJ) conducted extensive surveys on Beirut's buildings; collecting coordinates, construction year and number of floors of 7362 buildings in Beirut Salameh (2016). Due to security and political constraints at the time of the project, the buildings survey was restricted to the eastern and north-western sectors of the city as shown in Figure 4-4. The histograms in Figure 4-5 show the distribution of the surveyed buildings according to their number of floors and construction date.

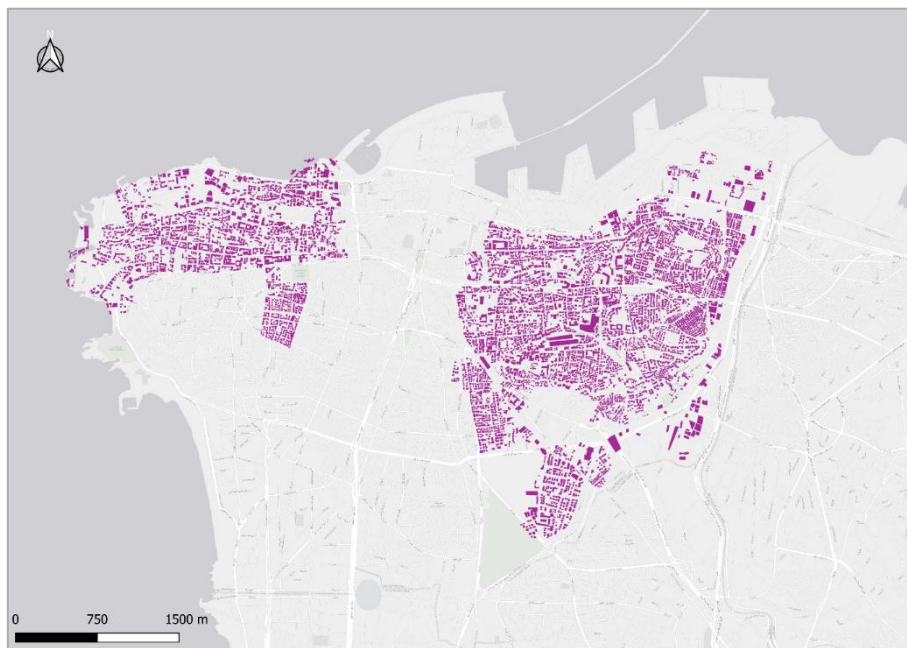


Figure 4-4: Buildings in Beirut surveyed in the framework of the LIBRIS project (Salameh, 2016)

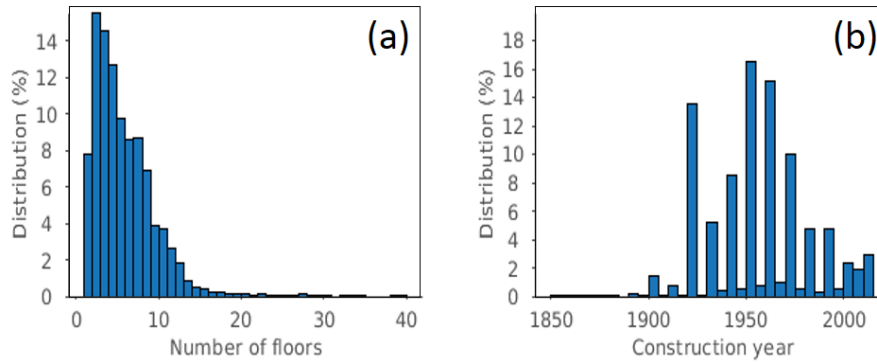


Figure 4-5 : Distribution of the surveyed buildings according to (a) their number of floors and (b) construction year

#### 4.2.3.1.3. Buildings fundamental resonance frequency and typology

Seismic noise measurements were carried out on another set of 330 buildings, which allowed the extraction of the fundamental resonance frequency of these buildings, in addition to the collection of their construction year and number of floors. From the measured resonance frequencies, the relationship between the number of floors, soil type and resonance frequency was derived (Salameh et al., 2016) as follows:

- $f_{\text{struct}} = 23/\text{number of floors}$ , for buildings constructed on rock sites;
- $f_{\text{struct}} = 18/\text{number of floors}$ , for buildings built on soft sites.

In addition, Salameh et al. (2017) proposed a classification of the buildings' typologies based on their number of floors and construction period. Buildings constructed before 1950 with less than 4 floors consisted mainly of masonry buildings (Class 1), buildings constructed before 1950 with 4 floors and more and buildings constructed between 1950 and 2005 were classified as non-designed reinforced concrete (Class 2), and buildings built after 2005 were considered as designed reinforced concrete with low ductility (Class 3). The distribution of the typology of the surveyed buildings in Beirut is shown in Figure 4-6.

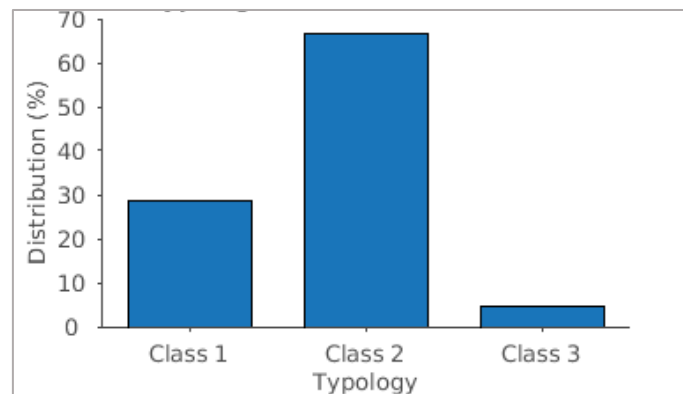


Figure 4-6: Distribution of the typology of the buildings surveyed in the framework of the LIBRIS project (Salameh et al., 2016)

#### 4.2.3.2. 3D building model for Beirut from OSM data, satellite images and machine learning tools

In countries like Lebanon, where comprehensive and openly accessible buildings databases are missing, volunteered geographic information, such as the data provided by OpenStreetMap (OSM) (<https://www.openstreetmap.org/>) can provide a suitable alternative. OSM is a digital cartography platform where volunteers contribute in mapping geospatial objects such as buildings, streets and leisure areas. Beirut buildings could be found in OSM; however in some areas, not all buildings were mapped (digitized). Consequently, we contributed to the digitization of missing buildings on OSM. Finally, the

OSM database of buildings in Beirut was extracted on 26/02/2021. The OSM database contains footprints of 15 089 buildings, displayed in Figure 4-7.

Applying the ANN trained in the previous section on the OSM database requires first to derive the typology of the OSM database buildings and their resonance frequency. This information can be inferred from the LIBRIS database. We derived statistical relationships between buildings' number of floors, resonance frequencies and construction periods and from high-resolution satellite images to estimate building height – and hereafter number of floors and construction - for each OSM building not included in the LIBRIS database.

**4.2.3.2.1. Subset of representative buildings from LIBRIS database**

Although the LIBRIS database contains valuable attributes (construction period and number of floors) for 7 692 buildings in Beirut, the attributes of the corresponding OSM buildings could not be directly identified from the LIBRIS database due to georeferencing incompatibilities between the LIBRIS and the OSM layers, as displayed in Figure 4-8, which make the spatial comparison of these two layers impossible. These georeferencing incompatibilities are due to the use of a combination of several projection systems when digitizing the building footprints in LIBRIS.

To overcome this limitation and to make use of the information provided in LIBRIS, a subset of 947 buildings from the LIBRIS buildings were manually identified in the OSM database by finding the footprints of identical buildings in the two datasets. The buildings were selected by picking all buildings that have more than 10 floors in LIBRIS, and a representative set of buildings with lower number of floors. We aimed to sample the overall distribution of number of floors and construction period in the LIBRIS database (Figure 4-5) while selecting buildings in the western and eastern parts of Beirut. The spatial distribution of the selected buildings is displayed in Figure 4-9. The attributes related to the number of floors and the construction year were added to the corresponding OSM buildings. The distribution of the building attributes in this dataset (referred to as LIB-STAT) is displayed in Figure 4-10. This subset is assumed to be representative of the Beirut buildings and was used to derive statistical relationships between different building attributes, in order to estimate the OSM buildings' number of floors and construction periods.

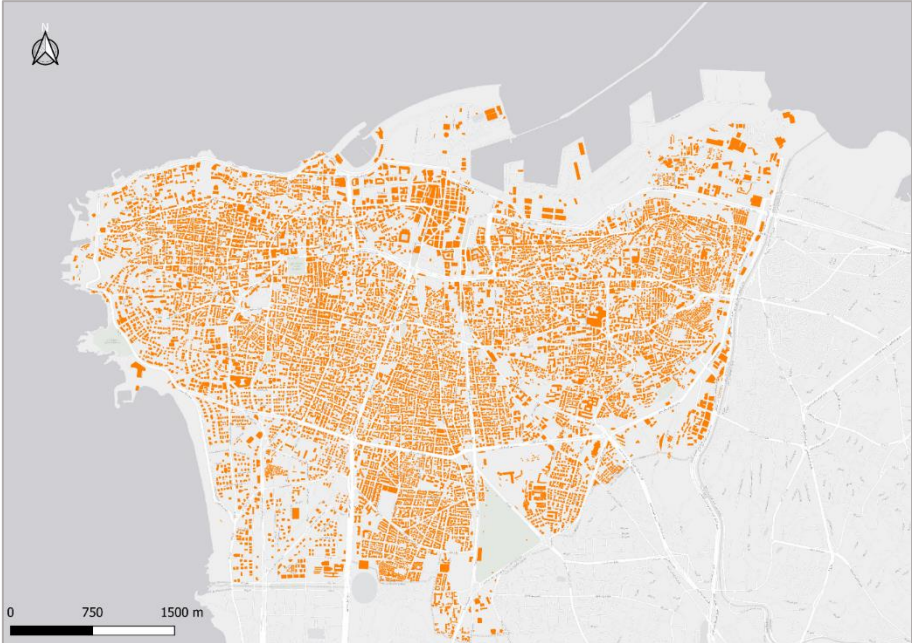


Figure 4-7: Buildings footprints retrieved from OSM



Figure 4-8 : Geolocalisation incompatibilities between the LIBRIS buildings (purple) and the OSM buildings (orange)

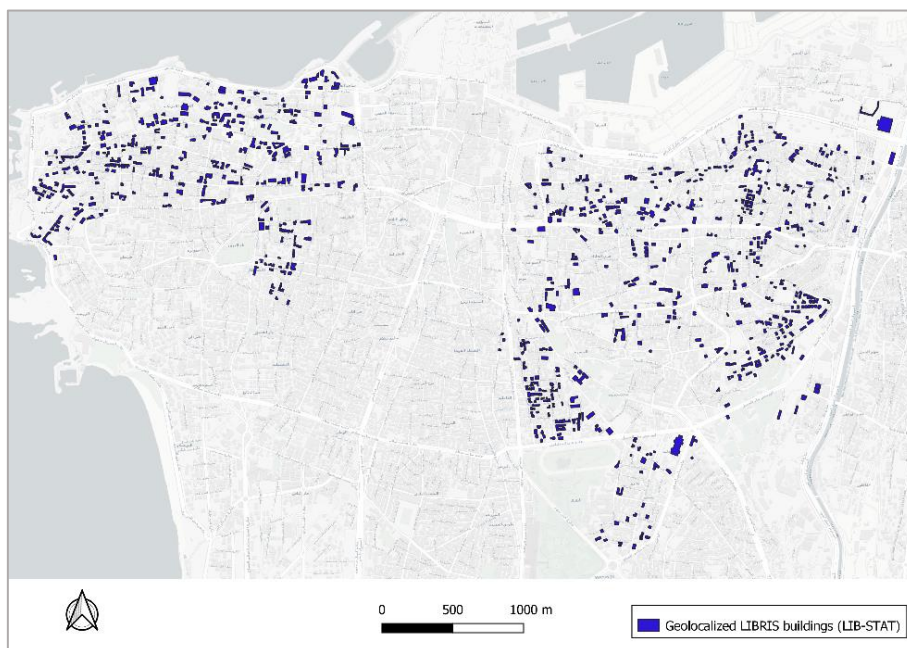


Figure 4-9: Spatial distribution of the 947 geolocalized LIBRIS buildings (LIB-STAT)

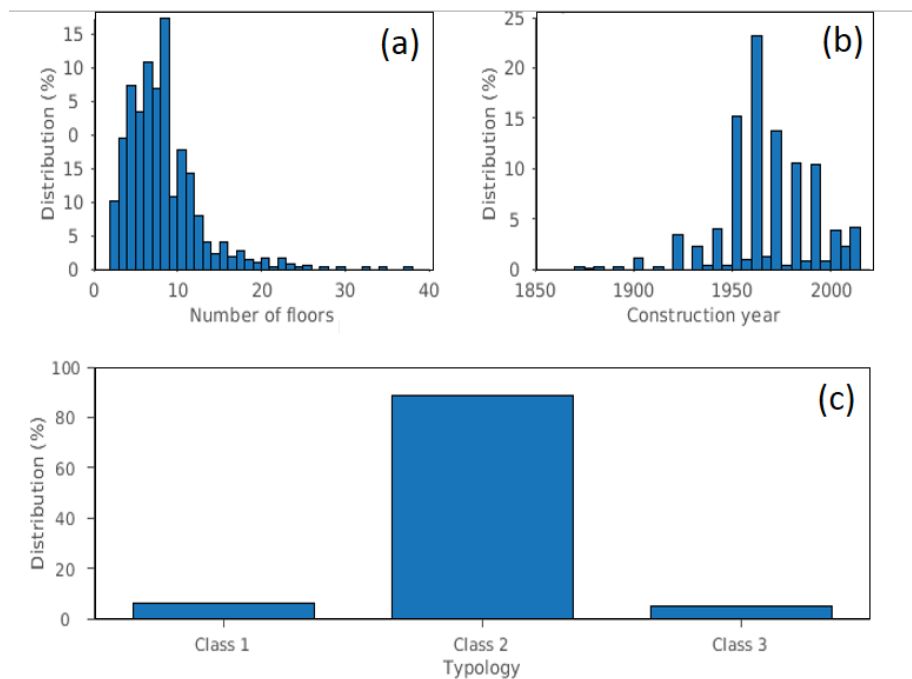


Figure 4-10 : Distribution of the buildings' number of floors (a), construction year (b) and class (c) in the subset of 947 extracted from LIBRIS for the statistical analysis (LIB-STAT)

#### 4.2.3.2.2. Estimation of the building's heights from satellite images

The heights of the buildings in Beirut was retrieved from processing of high-resolution satellite images. Tri-stereo Pleiades 1-B<sup>6</sup> satellite images (resolution 0.7 m) acquired in July 2016 on Beirut and its surroundings (Figure 4-11) were kindly provided by the Centre National d'Etudes Spatiales (CNES) through the DINAMIS<sup>7</sup> project.

The set of the three panchromatic images were processed using the Ames Stereo Pipeline software (Broxton and Edwards, 2008), an automated stereo processing software developed by the NASA Ames Research Center, capable of generating high-quality surface elevation models from satellite images. The processing steps can be summarized as follows:

- (1) Each image is map-projected using a low resolution (10 m) Digital Terrain Model (DTM) covering the area of Beirut.
- (2) Each pair of the tri-stereo image is then bundle adjusted (Triggs et al., 2000) by automatically extracting tie points, i.e. features that can be clearly identified in the two images and that can be selected as reference points. This step allows to find the disparities between each pair of images.
- (3) The final step is the triangulation step, in which the intersection between all the rays coming from the tie points are jointly found in the three images. This step leads to the derivation of a 3D point cloud, containing the information of the surface elevation at each point in the satellite images.

The point cloud is then converted into a grid mesh regularly spaced every 2 m, which is approximately three times the resolution of the initial images. This grid mesh constitutes the Digital Surface Model (DSM) (Figure 4-12, Figure 4-13 (a)), which represents the elevation model of the earth's surface including the elevation of the above-the-ground features (trees, buildings, etc...). As we are interested in the heights of the buildings in Beirut, we need to determine the height of the above-the-ground features, which we call the Digital Features Model (DFM). The DFM can be obtained by subtracting the

<sup>6</sup> <https://www.intelligence-airbusds.com/imagery/constellation/pleiades/>

<sup>7</sup> <https://dinamis.data-terra.org/organisation/>

elevations of the bare earth (DTM) from the DSM, as illustrated in Figure 4-12.

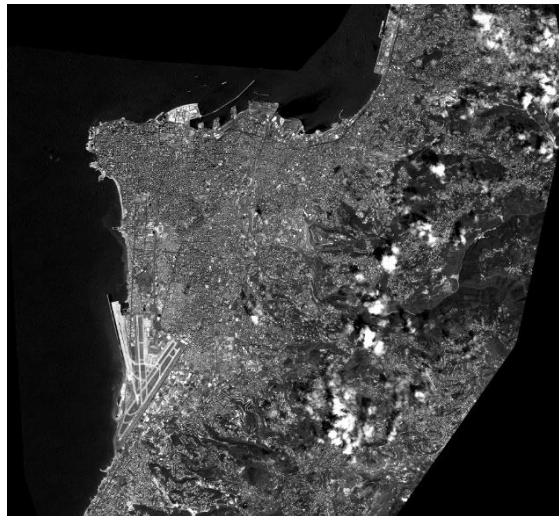


Figure 4-11: Preview of one of the Pleiades 1-B panchromatic satellite images taken over Beirut

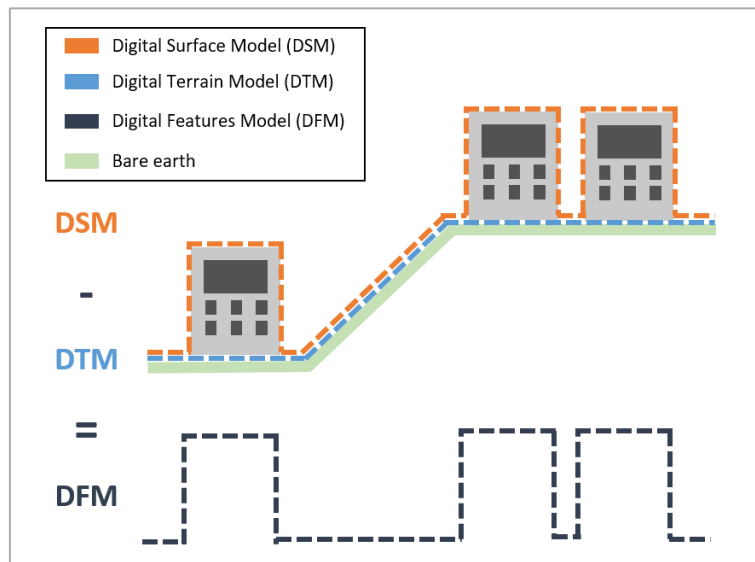


Figure 4-12: Digital elevation models

To derive a high-resolution DTM, the generated DSM was treated in the geographic information system software QGIS (Quantum GIS), using the SAGA-GIS module DTM-filter. This module allows the automatic detection of the cells in the DSM that correspond to bare earth and the cells that correspond to elevated objects. After identifying the bare earth cells, the gaps between these cells were filled by performing a Multilevel B-spline interpolation in QGIS, and therefore reconstructing a Digital Terrain Model (DTM) (Figure 4-13 (b)). The elevations of the DTM were then subtracted from the DSM, which resulted in the generation of a DFM for Beirut (Figure 4-13 (c)). Elevations less than 2 m in the DFM were filtered out, since they are too low to correspond to building heights. Then for each building, the mean DFM value of the cells occupied by the building's footprint was assigned as the building height.

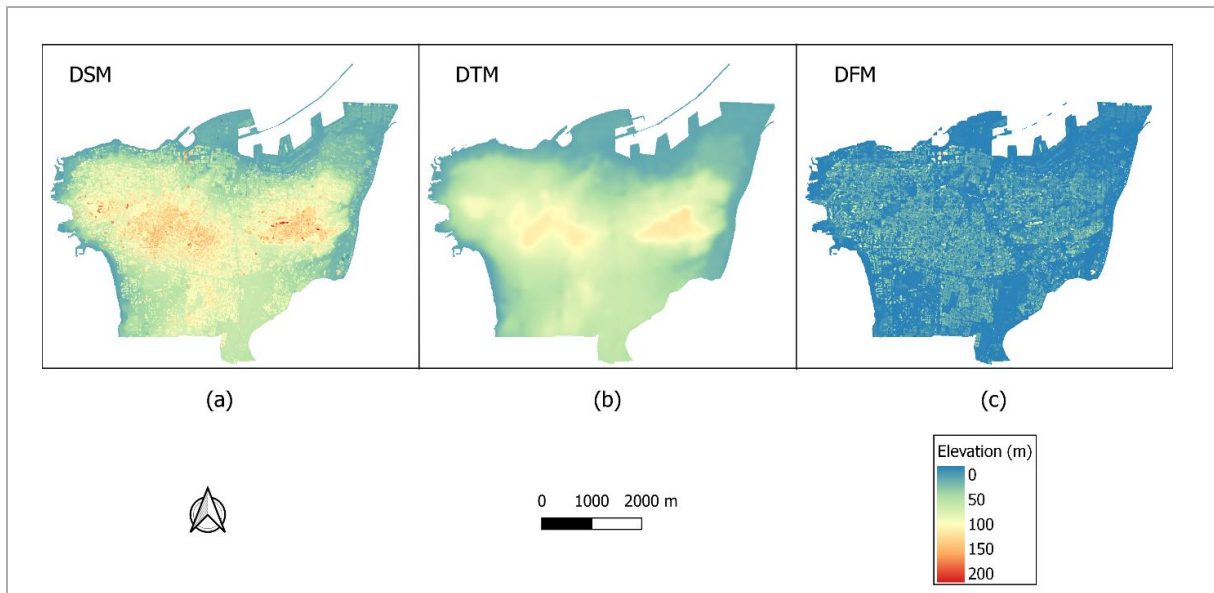


Figure 4-13: Beirut elevation models derived from processing high-resolution satellite images

To estimate the error in the prediction of the building's heights from the DFM, we have compared for the LIB-STAT dataset, the building heights retrieved from the DFM to the heights provided in OSM when available, or to the building heights estimated by multiplying the number of floors by an approximate story height of 3 m (Figure 4-14).

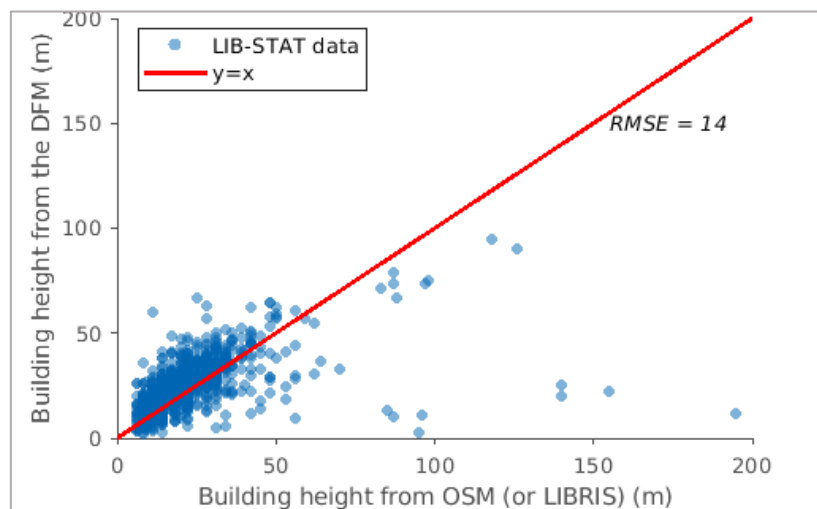


Figure 4-14 : Comparison of the DFM building heights to the building height retrieved from OSM or LIBRIS

On Figure 4-14, we can see that the DFM is able to reproduce the building height with an average error of 14 m. The height of the buildings having less than 50 m is slightly overestimated in the DFM, while the elevation of high-rise buildings (100 m and higher) is underestimated. We have investigated the possible causes of the poor identification of tall buildings by examining the distribution of the DFM values and the quality of the DSM at the location of 9 well-known skyscrapers in Beirut (Table 4-3 and Figure 4-15).

We can see in Table 4-3 that the the highest values taken by the DFM for the “Sama Beirut”, “20|30”, “Les domes de Sursock” and “Crédit Libanais” towers (35.1 m, 30.8 m, 60.4 m and 27.4 m high, respectively) are way less than the actual building heights which exceed 130 m for the four buildings. Furthermore, we can see in Figure 4-15 that the DSM is poorly constrained for these buildings, as the DSM has many “no data” cells (no color) at the buildings’ locations. Moreover, even when DSM data are available, the data are sparse and do not match the building’s footprint. We have verified that these

buildings already existed at the time when the satellite images were taken (July 2016), as they have all been constructed in 2016 or before. On the other hand, the DSM's quality is considerably better for the five other towers, as the DSM has very few no data points at the location of the buildings, and the buildings' footprints can be identified by the higher values taken by the DSM around and under the building footprint. This is also translated by the maximum and mean DFM heights for these buildings, which are close to the actual buildings' heights.

Table 4-3 : Distribution of the DFM values and the quality of the DSM over high-rise buildings in Beirut

Building name	End of construction date	Height (from OSM) (m)	DFM max. elevation (m)	DFM mean elevation (m)	DSM quality
Sama Beirut	2016	195 m	35.1	11.6	Poor
20 30	2016	155 m	30.8	22.4	Poor
Les domes de Sursock	2013	140 m	60.4	25.2	Poor
Crédit Libanais	2015	133 m	27.4	15.1	Poor
Platinum Tower	2008	152 m	141.9	122.6	OK
Marina Tower	2007	150 m	126.7	101.3	OK
Bay Tower	2011	125 m	100.5	107.5	OK
Four Seasons	2009	120 m	121.6	102.7	OK
Beirut Tower	2009	112 m	103.8	95.6	OK

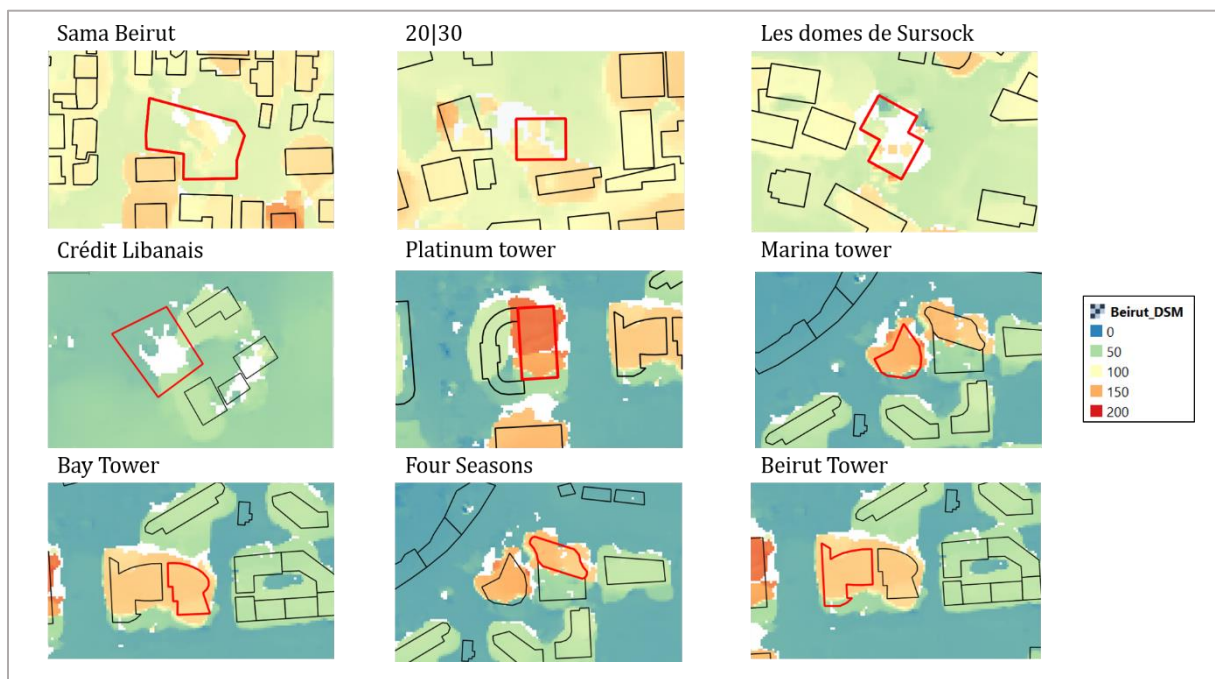


Figure 4-15: DSM elevations at the location of 9 high-rise buildings in Beirut. The building's name is indicated on the top the corresponding figure and the corresponding building's footprint is highlighted in red

It shows that although the processing of satellite images has shortcomings in the detection of high-rise buildings, the errors are not systematic, as some of the tall buildings in Beirut have been accurately identified. Therefore, despite the errors in the estimation, the processing of high-resolution satellite images allowed to retrieve the building heights in Beirut, with an average error of 14 m.

#### 4.2.3.2.3. Estimation of the number of floors from the building's height

The number of floors can be estimated by dividing the building's height by the average story height. The average story height in Beirut buildings has been defined in previous studies as follows: in Krayem et al.(2021), a building was considered to have 2.8 m per floor if it was built after 1923 and 4.5 m per floor otherwise. In Salameh (2016), the average story height was considered as 3.25 m in buildings built after 1950, and as more than 4 m for older buildings. As the average story height in Beirut varies according to different sources, and since the variation also depends on the building's construction period, it was difficult to generalize a floor height for the buildings in Beirut, especially since the construction date is not available for all the buildings in the OSM database.

In contrast, as both the number of floors and the building heights inferred from satellite images are available for the LIB-STAT buildings, a linear regression between the height of these buildings and their number of floors could be performed to obtain an empirical story height for the buildings in Beirut.

The LIB-STAT buildings were grouped by the buildings' number of floors. The distribution of the heights for each number of floors is shown in the boxplots in Figure 4-16. We can see that the median building height (red line) increases sharply for each additional floor for buildings having 2 to 5 floors, while the increase is slightly less steep for buildings with 6 floors and more. Buildings having more than 20 floors seem to have unusual low heights, as a consequence of errors in the DFM, and were therefore removed from the regression analysis.

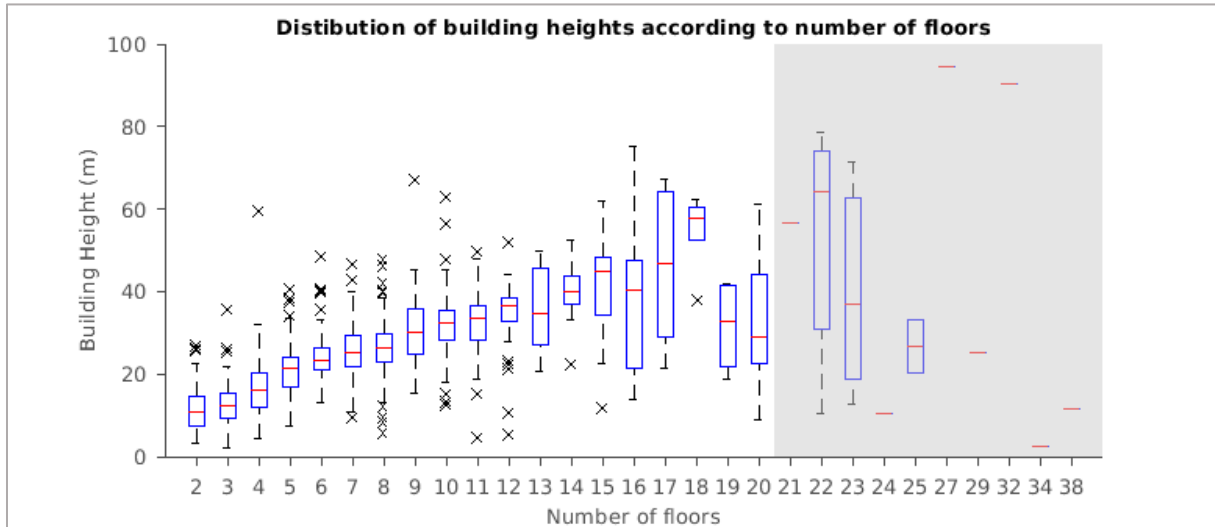


Figure 4-16 : Boxplot distribution of the building heights according to the number of floors in the LIB-STAT dataset. Outliers are represented by black crosses

A linear regression with no intercept was then performed between the number of floors and the heights of the LIB-STAT buildings (Figure 4-17), which resulted in the following equation:

$$Nb\ of\ Floors = 0.2822 \times Height \quad (4.9)$$

From the regression coefficient, we can deduce that the average story height is 3.5 m. The average story height is estimated with a coefficient of determination  $R^2$  of 0.5607 and a RMSE of 2.7. The RMSE value indicates that the number of floors can be estimated from the buildings height using equation (4.9) with a mean error of + or - 3 floors.

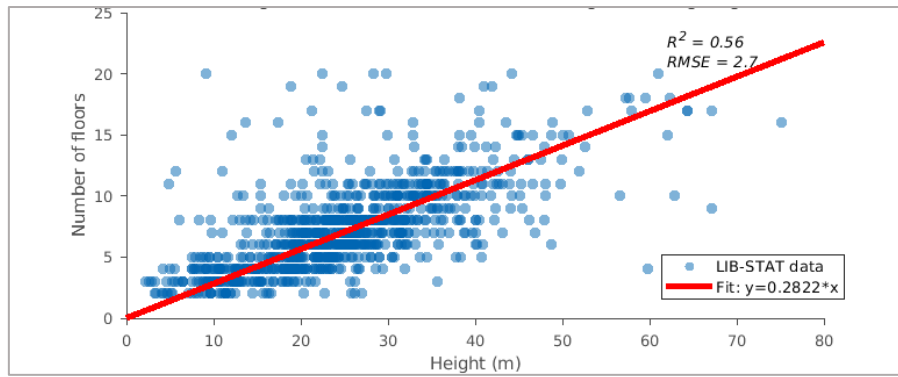


Figure 4-17 : Linear regression of the number of floors of the LIB-STAT dataset according to the building heights retrieved from the DFM

The estimation errors in terms of predicted number of floors as a function of the actual number of floors (Figure 4-18 (a)) and residuals between the predicted and the actual values (Figure 4-18 (b)) indicated that the number of floors are overestimated for low to medium-rise buildings (10 floors and less), while they are underestimated for buildings higher than 10 floors, as the residuals are mostly negative for these buildings. These errors are caused by the error in the detection of the building heights in the DFM (Figure 4-14).

With these uncertainties in mind, the number of floors of all buildings in the OSM database was estimated as of equation (4.9).

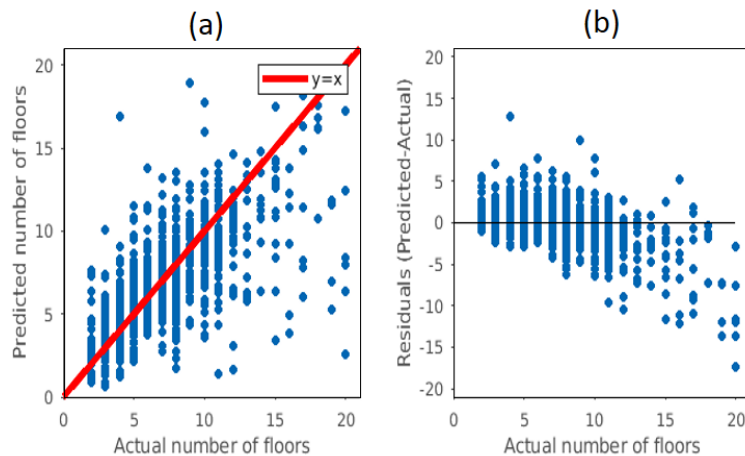


Figure 4-18 : Estimation errors in the linear regression between the number of floors and the building heights: (a) the predicted number of floors vs the actual number of floors, (b) the residuals between the predicted and actual value of the number of floors, according to the actual number of floors

#### 4.2.3.2.4. Prediction of the construction period

The prediction of the construction period can be achieved with a classification tree, a machine learning tool used to train a model to split a dataset into subsets according to rules learned from a set of predictor variables. The resulting model can then be applied to classify new data.

Classification trees were trained on the set of 947 buildings, to predict the buildings' construction periods that were categorized into the 3 classes used for the definition of the building typology (see section 4.2.3.1.3): before 1950, between 1950 and 2005 and after 2005. Different predictor variables were tested among the attributes available in the OSM database, namely:

- the building's number of floors, as the height of the building may reflect the evolution of constructions materials, building codes and architectural styles over time;
- the building's location (the X for longitude and Y for latitude coordinates of the building's centroid), which indicates the sector in which the building is located and can relate to the

evolution of the city's urbanization over time;

- the building's area and perimeter, as the geometrical properties and the size of the building may indicate the evolution of the construction practices over time.

Four different combinations of these variables were tested in order to find the optimal set of predictors. The classification trees were trained by splitting the dataset into 70% training set and 30% test set, and a 5-fold cross validation was additionally performed to prevent overfitting. The validation accuracy, i.e. the number of correct predictions divided by the total number of predictions, was computed for each classification tree to compare the trees' relative performances. The 4 different classification trees trained and their validation accuracies are displayed in Table 4-4.

Table 4-4 : The 4 different classification trees trained and their corresponding performance in terms of validation accuracy

Tree number	Predictors	Validation accuracy
Tree 1	Number of floors	0.7718
Tree 2	Number of floors, Area, Perimeter	0.7583
<b>Tree 3</b>	<b>Number of floors, X, Y</b>	<b>0.7958</b>
Tree 4	Number of floors, X, Y, Area, Perimeter	0.7838

The best accuracy was achieved by Tree 3 with predictors being the number of floors and the X and Y coordinates of the building. As for the predictors' importance, the number of floors is the most important predictor for the construction period, which is more than as twice as important as the X position of the building (Figure 4-19 (a)). The distribution of the predicted and true construction period classes in the LIB-STAT dataset shown in Figure 4-19 (b) shows that the buildings built between 1950 and 2005 are over-estimated using the classification tree, while the two other construction periods are underestimated in the predicted sample. This could be explained by the unbalanced input data set, where the buildings built between 1950 and 2005 are overly represented, which could create a prediction bias and affect the precision of the classification.

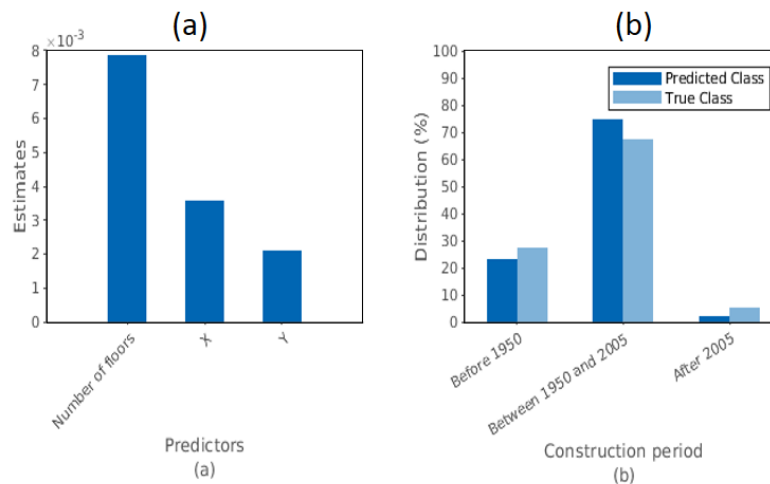


Figure 4-19 : Prediction of the construction period from the building's number of floors and X and Y coordinates using a classification tree. (a) Predictor importance estimates, (b) Comparison of the distribution of the predicted and true construction periods classes

Finally, Tree 3 was applied on the OSM database for the prediction of the Beirut buildings' construction period based on the number of floors (estimated in 4.2.3.2.3) and the X and Y coordinates of each building.

### 4.2.3.3. Application of the ANN to estimate the building damages at the scale of Beirut

After characterizing the construction period and number of floors of buildings in the OSM database, the ANNs trained in section 4.2.2.3 can be applied to estimate the seismic damages at the scale of Beirut. The inputs required for the ANNs are the building typology (as a separate ANN was trained for each building class), building and soil resonance parameters at the level of each building:  $f_{\text{struct}}/f_{\text{soil}}$  and  $A_{0\text{HV}}$  and indicators of the ground motion: PGA and PGV.

From the relationships identified in section 4.2.3.1.3, that relate the number of floors and construction period to the building's frequency and typology, the building typology and  $f_{\text{struct}}$  were derived. Figure 4-20 shows the distribution of the predicted buildings characteristics for the OSM database. The soil resonance parameters:  $A_{0\text{HV}}$  and  $f_{\text{soil}}$  at the location of each building were obtained from the interpolated maps in Figure 4-3, which also allowed computing  $f_{\text{struct}}/f_{\text{soil}}$  for each building.

For the remaining ANN inputs related to the seismic scenario, two near-fault earthquake scenarios were considered corresponding to a PGA of 0.3 g and 0.5 g. These scenarios correspond to earthquakes occurring at the Mount Lebanon Thrust (Epicentral distance  $R = 0$  km from Beirut) with different magnitudes. The moment magnitude ( $M_w$ ) and PGV values corresponding to each scenario were computed using the ground-motion prediction equation established by Akkar et al. (2014). The first scenario with PGA= 0.3 g corresponds to the recommended PGA for the design of earthquake-resistant buildings in Beirut (Huijer et al., 2016). This scenario stands for an earthquake with a  $M_w$  of 6.0 on the Mount-Lebanon fault with a PGV of 16 cm/s. The scenario with a PGA of 0.5 g corresponds to a  $M_w$  of 7.0 and a PGV of 40 cm/s. Although pessimistic, this scenario is plausible for near-fault ground motion in Lebanon (Fayjaloun et al., 2021).

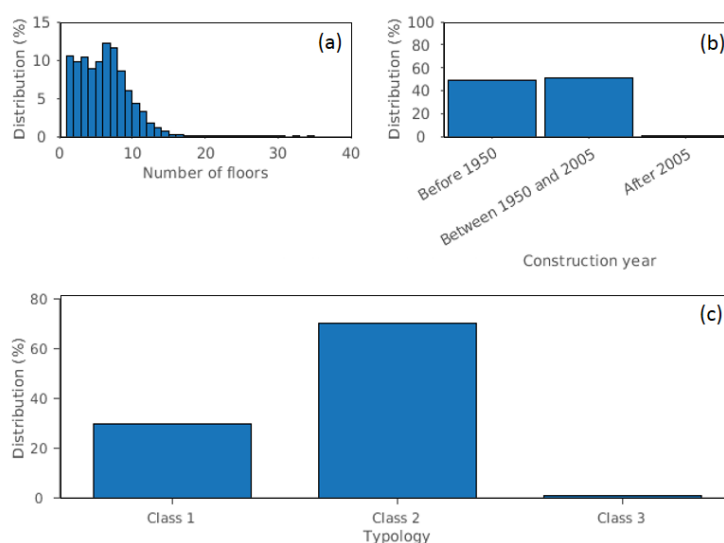


Figure 4-20 : Distribution of the predicted (a) number of floors, (b) construction year and (c) typology for the buildings in the OSM database

The distribution of the building damage states for the two considered scenarios is shown in Table 4-5. For an earthquake of PGA of 0.3 g, most of the damages predicted in Beirut are slight damages (60.7% of the buildings) followed by moderate damages (33.7%) and no damages (5.5%). 0.1% of the buildings are expected to suffer extensive damages, while no buildings would experience complete collapse (mean damage=4). For a PGA of 0.5 g, all buildings in Beirut would experience at least slight damages, 68.1% of Beirut buildings would suffer from moderate damages, while 31.4% would have extensive damages. For this scenario as well, no building will be completely damaged (collapsing).

Table 4-5 : Distribution of the buildings damage states for the two earthquake scenarios

Damage state	Scenario 1 (PGA = 0.3 g)	Scenario 2 (PGA=0.5 g)
None	5.5%	-
Slight	60.7%	0.5%
Moderate	33.7%	68.1%
Extensive	0.1%	31.4%
Complete	-	-

Nevertheless, as the buildings damages predicted for these scenarios are based on estimation models, the interpretation of these results should take into account the uncertainty in the predicted buildings' characteristics, especially the error on the buildings' number of floors that propagate to both the construction period and the typology.

The buildings' damages was thus predicted for the mean number of floors (N) plus and minus the standard error of 3 floors (N +3 and N - 3). The related ANNs inputs ( $f_{struct}/f_{soil}$  and the building's typology) were recomputed before applying the ANNs to estimate the damages. The distribution of the buildings damages for the 3 buildings' configurations is displayed in Figure 4-21.

For scenario 1 (PGA = 0.3 g) the subtraction of 3 floors (N - 3) leads to more pessimistic buildings damages, as the percentage of undamaged and slight damaged buildings decreases from 5.5% to 1.7% and from 60.7% to 47.5%, respectively, while the proportion of buildings with moderate damages increases from 33.7% to 50.5% (Figure 4-21 (a)). The opposite trend is observed for the addition of 3 floors (N + 3) as 15.2% of the buildings are undamaged for this scenario, while the damaged buildings have predominantly slight damages (72.6%).

For scenario 2 (PGA = 0.5 g, Figure 4-21 (b)), although as in scenario 1, the percentage of slightly damaged buildings increases with the increase of the number floors (0.1% for N - 3, 0.5% for N and 1.8% for N + 3), the percentage of moderately and extensively damaged buildings varies in the opposite direction compared to scenario 1 when considering the uncertainty in the number of floors. When considering N -3, the percentage of moderate damage increases from 68.1% to 78.3%, while the percentage of buildings with extensive damages decreases from 31.4% to 21.5%. Inversely, the addition of 3 floors, results in the decrease of the percentage of buildings with moderate damages (from 68.1% to 60.9%) and the increase of the percentage of buildings with extensive damages (from 31.4% to 37.3%).

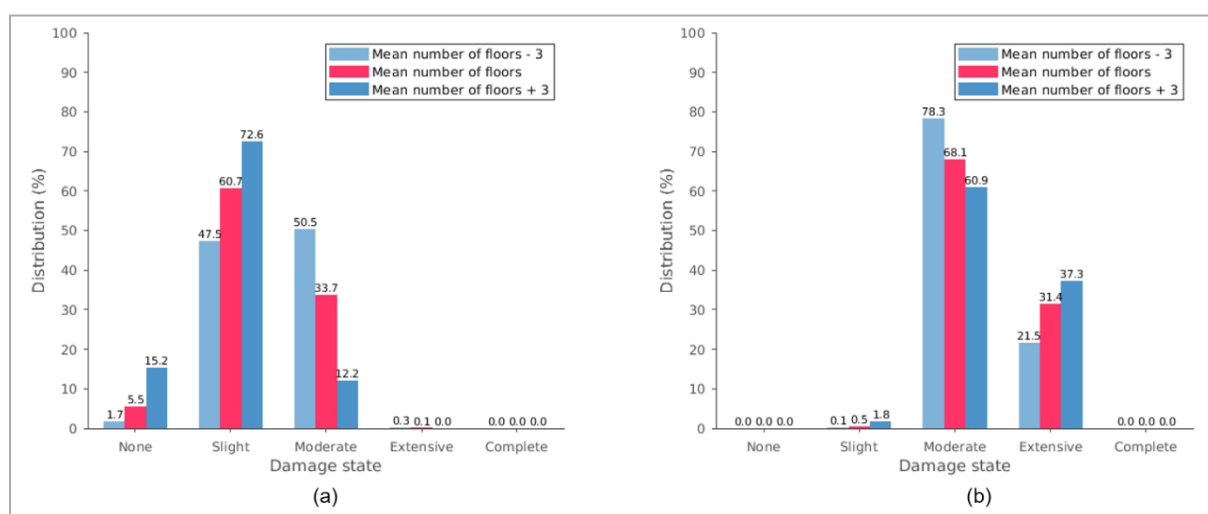


Figure 4-21 : Distribution of the buildings' damage states for the seismic scenarios 1 and 2, for the 3 buildings configurations obtained by considering: the mean predicted number of floors (N), the mean predicted number of floors -3 (N - 3) and the mean predicted number floors + 3 (N + 3)

In order to understand these variations in the buildings damages, we have displayed the spatial distribution of the buildings' typology and building to soil resonance frequency ratio ( $f_{\text{struct}}/f_{\text{soil}}$ ) for the 3 buildings configuration (N - 3, N, N+ 3) together with the resulting damages in the two seismic scenarios (Figure 4-22). Although, the damages were computed building by building, for presentation purposes, they were averaged on a radius of 100 m.

As the building's typology depends on the number of floors, the decrease in the number of floors results in the increase of the proportion of Class 1 masonry buildings (Figure 4-22 (a)), while the addition of 3 floors leads to the slight increase in the Class 3 buildings and the disappearance of the Class 1, as all buildings would have at least 4 floors (Figure 4-22 (c)). As the buildings' resonance frequency is inversely proportional to the number of floors, the change in the number of floors also translates to a decrease of  $f_{\text{struct}}/f_{\text{soil}}$  for N - 3 (Figure 4-22 (d)) and an increase for N + 3 (Figure 4-22 (f)).

Regarding the spatial distribution of the building damages for scenario 1 (PGA = 0.3 g), the buildings with the mean number of floors (N) experiencing slight damages (mean damage between 1 and 2) are concentrated in the east and the west of Beirut, which have been identified as rock sites in Figure 4-3. Heavier damages (mean damage between 2 and 3) are concentrated in the north and the south of the city prone to site effects (Figure 4-22 (h)). The spatial distribution of the damages are strongly correlated to the  $f_{\text{struct}}/f_{\text{soil}}$  map in Figure 4-22 (e) as higher levels of damages are observed for buildings having  $f_{\text{struct}}/f_{\text{soil}}$  around between 0.5 and 2 and the lowest buildings damages are observed when this ratio is less than 0.5. The buildings configuration with N-3 number of floors will overall suffer heavier damages (mean damages > 3) throughout the city (Figure 4-22 (g)) compared to buildings configuration with N+3 floors (Figure 4-22 (i)) with more damages in sediment sites compared to rock sites. The control of the coincidence of frequencies between soils and buildings on the spatial distribution of buildings' damages is remarkable when considering buildings configuration with N + 3 number of floors (Figure 4-22 (f) and (i)), since most of the buildings at sediment sites exhibit a  $f_{\text{struct}}/f_{\text{soil}}$  close to 1 (Figure 4-22 (f)). For buildings' configuration with lower number of floors (N - 3), even though larger damages (mean damage = 3) are located in narrow regions where  $f_{\text{struct}}/f_{\text{soil}}$  is close to 1 (between 0.5 and 2), most of the damages (mean damage = 2) are caused by more vulnerable buildings (most of the buildings are Class 1, Figure 4-22 (a)) located on sites exhibiting site effects, and thus subject to larger surface ground motion.

In scenario 2 (PGA = 0.5 g), most of the buildings suffer heavy damages (mean damage > 3, Figure 4-21) whatever the buildings' number of floors configuration (Figure 4-22 (j) (k) (l)). The building damages are less severe at the rock sites (mostly mean damage = 3 whatever the buildings' configuration) in the east and the west of Beirut compared to the north and south sediment sites. Interestingly, less severe damages at sediment sites are observed for the buildings' configuration with N-3 number of floors compared to N and N+3 number of floors. This can be explained by the reduction of the soil's amplification at the building resonance frequency due to the nonlinearity of the soil response, since most of the N-3 floors building resonance frequencies to correspond  $f_{\text{struct}}/f_{\text{soil}}$  larger than 2, this ratio being even increased when considering the decrease of soil's resonance frequency due to non-linearity. For the N+3 buildings configuration, most of the  $f_{\text{struct}}/f_{\text{soil}}$  are ranging from 0.5 to 2 at sediment sites (Figure 4-22(f)). When  $f_{\text{soil}}$  decreases due to soil non-linearity, this ratio will be reduced which will make buildings with  $f_{\text{struct}}/f_{\text{soil}}$  between 0.5 and 1 prone to more structural displacement because of the coincidence of resonance frequency, and the buildings with  $f_{\text{struct}}/f_{\text{soil}}$  between 0.5 and 1 to more amplified ground motion.

In summary, despite the differences observed in the distribution of the damages' severity when considering the uncertainty in the buildings' properties, the spatial distribution of the damages was more or less consistent. Heavier building damages are concentrated at sediment sites in the north and the south of Beirut, while the buildings located on the rock sites in the east and the west of Beirut witness the lowest levels of damages. These observations show that the site effects and coincidence of frequencies between soils and buildings control the spatial distribution of damages.

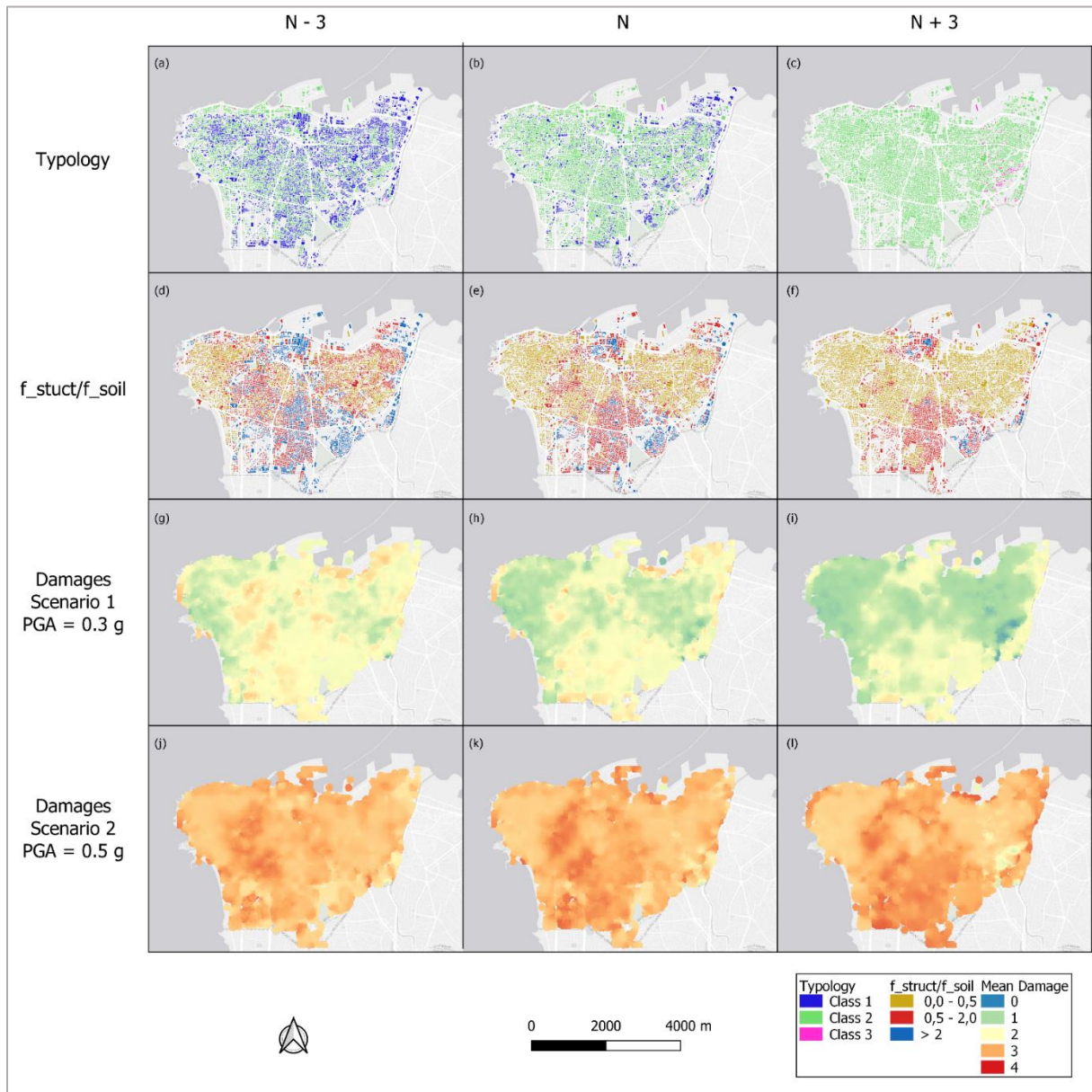


Figure 4-22: Beirut damages maps for scenarios 1 and 2 for buildings with the average predicted number of floors ( $N$ ), predicted number of floors +3 ( $N+3$ ) and predicted number of floors - 3 ( $N-3$ ). The damages were computed building by building, but for presentation purposes they were averaged on a radius of 100 m

#### 4.2.4. Conclusion

One of the challenges of the estimation of seismic damages in Beirut is the lack of comprehensive data on the building stock and the relevant building properties and their taxonomy. We have developed an approach to generate a 3D building model of the city using open source geographic data and high-resolution satellite images for estimating building heights. A subset of around 1000 buildings with known attributes taken from an existing database was used to derive statistical relationships between different buildings attributes (building height, number of floors, resonance frequency, typology) in order to extrapolate the building properties at the city scale. Seismic damages in Beirut were estimated using ANNs. These ANNs were trained on a comprehensive dataset of numerical simulations of non-linear site response and building damages to predict buildings' mean damages from simple indicators related to building, soil and signal properties. These indicators are the ratio between building and soil

fundamental resonance frequencies,  $f_{\text{struct}}/f_{\text{soil}}$ , the amplitude of the H/V peak estimation from seismic noise,  $A_{0\text{HV}}$ , PGA and PGV at outcropping rock. One of the most important results from the ANN is the strong control of  $f_{\text{struct}}/f_{\text{soil}}$  on the damages, higher damages occurring when  $f_{\text{struct}}/f_{\text{soil}}$  is close to 1.

For two earthquake scenarios corresponding to a PGA of 0.3 g and 0.5 g, the predicted damages at the building scale indicate that the damages are concentrated in sediment areas, larger damages occurring when ratio between soil and building resonance frequency is close to 1, while the damage levels depend on the seismic scenario considered.

The main source of error in the buildings' damage prediction comes from the difficulty in accurately quantifying the buildings' heights from satellite images, which in turn influences the number of floors and other building attributes such as the building's resonance frequency and its typology. The effect of this uncertainty on the predicted damages was explored by comparing the damages estimated for the average predicted number of floors and the damages computed for the average number of floors plus and minus the standard error of 3 floors. The changes in the number of floors translate into a possible change of building vulnerability class and an increase or decrease of  $f_{\text{struct}}/f_{\text{soil}}$ . While the overall distribution of damage states varies depending on the considered building configuration, the spatial distribution of the damages throughout the city is consistent with the damage distribution for the average predicted number of floors.

This highlights the control of the site effects on the buildings damages, as despite the variability of the building properties, the damages were still concentrated in the same areas in the city. Therefore, even though the generated 3D buildings model does not substitute a complete and detailed buildings exposure model, it can provide a starting point for the analysis of the distribution of seismic damages within the city. The approach developed in this study, which relies on simple measure parameters, may be particularly useful in other cities with a similar context to Beirut, where comprehensive building data stock is lacking. In future works we plan to complement this study with a more comprehensive analysis of the propagation of uncertainty from the estimated building parameters to the building damages.

### 4.3.DEBRIS ESTIMATION

In the literature, only few studies focused on the estimation of earthquake-generated debris. HAZUS (FEMA, 2012) proposes a methodology to estimate the quantity of generated debris due to an earthquake considering the buildings' typologies and damage levels: for each damage level, the corresponding fraction of the building material weight that transforms into debris is indicated. Knowing the unit weight of the building materials and the area of the building allows computing the total weight of debris at the building scale. However, one the main limitations of this approach is that it does not investigate the spatial distribution of debris outdoors, which is essential for the simulation of mobility during evacuation.

The spatial distribution of debris is still an open research question (Castro et al., 2019). The most common practice is to estimate the extent of debris around a building as a function of the building height. Nishino et al. (2012) assumed that debris fall uniformly from a collapsed building without any preferential direction. The extent of debris around a building is variable, as it follows a triangular distribution with minimum, maximum and mode equal to  $H/8$ ,  $H/2$  and  $H/4$  respectively (Figure 4-23 (a)). Similarly, in Ravari et al. (2016), the debris width is considered a function as the building's height, as the debris is assumed to form an angle of  $20^\circ$  between the between the front wall and a line that connects the top of the front wall to the farthest point of the debris (Figure 4-23 (b)).

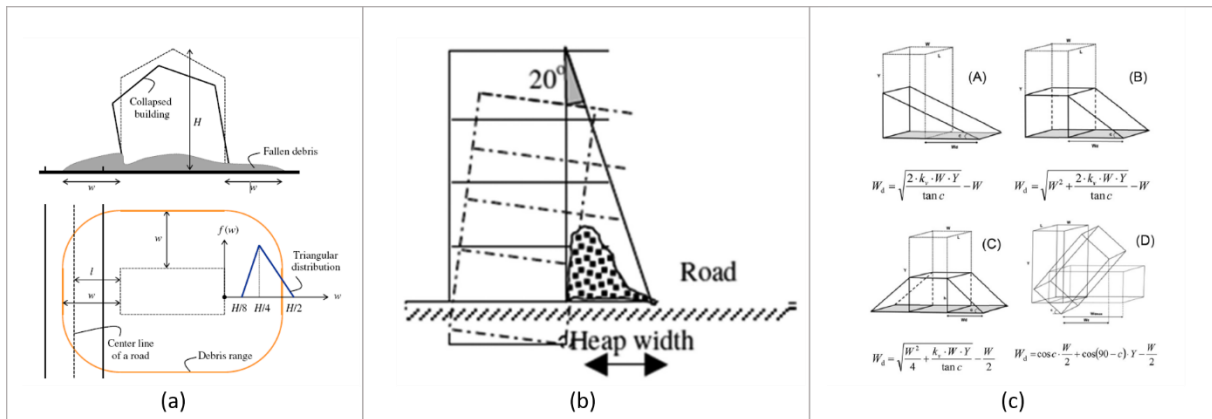


Figure 4-23: Models for the estimation of the spatial distribution of debris from the literature. Sources: (a) Nishino et al., 2012, (b) Ravari et al., 2016, (c) Argyroudis et al., 2015

Argyroudis et al. (2015) proposed a simplified geometrical model to estimate the debris resulting from collapsed buildings. This geometrical model assumes that the debris will form a volume with the shape of a triangular prism with the larger height next to the building (Figure 4-23 (c)). The model takes into account the collapse type: whether the collapse is in one direction, two directions, or an overturn. Under the assumption that adjacent buildings' façades are continuous and that the volume of debris is a fraction of the original volume of the building, an equation correlating the extent of the debris to the height and width of the building was defined for each collapse type. Although this geometrical approach is robust and simple, one of its main drawbacks is that it only accounts for cases of buildings' full collapse and not for partial damage states.

While the three previously mentioned approaches were rather empirical, a few studies have developed experimental approaches to analyze the debris formation due to an earthquake. Domaneschi et al. (2019) used numerical simulations to study different collapse scenarios of masonry buildings. After validating the numerical simulations by experimental tests on a shaking table, a simplified formula relating the geometric properties of the building and the area occupied by debris was extracted from the simulations results. However, the main limitation of this study is that it can only be applied for masonry buildings for the case of full building collapse, and not for partially damaged states. Santarelli et al. (2018) relied on machine learning tools to identify correlations between the extent of ruins on the streets facing masonry buildings observed in post-earthquake satellite images, and the buildings' vulnerability, seismic magnitude and the ratio between the building's height and street width. By relating the debris extent to the building's vulnerability and the seismic magnitude, this approach indeed takes into account the building's damage level. However, the results are expressed in terms of fraction of the street that is covered by debris, instead of an absolute debris width, which is difficult to generalize and to apply to studies in which knowing the width of streets is not a viable option.

The literature review allowed to identify a gap in models that could estimate the spatial distribution of debris around buildings while also accounting for the severity of the buildings' damage. Since we need to estimate the debris around buildings for the simulation of pedestrians' evacuation, we propose a methodology to estimate the height and extents of debris around buildings, while considering the level of damage attained by the buildings. The proposed model estimates the volume of generated debris in the case of full collapse, then, using correlations between the building's damage and the generated debris quantity, the debris volume corresponding to the building's damage level is estimated. Once the debris volume is estimated, a geometrical model is used to distribute this volume around the building, which allows to estimate both the debris width and height.

#### 4.3.1. Estimation of the debris volume corresponding to the damage level of the building

The first step in the proposed methodology is to estimate the volume of debris generated for the level of damage reached by the building. In HAZUS, the percentage of debris weight from damaged structural elements can be found for each building typology. Table 4-6 shows the values for the common building

types in Beirut: URM (Class 1 in our approach), C1 (Class 2 in our approach) and C3 (Class 3 in our approach). These correlations could be adopted for the relationship between debris volume and building damage state, by assuming that all building materials have the same unit weight. Under this assumption, the percentage of debris volume generated for a given damage level can be considered the same as the percentage of debris weight. For example, if total debris weight is of 100 kg and occupies a volume of 100 m<sup>3</sup>, 50% of the debris will weight 50 kg and occupy a volume of 50 m<sup>3</sup>.

Table 4-6 : Percentage of debris weight from damaged structural elements (source: HAZUS, FEMA 2012)

Building type	Percentage of debris weight from structural damage state			
	Slight	Moderate	Extensive	Complete
URM	0	2	25	100
C1	0	5	33	100
C3	0	4	32	100

To apply this methodology, the first step is to compute the volume of debris in the case of full collapse. We assumed that in case of full collapse, the debris would be generated from the building's construction materials, specifically the exterior walls and the floor slabs (Figure 4-24). The debris generated from interior walls and partitions, furniture and other objects in the buildings were not considered for simplification purposes. Also for the sake of simplification, buildings are assumed to have a regular rectangular shape. The debris volume in case of total collapse can therefore be computed as:

$$V_t = 2 \times W \times H \times e + 2 \times L \times H \times e + n \times W \times L \times s \quad (4.10)$$

Where  $V_t$  represents the total debris volume in case of full collapse (in m<sup>3</sup>),  $W$  is the building width (in m),  $H$  is the building's height (in m) and  $L$  is the building's length (in m).  $e$  and  $s$  represent respectively the thickness of the exterior walls and the thickness of the floors slabs (in m), while  $n$  represents the number of floors of the building.

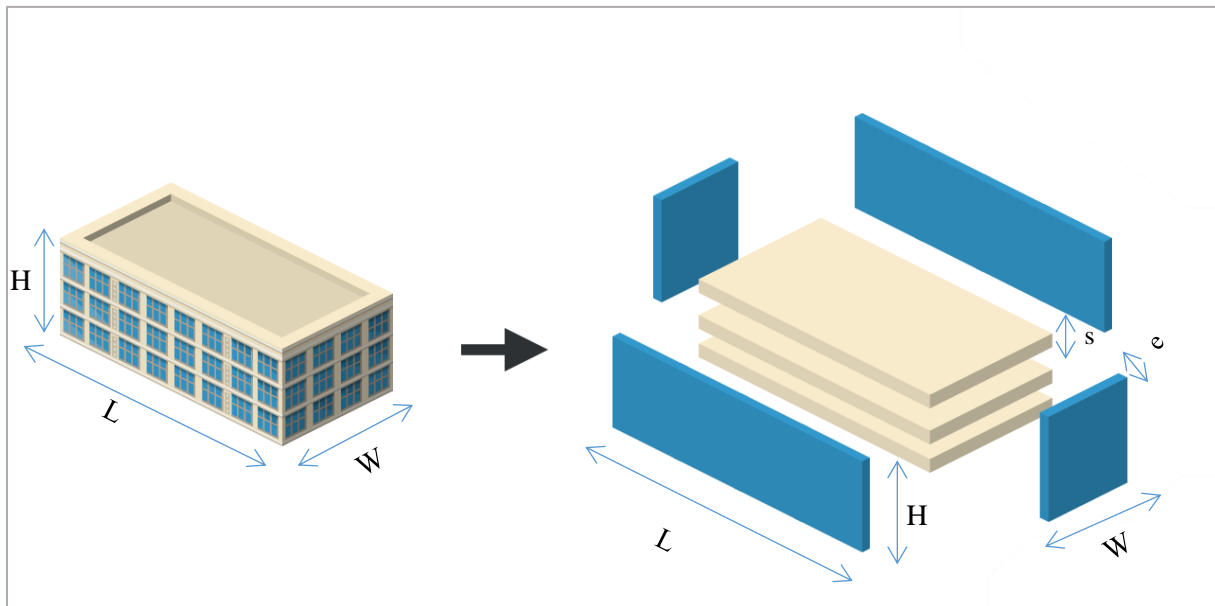


Figure 4-24 : Debris generation from the building's construction elements

In case of partial buildings damages, the generated volume of debris is considered to be a fraction of  $V_t$  computed as:

$$V_d = \alpha \times V_t \quad (4.11)$$

Where  $V_d$  is the volume of debris corresponding to the mean damage of the building and  $\alpha$  is the proportion of total debris volume that is generated at this particular damage level. The values of  $\alpha$  were

adapted from Table 4-6. Indeed, the mean damage computed in previous section is on a continuous scale from 0 to 4 while the values in Table 4-6 are given for discrete damage levels. Therefore, a Gaussian curve was fitted for each building typology in order to have continuous values of  $\alpha$  for mean damage values ranging from 1 (structural damage state = slight) to 4 (structural damage state = complete). The values taken for  $\alpha$  for each building type are shown in Figure 4-25.

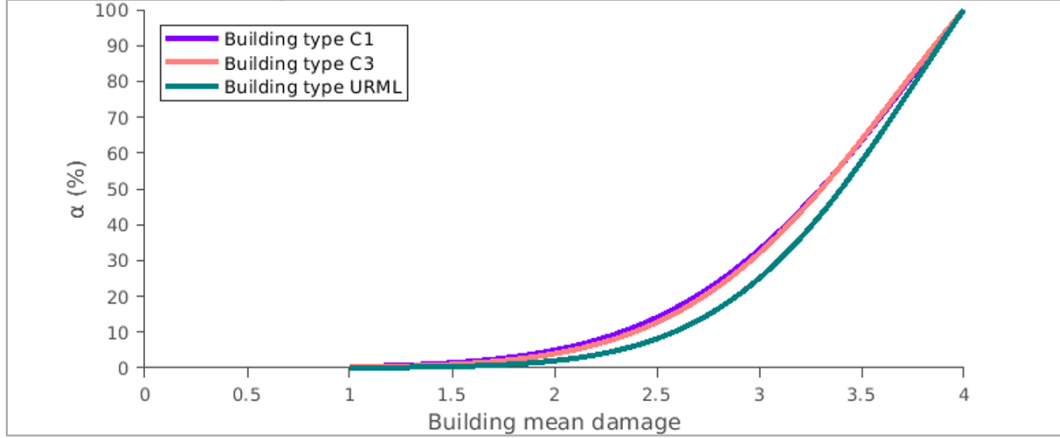


Figure 4-25 : Percentage of total debris volume generated depending on the mean damage for each building type

#### 4.3.2. Estimation of the debris footprints around a building

For the estimation of the debris footprints around a building, a geometrical model similar to Argyroudis et al.(2015) was developed. In contrast to the model of Argyroudis et al.(2015) in which all buildings façades were considered continuous, in this approach adjacent buildings were assumed to have separate façades; therefore, debris could fall in all four directions around the buildings. This results in the formation of debris in the shape of a truncated pyramid whose volume is filled by the volume of the generated debris  $V_d$  (Figure 4-26). The debris extent around the building can be computed by calculating the dimensions of the pyramid's base  $L_p$  and  $W_p$ . The height of the debris at the highest point next to the building façade can also be computed by finding  $H'$ , the truncated pyramid's height.

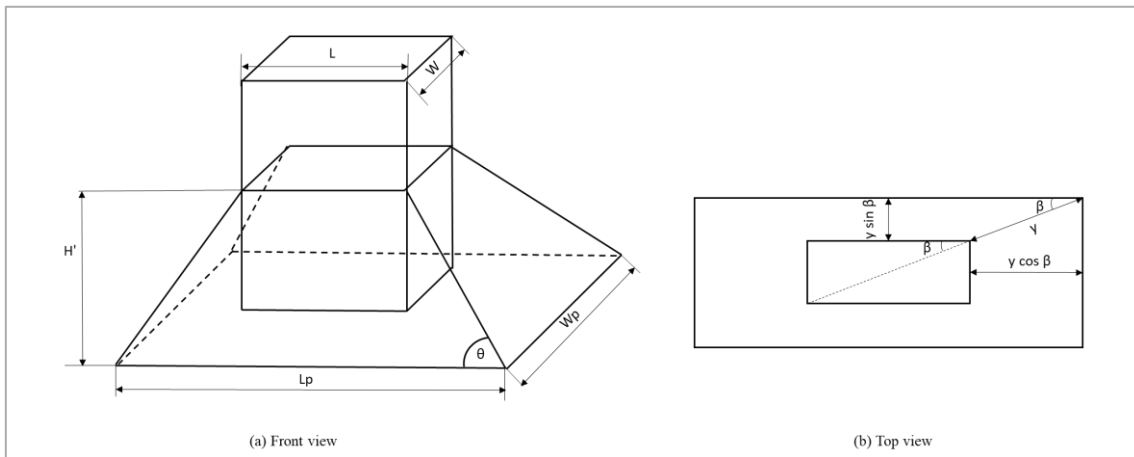


Figure 4-26 : Front and top views of truncated pyramid shaped debris

The truncated pyramid's volume is given by:

$$V_p = \frac{H'}{3} (B + b + \sqrt{B \times b}) \quad (4.12)$$

$$b = L \times W \quad (4.13)$$

$$B = L_p \times W_p = (L + 2 \times y \times \cos\beta) \times (W + 2 \times y \times \sin\beta) \quad (4.15)$$

$$H' = y \times \cos\beta \times \tan\theta \quad (4.16)$$

$$\beta = \tan^{-1}\left(\frac{W}{L}\right) \quad (4.17)$$

where  $B$  is the area of the truncated pyramid's base (m),  $b$  is the area of the truncated pyramid's top (in m) and  $H'$  is the height of the truncated pyramid (in m). On the top view,  $y$  represents the diagonal distance between the building's corner and the debris' corner (in m).  $\beta$  is the angle made between the building's length and its diagonal and  $\theta$  is the angle made between the debris and horizontal plane.

Under the assumption that the debris fall uniformly in all directions, filling the volume of the truncated pyramid:

$$V_p = V_d \quad (4.18)$$

Solving equation (4.18) with one unknown, gives the value of  $y$ , from which the debris height can be directly calculated as:  $y \times \cos\beta \times \tan\theta$ , and the debris extents can be calculated in both directions as:  $y \times \cos\beta$  and  $y \times \sin\beta$ .

### 4.3.3. Validation of the approach

Previous studies have highlighted the dependence of the extent of the debris around the building on the building's height. The debris widths were commonly found to be proportional to the building height ( $H$ ), with values ranging from  $H/2$  to  $H/8$  (Nishino et al., 2012). Since these relationships were established for cases of full building collapse only, the relationship between the debris width computed using the developed model and the building height was investigated for the case of complete collapse (mean damage=4).

A rectangular building with dimensions  $L = 20 \text{ m}$  and  $W = 10 \text{ m}$  was considered. The building's number of floors was varied from 1 floor to 40 floors, with a floor height set to 3.5 m. The angle at the diagonal of the building was calculated as:  $\beta = \tan^{-1}\left(\frac{10}{20}\right)$ . The angle  $\theta$  formed by the debris and the horizontal plane was assumed to be equal to  $30^\circ$ . The thicknesses of the walls and the floor slabs were considered to be respectively  $e = 0.2 \text{ m}$  and  $s = 0.5 \text{ m}$

The debris width in the diagonal direction,  $y$ , was computed for each building height by solving equation (4.18). The resulting debris width is shown in Figure 4-27 as a function of the building's height. It can be observed that as the height of the building increases, the extent of debris away from the building increases as well. For building heights less than 20 m, the debris width ranges between  $H/3$  and  $H/4$ . As the building becomes taller, the debris width tends gradually away from  $H/4$  and closer to  $H/8$ . The debris extent becomes less than  $H/8$  for buildings taller than 115 m. Therefore, in our model, as the building height increases, the ratio between the building height and the debris width increases as well. This observation has not been documented in the literature, as no other study offers a detailed comparison between debris width and building height. We believe it is mainly due to the geometrical considerations of the truncated pyramid shape, which highly depends on the ratio between building length and width that sets an upper limit to the debris width.

Consequently, we can safely assume that the debris estimated using the developed approach are within the range found in the literature; however the approach needs to be validated for high-rise buildings by conducting further experiments and collecting real life observations.

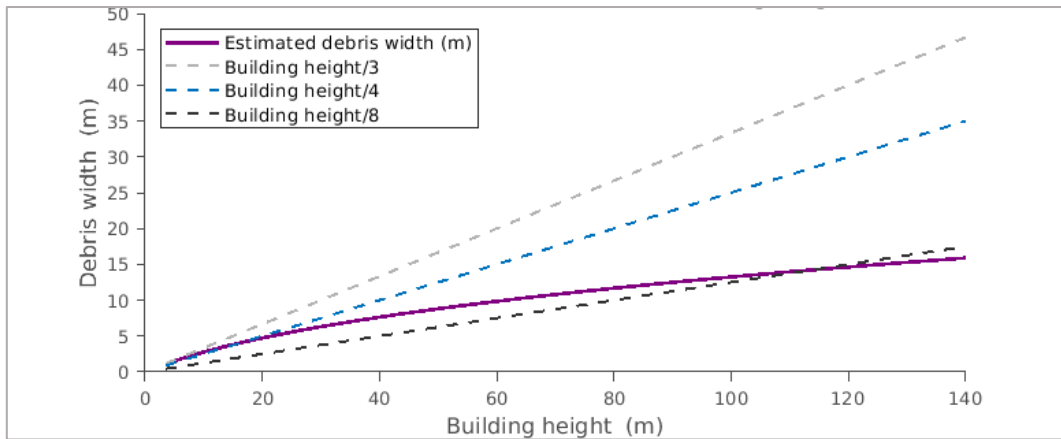


Figure 4-27 : Comparison of the debris width estimated following the developed methodology to the typical formulas found in the literature

#### 4.3.4. Application to Beirut

This approach is applied to the buildings in Beirut, for the two earthquakes scenarios with  $PGA = 0.3\text{ g}$  and  $PGA = 0.5\text{ g}$ . The generated debris width - i.e. the furthest distance reached by debris away from buildings- according to the building height and the mean damage is displayed in Figure 4-28. We can see that for a given building height, the debris width increases with increasing building damages. Similarly, for a given building damage level, the debris width increases with the increase of the buildings height. The maximum debris width for the scenario with  $PGA = 0.3\text{ g}$  (Figure 4-28(a)) is in the order of 1 m, attained by a building of 10 m for a mean damage around 3. The small debris widths observed in this scenario can be explained by the fact that tall buildings have very low damage levels, and consequently generate very little debris. On the other hand, for the scenario with  $PGA = 0.5\text{ g}$  (Figure 4-28(b)), as the buildings experience greater damages in this scenario, the extents of the debris around the buildings are higher than in the first scenario, reaching up to 6.5 m for heavily damaged tall buildings.

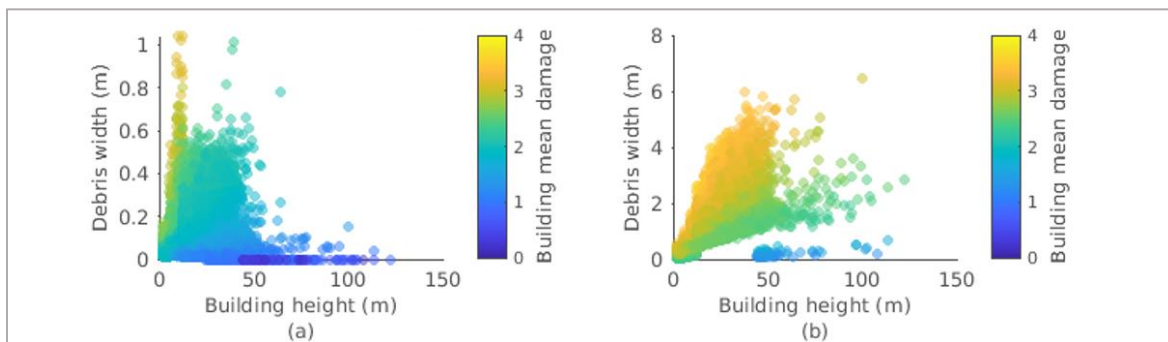


Figure 4-28 : Distribution of the debris width according to the building height and the mean damage. (a) Seismic scenario with  $PGA = 0.3\text{ g}$ , (b) Seismic scenario with  $PGA = 0.5\text{ g}$

As the debris height is also important for pedestrian's mobility in the aftermath of an earthquake, we have examined the distribution of debris heights for the two seismic scenarios (Figure 4-29). The debris height refers to the maximum height of the debris,  $H'$  in Figure 4-26. We can see that the debris height follows the same distribution as the debris widths in the two scenarios, as with increasing buildings heights and damage levels, the debris heights increase as well. While the maximum debris height in the scenario with  $PGA = 0.3\text{ g}$  (Figure 4-29 (a)) is of 0.6 m, in scenario with  $PGA = 0.5\text{ g}$  (Figure 4-29 (b)) the debris are considerably higher, reaching up to 4 m in the case of heavily damaged tall buildings.

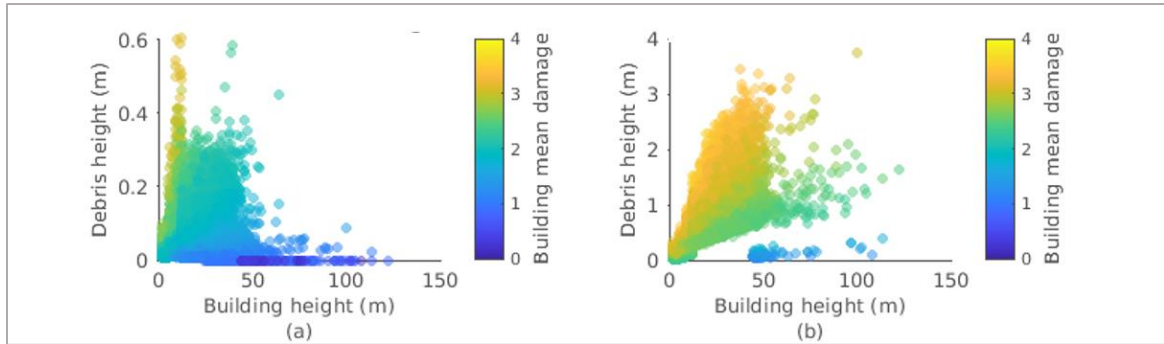


Figure 4-29 : Distribution of the debris height according to the building height and the mean damage. (a) Seismic scenario with PGA = 0.3 g, (b) Seismic scenario with PGA = 0.5 g

The computed debris were then transformed into debris zones around buildings through GIS processing: a buffer was applied around each building with a distance equal to its corresponding debris width. This created a new layer of debris zone around each building. The height of each debris zone was then added as an attribute in the layer. This process was performed for both seismic scenarios (0.3 g and 0.5 g). To illustrate this, Figure 4-30 shows an example of debris zones for a building for the two seismic scenarios. For this building, the width of the debris clearly increases between the scenario of PGA = 0.3 g (0.4 m) and the scenario of PGA= 0.5 g (3.3 m).

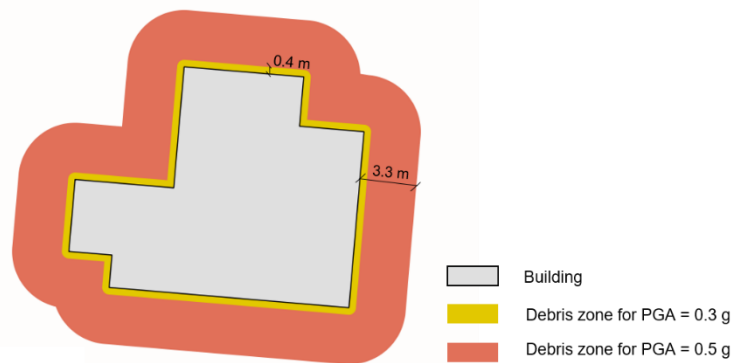


Figure 4-30: Debris zone for a building for a scenario PGA = 0.3 g and a scenario of PGA = 0.5 g

While all the debris zones have heights less than 1 m for an earthquake of PGA 0.3 g, the debris that reach heights greater than 1 m for a PGA = 0.5 g are mainly concentrated in the Mazraa and Moussaitbeh sectors in Beirut, as it can be seen in Figure 4-31.

#### 4.3.5. Summary

The literature is poor in models that estimate at the same time the quantity of debris generated per building according to its damage level and the distribution of the debris (width and height) around the building. In this section, we have developed a model for the estimation of the spatial distribution of debris as a function of the building's damage level. The model was validated by comparing it to the usual values found in the literature in the case of full building collapse. Although the calibration of the model should be improved for high-rise buildings, it showed good results for low-to-moderate rise buildings. The model was applied to estimate the distribution of debris for the damages predicted for the two earthquake scenarios in section 4.2. While for the scenario with PGA = 0.3 g the debris widths and heights are relatively low (maximum debris width 1 m and maximum height 0.6 m), for the scenario with PGA = 0.5 g the debris reach further extents around buildings (up to 6.5 m) and have heights over 1 m that could severely constrain the pedestrians' mobility.

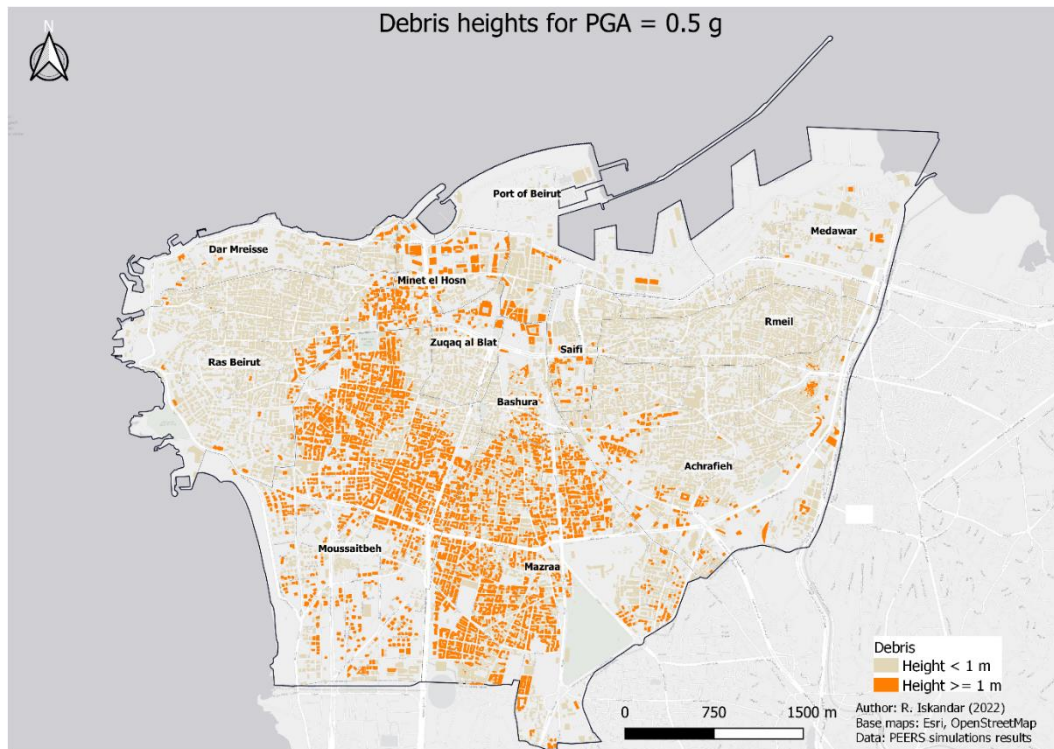


Figure 4-31: Spatial distribution of the debris' heights in Beirut for a seismic scenario of PGA = 0.5 g.

#### 4.4.ASSIGNMENT OF CASUALTY RATES TO BUILDINGS AND DEBRIS ZONES

The approaches used to estimate casualties in earthquakes have been classified into empirical (Jaiswal and Wald, 2010a; Wyss, 2005), semi-empirical (Jaiswal and Wald, 2010b; Pai et al., 2007) and analytical (FEMA, 2012; Porter, 2009) approaches (Maqsood and Schwarz, 2011). The main difference between analytical and empirical (or semi-empirical) approaches, is that the former consider the level of buildings damages when estimating casualties while the latter only correlate casualties to the intensity or magnitude of the earthquake. Consequently, analytical approaches are more appropriate for establishing casualty rates at the building-level.

The casualty rates provided by HAZUS were adopted in this study because in HAZUS:

- The casualty rates are given according to the building's structural damage, and according to the building type;
- The casualty rates are not only for fatalities, but for casualty severities ranging from 1 (light injury) to 4 (deceased).
- Indoor and outdoor casualty rates are provided. Indoor casualty refers to injuries that occur inside buildings, and outdoor casualty refers to injuries that occur due to the fall of objects from buildings (collapsing masonry parapets, wall panels... etc.).

Nevertheless, the casualty rates provided by HAZUS are for discrete damage levels, while the mean damages calculated in this study are on a continuous scale from 0 to 4. Consequently, the indoor and outdoor casualty rates provided by HAZUS for the building typologies in Beirut (URML, C1 and C3) were interpolated on a continuous scale from mean damages ranging from 1 (slight damages in HAZUS) to 4 (collapse in HAZUS) (Figure 4-32). We can see on this figure, that the indoor fatality (Severity 4) rates range from around  $10^{-5}$  % (or  $10^{-7}$ ) for a building with a mean damage equal to 1, up to 20% for building a mean damage equal to 4. Outdoor casualty rates range from  $10^{-6}$  for a mean damage equal to 1 and go up to 0.5% when the mean damage reaches 4.

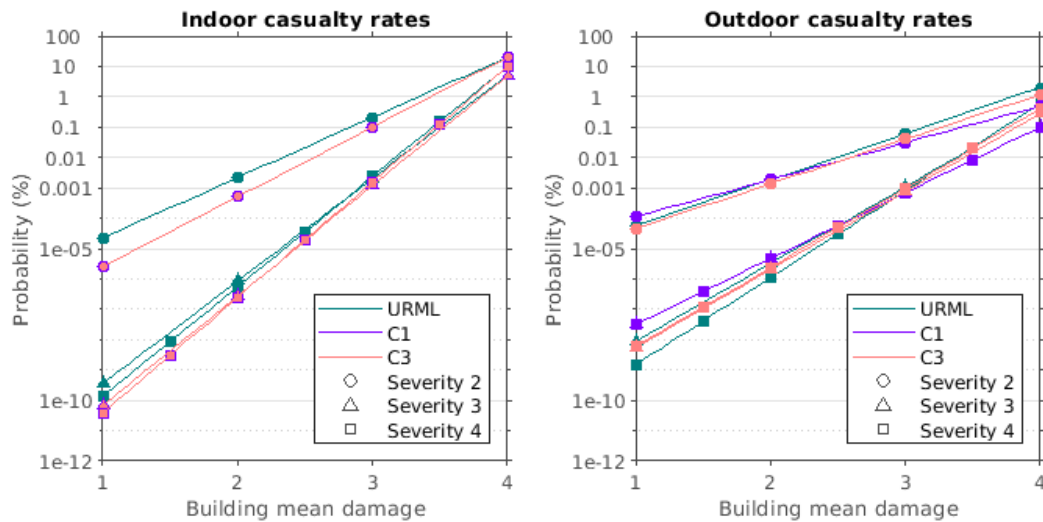


Figure 4-32: Interpolated indoor and outdoor HAZUS casualty rates according to the building mean damage for building types URML, C1 and C3. C1 and C3 buildings have the same indoor casualty rates.

The interpolated casualty rates were applied to the buildings and debris zones in Beirut. For each building, depending on its mean damage, the indoor casualty rates (severities 2 to 4) were added to its list of attributes, and the outdoor casualty rates were added to its corresponding debris zone. For a reference about the estimated casualty rates applied to Beirut for the two seismic scenarios, Table 4-7 shows the mean indoor and outdoor fatality (severity 4) rates. The mean rates were calculated by averaging the rates of all buildings in Beirut. The mean fatality rate inside buildings in Beirut is of  $1.5 \times 10^{-7}$  for an earthquake of PGA 0.3 and it increases to  $6.2 \times 10^{-5}$  for a PGA of 0.5 g. In debris zones (outdoor) the fatality rate is of  $7.2 \times 10^{-8}$  for 0.3 g and it reaches  $1.5 \times 10^{-5}$  for 0.5 g.

Table 4-7: Mean indoor and outdoor fatality rates in Beirut for seismic scenarios of PGA 0.3 g and 0.5 g. The standard deviation (std) is indicated in brackets

Seismic scenario	Mean indoor fatality rate (std)	Mean outdoor fatality rate (std)
PGA = 0.3 g	$1.5 \times 10^{-7}$ ( $2.14 \times 10^{-6}$ )	$7.2 \times 10^{-8}$ ( $6.4 \times 10^{-7}$ )
PGA = 0.5 g	$6.2 \times 10^{-5}$ ( $2.04 \times 10^{-4}$ )	$1.5 \times 10^{-5}$ ( $3.63 \times 10^{-5}$ )

#### 4.5.CONCLUSION

This chapter presented the estimation of the building seismic damages and resulting debris in Beirut. These damages were estimated for two seismic scenarios, the first corresponding to the regulatory PGA of 0.3 g, and the second to a more pessimistic scenario of PGA 0.5 g. We further developed the approach of Salameh et al. (2017), by including the PGV to the ANN indicators, in addition to the PGA,  $f_{\text{struct}}/f_{\text{soil}}$  and  $A_{\text{OHV}}$ . These ANN were applied to estimate the damages in Beirut on a building database covering the whole city, constructed using volunteered geographic information, high-resolution satellite images and machine learning tools. For a scenario of PGA of 0.3 g, the building damages in Beirut are mostly slight to moderate. For a PGA of 0.5 g, the damages are moderate to extensive. In both scenarios, the highest damage levels are concentrated in sediment areas that are prone to site effects and where the frequencies of soils and structures coincide.

To estimate the debris generated from these damages, we developed a methodology that computes the height and extents of debris around buildings according to the building damage. This methodology is applied to generate debris zones in Beirut. For the scenario of PGA 0.5 g, the debris heights and extents are remarkably high, exceeding 1 m, which significantly increases the challenges on mobility in the urban area. Finally, casualty rates were attributed to buildings and debris based on analytical rates provided by (FEMA, 2012).

# Chapter 5: Mixed approaches for the generation of spatial, social and behavioral data in Beirut

## 5.1. INTRODUCTION

Further to building damages and debris data, spatial data on open spaces and mobility constraints in Beirut are needed for the simulation of pedestrians' mobility and safety in the aftermath of an earthquake. Similarly, the estimation of a realistic population exposure, in terms of size and spatial distribution, is a key ingredient for the dynamic simulation of an earthquake crisis. As we simulate realistic human behaviors, the characteristics of the population and the social bonds between individuals should be represented in the population dataset as well. This condition is particularly challenging in Lebanon, due to the lack of comprehensive data on the population. Finally, as the behavioral responses to sudden emergencies are highly contextual and culture-dependent, behavioral data on the Lebanese population's reaction in previous events are needed as well to calibrate the behavioral model to the cultural context of Beirut.

This chapter presents the approaches that were developed for the generation of the aforementioned data. The generation of spatial data is covered in section 5.2 regarding open spaces and section 5.3 for the mobility constraints. Section 5.4 presents the approach for the generation of a synthetic population in Beirut and finally section 5.5 focuses on the survey that collected behavioral responses in the aftermath of the Beirut port explosions from which behavioral data were extracted.

## 5.2. DELIMITATION OF OPEN SPACES IN BEIRUT

In an urban area, open spaces are incredibly valuable during and after an earthquake as they are immediate evacuation locations (Godschalk, 2003; Shrestha et al., 2018). The great potential of open spaces for emergency response in the event of an earthquake and their role in enhancing the urban resilience has been highlighted by several studies (Allan et al., 2013; Jayakody et al., 2016; Koren and Rus, 2019). As suggested by Koren and Rus (2019), open spaces can be divided into three main types: green spaces, such as parks and gardens; built-up spaces such as streets, squares, parking, sports fields and playgrounds; and undeveloped urban spaces, which have been defined by Allan et al., (2013) as residual left-over space, or urban void.

### 5.2.1. Open spaces in Beirut

In Beirut, changing social, political, economic and environmental factors have encouraged a rapid rate urbanization, which has created critical challenges in the development and the sustainability of the city (Aouad and Kaloustian, 2021). Formal public open spaces in Beirut are scarce and poorly-managed: as identified by the Beirut Urban Lab<sup>8</sup> (BUL) at the American University of Beirut, they consist of 21 parks and gardens, a seaside Corniche, and a few publicly accessible coastal sites, displayed in blue and green in Figure 5-1. Indeed, formal public open spaces are very limited in Beirut with an area of green space less than 1 m<sup>2</sup> by inhabitant (Mazraani, 2020). Additionally, some public open spaces in Beirut have a highly controlled access through limited opening times and permissible activities. Horsh Beirut (also known as the Pine Forest) is a great example of a public open space with highly-controlled access, as the forest was closed for 40 years until 2015, which made it forgotten or rather unknown to a great proportion of the local residents (Mady, 2015).

Ideally, public open spaces should be managed in Beirut and purposed for varying communal practices, particularly crisis management. Alternatively, and as suggested by Mazraani (2020), the repurposing of public and private vacant parcels in Beirut for multiple social spatial practices would respond to the needs of the residents and contribute to the fortification of the communal life. Mazraani (2020) also highlighted the vital role that have played the urban vacant sites in the crisis management during and in

---

<sup>8</sup> <https://beiruturbanlab.com/en/Details/619/vacancy-as-opportunity-re-activating-public-life-in-beirut>

the aftermath of the August 4 Beirut Port explosion, as public and private vacant lots have been used by the community as spaces for the gathering of the population and for the provision of relief.

From this perspective, we have considered that in case of an earthquake in Beirut, people will take refuge in any place far from buildings with no differentiation between private and public spaces. Instead, the open spaces that can accommodate people in the event of an earthquake were defined in terms of their:

- safety: an open space should be a safe zone away from potentially harmful buildings and debris. This was achieved by imposing a minimal distance of 20 m between open spaces and buildings, which is more than twice the maximum debris width estimated for the pessimistic earthquake scenario of  $PGA = 0.5 g$ .
- size: large and smaller (less than  $1000 m^2$ ) open spaces are both important for sheltering populations (Villagra et al., 2014). Therefore, any unbuilt space with an area greater than  $500 m^2$  was considered to have the potential of accommodating people.

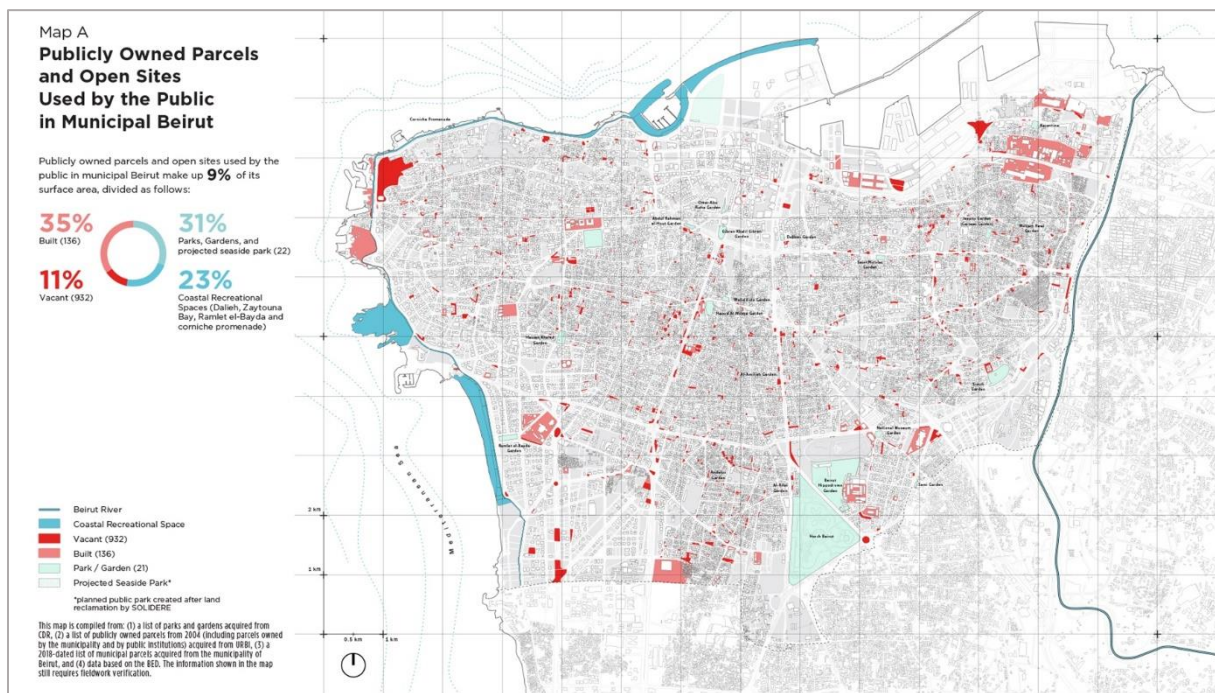


Figure 5-1: Public open spaces in Beirut identified by the BUL. Source: <https://beiruturbanlab.com/en/Details/619/vacancies-opportunity-re-activating-public-life-in-beirut>

Thus, we have relied on geographic information systems to delimit the open spaces in Beirut that correspond to these criteria. The processing steps and the results are presented in the following section.

### 5.2.2. Processing and results

The city's boundary layer was extracted from OSM. In QGIS, a buffer of 20 m was applied around the buildings, which allowed identifying the zones that could not be considered as open spaces. These zones were then subtracted from the geometry of the city, which led to the delimitation of all the spaces that are more than 20 m away from buildings. From these spaces, only the polygons with an area greater than  $500 m^2$  were preserved. Although land-use was not formally considered in the proposed open space definition, we have identified some land-use cases that would not be safe for sheltering populations. They include cemeteries, as the cemeteries in Beirut are heavily constructed with concrete and masonry structures that could possibly be damaged during an earthquake (Figure 5-2 (a)), the containers area at the port, where only narrow passages exist between long lanes of superimposed containers (Figure 5-2 (b)). Highways were considered unsafe too due to the high circulation speed and because they should be reserved for the use of emergency vehicles. Moreover, beachfront spaces that can only be accessed through an establishment (beach resort or restaurant) were also identified. Therefore, the container area at the port, the cemeteries, the highways and some beachfront spaces in Beirut were digitized and

subtracted from the identified open spaces. Finally, the geometry of the delimited open spaces was simplified, using the simplification tool in QGIS followed by the application of a buffer with a negative value, to smoothen the sharp edges resulting from the polygon subtraction.

This has resulted in the delimitation of 268 open spaces in Beirut, with surface areas ranging from 506 m<sup>2</sup> to 830 000 m<sup>2</sup>, with a total open space area of 4 028 220 m<sup>2</sup>. The identified open spaces were then characterized in terms of their:

- capacity: following the guidelines of ECPFE and OASP(2002), the capacity of each open space was calculated on the basis of 2 m<sup>2</sup>/person;
- access: open spaces that have restricted access due to a secured gate or a locked door have been identified. They comprise the Sanayeh Garden, Horsh Beirut, the Hippodrome, the Sioufi Garden and the port of Beirut. An attribute “can be locked” was added to these open spaces.



Figure 5-2 : Examples of unbuilt spaces in Beirut considered unsafe for the gathering of populations in the case of an earthquake. (a) Saint Dimitrios Cemetery in Achrafieh, Beirut. Photo by: Katrice Dustin, retrieved from: <https://www.travel-almanac.com/blogs/psychological-sightseeing/st-demetrius-mar-mitr>. (b) Container area at the port of Beirut. Photo by: Rami Rizk, retrieved from: <https://www.lebanoninapicture.com/pictures/port-of-beirut-lebanon-beirut-port-dji-drones-quadcopte>.

The final map of open spaces in Beirut is shown in Figure 5-3. We can see on this map that the largest open spaces in the city are spaces that have limited access: the port, the Hippodrome and Horsh Beirut. Large open spaces have also been identified on the maritime border; nonetheless, the safety level of these spaces is questionable, as in the case of earthquake-triggered tsunamis, the presence near the sea should be highly avoided. However, for simplification purposes, we have disregarded the possibility of occurrence of earthquake-triggered tsunamis, and the open spaces identified on the maritime border were preserved. The other open spaces identified were mainly located in the outskirts of the city, with a high concentration of open spaces in the Medawar sector and in the south of the Achrafieh and the Moussaitbeh sectors. In the center of Beirut, and particularly in the north of Mazraa and Moussaitbeh, the absence of open spaces is particularly noticeable, as only a few open spaces with very limited size were identified.

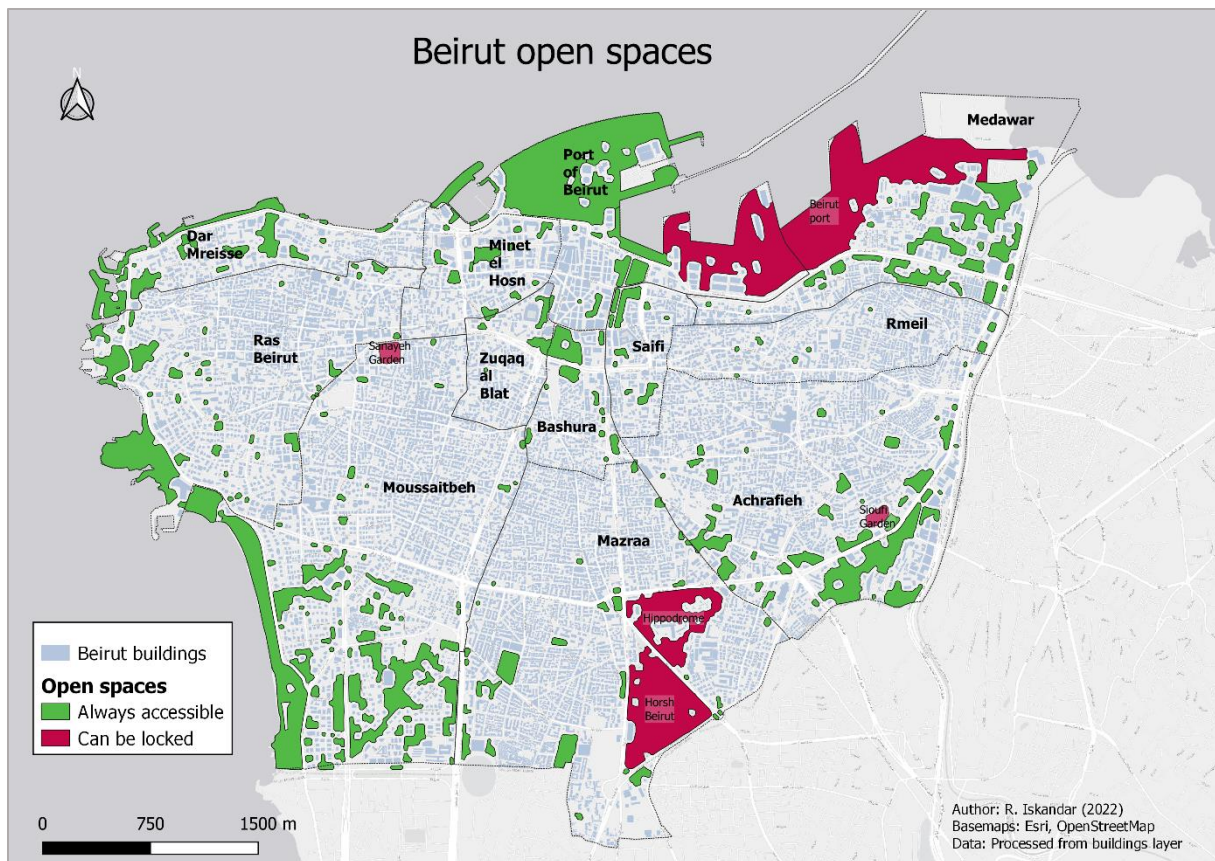


Figure 5-3 : Map showing the open spaces that are always accessible (green polygons) or can be locked (red polygons) in Beirut identified based on the proposed definition. Beirut buildings footprint is extracted from OpenStreet Map (last accessed: 26/02/2021)

### 5.2.3. Summary

Open spaces play a major role in the immediate aftermath of an earthquake, as they are safe spaces that people can evacuate to, away from buildings and debris. Although public open spaces should be included in city plans and managed by the local authorities, in Beirut, public open spaces are scant and access to these spaces is limited, as some of them may be locked and only accessible within certain hours. Nonetheless, in case of emergency, the population will gather in any place available away from buildings, whether this place is public or private. From this perspective, open spaces in Beirut have been identified following a GIS-based approach. The delimited open spaces are not uniformly distributed in the city: the outskirts of Beirut have a high concentration of open spaces, while the central area is particularly poor in open spaces. Moreover, some of the largest open spaces identified have critical conditions either due to their location near the sea or due to their restricted access, which may be problematic in case of mass evacuation of the population towards these spaces.

## 5.3. DELIMITATION OF NATURAL AND URBAN CONSTRAINTS ON PEDESTRIAN MOBILITY IN BEIRUT

The speed and route options of pedestrians in a city are affected by several constraints, which can be related to the city's natural environment or its urban features. As mentioned Chapter 2 (section 2.6.2.1) and evidenced by the DTM in (Figure 4-13 (b)) the topography in Beirut is not flat, therefore the slope of the terrain imposes additional challenges on the mobility of pedestrians. Regarding urban features, buildings are obstacles that constrain the routes of pedestrians; and in the aftermath of an earthquake, debris around buildings further obstruct mobility. Another type of mobility obstacle in Beirut, are the highways that are on a different level from the natural terrain, which make them inaccessible to pedestrians, i.e. barriers. As the buildings and debris were identified in the previous sections, in the

following the slope of the terrain is identified and barriers in Beirut are delimited.

### 5.3.1. Derivation of the terrain’s slope from the DTM

The slope of a terrain can be calculated in QGIS using the “Slope” tool, which takes as input a DTM and provides a raster layer, in which each pixel takes the value of the slope. Although a DTM of Beirut with a resolution of 2 m was derived (see Chapter 4 section 4.2.3.2.2), such a high-resolution is not needed for the movement of pedestrians. Additionally, having a raster with a high number of pixels increases the memory needs of the simulations, especially when simulating a large urban area, and negatively affects the speed of the simulations. Consequently, we derived a new DTM from the processing of the satellite images, with a resolution of 10 m (instead of 2 m). The slope of the terrain was calculated from this DTM. The resulting slope map is shown in Figure 5-4. In this figure, we can see the relief of the terrain, especially the hills in Achrafieh (highest slope values of 24 degrees) and Ras Beirut.

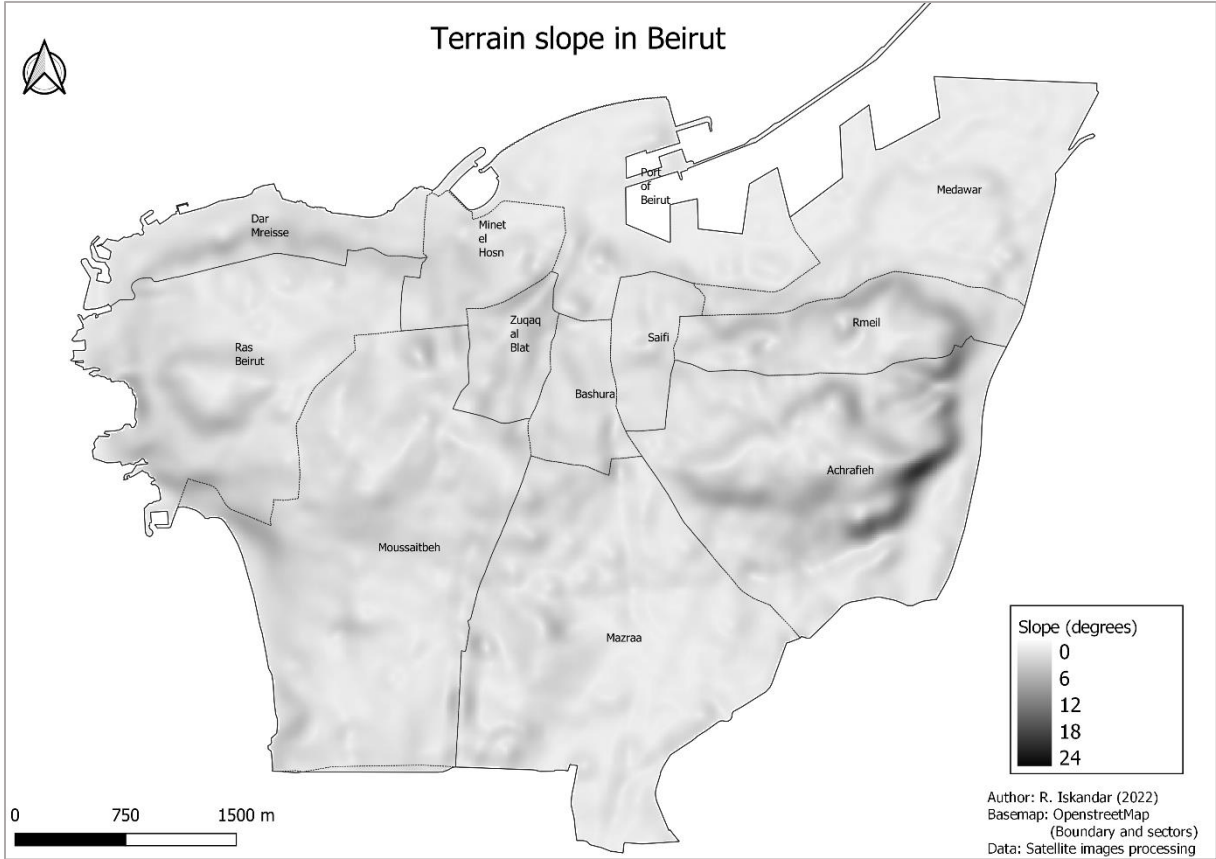


Figure 5-4: Slope of the terrain in Beirut

### 5.3.2. Delimitation of barriers

As for the anthropic barriers in Beirut, we considered that the highway that stretches from Zugaq el Blat sector to the south of Moussaitbeh (highway 51M) would be an obstacle for pedestrians’ mobility in Beirut at different locations. The elevation of this highway changes considerably as it has many tunnels and bridges, often with wall on the sides of the way to secure the structures (Figure 5-5).

Consequently, we digitized in OpenStreetMap the portions of this highway that would not be accessible to pedestrians. These portions were considered as barriers (Figure 5-6).



Figure 5-5: Stretch of the highway 51M in Salim Salam, Beirut with walls on the side of the road. Photography by: Jean ISENMANN

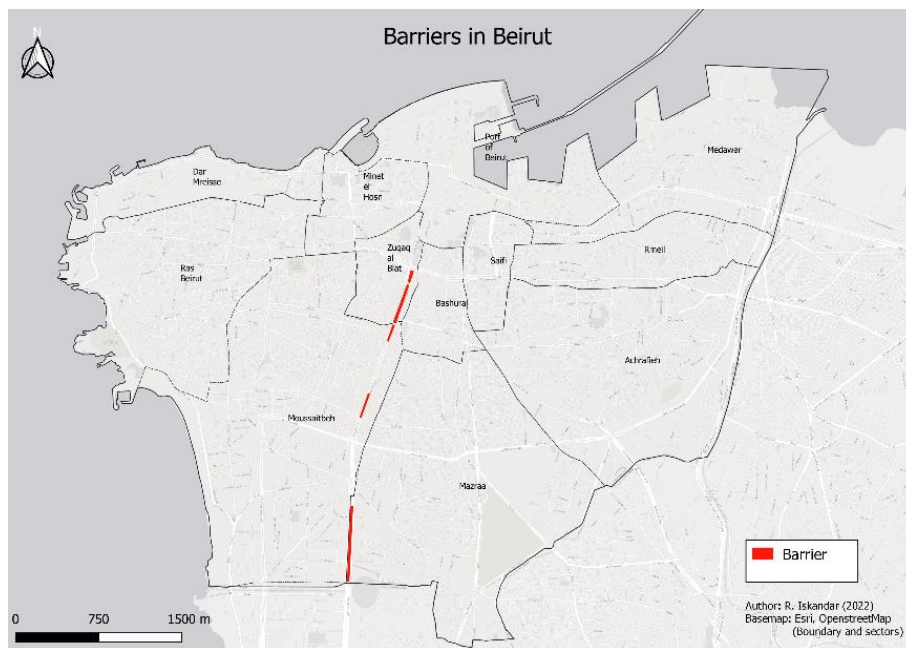


Figure 5-6: Barriers in Beirut digitized on the highway 51M

After delimiting the urban features needed for the simulations, the next section focuses on the generation of population data.

#### 5.4.ESTIMATION OF THE POPULATION'S SIZE AND DISTRIBUTION: SYNTHETIC POPULATION

For the simulation of human behavior in response to an earthquake, 3 main features of the population are needed: (1) its size, i.e. how many people are affected by the earthquake, (2) its spatial distribution, which is different depending on the time of the day and the activities of the individuals and (3) its characteristics, i.e. the distribution of the population's social and demographic attributes. Once these

data are available, synthetic population generation techniques can reproduce to a high degree of fidelity a “numerical” population that can be used in simulations of behaviors at the individual level.

Nevertheless, this task is particularly challenging in Lebanon due to the absence of census data and to the incompleteness of the available statistical data. In the following section, we further detail the challenges related to the collection of accurate population data, then we present our proposed approach and the generation of the synthetic population for Beirut.

#### **5.4.1. Challenges in the collection of accurate population data in Lebanon and proposed approach**

The collection of complete and accurate population data is a particularly challenging task in Lebanon, as the last national population census in Lebanon dates back to 1932 and no official population enumeration has been undertaken since (Maktabi, 1999). Despite the lack of complete enumerated population data in Lebanon, household surveys conducted by the Central Administration of Statistics in Lebanon (CAS) provide some insightful information on the Lebanese population. The latest household survey undertaken by the CAS, the Labour Force and Household Living Conditions Survey (LFHLCS) (CAS, 2020), was conducted between 2018 and 2019 and covered a national sample of 39 000 households. This survey produced estimates of indicators at the national level and at sub-national levels. These indicators are related to the labor market, the educational characteristics and the living conditions of the residents in Lebanon. However, the LFHLCS covered only the population of Lebanon living in residential dwellings and excluded people living in non-residential units, such as unfurnished buildings, construction sites, refugee camps and illegal settlements. Therefore, this study leads to an underestimation of the number of dwellers of the city (Fawaz and Peillen, 2003), which can be problematic for emergency planning.

Another challenge related to the assessment of the population exposure to earthquakes, is the prediction of the population’s spatial distribution at different times of the day. Moreover, the available population datasets usually represent residential populations, i.e. nighttime populations, and can consequently be highly inaccurate for daytime scenarios where population’s commuting occurs in both the directions: an outward flow of residents leaving the city, and inward population flow towards the city.

Having these challenges in mind and given the need for a realistic estimation of the population exposure to earthquakes in Beirut, we have relied on a geographic information system based approach to develop a population exposure model for Beirut. However, faced with the complexity of assessing the population’s migration flow from and to the city during the day, the model is developed for the residents of the city only. Nevertheless, the dynamic spatial distribution of the residential population is accounted for by locating the population in residential units during the night and in both residential buildings and places of work during the day. In addition to the population’s size and spatial distribution, the generated population is also characterized by social attributes related to the population’s age, gender and household composition.

The first step in this approach is the characterization of the buildings’ function, which allows classifying buildings as either residential or non-residential. The number of apartments in residential buildings is then estimated, from which the number of households in Beirut can be inferred. Then, a synthetic population of individuals and households is generated for Beirut, with age, gender and household composition distributions representing the actual population’s characteristics. In the final step, the spatial distribution of the population is performed for both night and day scenarios.

A detailed description of each of these steps is presented in the following sections.

#### **5.4.2. Identification of the buildings’ function**

The function of a building designates its primary purpose and its typical use. The classification of buildings into residential and non-residential is essential for the estimation of the population’s distribution at different times of the day. Although some buildings might have mixed-functions (retail and residential for instance) we did not consider mixed usages, and any building that hosts a residential activity was assigned as residential. Consequently, in order to classify the buildings’ function, we

focused on the identification of buildings that have a full non-residential use, and considered the others as residential. Additionally, for non-residential buildings, we are not interested in designating the building’s specific function (school, store, etc..), except for hospitals, since hospitals play an essential role in crisis management, as people evacuate towards hospitals for immediate emergency relief. Therefore, non-residential buildings that are not hospitals were classified as “work”.

As the dataset of buildings in Beirut was retrieved from OSM, the building’s use can be identified by the value taken by the “building” key in the attribute table. This key can take values related to different categories of use such as accommodation, commercial, religious and sports. Moreover, the building’s function may also be described by the value of the “amenity” key that is used to indicate useful and important facilities such as libraries, banks, restaurants and schools for example. In addition, the key “name” could also indicate the function of the building, when the name of the building designates a public institution or a medical facility for instance.

To identify non-residential buildings, values taken by “building” and “amenity” keys and designating non-residential usage were pinpointed. The retained values for both keys are indicated in Table 5-1. Buildings having these values as well as buildings having names related to ministries, official administrations and supermarkets were identified and classified as non-residential. This resulted in the identification of 570 non-residential buildings in Beirut. Then, from these non-residential buildings, those having the field attribute “building = hospital” or “amenity=hospital” were identified (86 buildings) and characterized as hospitals. The relatively high number of hospital buildings could be due to the fact that the same hospital could be composed of several adjacent but separate buildings, which increases the number of hospital buildings without being directly correlated to the number of medical institutions.

After identifying the non-residential buildings, we verified that these buildings corresponded to a full non-residential use. We validated, when it was possible, the buildings tagged as commercial, retail and supermarkets by looking at images of the building in Google Earth, in both satellite and street views. In the images, we verified that these buildings did not hold any residential functions, mainly by looking at the shape of the roof and whether or not the building had balconies. Through this process, we have validated that all the identified buildings had a full non-residential use.

*Table 5-1 : Tags in OpenStreetMap considered to refer to non-residential use of buildings*

<b>Building key</b>	<b>Amenity key</b>
“church” ; “civic” ; “commercial” ; “commercial;yes” ; “garage” ; “hospital” ; “hotel” ; “industrial” ; “kindergarten” ; “mosque” ; “office” ; “retail” ; “roof” ; “ruins” ; “school” ; “university” ; “warehouse” ; “construction”	“arts_centre”; “cinema”; “community_centre (mansion)” ; “courthouse” ; “embassy” ; “fuel” ; “hospital” ; “nightclub” ; “place_of_worship” ; “police” ; “school” ; “theatre” ; “university”

As non-residential buildings may not be all tagged in OSM, we have also relied on the Beirut Built Environment Database (BBED) developed by the Beirut Urban Lab (BUL), for the identification of additional non-residential buildings. This database was updated last in October 2019 and made available to us in September 2021. It contains a polygon layer of building footprints that covers 625 non-residential buildings in Beirut, as shown in Figure 5-7. Figure 5-8 shows the OSM buildings layer overlaying the BBED; we can see that the building polygons are highly compatible, which makes it possible to compare the superimposed buildings between the two layers. Therefore, a spatial join by location was performed in QGIS between the two building layers, which resulted in the identification of 589 additional buildings from the OSM layer that overlap non-residential buildings in the BBED layer. These buildings were classified as non-residential and were added to the previously identified non-residential buildings.

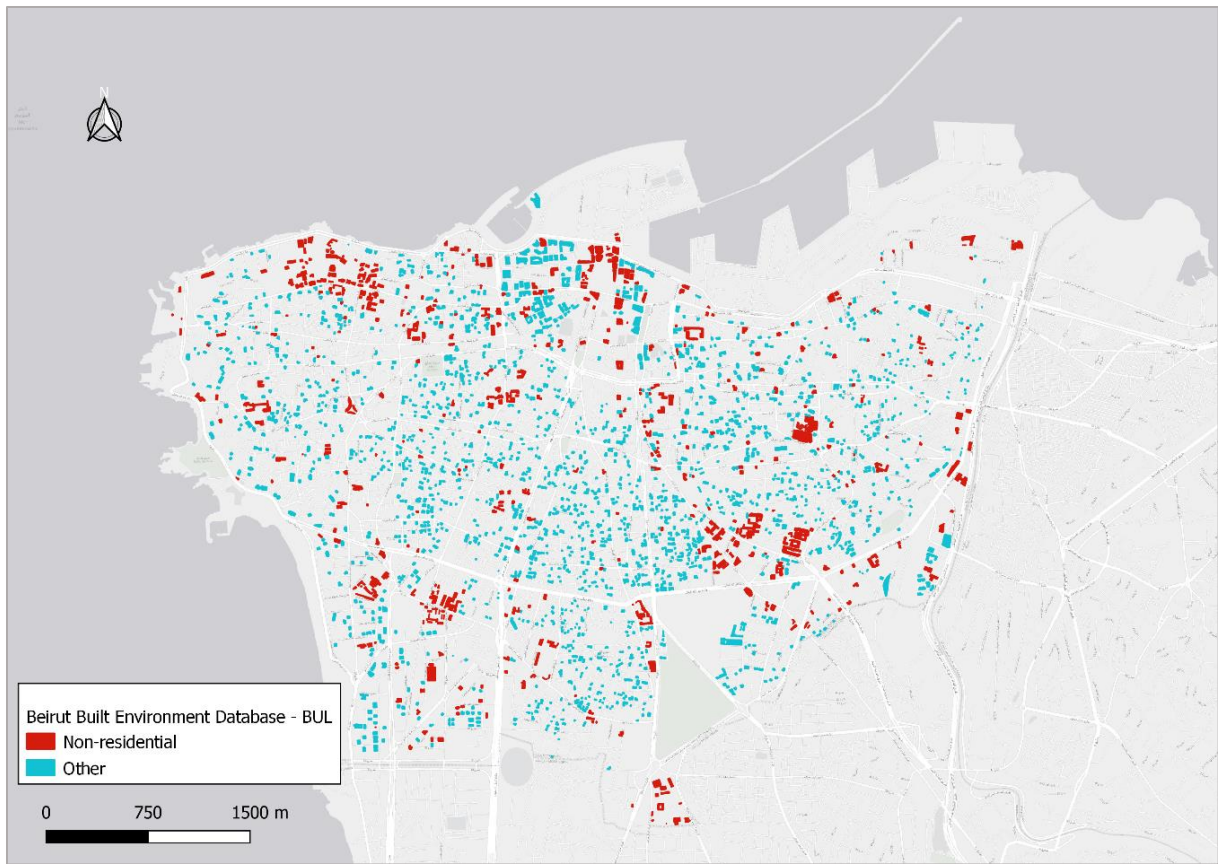


Figure 5-7: Map showing the buildings in Beirut retrieved from the Beirut Built Environment Database (BUL). Buildings function are indicated in colored polygons.

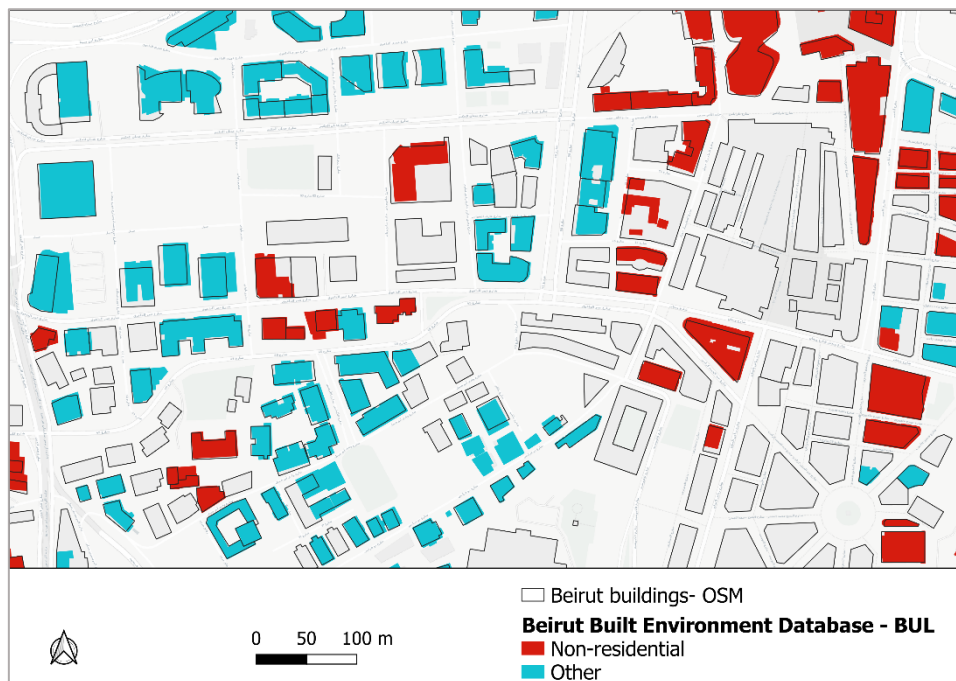


Figure 5-8 : Beirut buildings retrieved from OSM (black contour) overlaying the buildings from the Beirut Built Environment Database (red and turquoise).

In conclusion, Beirut buildings' function were characterized using a combination of the two complementary spatial datasets, OSM and BBED, one being rich in terms of geometry of objects and the other rich in terms of attributes. Figure 5-9 shows the 1 159 non-residential buildings identified in

Beirut, from which 86 buildings were designated as hospitals (and the 1 073 others as work). The remaining 13 930 buildings which were classified as residential buildings.

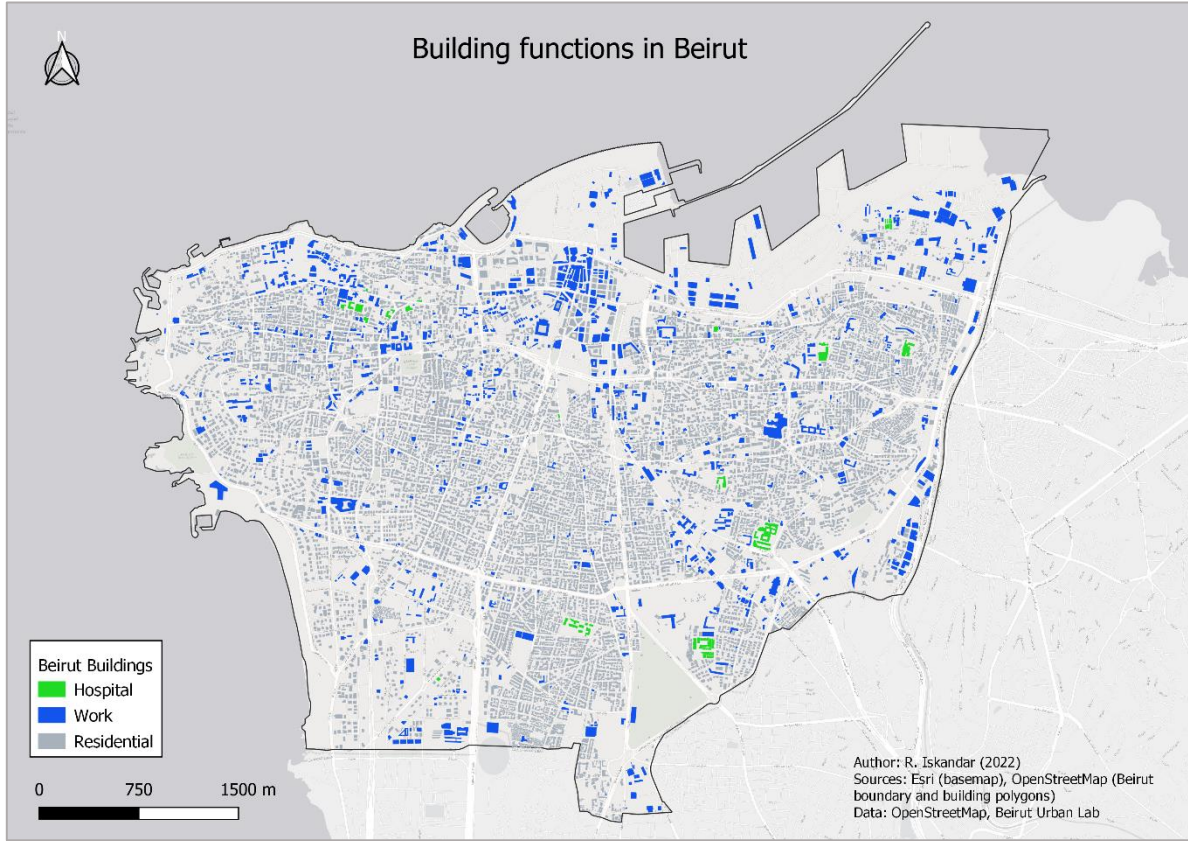


Figure 5-9 : Map showing the OSM buildings classified as: residential, hospital and work

### 5.4.3. Estimation of the number of residential apartments in Beirut

Having identified the residential buildings in Beirut, the total number of residential apartments in the city can be assessed by estimating the number of apartments per building. This can be achieved by estimating the average apartment surface in Beirut, and then, for each building, dividing the building's surface by this value to obtain the number of apartments per floor, which is then multiplied by the building's number of floors to estimate the total number of apartments in the building (equation 5.1):

$$N_{apartments} = \sum_{i=1}^n \frac{S_{b,i}}{AS_{app,i}} \times N_{floors,i} \quad (5.1)$$

Where  $N_{apartments}$  is the total number of apartments in Beirut,  $S_{b,i}$  is the building's surface area,  $AS_{app,i}$  is the average apartment surface in Beirut,  $N_{floors,i}$  is the building's number of floors and  $n$  is the number of residential buildings in Beirut.

To estimate the average apartment surface in Beirut, we have used the LIBRIS building database (Salameh, 2016) that contains a sample of 7 692 buildings from the city of Beirut for which both the number of apartments per building and the number of floors were collected by a field survey. The number of apartments per floor was obtained for each building by dividing the total number of apartments by the number of floors, which allowed computing the average apartment surface in each building by dividing the area of the building's footprint by the number of apartments per floor.

However, in order to reduce the estimation error, and as the use of building function was not specified in the LIBRIS database, we have disregarded buildings that have a floor area greater than 1500 m<sup>2</sup>, as these buildings were assumed too large to represent residential buildings. Moreover, buildings that have 1 apartment per floor were also disregarded, as the indicated number of apartments could be poorly

constrained as a result of missing observations during the LIBRIS field survey. Additionally, we have considered that high-rise buildings, with 15 floors and more, typically represent skyscrapers and luxurious buildings and consequently may have an apartment surface greater than low to mid-rise buildings. Therefore, the LIBRIS database was split into 2 subsets according to the buildings' number of floors: a subset for buildings with less than 15 floors, and another subset for buildings having 15 floors and more.

The distribution of the average apartment surfaces was evaluated for each of the two subsets, by calculating the mean apartment surface along with the standard deviation, as well as the median apartment surface (Table 5-2). As presumed, high-rise buildings have greater apartment surfaces than lower-rise buildings. As both subsets have a wide distribution of apartment surfaces, ranging from less than 50 m<sup>2</sup> up to 745 m<sup>2</sup>, the median value was chosen to represent the typical apartment size in each subset as it is less affected by the extreme values than the mean.

Table 5-2 : Distribution of apartment surfaces for low-rise and high-rise buildings in the LIBRIS buildings database

	<b>Buildings with less than 15 floors</b>	<b>Buildings with 15 floors and more</b>
<b>Number of buildings</b>	2780	34
<b>Minimum surface (m<sup>2</sup>)</b>	10	49
<b>Maximum surface (m<sup>2</sup>)</b>	736	743
<b>Mean surface (m<sup>2</sup>)</b>	128	232
<b>Standard deviation (m<sup>2</sup>)</b>	82	145
<b>Median surface (m<sup>2</sup>)</b>	113	192

Having determined the average apartment surface in Beirut, the total number of residential apartments in Beirut could be computed by the equation (5.1) updated as follows:

$$N_{apartments} = \sum_{i=1}^k \frac{S_{b,i}}{113} \times N_{floors,i} + \sum_{j=1}^l \frac{S_{b,j}}{192} \times N_{floors,j} \quad (5.1 \text{ bis})$$

where  $k$  and  $l$  represent the number of buildings having less than 15 floors and the number of buildings having 15 floors and more, respectively.

Accordingly, it was estimated that there are 246 325 residential apartments in Beirut, distributed in 13 930 residential buildings. If we consider that all apartments are inhabited, and that each apartment is occupied by one household only, the estimated number of households in Beirut is 246 325. In comparison to the 100 000 households estimated in Lebanon by the CAS in the LFHLCS, our estimation seems to exaggerate the number of households by around 2.46 times. The difference between the two estimations does indeed seem very important, and could have several possible explanations. It could be attributed to an underestimation of the number of households by the CAS, since in the LFHLCS, residents of refugee camps and informal settlements are not considered, while these buildings are digitized in OSM. This discrepancy could also be attributed to an error in the identification of residential buildings and an exaggeration of their number. Moreover, apartments in the city can be vacant and not occupied, which could also lead to an exaggeration of the number of estimated households when considering all apartments to be occupied.

Nevertheless, although the estimated number of households is likely to be exaggerated, the over-estimation of the population size is preferred to its underestimation, as it portrays more pessimistic conditions in which a greater number of pedestrians evacuate and look for shelter. Moreover, it may also compensate for not taking into account the “non-residential” population in Beirut, especially for a day scenario, as Beirut holds a large number of administrative institutions and business centers that are frequented by non-Beirut residents during the day. Therefore, the estimated number was retained for the subsequent analysis.

#### 5.4.4. Methodology for the generation of a synthetic population of households and individuals in Beirut

Micro-simulation models that simulate the dynamics of a large population with an explicit representation of each individual require a proper initialization with a population that represents the population of interest. Additionally, as behaviors are rarely individualistic and can be influenced by individuals' social ties, family ties between individuals need to be modeled as well, which also requires representing the organization of individuals into households. However, exhaustive individual data on the population, i.e. disaggregated or census data, are usually inaccessible for several possible reasons, including the privacy and the security of individuals. Occasionally, a subset of the census data, called public-use sample, may be available to the public (Müller and Axhausen, 2011). On the other hand, aggregate data, i.e. data showing the distribution of a particular attribute such as the population's age and gender, are usually available as results of large population surveys and are often accessible to the public. To overcome the lack of complete population enumeration data, synthetic populations can be created for micro-simulation models. The synthesized population is a simplified representation of the real population, since only the variables of interest are reproduced (Chapuis, 2019).

Several methods have been developed for the generation of synthetic populations of individuals and households. As described in Sun et al.(2018), these methods can be classified into three main categories: Synthetic Reconstruction (SR), Combinatorial Optimization (CO) and Statistical Learning (SL). A complete review and comparison of population synthesis methods can be found in Yameogo et al. (2020). The main findings of this review can be summarized as follows:

- SR is the most commonly used approach for population synthesis. SR usually requires both a census sample and aggregate data from which joint-distributions between the attributes of interest are determined. The population of individuals and households is created in a two-step process: the fitting stage in which weights are assigned to the individuals and households in the sample to ensure the sum of the weights corresponds to the marginal sums from the aggregate data. Then comes the allocation step that ensures that individuals from the sample are replicated in proportion to their corresponding weights.
- Similarly, CO techniques also require both sample and marginal data on individuals and households; however, unlike SR, CO does not explicitly determine the joint distribution across the controlled attributes. In CO, the study area is divided into mutually exclusive regions, similar to census blocks, and a subset of the sample is fitted to the given margins for each zone. Then, more households and individuals are added to each region in an iterative process, while ensuring the goodness of fit at each iteration.
- Finally, SL methods focus on the joint distribution of all attributes in the sample by directly computing a probability for each combination. In contrast to SR and CO, SL requires sample data only. In most SL techniques, a parametric model is first proposed, and then the model's structure and parameters are tuned until the proposed model converges with the original sample.

Although sample-based approaches have been widely developed and constitute the primary method for the generation of synthetic populations, their use is restricted to study areas for which sample data are available. To overcome this limitation, sample-free SR methods that rely on aggregate data only have been developed. Barthelemy and Toint (2013) developed a sample-free method based on a hierarchical three-step approach. First, the pool of individuals is created based on the distribution of individuals' attributes from aggregate data. Then, the joint distributions of household types are generated and finally, the households are created by grouping individuals based on ad hoc rules depending on the study area. Although some studies pointed that this approach does not guarantee the consistency of households and individuals in satisfying marginal constraints (Sun and Erath, 2015; Zhu and Ferreira, 2014), this approach remains relatively satisfying for cases where only limited data are available and inconsistencies between the data sources exist.

To construct a synthetic population that represents the distribution of individuals and households in Beirut as closely as possible and due to the unavailability of census data in Lebanon, we had to rely on a sample-free approach. Aggregate households and individuals' data could be found in the LFH LCS

demography survey conducted by the CAS. The survey provides data about the distribution of residents according to age, gender, marital status, nationality, place of registration (i.e. the locality in which individuals are registered) and place of residence (i.e. the locality where individuals live). The only variables we are interested in for the simulation of emergency behaviors are the age and gender of individuals as they are assumed to have the most impact on the behavioral choices. Regarding households, in addition to the distribution of household sizes, the survey provides several indicators related to the head of the household, i.e., the person who has more decision-making power than others in the household and more control over the household's resources (Posel, 2001). From these indicators, we are interested in the distributions of head of the households' sex and gender and the relations of the other household members to the head of the household. Therefore, the main idea behind the generation of a synthetic population for Beirut could be summarized by generating a population comprised of individuals grouped into households, which respect the constraints found in the data, summarized in Table 5-3:

*Table 5-3 : Data on the distribution of residents and households provided by the LFHLCs*

<b>Data</b>	<b>Possible values</b>
age of the residents	less than 5; 5-10; 10-15; 15-20; 20-25; 25-30; 30-35; 35-40; 40-45; 45-50; 50-55; 55-60; 60-65; 65-70; 70-75; 75-80; 80-85; 85 and more
sex of the residents	women; men
size of the households	1; 2; 3; 4; 5; 6; 7; 8
sex of the head of the household	women; men
age of the head of the household	15-20; 20-25; 25-30; 30-35; 35-40; 40-45; 45-50; 50-55; 55-60; 60-65; 65-70; 70-75; 75-80; 80-85; 85 and more
role in the household (relation with the head of the household)	head of household; husband; wife; son; daughter; son-in-law; daughter-in-law; grandson; granddaughter; father; mother; brother; sister; other kinship; no kinship and domestic worker

Although the separate distributions of individuals and households characteristics were provided at the level of Beirut, no joint distributions between the attributes were given at this level, as joint distributions were only provided at the level of Lebanon. The generation of joint distributions at the scale of Beirut being outside the scope of this work, we have decided to generate a synthetic population using the distributions provided at the level of Lebanon, under the assumption that they are representative of Beirut too. Thus, the data used for the generation of the synthetic population are:

- the distribution of the residents' age according to their gender at the scale of Lebanon;
- the distribution of households in Lebanon according to the household size;
- the distribution of the head of households according to their age and household size, at the level of Lebanon;
- the distribution of the head of households in Lebanon according to their sex and age;
- the distribution of residents in Lebanon according to their relation to the head of the household.

The distribution of the residents' age according to their gender provides the necessary data to generate a population of individuals whose characteristics correspond to the original population's characteristics. Nevertheless, the data provided by the LFHLCs on household compositions in Lebanon differ significantly from the typical data used for grouping individuals into households in population synthesis methodologies, which is often based on the type of the household (e.g. single man alone, couple with children, etc.). For instance, Barthelemy and Toint (2013) relied on data regarding household type and the numbers of adults and children per household to fit individuals into households. The same approach could not be applied in Lebanon, since the data only provide the household size and the relationships of

household members with the household head, without a clear specification of the household type.

To account for the specificity of the data available in Lebanon, an ad hoc methodology for the generating individuals and grouping them into households was developed in collaboration with Kevin Chapuis (UMMISCO, ESPACE-DEV, IRD). Figure 5-10 shows a graphical representation of the developed methodology, which can be described as follow:

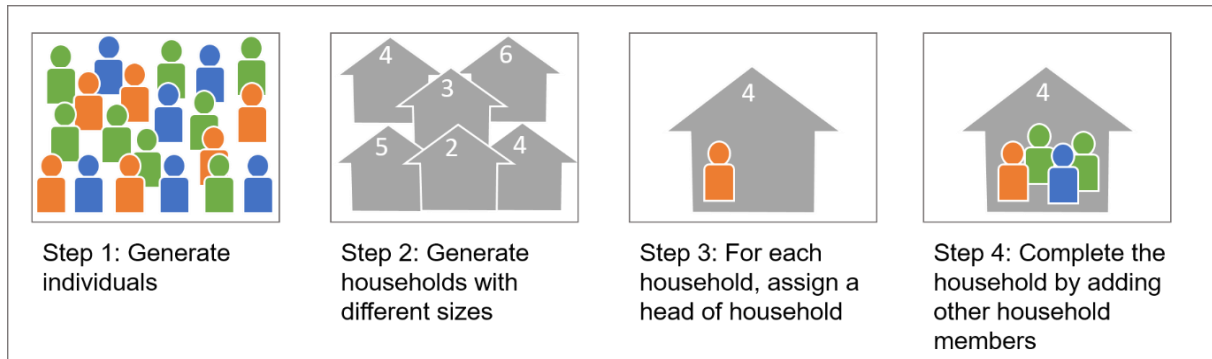


Figure 5-10 : Schematic representation of the methodology used to generate individuals in Beirut and aggregate them into households

1. The first step is the generation of the pool of individuals. After specifying the actual population size,  $N$ , the number of individuals to generate is obtained by multiplying the population size by an “expansion factor” greater than 1. The exaggeration of the size of the pool of individuals is intended to allow for more flexibility when choosing the individuals to fit into households. Subsequently, individuals are generated with attributes of sex and age corresponding to the distribution of the residents provided by the input data.
2. Based on the size of the actual population,  $N$ , and the distribution of the household sizes provided by the input data, the number of households and the corresponding household sizes needed to fit the population are determined.
3. For a given household, depending on the household size, a person that satisfies the distribution of the age and the gender of the head of the household with respect to this household’s size is drawn from the pool of individuals and assigned as the head of the household.
4. If the household is composed of more than one person, an additional person is drawn from the pool of individuals and assigned as a household member. For picking this person, the role he/she occupies is first chosen according to the distribution of the residents’ relations to the head of the household (spouse, child, etc.). The chosen role gives age and gender constraints according to which a person is drawn. For instance, constraints are specified on the gender of spouses (assuming all couples are heterosexual) and on the age difference between parents and children. Then successively, additional people are drawn and assigned to the household until the number of people in the household matches the household size.

Steps 3 and 4 are executed for each household until all households reach their target number of individuals. Finally, at the end of the generation process, the remaining individuals who were created but not attributed to households are deleted, which allows to restore the size of the population back to  $N$ .

#### 5.4.5. Application: generation of a synthetic population for Beirut

The methodology described in the previous section was applied to generate a synthetic population for the residents and households of Beirut. The size of the generated population was not limited to the population size in Beirut estimated by the LFHLCS survey (342 000 individuals gathered in 100 000 households); instead, it was determined by a target number of households to generate, set as the number of residential apartments estimated in section 5.4.3 (246 325 households).

The Gen\* plug-in (Chapuis et al., 2019) implemented in GAMA was used for the generation of the pool

of individuals. Gen\* was chosen as it handles the generation of synthetic population from all data types: sample data, a mix of sample and aggregate data, and aggregate data only, which was the case of the data available for Lebanon. As the generation of individuals was performed in GAMA, the methodology for fitting individuals into households was also implemented in the same platform. Since the population size was determined by a target number of households, the desired number of individuals to generate could not be accurately calculated. A first approximation could be obtained by multiplying the number of households (246 325) by the average household size (3.4), which results in approximately 837 505 individuals to generate. The computation time and the complexity of the algorithm increases with the increase of the population size. When fitting individuals into households, the search for individuals who fit all the desired constraints becomes significantly more time-consuming when the pool of individuals increases in size (i.e. in the order of 10 minutes for 10 000 individuals, and 2 days for 100 000 individuals). To reduce the computation time, the generation of the synthetic population was broken down into the parallel generation of 8 batches of 100 000 individuals, each batch fitted separately into households, followed by the generation of a final batch of 20 000 individuals, which resulted in the generation of a total of 246 408 households. The number of households was reduced to 246 325 by randomly choosing 83 households to be deleted along with their members. Finally, the generation process has resulted in a total population composed of 819 717 individuals fitted into 246 325 households.

The quality of the generated synthetic population was assessed by comparing the original (i.e. LFHLCS survey) and synthetic population's attributes, namely: the distribution of the age and sex of the residents, and the distribution of the household sizes, the head of households' age and gender and the relations of household members to the head of the household. The resemblance was assessed by the coefficient of correlation (R) between the predicted and original distributions. The error in the prediction was quantified by the Root Mean Square Error (RMSE), which shows the mean absolute error in the predicted distribution. Additionally, we have computed the average relative error in the classification of each attribute by computing the Average Absolute Percentage Difference (AAPD) as follows:

$$AAPD = \frac{1}{n} \sum_{i=1}^n \frac{|P_i - O_i|}{O_i} \times 100$$

Where  $P_i$  denotes the predicted distribution,  $O_i$  the original distribution and  $n$  the total number of classes for each attribute.

For the distribution at the individuals' level, as shown in Figure 5-11, the synthetic population's gender distribution (51% Women, 49% Men) is very close to the gender distribution observed in the original population with an AAPD of 1.2%. However, the generation process seems to lead to a synthetic population slightly more aged compared to the original residents. As shown in Figure 5-11, the percentage of young residents aged between 10 and 34 is under-represented in the synthetic population, whereas the proportion of older residents (50 year +) is over-estimated. The AAPD indicates that the relative classification error for the population's age is of 8.3%; nevertheless, the overall quality of the population's age classification is still satisfying with an R of 0.95 and a RMSE of 0.59.

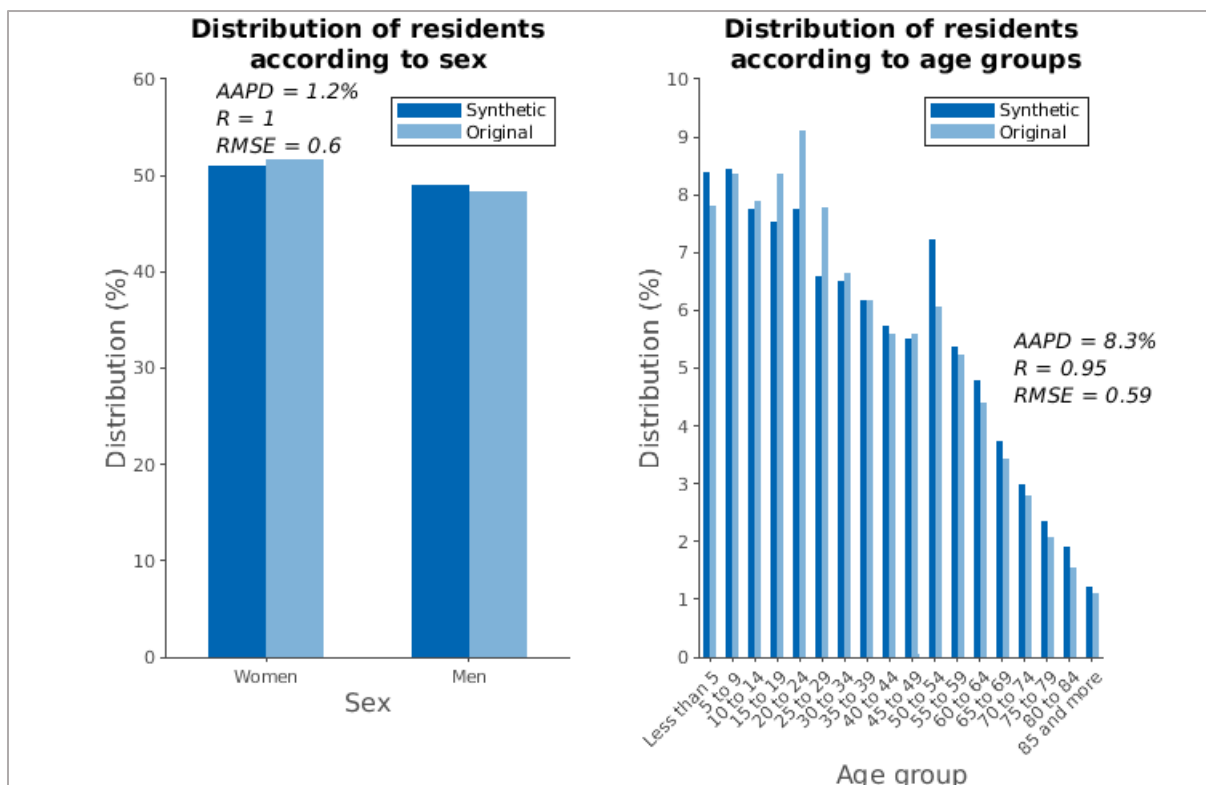


Figure 5-11 : Distribution of synthetic and original residents according to sex and age groups

For the households composition, as displayed in Figure 5-12, the generated household sizes follow the same distribution as the original household distribution, as demonstrated by the R value of 1 and the AAPD of 2.2%. The generated distribution of the head of household's gender is also very close to the original distribution with an AAPD of 1.2% only. The distribution of the head of the households' age groups correlates well with the original distribution (R=0.99) although the AAPD (7.8%) is slightly elevated. The family compositions inside households were successfully recreated, as the relations of the other household members with the head of the household were predicted with an R of 1 and an AAPD of 3.1% only.

In summary, the population generator provides a synthetic population with distributions that correlate highly with the data provided by the LFHLCS. A slight error is observed in attributes related to age: the age of the residents and the age of the head of the households. To explain the errors in the age prediction, two possibilities were identified: 1) a failure in the recreation of populations' distributions from aggregate data by Gen\*, and 2) the fitting process of individuals into households. In order to verify the first possibility, we have used Gen\* to create individuals only from the aggregate data available without fitting them into households. This resulted in a synthetic population with distributions in accordance with the input data, which allowed to verify that Gen\* was able to recreate the contingency tables of age and gender introduced in the inputs. Thus, the first possibility could be eliminated. This implies that the errors arise in the fitting process of individuals into households. The cause of this error could be the restrictions imposed on the age differences between the head of the household and the other household members. The algorithm seems to favor older individuals when choosing the people to add into households, which subsequently leads to the elimination of the younger individuals who were not attributed to households at the end of the fitting process. Although not confirmed, this appears to be a plausible explanation for the errors observed, which in future works could be analyzed further through a thorough sensitivity analysis on the model's parameters and the calibration of the age restrictions between the household members.

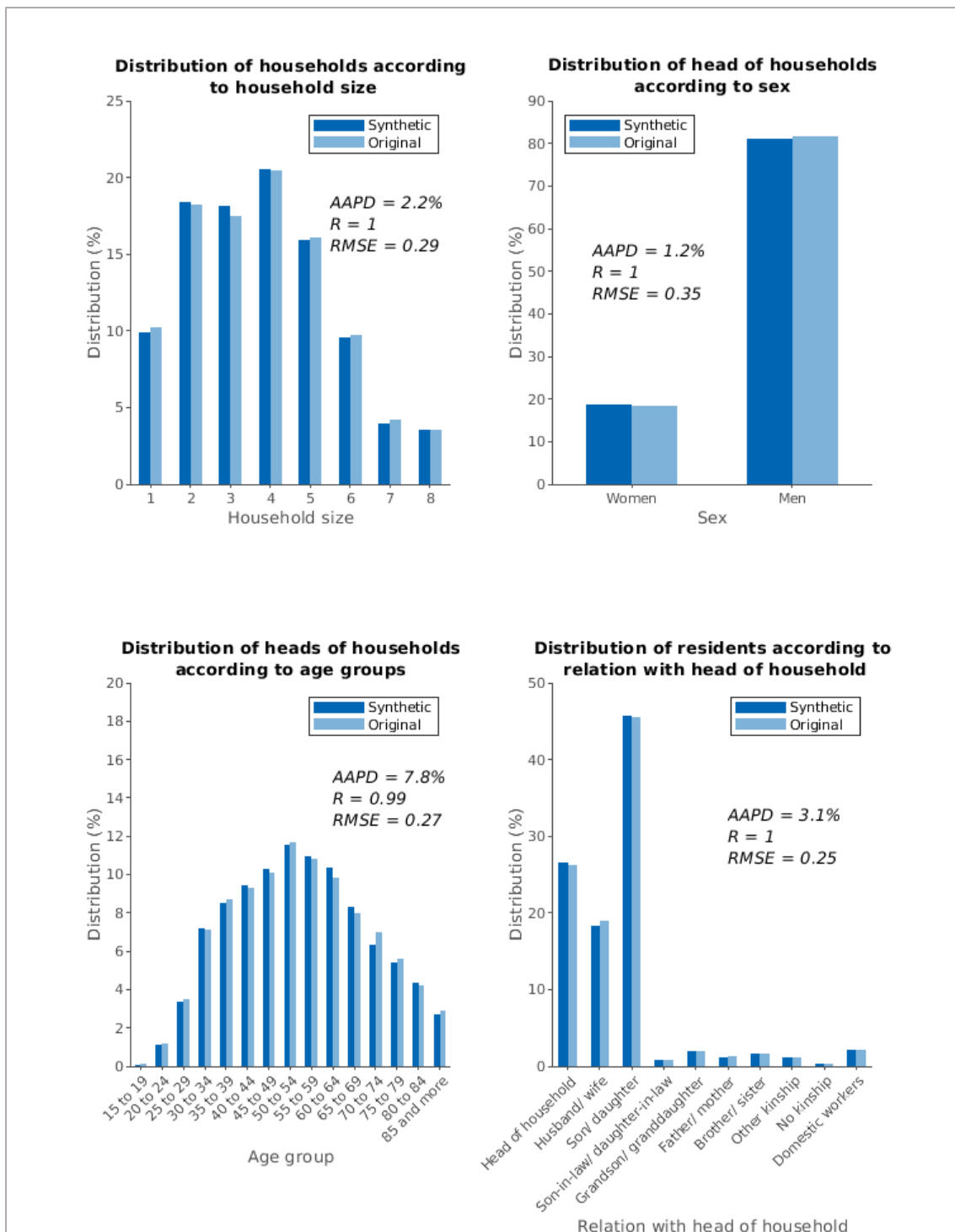


Figure 5-12 : Distribution of households' characteristics in both the synthetic and the original populations

Finally, the generated population was distributed in the city: each household was randomly assigned to an apartment in a residential building. This attributes home building for all the household members. Consequently, for each generated person, a household ID and a home building ID were assigned. For a night-time scenario the individuals are considered to be in their residential building, whereas during the day, it is assumed that 50% of people would be at places of work, 30% would be at home and 20% outdoors. The distribution of the population for day and night scenarios is handled directly by PEERS during the initialization of the simulation, nevertheless maps of the distribution of the population for day and night scenarios are provided in Appendix D.

#### **5.4.6. Summary**

The estimation of the size and distribution of the population is necessary for the simulation of human behaviors in the immediate aftermath of an earthquake. In the face of limited population data in Lebanon, we have developed an approach for the modeling of the residential population exposure to earthquakes in Beirut. The size of the population was estimated by identifying the residential buildings in the OSM building database, and calculating an approximate number of households given the buildings' surface area and the distribution of apartment sizes in Beirut. In addition to the population size, a synthetic population of individuals and households was generated for Beirut, using survey data provided by the CAS, and following an ad hoc approach that takes into account the specificity of these data. Each generated household was then affected to an apartment in a residential building, and the individuals were assumed to be located in their residential building for night scenarios, whereas for day scenarios, it was assumed that 50% of people would be at non-residential buildings, 30% would be at home and 20% would be located outdoors.

### **5.5. COLLECTION OF HUMAN BEHAVIORS IN RESPONSE TO THE AUGUST 4, 2020, EXPLOSION AT THE PORT OF BEIRUT**

The design of a data-driven model for the simulation of human behaviors in response to an earthquake requires identifying in the first place the common behaviors people adopt when facing seismic events, as well as the distribution of these behaviors among the impacted population needed to calibrate the model. As mentioned in Chapter 2, people's behavior in crisis is context-dependent. Individual behaviors are compelled by people's vulnerability, which is accentuated by structural and everyday constraints, that can be cultural (religion), social (demography), economic (poverty) and political (social protection) (Gaillard et al., 2008; Wisner, 2004). Additionally, the local physical environment and its interactions with the social environment can have a large influence on how people behave in crisis (B. L. Turner et al., 2003). Consequently, as behaviors are highly dependent on the social and physical local context, behavioral data had to be collected from previous events that happened in Lebanon.

During the time of this study, a major disaster occurred in Lebanon: the August 4, 2020 Beirut port explosion. This explosion provided valuable observations on how people in Lebanon behave to sudden onset events. Consequently, we launched an online survey for the collection of the behavioral responses, which were used for the design and calibration of PEERS. In the following, we present: (1) the motivation behind the survey, (2) the questionnaire, (3) the analysis of the survey responses. Finally, the findings are summarized and the data retained for PEERS are indicated.

#### **5.5.1. Motivation behind the collection of behavioral responses to the Beirut port explosion**

Our first attempt to gather data on the population's response to previous earthquakes in Lebanon was through a questionnaire that was specifically designed to collect data for designing an agent-based model for human behaviors in earthquakes. This questionnaire was developed by a multidisciplinary team, and was iteratively validated between computer and social scientists and tested by domain experts (Beck et al., 2020). The survey was adapted to the context of Lebanon in collaboration with researchers from the faculty of Social sciences in the USJ. The USJ team launched the survey online in October 2019. However, despite trying several diffusion strategies, the survey could not reach a satisfactory number of respondents (65 respondents only). This low response rate could be explained by the fact that no high-impact earthquakes had taken place in Lebanon around the time of the survey, which could have made the population insensible to the question of seismic risk.

Nonetheless, a few months later, a major catastrophic event took place in Lebanon. On August 4, 2020 around 6:10 p.m. (local time), a double explosion occurred at the Port of Beirut, after a fire that has started in Hangar 12. The first explosion was of small impact, and was mainly felt by the people near the port; however, the second explosion had devastating effects. The energy released from the second explosion generated a very powerful shock wave that pulverized the port and caused non-structural (including façade debris) and structural damages in nearly half of the city (Sadek et al., 2022), as shown

in Figure 5-13. The human toll of the disaster reached 218 dead, 7,000 injured (including 150 with permanent physical disabilities) among which 1 000 are children, and more than 300 000 people affected (Human Rights Watch, 2021). The explosion at the port generated seismic waves with a moment magnitude estimated at  $M_w$  3.5 (Pilger et al., 2021). Similar to earthquakes of tectonic origin, testimonies on the explosion’s felt intensities were collected by the US Geological Survey’s (USGS) “Did you feel it” (DYFI) system (Figure 5-14 (a)), as well the European Mediterranean Seismological Center’s (EMSC) Lastquake platform (Figure 5-14 (b)). These testimonies revealed that the earthquake (and explosion) was felt all over Lebanon and as far away as Cyprus, 200 km northwest of Lebanon. As it can be seen in Table 5-4, some of the application users who shared their felt experience on the Lastquake platform reported feeling the ground shaking and the rumbling of the explosion, observations that are commonly reported in the case of earthquakes.

Although the explosion at the Beirut port is a technological disaster, it shares similarities with an earthquake, mainly due to its unforeseen nature, its similar environmental signals to an earthquake (vibrations and noise) and the way it was perceived by the affected individuals. From this perspective, we have postulated that human behaviors during and immediately after an explosion of such magnitude are similar to those that can be observed in the event of an earthquake. This assumption can further be justified by the scientific paradigm that considers that individuals’ behaviors do not differ according to the type of disaster, but rather according to the social dimension of the disastrous event (Quarantelli, 1991). The social dimension includes the event’s predictability, recurrence, and rapidity of onset; the social centrality of the affected population and the proportion of the population involved. Therefore, two events of different origins, such as explosions and earthquakes may evoke similar individual behaviors due to their shared aspect of rapid onset. Another justification could be related to the observation that in the immediate aftermath of a sudden onset event, the affected population may not have all the necessary information to accurately identify the nature of the event they witnessed, which leads them to make their own interpretation according to the environmental clues they have perceived. This has been observed in the case of the Teil earthquake in Ardèche, France (2019,  $M_w$  5.1), where in the opposite direction, the earthquake was thought to be an explosion by 21% of the respondents of the survey of the French Association of Paraseismic Engineering (Taillefer et al., 2021), in comparison to only 14% of the respondents who thought it was an earthquake.

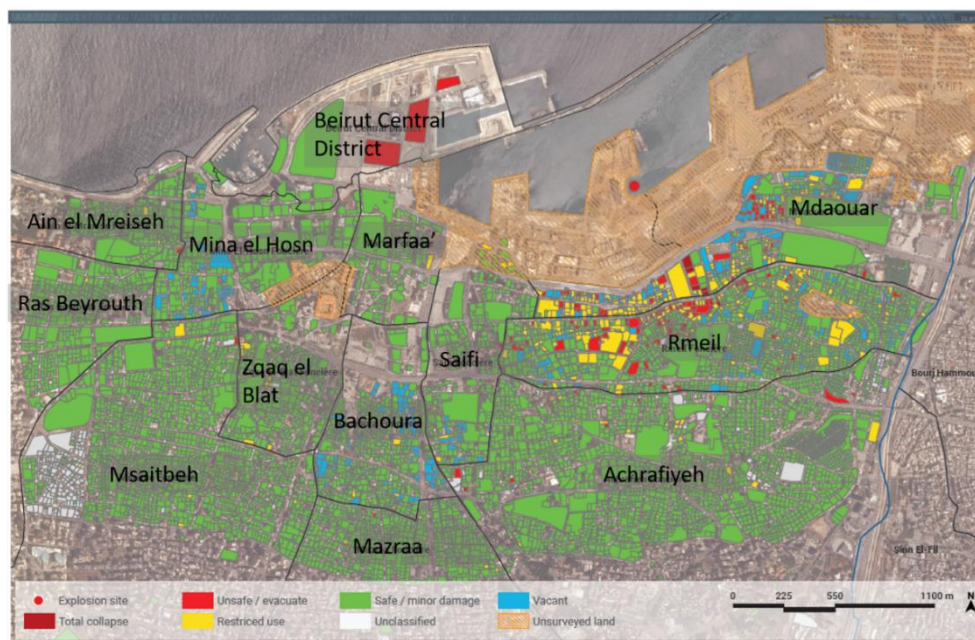


Figure 5-13: Map of the damages caused by the explosion at the port of Beirut (edited from Municipality of Beirut and UN Habitat, 2020)

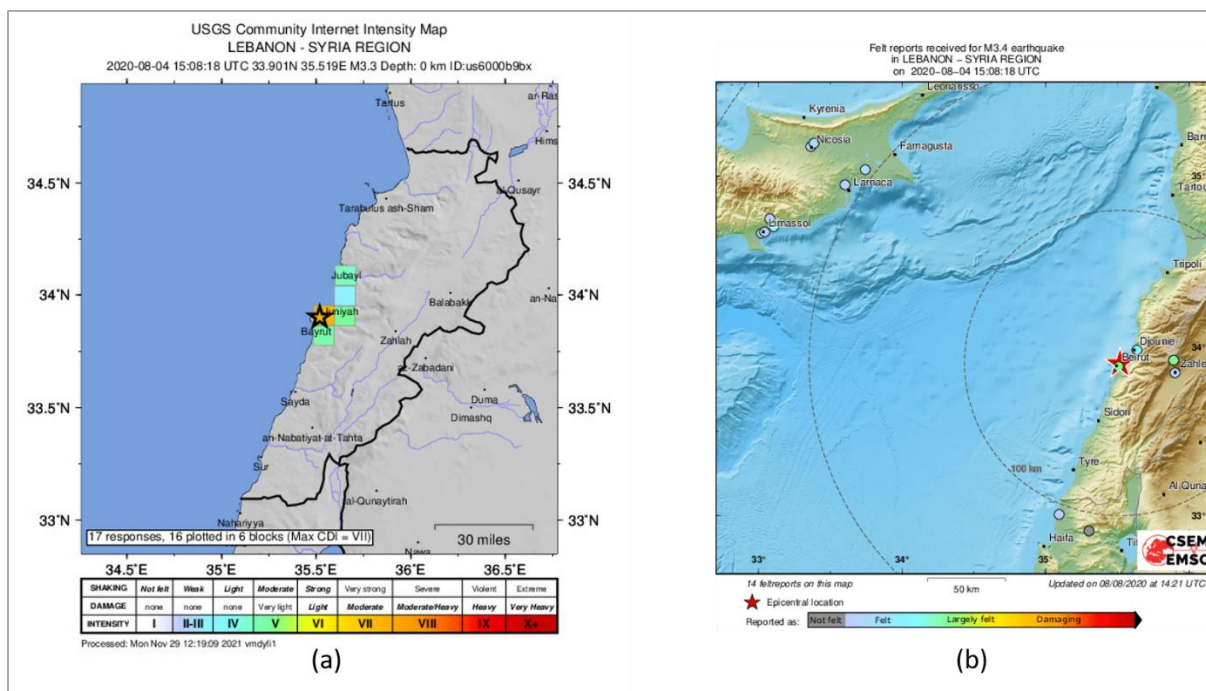


Figure 5-14: Maps of the reported felt intensities of the Beirut port explosion, according to: (a) the USGS DYFI and (b) the CSEM's Lastquake

Table 5-4 : Extracts from the users' testimonies on the Lastquake app with their corresponding locations and approximate distance from the explosion site (source: CSEM-EMSC)

Location	Distance (km)	Comment
Nahariya, Israel	107	"Shook my windows, heard it"
Xylotymvou, Cyprus	206	"Intense shaking for about 5 seconds"
Aradippou, Cyprus	211	"I'm not sure but house shook"
Nicosia, Cyprus	243	"Noise and sudden downward movement"
Mouttagiáka, Cyprus	244	"Windows and walls shook"
Limassol, Cyprus	245	"Felt it in Limassol"

### 5.5.2. Questionnaire on the behavioral response to the Beirut port explosion

To collect behavioral data on individual responses to the Beirut port explosion, I coordinated the adaptation of the previous questionnaire to the context of the explosion in collaboration with Elise Beck, Cécile Cornou, Julie Dugdale, Stéphane Cartier (Pacte, CNRS), and researchers in Lebanon affiliated to the Lebanese-French Observatory of the Environment (O'LIFE), Jocelyne Adjizian Gérard (USJ) and Jacques Harb (Notre Dame University). The aim of the questionnaire was to collect data on human behavior in Lebanon in response to the explosion, as well as the environmental and social factors that influenced them. The results of the survey should contribute to the design and the calibration of the agent-based model for the simulation of seismic crises in Beirut.

The online survey was launched on August 18, 2020, around 2 weeks after the explosion, via the Sphinx Online platform. The survey responses were anonymous, and we did not collect any personal data or any data allowing the identification of individuals by cross-referencing social data or by geographical location (address, IP address...).

The link to the survey was shared through our personal and professional networks, as well as social media platforms and websites of Lebanese and French institutions: Pacte (Grenoble), ISTerre (Grenoble)

and O'LIFE (Beirut). Although Arabic is the official language in Lebanon, most of the people in Lebanon are fluent in French or English (or both), therefore the questionnaire was made available in these 3 languages and the respondents could choose their preferred language when answering the survey. The questionnaire was composed of 50 close-ended (single and multiple choice) and semi-open (free response "other") questions and around 10 open-ended questions, and was structured in five sections, namely:

- i) the district (if in Beirut) or the city (if outside Beirut) of the respondent at the time of the explosion and the accompanying persons (e.g. children, elderly);
- ii) the first explosion experience (e.g. perception of the 1st explosion and search for information...);
- iii) the second explosion experience (e.g. identification of the phenomenon, intensity of the damage and immediate reaction...);
- iv) the mobility behaviors adopted in response to the explosion (e.g. exit time, destination, mode of transport...);
- v) the respondent's profile that could explain the behaviors (e.g. age, gender, education, knowledge of safe areas...etc.).

A complete list of the survey questions can be found in Appendix E.

The survey had collected 571 responses when it was closed on 09/03/2021. The raw data were then extracted from the survey website and introduced into the Sphinx IQ2 software, which was used to process and analyze the responses.

Before analyzing the survey responses, the database was cleaned by filtering out the individuals who answered the survey although they had no direct link to the explosion. The question "In which city were you when the explosions occurred?" made it possible to remove individuals who answered "Outside of Beirut" and indicated that they had been outside Lebanon during the explosions (e.g., Atlanta, Australia, Budapest, Riyadh). A second exclusion criterion concerned the individuals who answered "No" to the question "Did you feel the second explosion?", as these individuals did not experience the explosion and their responses were not relevant to the study. An additional clean-up was performed by filtering out the individuals from the "Under 18" age category (4 responses). These responses were removed to be in accordance with Article 8 of the GDPR regarding personal data relating to children, and also because the number of observations in this category was lower than 5, the minimum number of observations required to perform a Chi-square test (Caumont and Ivanaj, 2017). After the clean-up steps, the final sample was composed of 481 observations (N =481). The survey was answered in English by 51% of the respondents, in French by 40.5% and in Arabic by 8.5%. As English was the dominant language, a further processing step was carried out to translate all the open-ended responses to English, which allowed to perform a semantic analysis of the open-ended questions. Additionally, the terms in the responses related to the cities/districts were homogenized (for instance Achrafiyeh was also sometimes spelled Ashrafiyeh or Achrafieh) and the open-ended questions were categorized according to the relevance of the answers.

The filtering out and analysis of the survey on the behavioral response to the August 4 Beirut port explosions was done by Antonin Méjean, in the framework of his master internship in 2021 at Pacte, Grenoble. In the following sections, we will only present the analysis of the responses that are relevant to the individual behavioral choices; nevertheless the complete analysis of the survey responses can be found in (Méjean, 2021).

### **5.5.3. Analysis of the survey responses**

In the following sections, the analysis of the survey responses is presented. The analysis is structured as follows: (1) description of the respondents' profile and location at the time of the explosion; (2) the respondents' felt experience during the explosion and knowledge of safe areas; (3) behaviors adopted by respondents who were indoors and explanatory variables that explain the evacuation behavior and

(4) behaviors adopted by respondents who were outside. Some extracts have been re-interpreted from Méjean's master thesis (Méjean, 2021).

### 5.5.3.1. Respondents' profile and localization

The distribution of the demographic characteristics of the survey respondents and their spatial and social contexts at the time of the explosion is summarized in Table 5-5.

Table 5-5 : Demographic characteristics, spatial and social contexts of the participants of the survey (N=481)

Variable	N	%
Male	168	34.9%
Female	313	65.1%
<b>Gender</b>	<b>481</b>	<b>100.0%</b>
<24	99	20.6%
25-39	222	46.2%
40-64	135	28.1%
>65	25	5.2%
<b>Age</b>	<b>481</b>	<b>100.0%</b>
Never been to school	1	0.2%
Primary level	4	0.8%
Secondary level	5	1.0%
Higher level	471	97.9%
<b>Education level</b>	<b>481</b>	<b>100.0%</b>
In Beirut	143	29.7%
Outside Beirut	338	70.3%
<b>City</b>	<b>481</b>	<b>100.0%</b>
At home	301	62.6%
At work	47	9.8%
At friends'/family	25	5.2%
In a public building	48	10.0%
In a park, a square, a field	8	1.7%
On the road	52	10.8%
<b>Location</b>	<b>481</b>	<b>100.0%</b>
Alone	93	19.3%
With other people	388	80.7%
<b>Presence of other people</b>	<b>481</b>	<b>100.0%</b>

The percentage of female participants is greater than males (65.1% vs 34.9%). The 25-39 age group is over-represented as almost half of the participants (46.2%) were from this age category. The educational level of the respondents is almost homogeneous, with 97.9% of the respondents having achieved higher-level education. From the point of view of location at the time of the explosion, most individuals were at home when the explosion occurred (62.6%). For the social context, we can observe that only 19.3% of the respondents were alone when the explosion occurred. At the time of the explosion, 29.7% of the respondents were in the municipality of Beirut, compared to 70.3% outside Beirut. The respondents who were outside Beirut were asked to specify in which city they were located, which allowed to map the distribution of respondents per municipality in Lebanon (see Figure 5-15). The responses are not homogeneously distributed on the Lebanese territory, as the survey respondents were mainly located in Beirut and the governorate of Jabal Loubnane (Mount Lebanon). The respondents who were outside Greater Beirut during the explosion but present in the governorate of Mount Lebanon were mainly in Jounieh (N=26), Jbayl (N=11) and Zouk Mosbeh (N=8). The participants who were in Beirut were asked to specify the district they were in (see Figure 5-16). The respondents were mainly in the district of Achrafiyeh (40.6%), in Msaitbeh (10.5%), Mdaouar (9.8%), Marfa' (9.1%) and Rmeil (4.9%) which are the most affected neighborhoods in Beirut as it can be seen on the map in Figure 5-13.

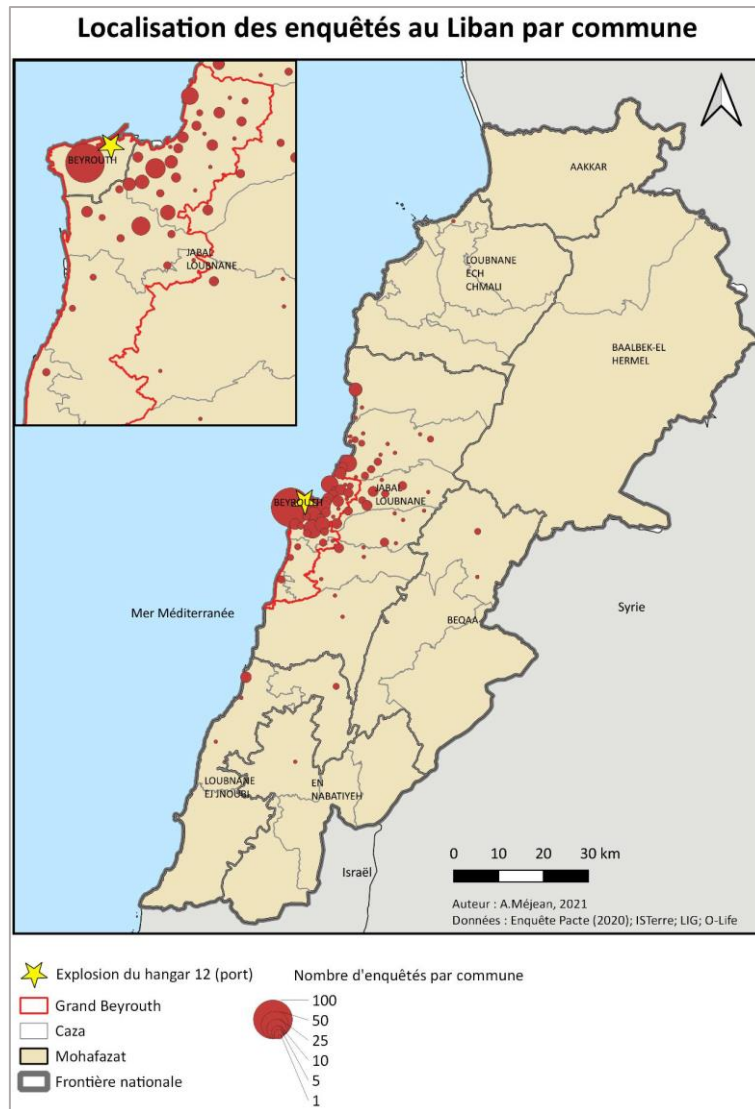


Figure 5-15 : Distribution of the number of the respondents per municipality in Lebanon (source: Méjean, 2021)

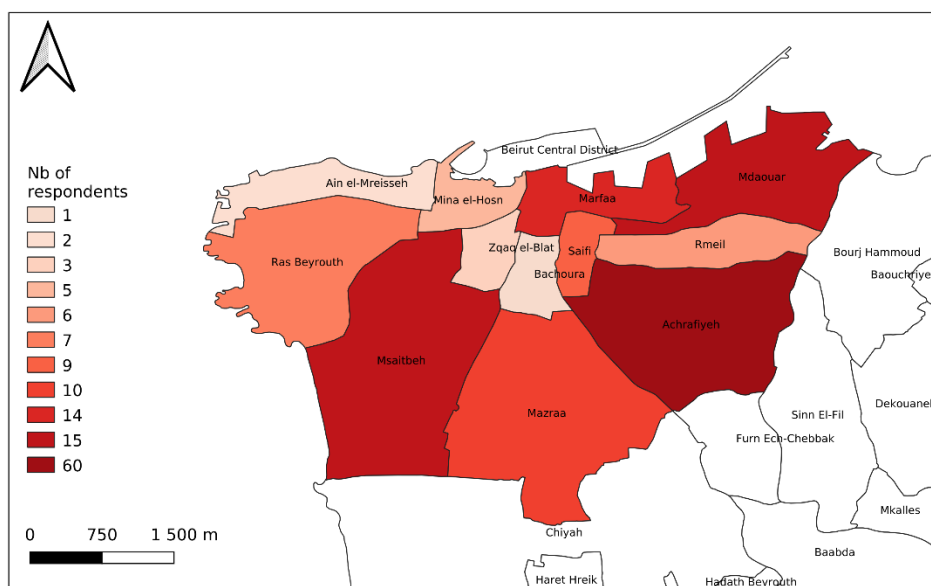


Figure 5-16: Distribution of the respondents in Beirut per district (adapted from Méjean, 2021)

### 5.5.3.2. Felt experience during the explosion and knowledge of safe areas

In this study, we are only concerned about how the second the explosion was perceived by the respondents, as it is considered as the main catastrophic event, while the first explosion can be considered as a precursor. We have analyzed the responses to the closed-ended question “What environmental clues have you felt?” (Table 5-6). Out of 481 individuals, 83.2% reported hearing the sound of the explosion, 65.1% felt the vibrations of the ground, 42% had damage/debris around them and 3.7% answered “Other” (e.g., sensation from the blast of the explosion, pressure in the ears). The sum of the percentages exceeds 100%, as multiple answers were possible to this question.

To the open-ended question "Before you knew it was an explosion, what did you think was the origin of this event?" there were 71 quotations of the word "explosion" and 63 quotations of the word "earthquake". The other most cited terms were “bombing” (58 citations), “attack” (54 citations), “bomb” (40 citations) and “Israeli” (37 citations). These words suggest a strong reference to war-related bombing, which could be related to the tense political context between Lebanon and Israel or to the revival of the respondents’ memories from previous wars. The free responses were then classified into three modalities according to their origin (see Table 5-6). The “Earthquake” modality (cited by 15.7% of respondents), the “Explosion” modality (75.9% of the responses), which includes all possible explosive causes (e.g., attack, bombing, industrial accident) and the “Other” modality (8.5%), which includes various causes often cited in small numbers (e.g., car accident, elevator crash, sound barrier, thunder... etc.).

80.5% of the survey respondents answered “yes” to the question “Were you in a building at the time of the second explosion?”, and were then asked the following question “Was the building you were in damaged?”. As Table 5-6 shows, about 54% of the individuals who were in buildings have witnessed buildings damages; knowing that damage level reported by respondents is not strictly related to classical damage classification after earthquake (Grünthal, 1998) or the structural damages of façade damages classification elaborated by Sadek et al. (2022) after the explosion.

The participants’ knowledge of safe areas was assessed by asking “Do you know where the safe areas are near you?”, which was followed by the explanation of the term “safe area” to limit the possibilities of misinterpretation (Table 5-6). Surprisingly, 72.6% of the respondents answered that they do not know the location of safe areas, while only 27.4% knew where the safe areas are located near either their home or their work.

Table 5-6: Distribution of respondents’ answers to questions related to the felt experience during the explosion and knowledge of safe areas. N is the number of respondents

<b>What environmental clues have you felt?</b>		
	N	%
I heard the sound of the explosion	400	83.2%
I felt the vibrations on the ground	313	65.1%
There was damage/debris around me	202	42.0%
Other	18	3.7%
Total number of respondents	481	
<b>Before you knew it was an explosion, what did you think was the origin of this event?</b>		
	N	%
Earthquake	63	15.7%
Explosion	305	75.9%
Other	34	8.5%
Total number of respondents	402	
<b>Was the building you were in damaged?</b>		
	N	%
No	178	46.0%
Yes, low damage	89	23.0%
Yes, moderate damage	69	17.8%
Yes, strong damage	42	10.9%
Yes, totally destroyed	7	1.8%

No response	2	0.5%
Total number of respondents	387	

**Do you know where the safe area is near you ? (Safe area : area away from buildings in which you are protected in the event of emergencies like fires, earthquakes, etc.)**

	N	%
No I do not know	349	72.6%
Yes, I know the safe zone near my home and/or my work	132	27.4%
Total number of respondents	481	

### 5.5.3.3. Behaviors of respondents who were indoors during the explosion

We have investigated how the respondents who were indoors reacted to the explosion by analyzing the answers to the multiple-choice question “What did you do at the time of the second explosion ?” (see Table 5-7), which was asked to the participants who were in a building during the second explosion.

*Table 5-7: Indoor respondents’ reactions to the explosion. N indicates the number of answers*

<b>What did you do at the time of second the explosion?</b>	N	%
Recovering and continuing previous activities	100	28.3%
Escape	77	21.8%
Reaching and protecting	65	18.4%
No reaction	52	14.7%
Seeking shelter	45	12.7%
Seeking information	8	2.3%
Other	6	1.7%
Total number of respondents	353	

The most common behavior was “Recovering and Continuing activities” cited by 28.3% of the respondents, followed by the “Escape” behavior adopted by 22% of the respondents. Additionally, a closed-ended question “Did you get out of the building you were in?”, was asked in the survey to all respondents who were in buildings, and 24.8% answered “yes”.

Since in the agent-based model we simulate pedestrians’ outdoor mobility, we are particularly interested in the escape behavior, as it highlights the transition of an individual from an indoor to an outdoor situation. Therefore, we analyzed the bi-variate relationship between the answer to the question “Did you get out of the building you were in?”, and variables that could explain the evacuation behavior. The selected variables were the gender and the age of the respondents, the city in which the respondents were located, the presence of other people, the building’s reported damage level and the knowledge of safe areas.

The Chi-square test (Chi<sup>2</sup>) was performed to evaluate the dependence of the evacuation behavior on the chosen indicators. The significance of the relationship is indicated by the p-value which takes value <0.01 in case of strong significance. The results of the bi-variate analysis summarized in Table 5-8 reveal that:

- Gender: males were slightly more inclined towards evacuating than women (29.4% of men evacuated, compared to 22.3% of women); however, there is low significance between gender and evacuation (p = 0.12).
- Age: although people aged 25-39 were more likely to evacuate compared to other age groups, there is no clear statistical significance between age and evacuation (p = 0.33).
- Location of respondents: the city in which the individuals were located when the explosion occurred is significantly related to the evacuation behavior (p<0.01), as people located in Beirut were more likely to evacuate (37%) than people who were outside of Beirut (18.8%).

- Presence of other people: the presence of other people did not have a significant influence on the evacuation decision ( $p = 0.27$ ), despite people alone being more inclined to evacuate than people who were with other people (30.5% of people alone evacuated, while only 23.8% of accompanied people evacuated).
- Buildings damage: The relationship between the building's reported damage and the evacuation behavior is very significant, as people who did not witness any buildings damage were more likely to remain in the building (91.0%). As the damage level increased, the percentage of the people who evacuated increased as well (23.6% for low damage, 40.6% for moderate damage, 57.1% for strong damage and 85.7% for total destruction).
- Knowledge of safe area: the knowledge of the location of safe areas is not significant to the evacuation behavior ( $p = 0.2$ ), although people who did not know where safe areas were located were more likely to evacuate (26.5%) than the people who did (20.2%).

Table 5-8 : Results of the bi-variate analysis of the evacuation behavior.

Did you get out of the building you were in?							
	Yes		No		Chi2	p-value	Significance
	N	%	N	%			
<b>Gender</b>					2.38	0.12	Low significance
Female	56	22.3%	195	77.7%			
Male	40	29.4%	96	70.6%			
<b>Age</b>					3.4	0.33	Not significant
18-24	20	23.5%	65	76.5%			
25-39	48	28.4%	121	71.6%			
40-64	25	22.9%	84	77.1%			
65 and more	3	12.5%	21	87.5%			
<b>City</b>					15.09	<0.01	Very significant
In Beirut	47	37.0%	80	63.0%			
Outside of Beirut	49	18.8%	211	81.2%			
<b>Presence of other people</b>					1.21	0.27	Not significant
Alone	18	30.5%	41	69.5%			
With other people	78	23.8%	250	76.2%			
<b>Buildings damage</b>					70.86	<0.01	Very significant
No	16	9.0%	162	91.0%			
Yes, low damage	21	23.6%	68	76.4%			
Yes, moderate damage	28	40.6%	41	59.4%			
Yes, strong damage	24	57.1%	18	42.9%			
Yes, totally destroyed	6	85.7%	1	14.3%			
<b>Knowledge of the safe area</b>					1.62	0.2	Not significant
No, I don't know a safe area	75	26.5%	208	73.5%			
Yes, I know a safe area	21	20.2%	83	79.8%			

Furthermore, a binary logistic regression with multivariate categorical variables was performed on the survey data in XLSTAT, including the damage level of the building and the gender and age of the person as explanatory variables. This analysis is done to derive the individual evacuation probability of each agent in PEERS. The results of the regression analysis are displayed in Table 5-9.

The building's damage level was considered as an explanatory variable due to its strong significance on evacuation behavior. Although the presence in or outside of Beirut showed strong significance with the evacuation behavior, it was not included in the regression analysis because in PEERS all individuals are considered to be in Beirut. On the other hand, although gender and age had little significance on evacuation behavior, they were included in the logistic regression model to incorporate the difference in the behavioral choice across people of different genders and age groups.

Table 5-9 : Results of the multivariate binary logistic regression analysis between the evacuation behavior and the building damage, age and gender

Variable	Reference category	Coef.	Standard Error	Wald Square	Chi- p-value	Odds ratio
<b>Constant</b>		0.893	1.252	0.509	0.476	
<b>Building damage</b>	<i>Totally destroyed</i>					
No damage		-4.584	1.201	14.579	0.000	0.010
Low damage		-3.427	1.197	8.202	0.004	0.032
Moderate damage		-2.406	1.189	4.097	0.043	0.090
Strong damage		-1.707	1.212	1.986	0.159	0.181
<b>Age</b>	<i>65 and more</i>					
24 and less		1.825	0.757	5.815	0.016	6.204
25-39		1.911	0.718	7.088	0.008	6.757
40-64		1.208	0.733	2.719	0.099	3.348
<b>Gender</b>	<i>Male</i>					
Female		-0.543	0.280	3.756	0.053	0.581

Finally, from the results of the binary logistic regression, the probability of evacuation can be calculated by multiplying each variable by its corresponding coefficient (coef. in Table 5-9):

$$p_{i, \text{evac}} = 1 / (1 + e^{-(0.893104 - 4.584032 \times D_N - 3.427137 \times D_S - 2.405917 \times D_M - 1.707436 \times D_E + 1.825227 \times A_{24} + 1.910626 \times A_{39} + 1.208290 \times A_{64} - 0.543178 \times S_F)}) \quad (5.2)$$

where  $D_N$ ,  $D_S$ ,  $D_M$  and  $D_E$  are binary variables corresponding to the damage level of the building, representing respectively none, slight, moderate and extensive damages. The binary variables  $A_{24}$ ,  $A_{39}$  and  $A_{64}$  are variables related to the age of the person, representing respectively being aged less than 24, between 25 and 39, and over 64. Finally, the variable  $S_F$  refers to the gender of the person, being a female in this case.

#### 5.5.3.4. Respondents' outdoor mobility behaviors

Regarding outdoor behaviors, the multiple-choice question “When you were outside, what did you do?” was asked to the people who were outdoors during the explosion and to the respondents who had answered “Yes” to the question “Did you get out of the building you were in?”. The most common response was “I tried to meet up with family” (50%), followed by “I went to a safe area” (30.2%). 15.6% of the respondents helped people around them, 5.2% followed someone and 4.2% went to hospitals (Table 5-10).

Table 5-10 : Distribution of the behaviors adopted outdoors. N denotes the number of respondents.

When you were outside, what did you do?		
	N	%
I tried to meet up with family	96	50.0%
I went to a safe area	58	30.2%
I helped people near me	30	15.6%
I followed someone	10	5.2%
I went to hospital	8	4.2%
I contacted relatives	5	2.6%
I stayed where I was	4	2.1%
Other	25	13.0%
Total number of respondents	192	

To determine the actual mobility destination of individuals, the open-ended question “Where did you go?”, was also asked to the people who were outdoors in the immediate aftermath of the explosion. The question received 151 free responses, which were translated to English and grouped into relevant categories according to the destination mentioned (Table 5-11). The most common mobility destination was going home (38.4% of the respondents), followed by going to the streets (19.9% of the participants). 11.9% of the respondents went to a hospital, while 10.6% headed towards a relative’s home. Some people mentioned staying in place (8.6%) while only 4 respondents went to their workplace.

Table 5-11: Destination reached in the aftermath of the explosion. N denotes the number of respondents

<b>Where did you go?</b>	<b>N</b>	<b>%</b>
Home	58	38.4%
Street	30	19.9%
Hospital	18	11.9%
Relatives home	16	10.6%
Stayed in place	13	8.6%
Work	4	2.6%
Other	12	7.9%
Total number of respondents	151	

As for the means of transportation used in case of mobility, the two most chosen categories for the multiple-choice question “What mean(s) of transport did you use for your travels?” were “Car” (69.7%) and “Walk” (30.9%). Two-wheeled vehicles (motorcycle/scooter) were used by 2.8% of the respondents, while only 2.2% used public transportation means (service, taxi, bus) (Table 5-12). However, as shown in Table 5-13, a very significant relationship exists between the city in which the respondents were located and their mode of transportation ( $p < 0.01$ ,  $\chi^2 = 18.92$ ). People outside Beirut were more likely to use cars, whereas people in Beirut were more likely to walk, use two-wheeled vehicles and public transportation.

Table 5-12 : Mean of transports used for travels. N denotes the number of respondents

<b>What mean(s) of transport did you use for your travels?</b>	<b>N</b>	<b>%</b>
Car	124	69.7%
Walk	55	30.9%
Motorcycle / scooter	5	2.8%
Service, taxi, bus ...	4	2.2%
Other	3	1.7%
Total number of respondents	178	

Table 5-13 : Bi-variate analysis of mean of transport used and the city where the respondents were located when the explosion occurred. Blue and red colors indicated under- and over-represented elements respectively

	In which city were you when the explosions occurred?			
	In Beirut		Outside of Beirut	
	N	% obs.	N	% obs.
<b>Means of transport used for travel</b>	<b>65</b>	<b>36.5%</b>	<b>113</b>	<b>63.5%</b>
Car	<u>37</u>	29.8%	<u>87</u>	70.2%
Walk	<u>31</u>	56.4%	<u>24</u>	43.6%
Motorcycle / scooter	<u>4</u>	80.0%	1	20.0%
Service, taxi, bus ...	<u>3</u>	75.0%	1	25.0%
Other	0	0.0%	<u>3</u>	100.0%

$p = <0.01$  ;  $\text{Chi}^2 = 18.92$  ;  $\text{dof} = 4$  (VS)

The relation is very significant.  
elements over (under) represented are coloured.

#### 5.5.4. Summary

Although Lebanon did not witness any major earthquake in the recent past, the catastrophic Beirut port explosions provided valuable observations on the Lebanese population's responses to a rapid onset disaster. An online survey was launched to collect behavioral data on the individuals' immediate reactions to the explosion. From the survey results, it was observed that only 25% of the respondents who were indoor at the time of the explosion evacuated the building they were located in, while the other respondents continued previous activities, tried to protect others and looked for shelter indoors. The evacuation behavior appears to be dependent on the building's perceived damage level. Although gender was slightly significant to the evacuation behavior, the age of the respondent, the presence of other people and the knowledge of safe areas did not have a significant influence on the decision to evacuate.

In outdoor situations, the most common behavior adopted in immediate aftermath of the explosion was meeting up with family members, followed by going to a safe area. The individuals' tendency to join their family members is also highlighted by the distribution of the mobility destinations, as the most common destination was "home", while "relative's home" occupied the fourth place after "street" and "hospital". The population's influx towards hospitals could be related to the high number of casualties caused by the explosion who needed emergency treatment. Although this behavior is not commonly mentioned in the literature on human behaviors in response to earthquakes, it is very important to consider it for the crisis management in the aftermath of catastrophic events as the rush of injured people towards hospitals could lead to the saturation of the medical facilities. Although 30.2% of the survey participants indicated they went to a safe area, "safe area" did not appear in the list of destinations reached, and "street" was mentioned instead. In addition, the survey showed that most of the population do not know the designated safe areas they should head to in case of emergency, as only 27.4% of the participants know where a safe area is located near their home and/or their work.

In conclusion, from this survey, the target mobility destinations of pedestrians' evacuation in PEERS were defined as: home, hospital, open space and undefined location (street, or any other location). Additionally, the results of this survey provided quantifiable data on the behaviors in Lebanon in the aftermath of sudden onset events that were used for the calibration of PEERS, namely:

- (1) The probability of evacuation depending on the building's damage level, age and gender:

$$p_{i, \text{evac}} = 1 / (1 + e^{-(0.893104 - 4.584032 \times D_N - 3.427137 \times D_S - 2.405917 \times D_M - 1.707436 \times D_E + 1.825227 \times A_{24} + 1.910626 \times A_{39} + 1.208290 \times A_{64} - 0.543178 \times S_F)})$$

- (2) The probability of joining a family member: 50%;
- (3) The probability of knowing the locations of open spaces: 27.4%.

## 5.6. CONCLUSION

Due to the lack and incomplete data in Beirut, approaches and methods had to be developed for the collection of data needed for the model. This chapter focused on the generation of additional spatial data in Beirut, namely open spaces, terrain slope and barriers. These data were generated from the processing of volunteered geographic information (OpenStreetMap) and satellite images. Open spaces were not restricted to the public urban spaces, but rather to any space that is safe in the event of an earthquake and can accommodate people. The spaces that correspond to this definition were delimited by GIS processing. The terrain slope was extracted from a DTM constructed by the processing of satellite images. Barriers were also digitized based on satellite images.

Additionally, due to the lack of complete information on the population's size and spatial distribution, a GIS-based approach was also developed for the estimation of the population's exposure to earthquake. Buildings were categorized as residential and non-residential (work or hospital) using OpenStreetMap and a complementary building database (BBED from the BUL). Furthermore, the number of residential apartments in Beirut was estimated based on the average apartment sizes, derived from an existing, but incomplete, building database (LIBRIS). The number of apartments allowed estimating the number of households in Beirut, which was used for determining the size of the residential population. Based on this, a synthetic population for Beirut was generated, and was qualified in terms of age, gender and social bonds from data derived from the most recent household survey in Lebanon (CAS, 2020). Consequently, according to the categorized building functions, home buildings were assigned to the generated population. The building functions will be used for the spatial distribution of the population during the simulation, as for a night scenario all individuals are assumed to be at home and for a day scenario 50% of the population is assumed to be at work, 30% at home and 20% outdoors.

Finally, this chapter also presented the survey that was launched just after the Beirut port explosion, which allowed us to collect behavioral data on the individuals' responses to a sudden onset event in Lebanon. The most important results of the survey that were used for the model are the characterization of the target destinations of individuals -home, hospital, open spaced and undefined location-, the individual probability of evacuation based on the building damage level, and the person's age and gender and finally the probabilities of knowing the location of open spaces and joining a family member.

Once these data were prepared, and with the building damages and debris prepared in Chapter 4, PEERS was calibrated with the appropriate GIS population and behavioral data related to the study area (Figure 5-17), which allows to running dynamic simulations of pedestrians' evacuation in an earthquake event in Beirut. Next chapter will cover the simulations in PEERS: the technical aspects and the outputs, before presenting the simulations performed at the scale of Beirut.

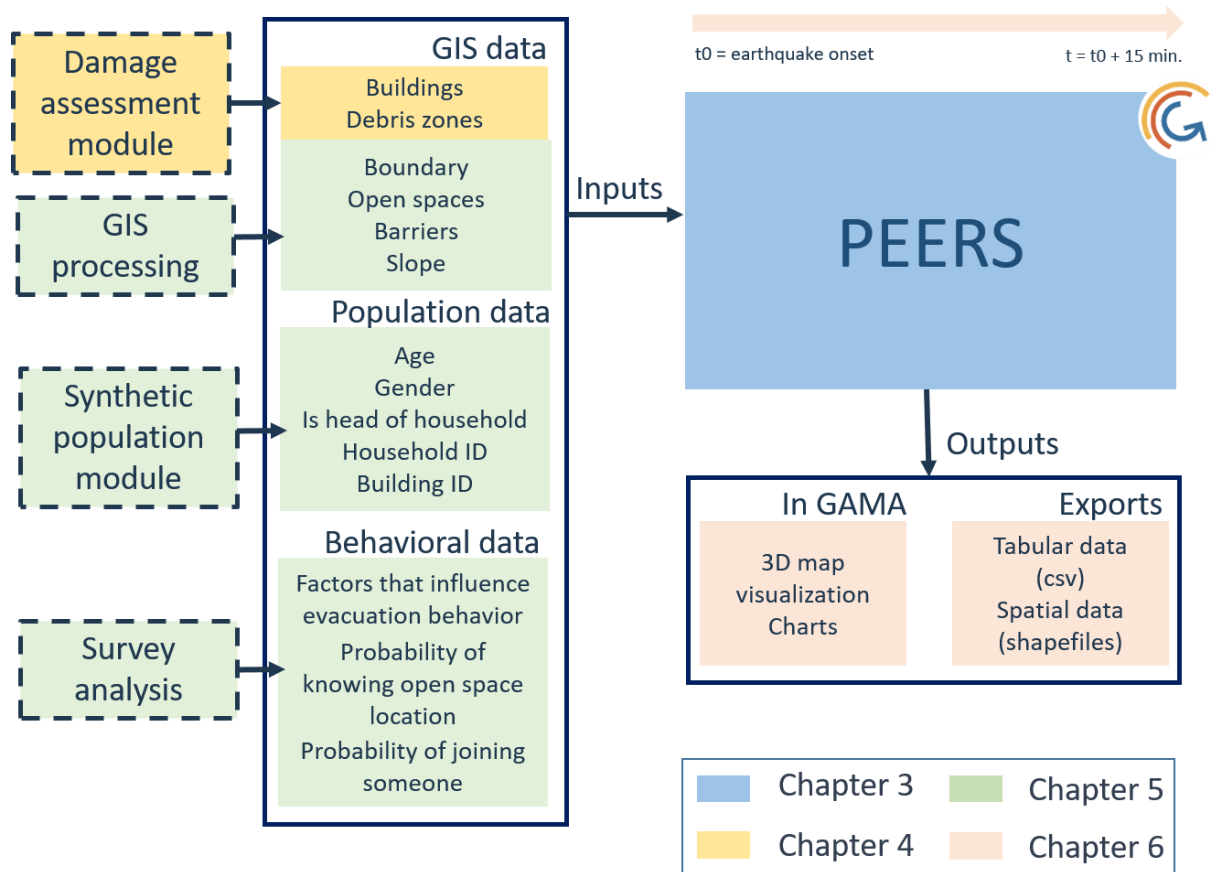


Figure 5-17 : Overview of the inputs and outputs of PEERS and their dedicated chapters in this manuscript



# Chapter 6: Simulation of pedestrian earthquake evacuation in Beirut

## 6.1. INTRODUCTION

The hybrid characteristics of PEERS allow the dynamic simulation of a seismic event by recreating the consequences of an earthquake on the urban environment and the individuals' behavioral adaptations to the earthquake. As individuals move in the environment, they have varying exposure levels, depending on whether they are in a building, a debris zone or in an open space. The behaviors that individuals adopt can also influence their exposure, and consequently their injury and safety status. PEERS was used to investigate about the individuals' safety in the immediate aftermath of an earthquake. In that context, we defined that a person is safe only if he/she is in an open space.

The simulations in PEERS were first run on a small spatial scale using GAMA's graphical interface to develop, test and verify the model. Then the simulations were performed at the scale of Beirut on a cluster using the headless (i.e. command-line) mode.

The following sections detail: (1) the general technical configurations and outputs of the simulations in PEERS, (2) the verification of the model which was done before running simulations, (3) the technical aspects behind launching simulations at a large scale, (4) the design of the experiment plan, (5) the pre-processing of the simulations results and (6) the analysis of the results of the simulation of pedestrians' earthquake evacuation in Beirut.

## 6.2. SIMULATIONS IN PEERS

The simulations in PEERS allow to follow the evolution of the states of the population and the open spaces in the city, by capturing at each simulated step, the location of the individuals, whether they are safe, in a debris zone, indoor, or outside a full open space. PEERS can also estimate the number of casualties and their severity. PEERS also captures the arrivals of people to open spaces, and monitors for each open space the number of occupants and its occupation rate, as well as the time required for the population to reach the open space.

The modular framework of PEERS allows the exploration of several scenarios, namely by varying:

- the seismic scenario and choosing different values of PGA, which changes the buildings' damage levels, the extent and the height of the debris as well as the injury rates;
- the time of day, which changes the population's initial spatial distribution;
- the human behaviors, which changes the percentage of the population that evacuates from buildings, and the target destinations that people adopt, as well considering individualistic or group behaviors;
- the locked state of the open spaces, which varies the number of open spaces that people can access and forces them to travel further to reach an unlocked open space if some of the open spaces are locked.

PEERS can also be used to simulate an evacuation drill in the city (earthquake PGA=0 and behaviors=ideal). In this scenario, buildings are not damaged, there are no debris in the environment and no casualties occur.

The technical configuration for running the simulations as well as the outputs are detailed in the following sections.

### 6.2.1. Technical configuration

To run simulations with PEERS, GAMA 1.8.1 should be installed on the machine. The machine can be a local machine (desktop) or a distant server.

The simulations can be run in the interactive mode of GAMA, by launching the application in which the user controls the start and the end of the simulation (the user can pause the simulation before 900 cycles have elapsed) through the user interface. The interactive mode is especially useful in the development stage of the model, since the evolution of the agents can be directly visualized on the simulation's map window, as well as the charts and monitors within the simulation interface. Additionally, the agents' attribute tables that contain the characteristics of each agent allows the user to monitor the agents' evolution throughout the simulation.

Alternatively, the simulation can also be run in the headless mode, i.e. with no user interface. In this mode the access to GAMA and the execution of the simulations are managed through command lines. Running GAMA in headless mode reduces the memory footprint of the simulations, and consequently improves their speed. The headless mode is also intended to facilitate launching simulations on grids and clusters, as different experiments can be launched by varying the model's input parameters directly in a bash script.

### 6.2.2. Simulation outputs

When launching simulations in the interactive mode, a panel for the specification of the parameters appears in the simulation window (Figure 6-1(a)). In this panel, the user can change the parameter values and run different experiments (however, for the changes to take effect, the simulation should be restarted (re-initialized)). Moreover, in the interactive mode, PEERS has a graphical display of the model's species (Figure 6-1(b)). Buildings can be displayed in 3D, with a z value proportional to the building's number of floors. The graphical display allows to visualize the dynamic evolution of the agents, following the mobility of agents and groups of agents, and their interactions with the buildings, debris and other agents. We also added monitors (Figure 6-1(c)) to follow at each time step the evolution of the number of safe agents, the number of agents who are still moving, the number of people outside saturated open spaces and the number of casualties. Similarly, the number of saturated open spaces is also monitored. The monitors are especially useful in the development stage of the model for debugging and verifying that the model behaves as expected.

We also defined charts that display within the simulation interface:

- (a) the evolution of the agents' states (indoor, safe, not arrived, outside saturated open space) over time (Figure 6-2);
- (b) the occupancy rates of the open spaces;
- (c) the arrival times to the open spaces.

Finally, we defined the export of simulation's logs, namely the export of the agents' attribute tables in csv and shapefiles to be analyzed and treated outside of GAMA. These exports allow to retrieve the exact location of the agents at each time step, the number of people arriving to each target destination at each time step, the number of casualties, the states of the open spaces: their saturation rates, how many agents are in each open space, the average time taken to reach each open space, etc. These logs are exported when running simulations in both the interactive and headless modes.

In the next section, we cover how the simulations were run in the graphical interface for the verification of the model.

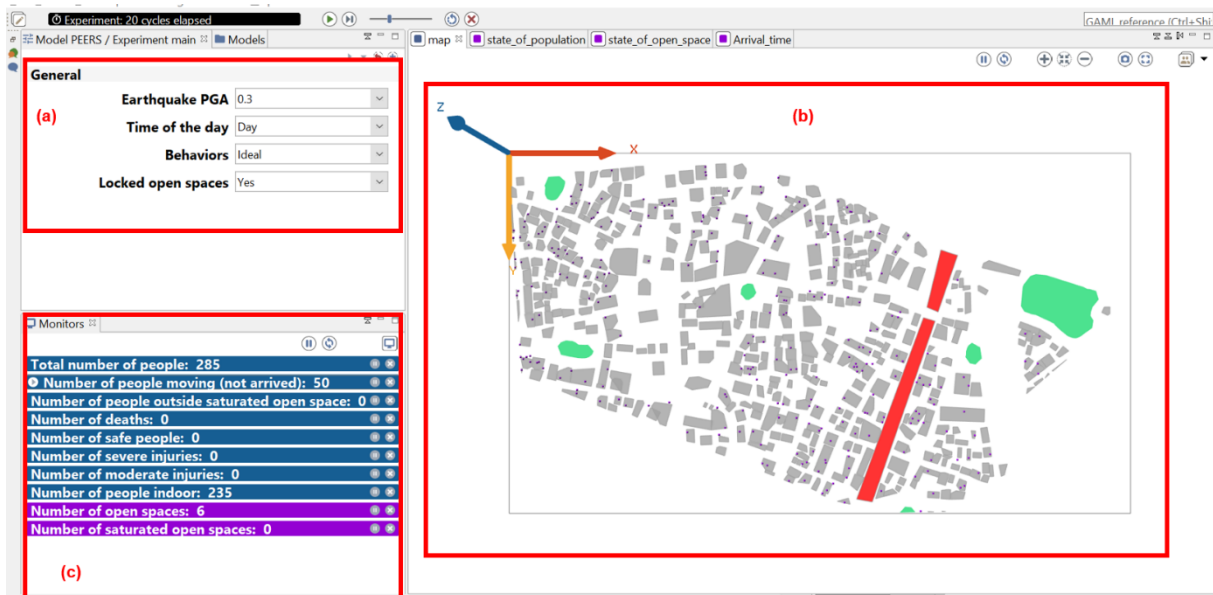


Figure 6-1: Simulation interface in GAMA showing, (a) the simulation's parameters, (b) the graphical display of the agents and (c) the monitors of the population's and open spaces' states

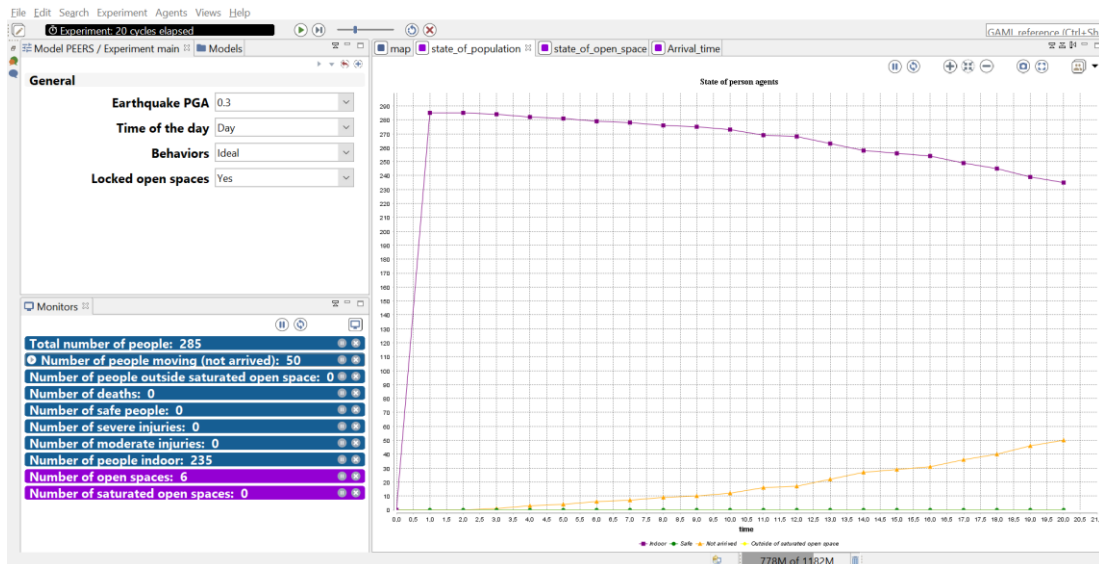


Figure 6-2: Chart displaying the evolution of the agents' states over time in GAMA's simulation interface. The purple line shows the number of agents indoor, the yellow line shows the number of moving agents, i.e. those who have not arrived, and the green line shows the number of safe agents in open spaces

### 6.3. MODEL VERIFICATION

The model was implemented using a gradual approach by increasing the complexity at each development stage. Each implemented code block was tested in order to verify that the implemented code corresponds well to the conceptual model. For the verification of the implemented model, we ran simulations on a small zone in Beirut using the interactive mode of GAMA. The verification was done by both a visual inspection of the graphical output (map visualization) and an examination of the agents' attributes from the attribute tables in GAMA.

The following sections present how the implementation of the key features of PEERS related to the agents' behaviors and movement (see Chapter 3) was verified. These features are: 1) the agent's navigation towards a target while avoiding obstacles; 2) the modification of the agent's speed caused by the slope and debris; 3) the spatial distribution of agents for day and night scenarios; 4) the agent's

evacuation decision and the assignment of the evacuation delay and 5) the group behavior, namely the homogenization of the attributes of agents that belong to the same group.

Each feature was verified by running at least 10 simulations and doing a thorough inspection of the agents' attributes in each simulation. Nevertheless, in the following, only illustrative examples of the verification process are shown.

### 6.3.1. Verification of the agent's navigation towards a target and around obstacles

In PEERS, the agents move in a free space towards a target, and when confronted by an obstacle (a building or a barrier), they move around it before heading back towards their target (see Chapter 3 section 3.7.2.4). The agents' navigation in PEERS was verified by running simulations with the graphical interface, in which the agent's movement was visually inspected. Effectively, the agents navigated towards their targets while avoiding buildings and barriers.

In order to illustrate how the visual verification was done, Figure 6-3 shows snapshots at different time steps of a simulation in PEERS, in which the movement of one agent was followed. We represented only one agent here in order to facilitate the traceability of the agent's movement. The snapshots were taken at different times that show: the navigation around a barrier, the navigation around a building and the arrival to the target.

In Figure 6-3 we can see that the agent (represented by a purple point) is outdoors at  $t = 110$  s. The agent's target is to arrive to the open space in the lower right corner (represented by a green polygon). At  $t = 120$  s, the agent is next to a barrier (in red) and needs to move around it. The navigation of the agent around the barrier can be followed by comparing the position of the agent at  $t = 120$  s to its position at  $t = 185$  s. We can clearly see that the agent is moving around the barrier without being stuck. At  $t = 200$  s, the agent is at the top right corner of the barrier, and we can see it navigating around a building (in gray) between  $t = 205$  and  $t = 235$  s. At  $t = 245$  s, we notice that there are no more obstacles in the path of the agent towards the open space, so the agent keeps moving straight towards the open space. The agent arrives at  $t = 300$  s.

These observations show that an agent in PEERS is capable of identifying the path towards its target and modifies it when confronted by an obstacle. As these observations were consistent in all the test simulations, we verified that the navigation of the agents towards their target has been correctly implemented.

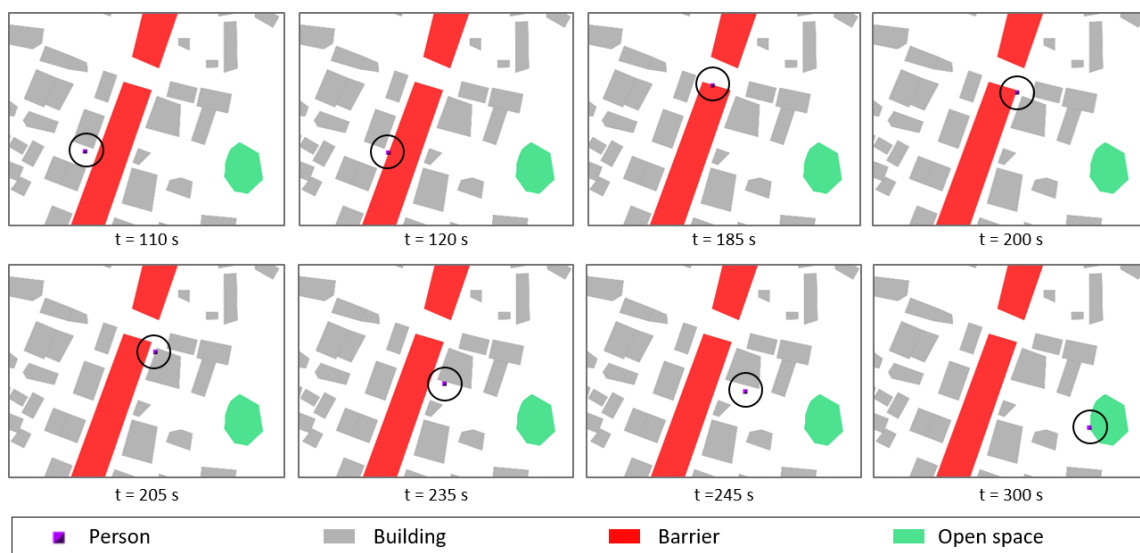


Figure 6-3: Snapshots from GAMA showing an agent (in purple) moving towards an open space (in green) while avoiding obstacles represented by buildings (in gray) and barriers (in red). A black circle is added around the agent to facilitate its traceability

### 6.3.2. Verification of the modification of the agent's speed due to the slope and the debris

As detailed in Chapter 3 (section 3.4.5.3) each agent in PEERS has a preferred speed that depends on its age. However, the effective speed at which an agent moves depends on:

- the value of the terrain's slope: the speed is reduced by a factor  $\gamma$ , that depends on the slope (see Chapter 3 equation 3.4)
- and if the agent is in a debris zone: the speed is reduced by 50% if the debris height is less than 1 m, and set to 0.16 m/s if the debris are higher than 1 m.

In order to verify the modification of the agent's speed due to the slope and the debris zones, we monitored the speed in the agents' attribute table in GAMA during simulations in PEERS. In the following, we give illustrative examples of how this verification was done.

Figure 6-4 shows a snapshot of the agent's attribute table, displaying for each agent its age (*Age*), its preferred speed (*natural\_speed*, m/s), the slope of the terrain at the location of the agent (*theSlope*, degrees), and the resulting speed after the modification due to the slope (*modified\_speed*, m/s). Additionally, the attribute (*is\_in\_danger*) indicates whether the agent is in a debris zone or not. Finally, the speed resulting from all the environmental modifications is stored in the attribute *speed* (m/s).

In Figure 6-4, in the first row of the table, we can see that agent #77 is at a location where *theSlope* is 2.84 degrees. From equation 3.4, the reduction factor  $\gamma$  due to the slope is equal to 0.84. Therefore, the slope should result in a reduction of the agent's speed to  $0.84 * \textit{natural\_speed} = 2.3$  m/s. This is in line with the value of the *modified\_speed* attribute observed in the table. The agent is not in a debris zone (i.e. the *is\_in\_danger* attribute is *false*), therefore the *speed* of the agent should be equal to the *modified\_speed*, which is confirmed in the table.

If we consider agent #918 in the 3<sup>rd</sup> row of the table, the agent's *is\_in\_danger* attribute is set to *true*, and the agent's *speed* is therefore set as 50% of the *modified\_speed*. Although not displayed, the reduction of the speed by 50% indicates that the debris' height is less than 1 m. Another example of a modified agent's speed caused by the debris can be seen in the 10<sup>th</sup> row of the table. Agent #3183 is in a debris zone (*is\_in\_danger* = *true*) and the agent's *speed* is set as 0.16 m/s, which indicates that the height of the debris exceeds 1 m.

In conclusion, from the observations of the agent's attributes, we have verified that the modification of the speed by the environmental factors has been correctly implemented.

#	Age	natural_speed	theSlope	modified_speed	is_in_danger	speed
77	21	2.74163765...	2.84268617...	2.304268111127...	false	2.3042681111279015
131	1	2.03048212...	3.86651086...	1.602752596165...	false	1.6027525961654812
918	31	2.69911553...	4.03616189...	2.108465767305...	true	1.0542328836529735
1327	53	2.56502525...	2.46647715...	2.206057029452...	false	2.206057029452826
2154	37	2.82555174...	2.13043189...	2.480606420245...	true	1.2403032101225282
2612	35	2.89442458...	2.51784205...	2.481544457059...	false	2.4815444570599654
2753	59	1.55805071...	3.61456489...	1.248997280704...	false	1.2489972807044498
2848	31	2.03345357...	3.02878046...	1.689690772005...	false	1.6896907720051344
2981	62	0.98335477...	4.82846832...	0.731659748960...	false	0.7316597489603501
3183	8	2.14090474...	1.37107133...	1.968867691129...	true	0.16
3225	48	2.20062087...	6.58435106...	1.469239171756...	true	0.734619585878403
3270	82	1.09845339...	2.63556027...	0.935001098651...	false	0.9350010986518341
3287	6	2.08049851...	5.45353412...	1.489529988881...	true	0.7447649944407596
3344	44	2.87720964...	4.34603357...	2.205218742923...	true	1.1026093714619465
3806	68	0.95409210...	3.23056578...	0.783058112951...	false	0.7830581129516718

Figure 6-4: Snapshot from the agents' attribute table in GAMA. The columns (left to right) show the identifier of the agent, its age, its natural speed in m/s (i.e. preferred speed that depends on the person's age), the slope in degrees at the location of the agent, the modified speed resulting from the effect of the slope, and whether or not the person is in danger, i.e. in a debris zone. The final column shows the final speed of the agent that depends on whether the person is in a debris zone or not and on the height of the debris in the zone.

### 6.3.3. Verification of the spatial distribution of agents for day and night scenarios

The distribution of the agents' initial locations varies according to the time of day. In a night scenario, all agents are supposed to be in residential buildings while in a day scenario agents should be in both residential and non-residential buildings as well as outdoors.

For the verification of the agents' distribution for day and night scenarios, we evaluated the location of the agents at the initialization of the simulation for the two times of the day. In Figure 6-5 (a) displaying the distribution of the agents in the simulation zone during a night scenario, we can see that no agents are located outdoors. The close-up view in Figure 6-5 (b) shows that the agents are in residential buildings (in gray), while the work buildings (in blue) are not populated. For a day scenario, shown in Figure 6-5 (c), we can observe that many agents are outdoors. In the close-up view in Figure 6-5 (d), we can see that indoor agents are located in both residential and work buildings.

From these observations, we have verified that the agents' spatial distribution varies between day and night scenarios in accordance with the model implemented.

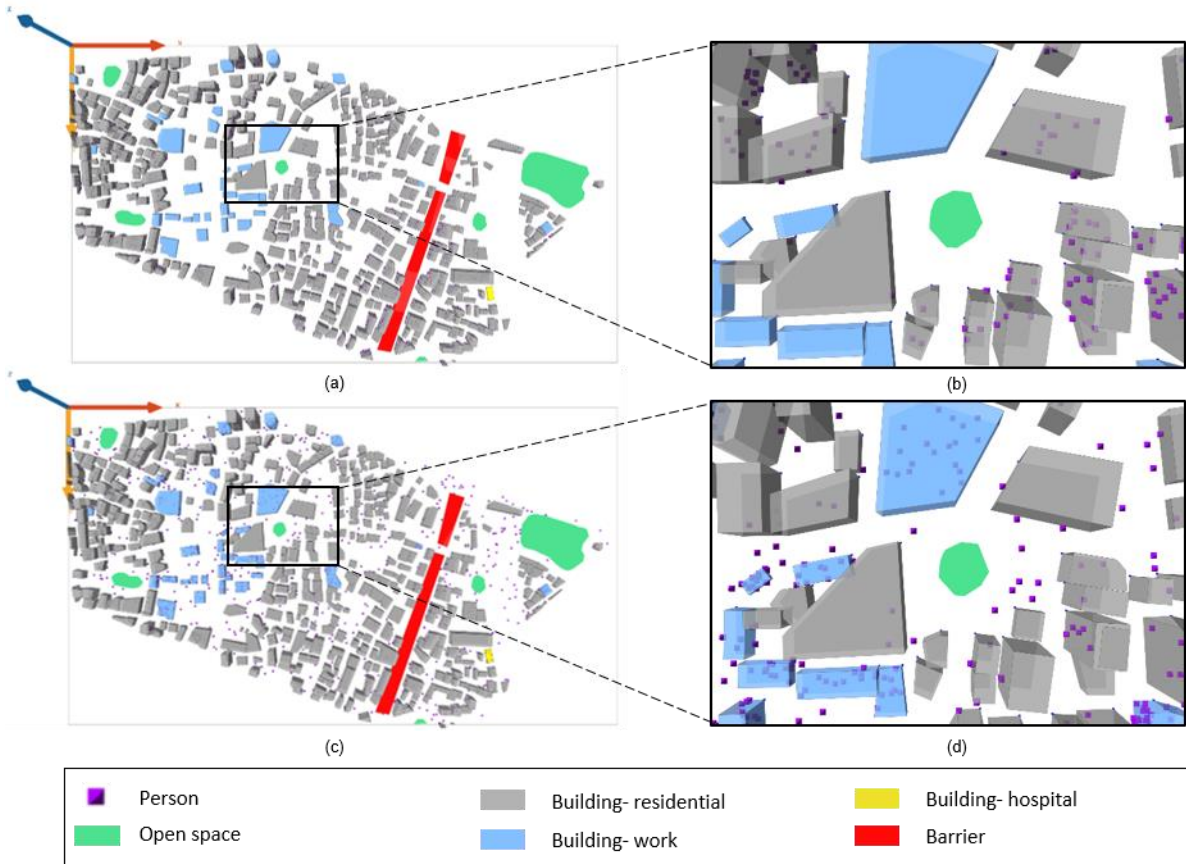


Figure 6-5: Snapshots from GAMA displaying the population distribution in PEERS at the initialization of the simulation for night and day scenarios. Buildings are displayed in 3D with a transparency factor in order to see the agents inside. The buildings have different colors according to their function. (a) Night scenario, (b) Close-up view for the night scenario, (c) Day scenario, (d) Close-up view for the day scenario

### 6.3.4. Verification of the agent's evacuation decision and the assignment of the evacuation delay

We verified that for a scenario in which realistic human behaviors are considered, the computation of the indoor agents' probability of evacuation is correctly implemented as of equation 5.2 (see Chapter 5), and that the evacuation delay is correctly assigned (i.e. between 0 and 180 s for realistic behaviors).

Figure 6-6 (a) shows a snapshot from the agents' attribute table, displaying each agent's age, gender (*Sexe*), the ID of the building in which the agent is located in during the earthquake (*building\_at\_EQ\_ID*), the probability of evacuating (*proba\_evacuation*), the evacuation decision

(*decision\_to\_evacuate*) and the evacuation delay (*evac\_delay*, in s). Figure 6-6 (b) is a snapshot from the buildings' attribute table, showing for each building, its ID (*building\_ID*) and damage state (*damage\_state*).

We present here an example of verification of the calculation of an agent's evacuation probability, considering the agent in the first row of Figure 6-6 (a):

Person #63 is a 51-year-old female, located in building #28 (*building\_ID* 809) whose damage state is moderate (Figure 6-6 (b)). Using equation 5.2, the probability of evacuation for the person #63 is:

$$p_{evac} = \frac{1}{1 + e^{-(0.893104 - 2.405917 + 1.208290 - 0.543178)}} = 0.299$$

which corresponds to the value of *proba\_evacuation* in the attribute table for this agent. Therefore, person #63 has a 29.9% probability of evacuating. When the probability of evacuation was evaluated, the *decision\_to\_evacuate* resulted in a *true* value. An *evac\_delay* of 21 s was then randomly assigned to this agent. We can also see in Figure 6-6 (a) that for agents whose *decision\_to\_evacuate* is *true*, their evacuation delay is between 0 and 156 s (although it can reach up to 180 s).

Consequently, the implementation of the evacuation decision and delay of the agents was verified; the probability of evacuation calculated in GAMA matches the theoretical probability and the evacuation delays are assigned within the specified limits.

#	is_indoor	Age	Sexe	building_at_EQ_ID	proba_evacuation	decision_to_evacuate	evac_delay
63	true	51	'Female'	'809'	0.29991534750...	true	21
240	true	82	'Female'	'4885'	0.11344842235...	false	0
254	true	51	'Female'	'928'	0.29991534750...	false	0
262	true	64	'Female'	'3366'	0.29991534750...	false	0
441	true	21	'Female'	'3475'	0.44256365752...	true	0
496	true	64	'Female'	'1683'	0.29991534750...	false	0
779	true	32	'Female'	'1680'	0.46372260892...	true	70
790	true	72	'Female'	'3367'	0.11344842235...	false	0
830	true	70	'Female'	'3543'	0.11344842235...	false	0
840	true	36	'Male'	'3797'	0.59816209663...	false	0
960	true	71	'Female'	'3576'	0.11344842235...	false	0
1070	true	53	'Female'	'3495'	0.29991534750...	false	0
1120	true	60	'Male'	'4901'	0.42445217229...	false	0
1281	true	32	'Female'	'3584'	0.46372260892...	false	0
1283	true	54	'Female'	'3371'	0.29991534750...	false	0
1431	true	8	'Female'	'6102'	0.44256365752...	false	0
1483	true	16	'Female'	'3793'	0.44256365752...	true	156
1609	true	53	'Female'	'3503'	0.29991534750...	false	0
1673	true	21	'Male'	'3482'	0.57747438152...	false	0

#	building_ID	damage_state
23	'28'	'Extensive'
24	'189'	'Extensive'
25	'785'	'Moderate'
26	'789'	'Moderate'
27	'808'	'Moderate'
28	'809'	'Moderate'
29	'923'	'Extensive'
30	'924'	'Extensive'
31	'928'	'Moderate'
3	'1046'	'Moderate'
5	'1047'	'Moderate'
6	'1048'	'Moderate'

Figure 6-6 : Snapshots from the agent and building attribute tables, showing the evaluation of the evacuation decision of an agent. (a) Agents' attribute table and (b) buildings' attribute table

### 6.3.5. Verification of group behavior: homogenization of the attributes of the agents that belong to the same group

In scenarios with realistic behaviors, agents from the same household can form groups, share decisions and navigate together. Some of the important aspects to verify for a group and its members are:

- the designation of the group's leader;
- the homogenization of the group members' evacuation decisions and evacuation delays;
- the homogenization of the group members' speed;
- the homogenization of the group members' target.

In order to verify these aspects, we inspected the attributes of the group agents in the attribute table.

As an illustrative example, we consider *group3*, displayed in Figure 6-7 (a), which has two members (*group\_size* = 2). The most relevant attributes of the group members are displayed in Figure 6-7 (b) to (d). For the group members, we distinguish between the *individual* attributes of the agents, i.e. the

attributes that would control their behavior if they were to behave individually, and their actual attributes that are influenced by the group and that are taken into account in the simulation. For instance, in Figure 6-7 (d) we can see that each group member has an *individual\_speed* that depends on the person’s age, the slope and the debris. However, the actual speed that they will move at in the simulation is the speed of the slowest group member, stored in the *speed* attribute.

We can see in Figure 6-7 (a) that the *group\_leader* is *people\_in\_group(0)*, i.e. the first agent in the list of group members. If we look at the attributes of the group members related to the designation of the leader displayed in Figure 6-7 (b), we can see that neither of the group members is the head of the household and that the *leadership\_score* of the first member (in the first row) is higher than that of the second member. Therefore, the first member is chosen as the group’s leader.

Regarding the group’s evacuation decision and delay, we can see in Figure 6-7 (c) that for both group members *individual\_decision\_to\_evacuate* is *true*, therefore, the group’s decision to evacuate is also set to *true*. The evacuation delay of the group, *group\_delay*, is set at the highest value of the group members’ *individual\_evac\_delay* (i.e. 36 s). Consequently, the *evac\_delay* of the two group members is also set as 36 s.

Regarding the homogenization of the speed, the *group\_speed* is taken as the lowest value of the group members’ *individual\_speed* (i.e. 0.458 m/s), and the *speed* of the two group members is set as the *group\_speed*, as shown in Figure 6-7 (d).

Finally, the target location of the group, *group\_target\_loc*, is set as the *individual\_target\_loc* of the group’s leader, i.e. the *individual\_target\_loc* of the group member in the first row which has a value of {352.4, 538.6}. The *target\_loc* of both the group members is then homogenized as the *group\_target\_loc*.

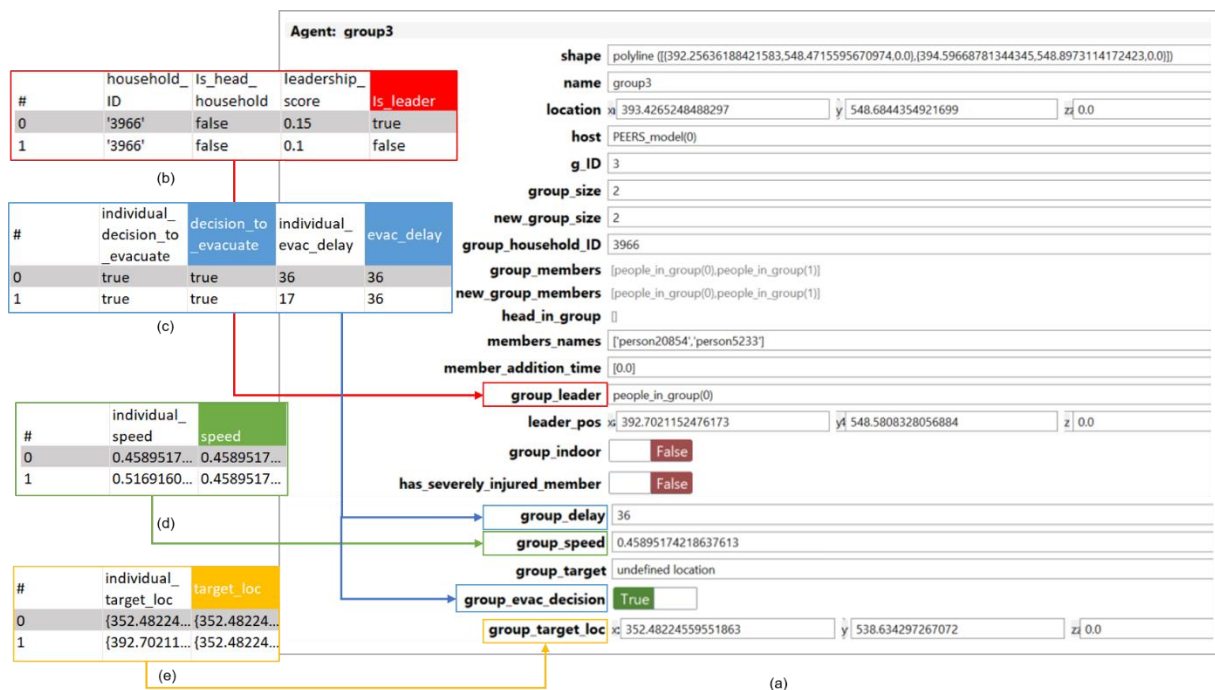


Figure 6-7: Snapshots from GAMA showing (a) the attributes a group (group3), and the attributes of the group’s members related to the designation of (b) the group’s leader (in red), (c) the group’s evacuation decision and delay (in blue), (d) the group’s speed (in green) and (e) the group’s target location (in yellow)

The inspection of the attributes that govern the behaviors of groups has resulted in the verification of the homogenization of the group’s attributes.

In conclusion, the different verification steps presented previously have allowed us to verify that the implementation of the core aspects of PEERS corresponds to the conceptual model, and that the simulations can be executed without bugs in the code. Once the code has been verified on simple test cases, the graphical interface was no longer needed since we had confidence in the functioning of the

model. This allowed us to use the headless mode for large scale simulations, which will be detailed in the next section.

## 6.4. LARGE-SCALE SIMULATIONS

Although the interactive mode was used for developing and testing PEERS, the headless mode was preferred for running simulations at the scale of Beirut. In fact when simulating at the city-scale, the model's environment represents an area of 20 km<sup>2</sup>, containing around 820 000 person agents, 15 000 buildings and thousands of other agents, which all use up a lot of memory to be displayed. Therefore, important performance gains can be achieved by removing the graphical interface and using the headless mode. Simulations were run on a cluster instead of a local laptop since the computational performances of a cluster in terms of processors and RAM surpass those of a desktop machine. Indeed, by using a cluster we can run several simulations simultaneously, therefore reducing the total time taken to run all the desired experiments. In the following sections, we detail how PEERS simulations were executed in GAMA's headless mode as well as the hardware considerations of the cluster.

### 6.4.1. The headless bash script

Upon the installation of GAMA, a bash script (*gama-headless.sh*) is provided in the application's main directory, which can be used to run GAMA in the headless mode. The only modification we have made to the bash script was the specification of the memory that needs to be allocated to GAMA for running simulations in the headless mode. We have allocated a maximum memory of 16 GB for running PEERS at the scale of Beirut, since the simulations handle an important number of agents that interact with their environment, which consumes a lot of RAM.

Using this script, simulations with PEERS in GAMA's headless mode were launched using the command line displayed in Figure 6-8.

```
bash gama-headless.sh PEERS_simulations/PEERS_headless.xml outputHeadLess/PEERS_simulations
```

Figure 6-8: Command line used to launch simulations with GAMA in headless mode

In this command line, *PEERS\_headless.xml* refers to the experiment file that should be executed in GAMA. The experiment file contains the source path of PEERS, as well as the experiment's parameters (i.e. the earthquake's PGA, the time of the day, etc.).

Since the headless mode does not use a graphical interface the simulation's outputs were specified by export statements in PEERS and were saved as the simulation was running. The exported simulation's outputs (\*.csv and \*.shp) could then be treated post-simulation in any data analysis software.

### 6.4.2. Cluster configuration: hardware specifications and limitations

The simulations of PEERS in headless mode were executed on the cluster of ISTerre. The cluster is composed of several computation nodes shared across several teams of the laboratory. The hardware specifications of the nodes used for the simulations are presented in Table 6-1. The nodes are configured with a Debian Linux operating system and are all equipped with Intel(R) Xeon(R) processors with frequencies ranging between 2.2 and 3 GHz, and with a RAM capacity of 192 GB per node.

Table 6-1: Hardware specifications of the nodes on the ISTerre cluster used for running PEERS

Node	Processor	Architecture	CPUS	Cores per socket	RAM (GB)
ist-clacul1	Intel(R) Xeon(R) CPU E5-2680 v3 @ 2.50GHz	x86_64	48	12	192
ist-calcul2	Intel(R) Xeon(R) CPU E5-2695 v2 @ 2.40GHz	x86_64	48	12	192
ist-calcul4	Intel(R) Xeon(R) CPU E5-2660 0 @ 2.20GHz	x86_64	32	8	192
ist-calcul7	Intel(R) Xeon(R) CPU E5-2680 v3 @ 2.50GHz	x86_64	48	12	192
ist-calcul10	Intel(R) Xeon(R) CPU E5-2687W v4 @ 3.00GHz	x86_64	40	12	192
ist-calcul14	Intel(R) Xeon(R) Gold 5220R CPU @ 2.20GHz	x86_64	96	24	192

As the cluster is a computing environment shared by several users, restrictions are imposed on the maximum resources a user can occupy at a time. A user can not occupy simultaneously more than 96 cores, and any job launched on the cluster should be executed within a wall time of 480 hours (20 days). These conditions imposed limitations on the experiments in PEERS and countermeasures had to be found to deal with these limitations. They are summarized as follows:

- 1) The core limitation imposed a limit on the number of experiments that could be executed simultaneously, which became even more restricted if a single experiment was set to run on multiple cores (by scheduling agents in parallel). In order to maximize the number of experiments that we could do at the same time, each experiment was run on a single core.
- 2) Although the nodes have high memory capacities, given that each simulation takes up to 16 GB of RAM, running a large number of simulations simultaneously led to the saturation of the nodes' memory and consequently to the stalling of the simulations. We should also mention that the resources of each node are shared between the jobs of all its users. Therefore, in periods where other users were running extensive computations, the nodes availability was limited. Consequently, we had to reduce the number of experiments to be done with PEERS.
- 3) Another limitation was the wall time of 480 hours for a job. In order to reduce the time taken for the execution of a simulation the model had to be optimized. The optimization steps that we took were:
  - a. Deleting the inactive agents from the simulation, i.e. the agents that arrived to their destination or those who decided to stay indoors.
  - b. Limiting the number of saved outputs and reducing the frequency at which the outputs were exported. Aggregate data on the population's states (number of agents indoors, safe, etc.) were still exported at every cycle. However, the frequency at which the full attributes of the agents were exported was reduced from every 1 cycle to every 100 cycles. Given that a simulation runs for 900 cycles, this would allow having the full information on the agents at 10 different times during the simulation to make sure there are no inconsistencies or errors. This decision was taken to reduce the time taken to save simulation outputs. Indeed, the data transfer took at least a couple of minutes per cycle, mainly due to the size of the files that were transferred (up to 700 MB for the attribute table of the person agents). This consequently meant that more time could be spent on the execution of the simulation, but limited the possibility of having the complete trajectory of agents at each time step.

Before running experiments, we verified the feasibility of running the simulations on the cluster. A large-scale simulation was launched on a single core (no parallel computing). The simulated scenario corresponds to scenario 2 in the experiments plan (detailed in the next section). The scenario was selected because it is expected to be one of the longest to execute as it simulates ideal behaviors where all agents are active.

The execution of the simulation took 360 h (around 15 days), including 15 h for the initialization of the simulation. On average, the execution of one cycle took 23 min. The duration of each cycle, i.e. the time taken to run one iteration or increase one time step in the simulation is shown in Figure 6-9. We can see that the cycle's duration started at a relatively low value and increased as the simulation progressed until a maximum cycle duration was reached after around 150 cycles, which was followed by a decrease of the cycles' durations. The comparison with the number of active agents at each cycle shows a clear correlation between the number of active agents and the duration of a cycle (see Figure 6-9).

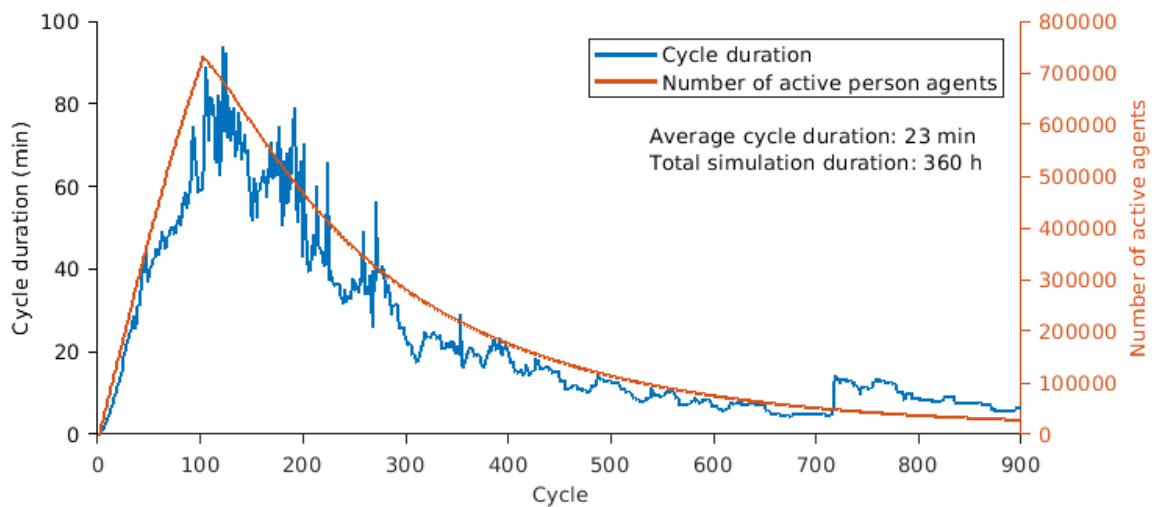


Figure 6-9: Time taken (in min) to execute each cycle of the large-scale PEERS simulation on the ISTERre cluster. The number of active agents is also plotted for reference

As the simulation was performed within the wall time of 480 h, we can confirm that it is possible to run a simulation at large scale on a single core on the cluster. However, the simulation requires very large computation resources, namely in terms of RAM (16 GB) and time (around 15 days). This restricted the number of experiments that could be executed at a large scale without changing the structure and the implementation of the model. Given these restrictions, experiments that explore the whole parameter space of PEERS could not be executed at a large scale. A concise experiment plan had thus to be defined to answer the most important research questions related to the population's arrival to safe areas in Beirut in the immediate aftermath of an earthquake. The experiment plan is presented in the next section.

## 6.5.DESIGN OF THE EXPERIMENT PLAN

The large-scale experiments with PEERS were designed to answer the two research questions related to the safety of Beirut's population in the immediate aftermath of an earthquake (defined Chapter 1).

**The first research question** related to Beirut's urban form, and particularly to the open spaces and their capacity in providing shelters for the residents in the immediate aftermath of an earthquake. This question was investigated by 3 experiments that represent ideal (or near ideal) conditions, however with varying complexity levels.

- We defined a first scenario (**Scenario 1**) that represents a baseline scenario. No earthquake (meaning no debris) does occur, all the open spaces are unlocked, all the individuals go to the open spaces with a minimal delay (ideal behavior) and the residents are all located in their homes (night scenario). A night scenario is considered in the "ideal" case, as it contains less uncertainty

about the spatial distribution of the population compared to a day scenario. Due to its characteristics, this scenario can also be assimilated to an evacuation drill, in which the population is given an order to leave their place of residence and head to the nearest open space.

- In the second scenario (**Scenario 2**), we add a slight deviation from the evacuation drill case, by considering an earthquake with a PGA of 0.3 g at outcropping rock, which is the recommended acceleration for the design of earthquake-resistant buildings in Beirut. All the other conditions remain similar to Scenario 1. This scenario allowed us to analyze whether the environmental modifications, i.e. the debris, caused by a moderate earthquake impose considerable constraints on the population's arrival to safe areas.
- Finally, we add to the previous scenario an additional complexity factor by defining a scenario that represents the realistic access conditions to the open spaces in Beirut (**Scenario 3**). In this scenario, all the open spaces in Beirut that have gates are considered locked. As a reminder, the open spaces that can be locked are: the Sanayeh Garden, Horsh Beirut, the Hippodrome, the Sioufi Garden and the port of Beirut (see Figure 5-3). The earthquake's PGA is 0.3 g at outcropping rock, the population adopts ideal behaviors, and the scenario occurs at night-time.

**The second research question** is centered around the increasing challenges on the population's safety that are imposed by more complex physical and social contexts. The complexity factors that we study are: a stronger earthquake, realistic behaviors and the spatial distribution of the population in a day-time scenario.

- **Scenario 4** is defined as a scenario with a stronger earthquake. In this scenario, we consider an earthquake with a PGA of 0.5 g at outcropping rock. The other parameters related to the open spaces and the population's distribution and behaviors remain ideal. The objective behind this scenario was to analyze the impact of the increased debris in the environment on the population's safety.
- In **Scenario 5**, we introduce more complex realistic human behaviors by considering group behaviors and the possibility of adopting different behavioral choices. The other parameters are considered ideal: the earthquake's PGA is of 0.3 g at outcropping rock, the open spaces are unlocked, the scenario takes place at night-time. The goal of this scenario is to analyze the effects of the realistic behaviors on population's arrival to safe areas.
- Finally, in **Scenario 6**, we add to the previous scenario the complexity of a day-time scenario, in which the population is distributed between residential buildings, work buildings and outdoors. The intention behind this scenario is to analyze the effects of the population's distribution when realistic behaviors are considered.

The simulated scenarios and the parameters related to each scenario are summarized in Table 6-2.

*Table 6-2 : Research questions and parameters of the experiments in PEERS. The cell indicating the parameter of interest in each scenario is highlighted in green*

Research question	Conditions	Scenario number	Earthquake PGA	Open spaces locked	Behaviors	Time of the day
Does Beirut's urban form, particularly its open spaces, have the capacity to provide shelters	No earthquake	1	-	True	Ideal	Night
	Earthquake PGA= 0.3 g	2	0.3 g	True	Ideal	Night
	Earthquake PGA= 0.3 g	3	0.3 g	False	Ideal	Night

<b>for the residents in the immediate aftermath of an earthquake?</b>	and locked open spaces					
<b>How do more complex physical and social contexts, increase the challenges to the population's safety?</b>	Earthquake PGA= 0.5 g	4	0.5 g	True	Ideal	Night
	Earthquake PGA= 0.3 g and realistic behaviors	5	0.3 g	True	Realistic	Night
	Earthquake PGA= 0.3 g, realistic behaviors and day scenario	6	0.3 g	True	Realistic	Day

Given the large demand on the computation resources needed to run the simulations at a large-scale and the increased execution times due to the data transfers (explained earlier), the simulation's outputs had to be limited to key indicators related to the population's states and to the open spaces' capacity and saturation. The outputs retrieved from the simulations are detailed in Appendix F and can be summarized as follows:

- The attribute tables of the person and group agents, exported as csv files and shapefiles every 100 cycles.
- Aggregated indicators describing the states of the population (person and person in group). Those indicators are: the number of people indoors, the number of people who have not yet arrived to their destinations, the number of people who arrived to their destination, the number of people in open spaces, the number of people outside of saturated open spaces, the number of injured people (with different injury levels). A csv file containing these indicators was updated at each simulation cycle.
- The arrival data of the population compiled in a csv file for each destination type: open space, hospital, home and undefined location. Each csv file contains the identifier of the agent who has arrived, its initial and final location (x and y coordinates) and its time of arrival.
- The attribute table of the open spaces, containing for each open space the arrival times, the number of occupants, the occupancy rate, if the open space is fully occupied or not, and if the open space is locked or not. The attribute table was saved as a csv file every 100 cycles.

These outputs could be compared between each other for the different scenarios in order to answer the research questions.

After defining the experiment plan and the desired outputs, the simulations in PEERS were executed on the ISTERre cluster. As the agents' behaviors and their interactions with the environment are not deterministic, 5 runs of each scenario were performed in order to avoid exaggerating any particular condition. A few pre-processing steps were taken on the results before their analysis, as it will be detailed in the following section.

## 6.6.PRE-PROCESSING OF THE SIMULATIONS RESULTS

5 runs for each of the 6 scenarios defined in the previous section were simulated. The average cycle duration for each scenario is displayed in Figure 6-10. Scenario 4 had the longest cycles with an average

of 23.7 min/cycle, while Scenario 6 had the shortest cycles with an average of 8 min/cycle. This large difference in the average cycle duration can be explained by the difference in the number of active agents between simulations with ideal behaviors (i.e. scenario 4) in which all agents have mobility behaviors, and simulations with realistic behavior (i.e. scenario 6), where only a percentage of the population is active. The differences in the cycles durations among scenarios of ideal behaviors (i.e. scenarios 1, 2, 3 and 4) and among scenarios of realistic behaviors (i.e. scenarios 5 and 6) could be related to the longer (or shorter) times that agents take to arrive to their target destinations depending on each scenario's considerations. Longer arrival times means that more cycles are performed with a high number of agents, which consequently increases the average cycle duration.

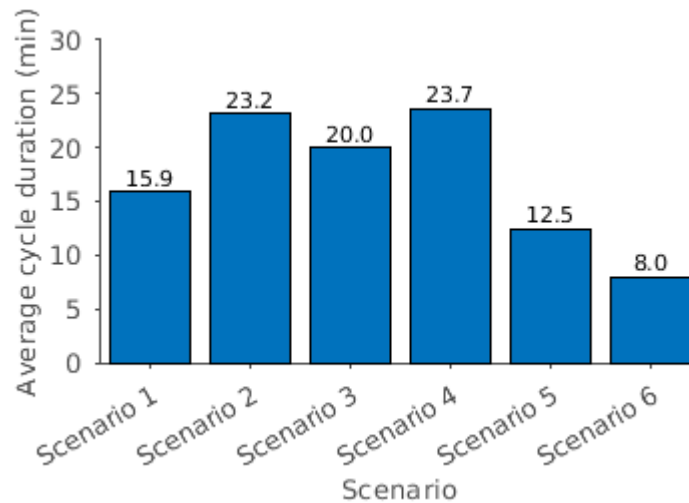


Figure 6-10 : Average cycle duration for each of the simulated scenarios

Before analyzing the simulation results related to the questions formulated in section 6.5, we analyzed the variability between the different runs of the same scenario. We also analyzed the estimated casualties to assess the realism of these estimates.

### 6.6.1. Variability between different runs of the same scenario

The variability of the simulation's behaviors between different runs of the same scenario was assessed by investigating one of the core metrics of PEERS, namely the arrivals to open space. We considered scenario 6, as it is the scenario in which we expect the most variability due to the probabilistic distribution of the population (day scenario) and the probabilistic choice of behaviors (realistic behaviors).

At a first level, we analyzed the variability at the scale of one open space, by considering a random open space (open space 8) and comparing the number of people in the open space at every simulation cycle across the 5 runs. We can see in Figure 6-11 that the total number of people in the open space varies from 40 in run 1 to 55 in run 3. Additionally, the rates of arrivals to the open space vary from one run to the other. The last arrival in run 1 was at 190 s, while in run 2 the latest arrivals to the open space occurred at 300 s. Therefore, at a micro-level, the number of people and their times of arrivals to open spaces show an important variation from one run to another.

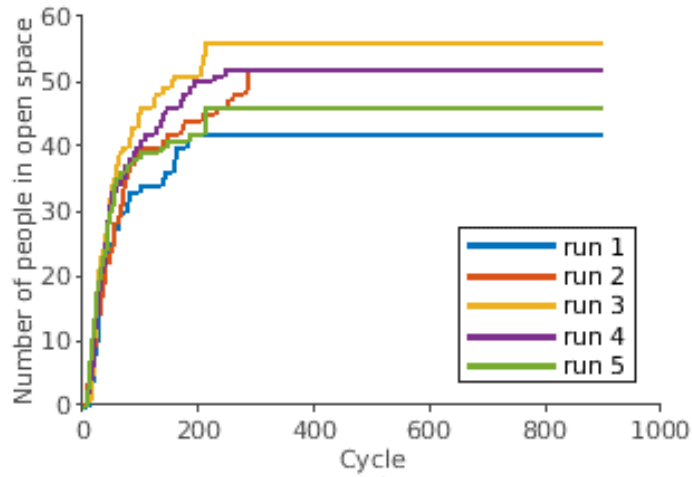


Figure 6-11: Number of people in open space 8 at each simulation cycle in runs 1 to 5 of Scenario 6

However, if we consider the macro-scale and look at the total number of people in all open spaces at each cycle of the simulations, displayed in Figure 6-12, the variations between the different runs are hardly perceptible.

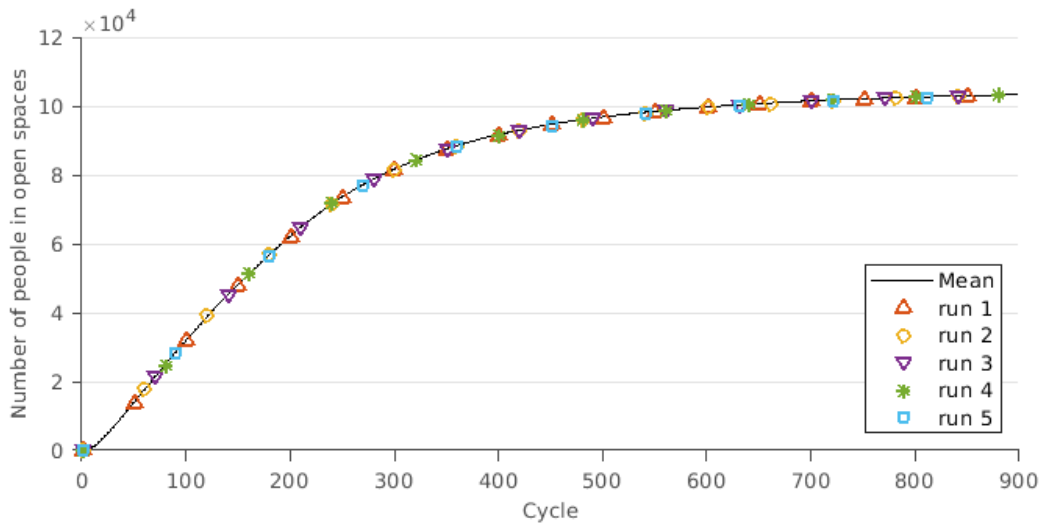


Figure 6-12 : Total number of people in open spaces in the 5 runs of Scenario 6

In order to compare the relative difference between the runs, we calculated the relative variation in the number of people in open spaces in the different runs with respect to run 1 (considered as a reference). We can see in Figure 6-13 that in the first 10 cycles, the variation between the open spaces' arrivals is rather large and reaches up to a 50% difference between run 3 and run 1. However, the variation becomes less important in the subsequent cycles, and no variation between the runs can be seen at the end of the simulations.

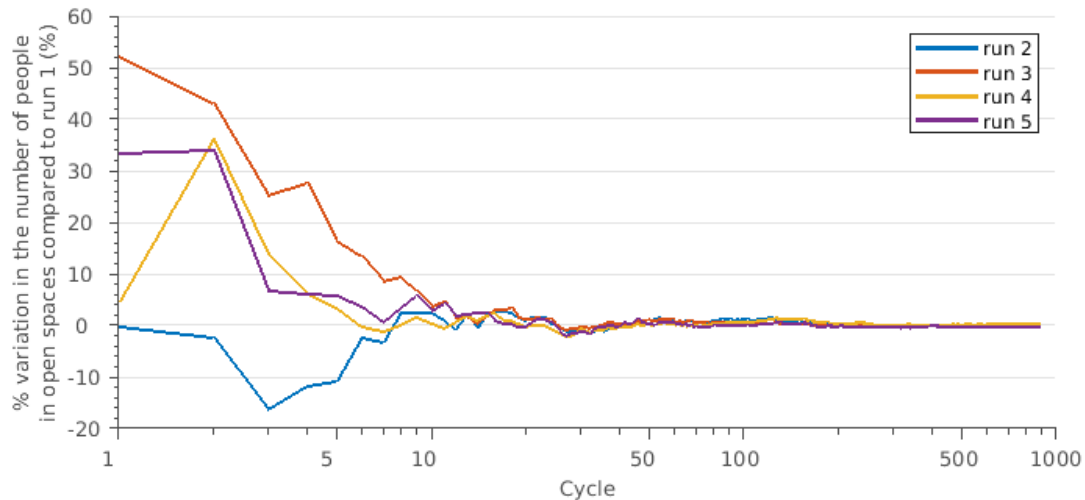


Figure 6-13 : Relative variation in the number of people in open spaces in the different runs of Scenario 6 with respect to run 1. The horizontal axis is in logarithmic scale

From these observations we concluded that despite the multiple factors that cause variability in the simulation's environment, the variability in the simulation's output for one given scenario is only seen at a micro-scale. At a macro-scale, although in the first few cycles of the simulations the outputs show variability from one run to another, the system stabilizes after around 100 runs, and different runs of the same scenario lead to almost identical states at the end of the simulation.

In order to minimize the effect of this variability in the first cycles of the simulations, we averaged the simulation outputs for the 5 runs of each scenario before analyzing the simulations' results.

### 6.6.2. Casualties estimated in the simulations with PEERS

In PEERS each person located in a building or in a debris zone during the earthquake has a probability of being moderately, severely or fatally injured depending on the building's (or debris zone) damage level (Chapter 3, section 3.3.4). The simulations allow to estimate the total number of casualties resulting from a seismic event. In order to assess the realism of the estimated casualties, we analyzed the estimated casualties for the two simulated seismic scenarios: PGA = 0.3 g and PGA= 0.5 g at outcropping rock, for night-time where all the population is located at home.

In Figure 6-14, we can see that for the scenario of PGA= 0.3 g, it was estimated that 16 people would have moderate injuries, and no severe injuries or fatalities would occur. On the other hand, for an earthquake with a PGA of 0.5 g, the number of moderate injuries increases to 2009, while the number of severe injuries and fatalities are 65 and 60 respectively.

To verify that the order of magnitude of the estimated casualties corresponds well to the input casualty rates, we compared the number of fatalities for the two seismic scenarios to the mean indoor fatality rates per building derived from HAZUS (FEMA, 2012) (Chapter 4 section 4.4). For PGA of 0.3 g, the mean indoor fatality rate is  $1.5 \times 10^{-7}$ . When the entire simulated population is indoors during the earthquake, the average number of fatalities should be around 0.12 ( $819\,717 \times 1.5 \times 10^{-7}$ ), which is less than 1. Therefore, having 0 fatalities in the first seismic scenario corresponds well with the input data. Similarly, for an earthquake of PGA= 0.5 g, the average number of fatalities should be around 50 ( $819\,717 \times 6.2 \times 10^{-5}$ ). Therefore, the estimated number of fatalities of 60 is of the same order of magnitude as the input rate.

Although the estimated casualties correspond to the casualty rates given by HAZUS and to the building damage level in each seismic scenario, we question if the HAZUS casualty rates are adapted to the case of Lebanon.

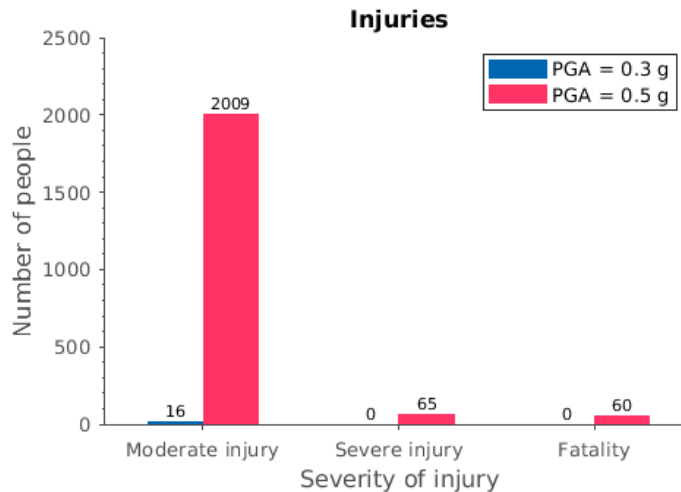


Figure 6-14: Injuries resulting from the simulations results

If we look at other studies, namely the empirical fatality estimation model implemented in the USGS Prompt Assessment of Global Earthquakes for Response (PAGER) system (Jaiswal and Wald, 2010a), the relationship between the fatality rate and the macroseismic intensity (MMI) witnessed large variations from one country to another. If we convert the MMI intensity to PGA using the relationships defined in (Wald et al., 1999b), a PGA of 0.5 g would correspond to an MMI VIII. We can see in Figure 6-15 that for an intensity VIII, the fatality rate for the U.S. is in the order of  $8 \times 10^{-6}$ , while that of Iran is in the order of  $4 \times 10^{-2}$ . Hence, for a seismic event having a MMI VIII, a ratio of 5 000 can be estimated between the fatalities estimated for Iran and those for the U.S.

Given the fatality rates in HAZUS, which are of the same order of magnitude as the empirical fatality rate models for the US given in (Jaiswal and Wald, 2010a), we can assume that the number of fatalities estimated for the U.S. for a PGA of 0.5 g using the empirical model would be of 60. On the other hand, if we consider that the fatality rate for an MMI VIII in Lebanon is somewhere between that of the U.S. and that of Iran, the possible range of fatalities in Beirut would be between 60 and 300 000. In our current state of knowledge, we can not accurately assess the validity of the application of any empirical model to the case of Lebanon. Although PEERS has the capacity to give an estimation of the number of casualties, it needs to be calibrated to the case-study. As the realistic prediction of the casualties resulting from an earthquake is not the core of this work, we did not perform any further research in this direction.

Given the sensitive nature of this topic, and the uncertainty of the HAZUS model when applied to Lebanon, we will not interpret further the casualties estimated using PEERS for Beirut. Therefore, in the subsequent analysis, the casualties estimated in PEERS will not be discussed. Similarly, as the arrivals to hospitals depend on the estimated number of moderate injuries, the arrivals to hospitals will not be included in the analysis. Removing the arrivals to hospitals from the analysis does not affect the analysis related to our two research questions, as less than 1% of the population arrived to hospitals in scenarios 5 and 6 (realistic behaviors with PGA 0.3 g).

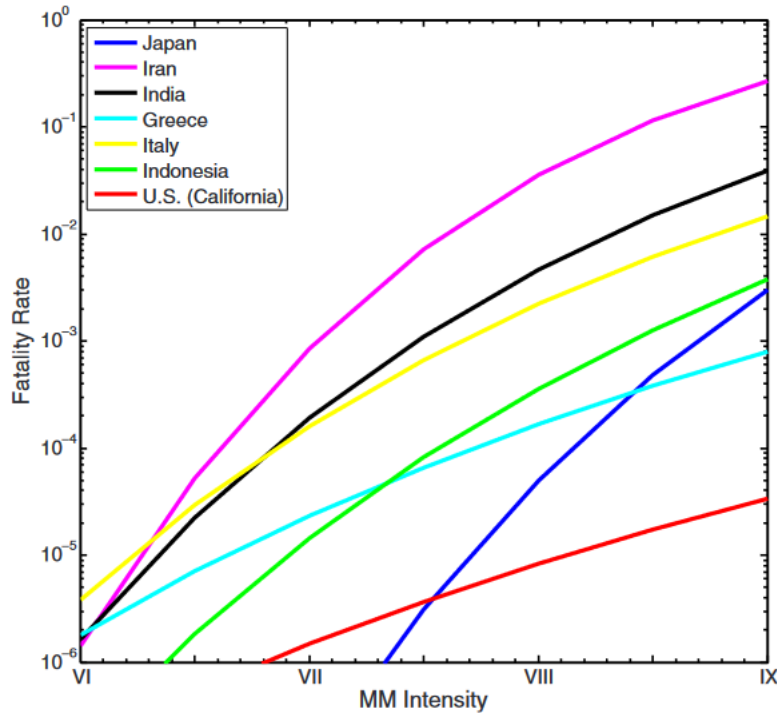


Figure 6-15: Fatality rates derived in the framework of the USGS PAGER for selected countries using an empirical model. Source: Jaiswal and Wald, 2010

## 6.7. ANALYSIS OF THE SIMULATIONS RESULTS

After running the simulations at the city-scale, the simulation's outputs were analyzed to answer the research questions formulated in section 6.5. The first research question is around the open spaces' capacity in providing shelters for the residents in the immediate aftermath of an earthquake. This question is analyzed through 3 scenarios representing ideal conditions with varying levels of complexity. The second research question is about the analysis of the effects of increasing challenges on the population's safety that are imposed by a stronger earthquake, by realistic behaviors and by the spatial distribution of the population for a day-time scenario with realistic behaviors.

In order to determine the effect of a parameter of interest, the scenarios were compared in pairs. The pairs of scenarios to compare were chosen on the basis of having identical parameters in the two scenarios, except for the parameter of interest. The simulation's outputs that are analyzed in this section are the distribution of the population's states during and at the end of the simulations, as well as the open spaces' arrival times and occupancy rates at the end of the simulations. Before presenting the analysis of the simulations' results, we explain the terms used in the analysis.

The population's states are categorized as follows:

- *Indoor*: people who are inside buildings;
- *Not arrived*: people who are outdoors, have not reached their destination, and who are still moving;
- *Arrived to an undefined location*: people who moved towards a target, which was an undefined location and arrived there;
- *Arrived to home*: people who moved towards their home building and arrived there;
- *Safe- in an open space*: people who moved towards an open space, and arrived to an unsaturated open space. Therefore they could access it and they are safe;

- *Arrived to a saturated open space*: people who moved towards an open space, but arrived to a saturated open space. Therefore, they remained outside this open space.

Regarding the open spaces, we distinguish between:

- The *occupancy rate* of an open space, which is the percentage of the area of the open space that is occupied, given that a person occupies 2 m<sup>2</sup>;
- The *number of people outside of a saturated open space*, which refers to the number of people who arrived to a given open space after it was saturated, and therefore could not access it.

Regarding the time:

- The simulations start at the time of occurrence of the earthquake and a cycle represents 1 s. Therefore as 900 cycles were executed, the end of the simulation is after 900 s or 15 min from the time of occurrence of the earthquake.

After defining the terms used in the analysis, the simulation results are presented in the following sections.

### **6.7.1. The capacity of the open spaces in Beirut for immediate disaster shelter**

In this section, we investigate if the open spaces in Beirut have the capacity of sheltering the residents of the city in case of an earthquake. This question is analyzed by 3 scenarios with increasing levels of complexity which are presented in the following subsections.

#### **6.7.1.1. Ideal conditions with no earthquake**

In this scenario as no earthquake occurs, it can be assimilated to an evacuation drill, in which an evacuation order is given at the start of the simulation. The whole population is assumed to be located at home and everyone leaves individually within the first 100 seconds from the beginning of the evacuation (i.e. time to go to down the stairs) and goes to the nearest open space, which are all unlocked.

From Figure 6-16, we can see that the percentage of the population who is indoor (purple line) decreases gradually from 100% to 0 within the first 100 s. As implemented, all the residents of Beirut are indoors at the start of the simulation and they evacuate within 100 s. We can also see that, as the percentage of the population who is indoors decreases, the percentage of the population who is traveling, i.e. not arrived (orange line) increases. The percentage of the population who has not arrived decreases over time as the percentages of the population who reach open spaces (saturated and non-saturated, yellow and green lines) increase. The percentage of safe population (green line) increases sharply in the first seconds, while after 200 s the increase becomes slower, and after around 500 s the percentage of the population who is safe sees little to no increase. In contrast, the percentage of the population arriving to saturated open spaces starts increasing at around 100s, and keeps increasing as more and more people arrive to open spaces that are saturated. After 15 minutes, i.e. at the end of the simulation, only 38% of the population is safe in an open space, while 60% arrived to a saturated open space and 2% have not arrived (Figure 6-17).

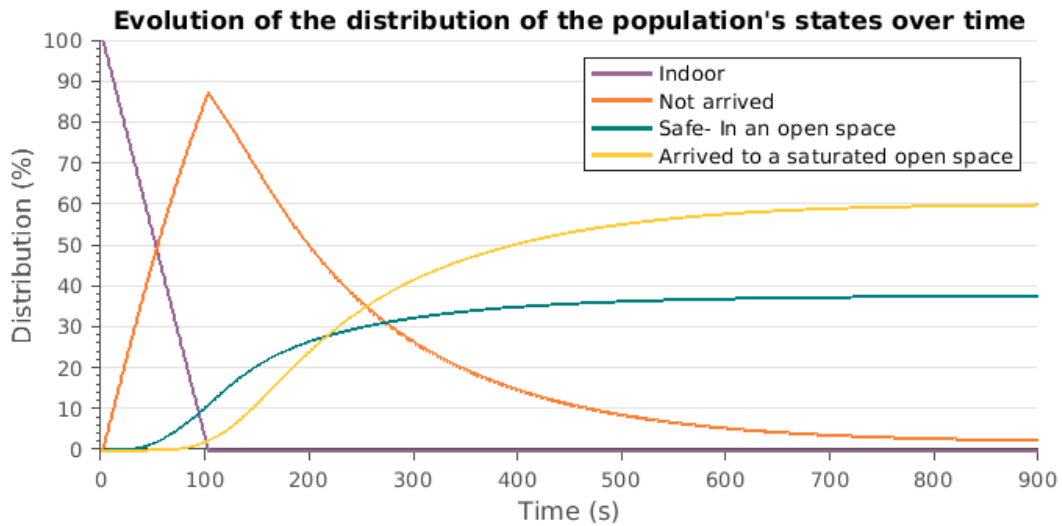


Figure 6-16: Evolution of the percentage of the population: indoor (purple), not arrived (orange), safe (green) and arrived to a saturated open space (yellow) from the start of the earthquake to 15 minutes after its occurrence

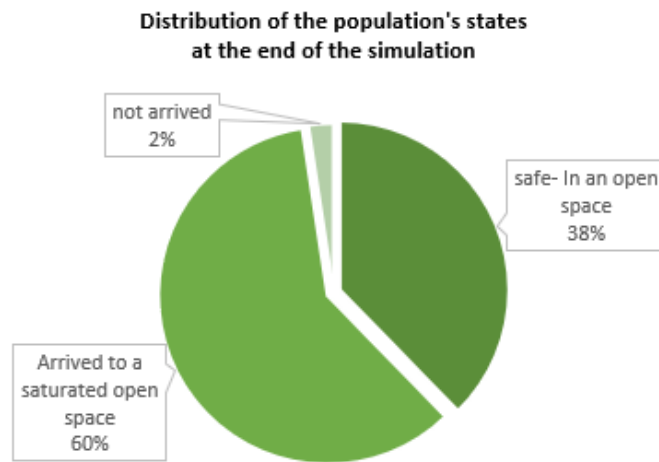


Figure 6-17: Distribution of the population's states at the end of the simulation in Scenario 1

In Figure 6-18 we can further analyze people's arrival times to unsaturated open spaces. In this figure, we observe the minimum, maximum, median, average (and standard deviation) arrival times to open spaces. We can see that the first arrival to an open space was after 8 s from the start of the simulation. Such a fast arrival time could represent the arrival of a person who lives at the ground floor of a building located just next to an open space. Overall, 50% of those who arrived to unsaturated open spaces did so in the first 139 s. The average arrival time to an open space is 181 s with a standard deviation of 133 seconds. The maximum arrival time of 899 s, suggests that people were still arriving to unsaturated open spaces at the end of the simulation.

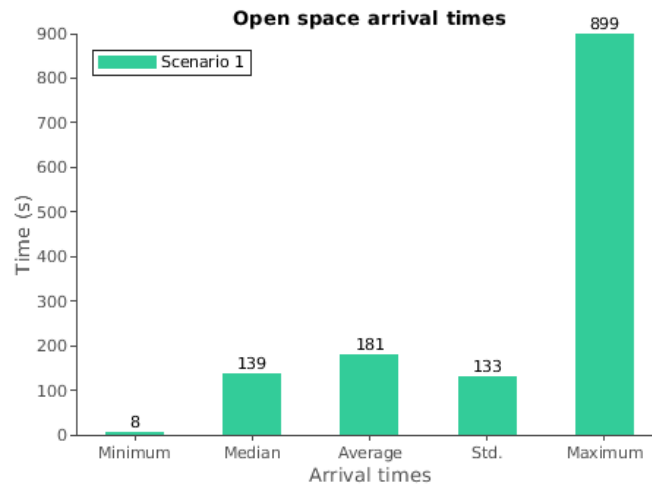


Figure 6-18: Times of arrivals to unsaturated open spaces in Scenario 1

On the other hand, if we look at the distribution of the open spaces' occupancy rates at the end of the simulation displayed in Figure 6-19, we can see that around 50% of the open spaces in Beirut are between 80 to 100% occupied, with 121 out of 268 open spaces being totally saturated. In contrast, we can see that 29% of the open spaces received less than 20% of their maximum capacity. This raises serious questions about the distribution of the open spaces in the city, because although there are still a considerable number of open spaces that have the capacity to shelter the population, the people did not get there, but were outside saturated open spaces.

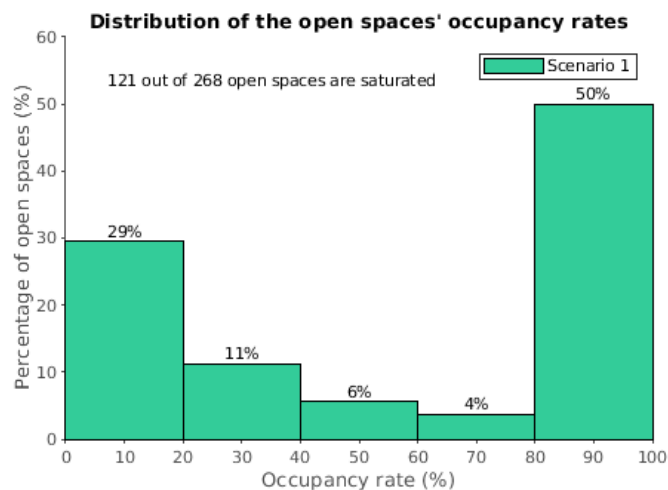


Figure 6-19: Distribution of the open spaces' occupancy rates in Scenario 1

To further analyze this question, we have displayed on the map in Figure 6-20 the occupancy rates of the open spaces in Beirut at the end of the simulation. We can see that in the center of the city, specifically in the northern parts of the Moussaitbeh and Mazraa sectors, the open spaces are small and they are all saturated, with the number of people outside the saturated open spaces reaching up to 25 000 people per open space. In contrast, the open spaces that have the lowest occupancy rates are mainly large open spaces located at the border of the city. We can see, for instance, that the port of Beirut, the maritime border in the southwest of Beirut, Horsh Beirut as well as the Hippodrome (see Chapter 5 Figure 5-3) are less than 20% occupied. The size of these open spaces, but also their location at the border of the city resulted in the low occupancy rates.

In order to have an idea of the total open space surface that can be occupied by the population in ideal conditions, we have computed the percentage of the open space surfaces that was occupied by the population in this scenario as of equation 6.1.

$$\% \text{ Occupied open space surface} = \frac{\text{Number of people in open spaces} \times 2}{\text{Total open space surface}} \times 100 \quad (6.1)$$

In this scenario, 309 033 people are in open spaces. As each person occupies 2 m<sup>2</sup> in the open space, and the open spaces surface in Beirut is of 4 028 220 m<sup>2</sup>, only 15% of the open spaces surface could be used by the population. From this observation, we can deduce that it is not only the capacity of the open spaces that determines the population's safety, but also the distribution of the open spaces' sizes and distance from populated areas.

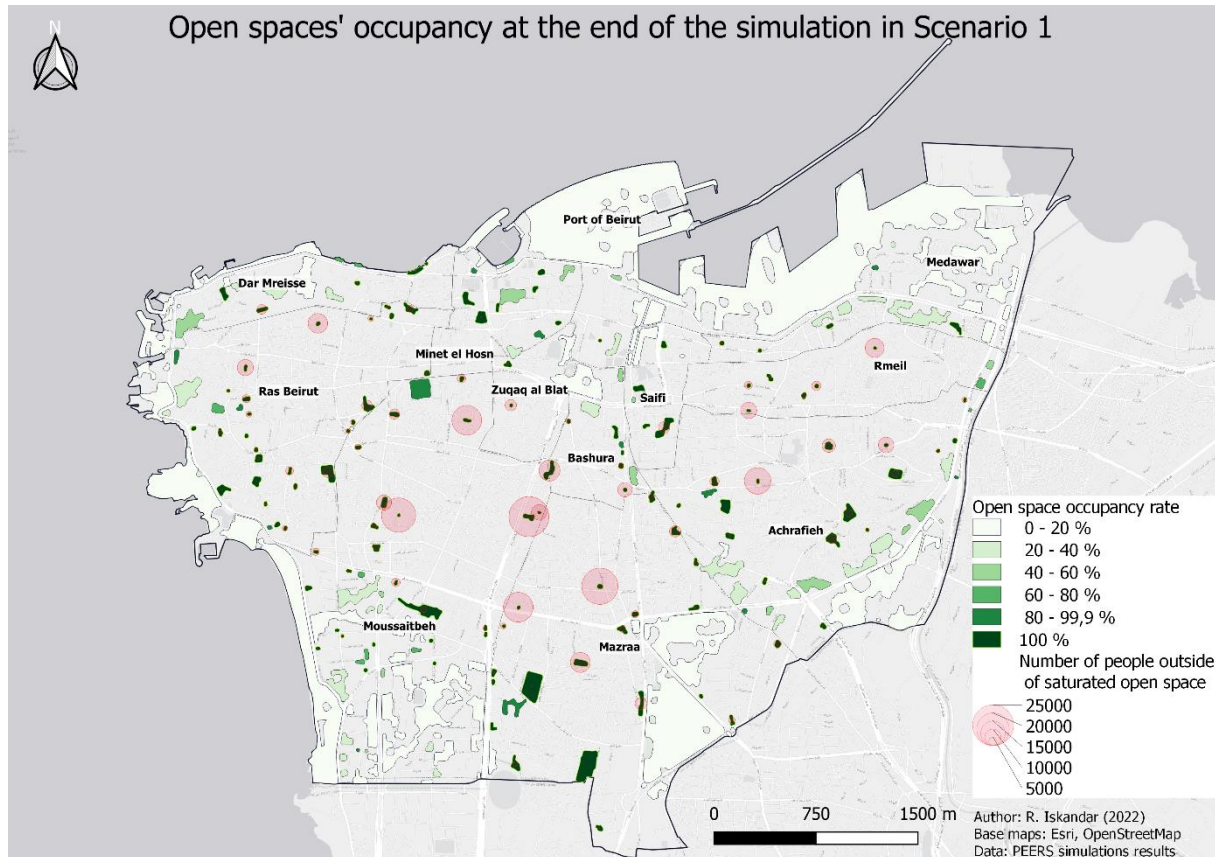


Figure 6-20: Occupancy rates of the open spaces in Beirut at the end of the simulation in Scenario 1

To summarize, in ideal conditions, if all the residents in Beirut were to evacuate from their home and go to the nearest open space, only 38% of the population would arrive to an unsaturated open space. It would take each person on average 3 minutes to reach an open space, however, even after 15 minutes around 2% of the residents would still not have reached an open space. 60% of the population would arrive to open spaces, without being able to access them, as these open spaces would be saturated. This is particularly the case of the open spaces located at the north of the Moussaitbeh and Mazraa sectors, as these open spaces are very scarce and have a small surface. Despite nearly half of the open spaces in the city being saturated, the percentage of the available open spaces surface that was occupied by the population is only 15%. This can be explained by the contrast between the occupancy rates of the large open spaces that are on the outskirts of the city, and the smaller open spaces that are within the city. Therefore, we can conclude that although in theory there is enough capacity of open spaces in Beirut, the distribution of these open spaces in terms of size and location does not match the population's need and does not ensure the arrival to safe areas within 15 minutes to more than 38% of the population, even in ideal conditions.

#### 6.7.1.2. Complexity level 1: Ideal conditions with an earthquake of PGA 0.3 g

In this section, we analyze the results of Scenario 2, which represents the evacuation of the population in the immediate aftermath of an earthquake of PGA 0.3 g at outcropping rock. As in Scenario 1, human

behaviors are considered ideal, the open spaces unlocked and the scenario occurs at night-time, therefore the population is distributed in residential buildings. The only difference with Scenario 1 is the presence of the debris in the environment caused by the building damages. We compared the results of Scenario 2 to those of Scenario 1 to identify the effects of the debris on the population’s arrival to safe areas in the case of an earthquake of PGA of 0.3 g.

Figure 6-21 shows the comparison between Scenario 2 and Scenario 1 in terms of the distribution of the population’s states at the end of the simulation, and the arrival times to unsaturated open spaces. We can see in Figure 6-21 (a) that the percentage of population safe in open spaces is almost identical in the two scenarios (37.5% in Scenario 2 compared to 37.7% in Scenario 1), while the percentage of the population arriving to saturated open spaces decreases in Scenario 2 by 1% compared to Scenario 1 (59.9% in Scenario 1 to 58.9% in Scenario 2). In parallel, the percentage of the population who has not yet arrived to an open space at the end of the simulation increases by 1%, from 2.4% in Scenario 1 to 3.6% in Scenario 2. Nonetheless, despite these slight changes in the distribution of the population’s states, globally the population’s situation after 15 minutes is not significantly affected by the presence of debris in the environment in the case of an earthquake of PGA= 0.3 g. This is because of the relatively low debris width (maximum width of 1 m) and height (maximum height of 60 cm) for an earthquake of PGA of 0.3 g (see Chapter 4 section 4.3.4.).

Regarding the times of arrivals to open spaces, we can see in Figure 6-21(b) that the median time taken to reach an unsaturated open space increases from 139 s in Scenario 1 to 150 s in Scenario 2 (increase of 11 s). Similarly, the average time increases from 181 s to 198 s (17 s increase). Therefore, on average, the arrival time to open spaces witnesses a 9% increase due to the presence of the debris in the aftermath of the earthquake of PGA= 0.3 g. Again, this relatively low delay in arrival times caused by the debris is directly related to the marginal presence of debris around buildings for an earthquake of PGA= 0.3 g.

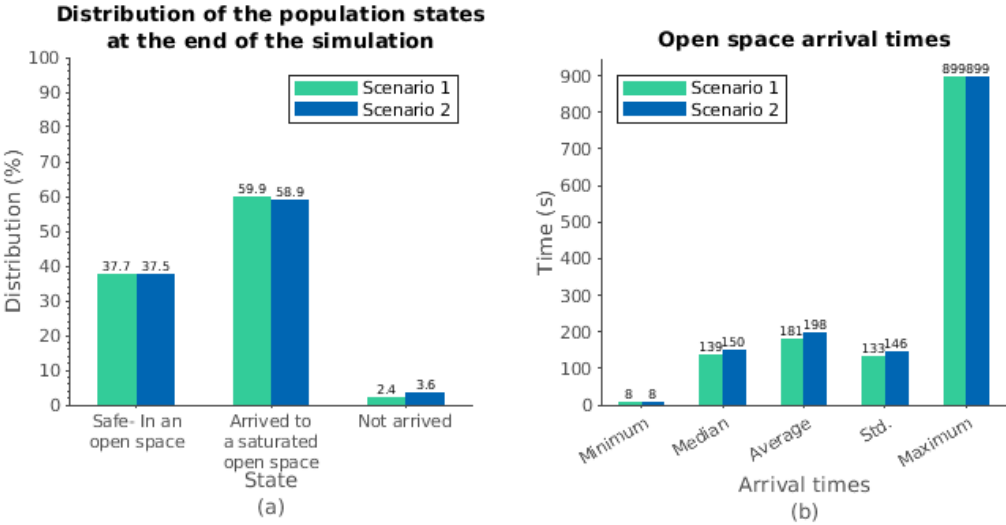


Figure 6-21 : Comparison of the simulation outputs between Scenario 1 and Scenario 2. (a) Distribution of the population’s states at the end of the simulation, (b) Arrival times to open spaces

In summary, an earthquake scenario of 0.3 g with ideal conditions does not induce significant changes on the population’s state in the 15 minutes that follow the earthquake. The only observed changes are in terms of the average time taken for people to reach open space, which is increased by 9% in the case of an earthquake of PGA= 0.3 g compared to a scenario with no earthquake.

### 6.7.1.3. Complexity level 2: Case of an earthquake of PGA 0.3 g with some open spaces locked

In this section, we analyze the effects of locking the open spaces in Beirut that are equipped with gates (Scenario 3) on the safety of the population and their arrivals to open space within 15 minutes from an earthquake of PGA= 0.3 g. Therefore, we compare the distribution of the population's states and open spaces occupancy rates in Scenario 3 to those in Scenario 2 (with the same conditions as Scenario 3, except for the open spaces which are all unlocked in Scenario 2).

In Figure 6-22, we observe that the percentage of the safe population decreases from 37.5% in Scenario 2 to 35.2% when the open spaces that have gates are locked. Conversely, the percentage of the population arriving to saturated open spaces increases from 58.9% in Scenario 2 to 61.3% in Scenario 3. Therefore, as expected, less people are able arrive to open spaces when some of the open spaces are locked, whereas more people arrived to saturated open spaces.

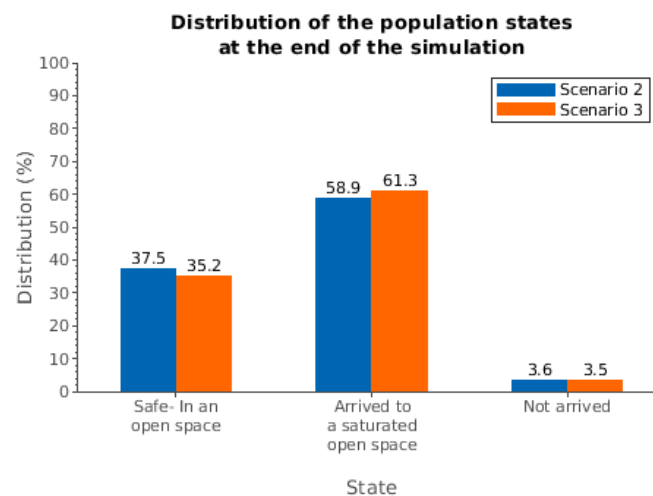


Figure 6-22: Distribution of the population's states at the end of the simulation in Scenario 3 compared to Scenario 2

From the comparison between the occupancy rates of the open spaces in Scenario 3 (Figure 6-23) and those in Scenario 1 (Figure 6-19), we observe that at a macro-scale, there are no major changes in the open spaces' occupancy rates. The only perceptible change is the increase in the number of saturated open spaces from 121 in Scenario 1 to 123 in Scenario 3. Therefore, locking the open spaces in the city does not have any significant consequences on the occupancy of the open spaces at a macro-scale, except a slight increase in the number of saturated open spaces.

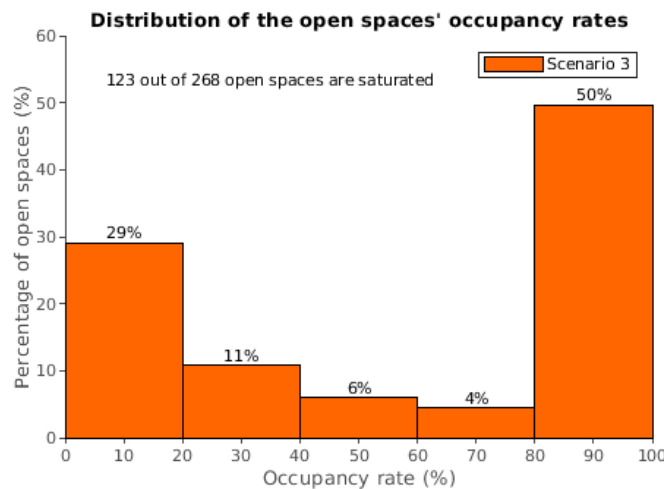


Figure 6-23: Occupancy rates of open spaces in Scenario 3

In order to inspect the changes at the micro-scale, especially in the open spaces located around the locked open spaces, we calculated for each open space, the difference in its occupancy rates between Scenario

3 and Scenario 2 as well as the difference in the number of people in the open space. Additionally, for saturated open spaces, we calculated the difference between the number of people outside of each open space between Scenario 3 and Scenario 2. The map showing the changes at the scale of Beirut is in Appendix G. In Figure 6-24, we can see the changes between Scenario 3 and Scenario 2 with focused views on the locked open spaces. Horsh Beirut and the Hippodrome were analyzed jointly, as they are next to each other and the effects of locking these open spaces can not be treated separately. We see that when an open space is locked, the open spaces around it show up to a 74% increase in their occupancy rates. Additionally, for the saturated open spaces, the increase of the number of people outside reaches up to 6 762 additional people.

When we analyze the individual situation of each open space, we see in Figure 6-24(a) that locking the Sanayeh Garden resulted in an increase of the influx towards the two already saturated open spaces nearby, which showed an increase of 6 762 and 1 214 people outside each open space. Similarly, for Horsh Beirut and the Hippodrome displayed in Figure 6-24(b), although around 2 225 people could go to the unsaturated open spaces in the south of Horsh Beirut and the west of Hippodrome, more than 10 000 people arrived to saturated open spaces that do not guarantee their safety. If we look at the case of Sioufi Garden displayed in Figure 6-24(c), the open spaces around it gave shelter to around 1 600 people, while 823 people were found in a saturated open space at the northwest of the locked open space. Finally, for the port of Beirut displayed in Figure 6-24 (d), we observe that most of the population could find a safe space in the unsaturated open spaces nearby, while only 246 people went to a saturated open space.

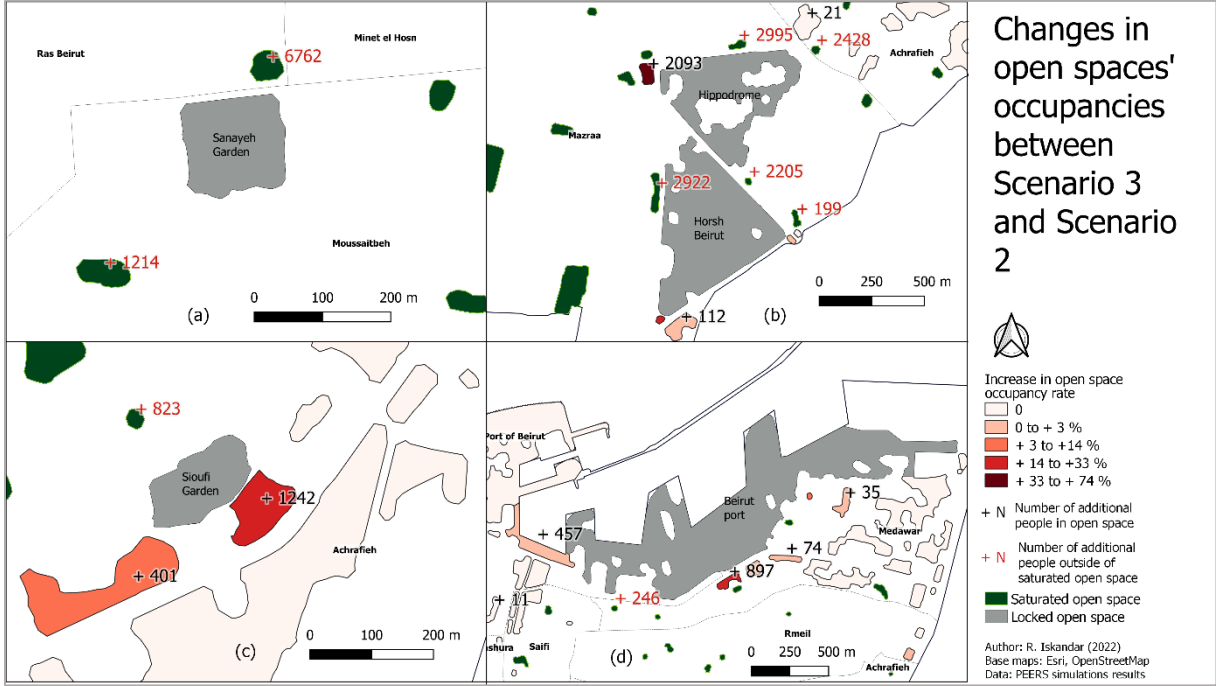


Figure 6-24 : Changes in the occupancy of the open spaces between Scenario 3 and Scenario 2. Close up on locked open spaces: (a) Sanayeh Garden, (b) Horsh Beirut and Hippodrome, (c) Sioufi Garden, (d) Beirut port

We can conclude that locking some open spaces in Beirut does not have a major impact on a global level, especially when most of the open spaces that can be locked are located at the outskirts of the city. However, at a local level, it results in an increase of the population’s influx towards the open spaces around the locked open spaces. The effect on the population’s safety varies from one open space to another. When the Sanayeh garden was locked, 100% of the population who was coming to this open space ended up outside a saturated open space, and therefore could not find another shelter. In the case of the Hippodrome and Horsh Beirut, only 17% of the people who were heading towards these two open spaces could find a safe space. For the Sioufi Garden, only 30% of the people could find a safe space, while in the case of the port 86% of the people went to another safe open space.

#### **6.7.1.4. Conclusion on the capacity of the open spaces in Beirut for immediate disaster shelter**

From the analysis of the 3 scenarios representing “near ideal” conditions, we conclude that in Beirut, the distribution of the open spaces in terms of size and location can only ensure the safety of less than 40% of the residents. Although the theoretical open space capacity is sufficient for the needs of the population, only 15% of this capacity can be exploited. When more complex scenarios were considered, despite small variations observed due to the consideration of the conservative earthquake and to the locking of the open spaces, these variations did not induce major changes at the macro scale. This is because the dominant effect in the urban area is the saturation of the small open spaces located in the center of the city, while the open spaces with the largest surface are at the outskirts of the city.

In the next section, we analyze how the safety of individuals is affected by more complex physical and social contexts.

#### **6.7.2. Analysis of the effects of more complex physical and the social contexts**

In this section, we analyze the effects of more complex physical and social environments on the population’s arrivals to safe areas in the immediate aftermath of an earthquake. We study the effect of a stronger earthquake, by considering an earthquake of a  $PGA = 0.5$  g at outcropping rock. Then, we analyze the effects of realistic human behaviors, and finally we examine the effects of the population’s spatial distributions when realistic behaviors are considered. The analysis is performed by answering three what-if questions.

##### **6.7.2.1. What-if we consider a stronger earthquake?**

In this section, we analyze the effects of considering an earthquake of  $PGA = 0.5$  g (Scenario 4), compared to a more conservative earthquake of  $PGA = 0.3$  g (Scenario 2) on the population’s arrival to safe areas. In these two scenarios, the population is distributed in residential buildings when the earthquake occurs. All the population evacuates individually, heading towards the nearest open space, and all the open spaces are unlocked. The only difference between these two scenarios is the width and the heights of the debris around the buildings.

The comparison between the distribution of the population’s states at the end of the simulation in Scenario 4 and Scenario 2 is given in Figure 6-25 (a). We can see that the percentage of arrival to safe areas decreases by 1% in Scenario 4 (from 37.5% in Scenario 2 to 36.5% in Scenario 4). The most significant changes are the decrease of the percentage of the population outside of saturated open spaces, from 58.9% in Scenario 2 to 50.4% in Scenario 4, and the increase of the percentage of the population who is still moving towards open spaces from 3.6% in Scenario 2 to 13% in Scenario 4. The increase of the percentage of the population who is still moving after 15 minutes from the onset of the earthquake can be explained by the effect the debris have on the speed of the individuals. With an earthquake of  $PGA = 0.5$  g the debris are higher and wider than with an earthquake of 0.3 g. Therefore, people take longer to travel in the environment and at 15 minutes a higher percentage of people is still moving.

The effect of the debris can also be seen on the time people took to arrive to a safe area. In Figure 6-25 (b), we can see that the average time to reach an open space increases from 198 s in Scenario 2 to 263 s in Scenario 4, which corresponds to a relative increase of 33%.

In order to analyze the spatial effects of the debris on the arrivals to the open spaces, the changes in both the number of people in open spaces and the number of people outside of saturated open spaces between Scenario 4 and Scenario 2 are displayed on the map in Figure 6-26. We can see that an open space may show a decrease reaching - 2500 arrivals after an earthquake of  $PGA$  of 0.5 g. Similarly, the number of people outside saturated open spaces can be reduced by as far as -12 000 people. On the map (Figure 6-26), we can also see that the highest changes in the number of people arriving to open spaces (unsaturated and saturated) occur in the southern part of the city. This is correlated with the distribution of the debris having heights exceeding 1m.

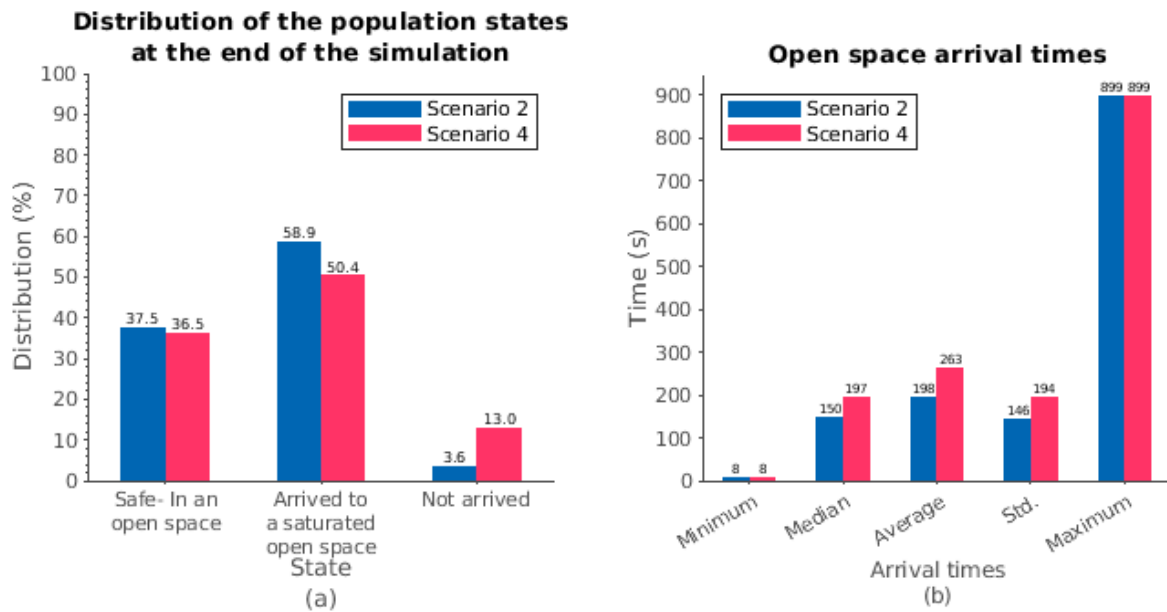


Figure 6-25: Comparison of (a) the distribution of the population's states at the end of the simulation and (b) the open space arrival times, in Scenarios 2 (PGA=0.3 g) and 4 (PGA=0.5 g)

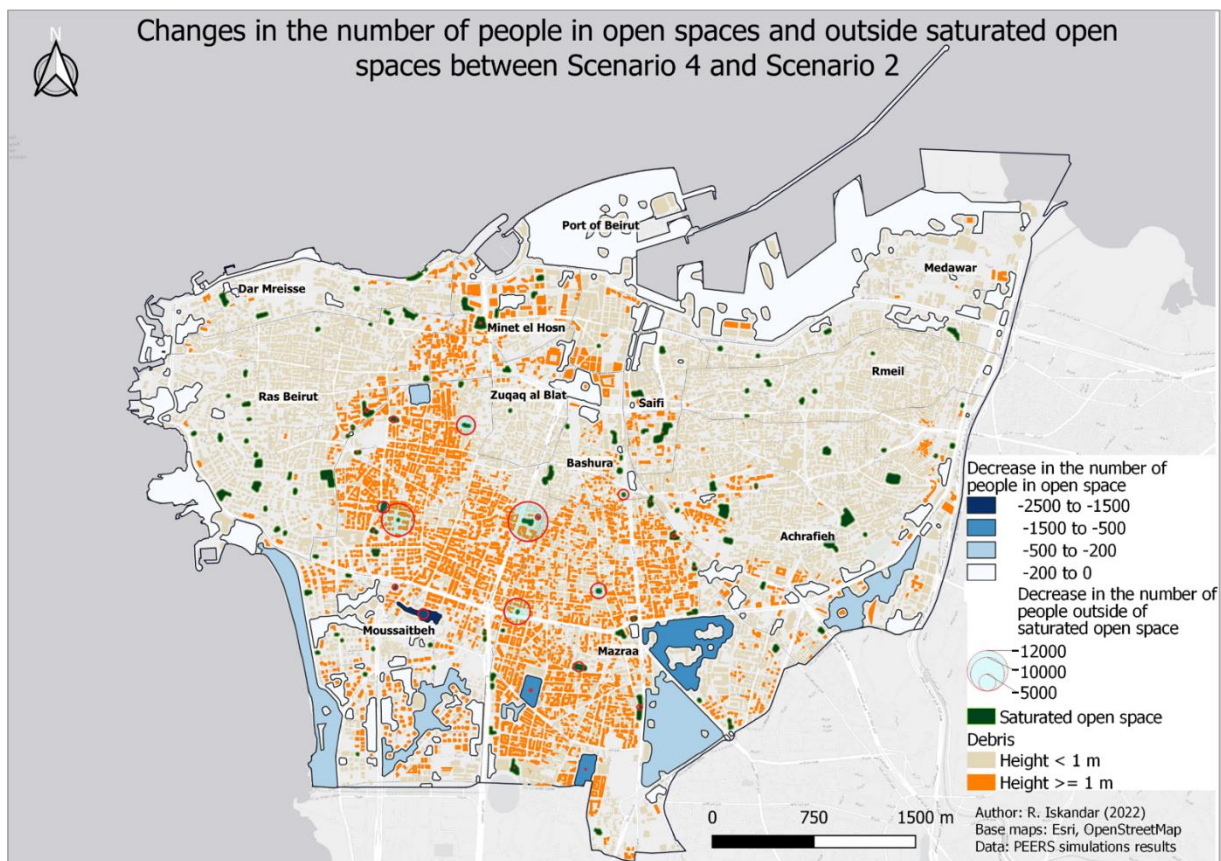


Figure 6-26: Changes in the number of people in open spaces and outside saturated open spaces between Scenario 4 and Scenario 2

In conclusion, the consideration of a stronger earthquake affects the arrivals in open spaces by increasing the time taken to reach open spaces. This is mainly caused by the environmental modifications due to the earthquake as the debris are higher and wider and cause more mobility constraints. On average, the time taken to reach an open space is increased by 32% in comparison with a more conservative scenario of PGA= 0.3 g.

### 6.7.2.2. What-if we consider realistic human behaviors?

In this section, we analyze the effects of considering realistic human behaviors on the population's arrival to safe areas in the immediate aftermath of an earthquake. As a reminder, realistic human behaviors differ from the ideal behaviors in 4 aspects. When realistic behaviors are considered:

- the people who are in buildings when the earthquake occurs can choose to evacuate or to stay indoors;
- before evacuating, the people who are indoor can do additional pre-evacuation behaviors. Therefore, the maximum evacuation delay increases from 100 s for ideal behaviors to 180 s for realistic behaviors;
- the target destination is not necessarily an open space. The behavioral choice can be either going to an open space, either going to an undefined location or going home if the person was not at home at the occurrence of the earthquake.
- people from the same households who are at a close distance form a group and share the same behaviors, typically the behaviors of the group's leader.

To analyze the effect of considering realistic behaviors, a scenario of an earthquake of  $PGA=0.3$  g occurring during the night with all the open spaces unlocked, in which the population adopts realistic behaviors (Scenario 5) is compared to a scenario with the same conditions but with ideal behaviors (Scenario 2).

When realistic behaviors are considered (Scenario 5), 72.5% of the population remains indoor at the end of the simulation, which means that only 27.5% of the population evacuates in this scenario. This observation seems reasonable, as it is close to the percentage of evacuation in the dataset on which the logistic regression model was trained (see Chapter 5 section 5.5.3.3).

When comparing the distribution of the population's states at the end of the simulation between Scenario 5 and Scenario 2 (Figure 6-27), we observe that in Scenario 5, the majority of the population is indoor, while no one is indoor in Scenario 2. As for the 27.5% of the population who are outdoors in Scenario 5, at the end of the simulation they are distributed as follows:

- 6.3% of the population is in an open space (37.5% in Scenario 2);
- 1% of the population has arrived to a saturated open space (58.9% in Scenario 2);
- 19.6% of the population arrived to an undefined location (a behavior that is not implemented in Scenario 2);
- 0.6% of the population still has not arrived to their target (3.6% in Scenario 2).

Therefore, we observe that when realistic behaviors are considered, the number of safe people in open spaces is significantly reduced. The decrease in the number of people in open spaces is mainly due to the fact that less than 30% of the population evacuated from their homes. In addition, the majority of the people who evacuated went to an undefined location rather than going to an open space. As the influx towards open spaces is reduced when realistic behaviors are considered, the percentage of the population arriving to open spaces also decreases.

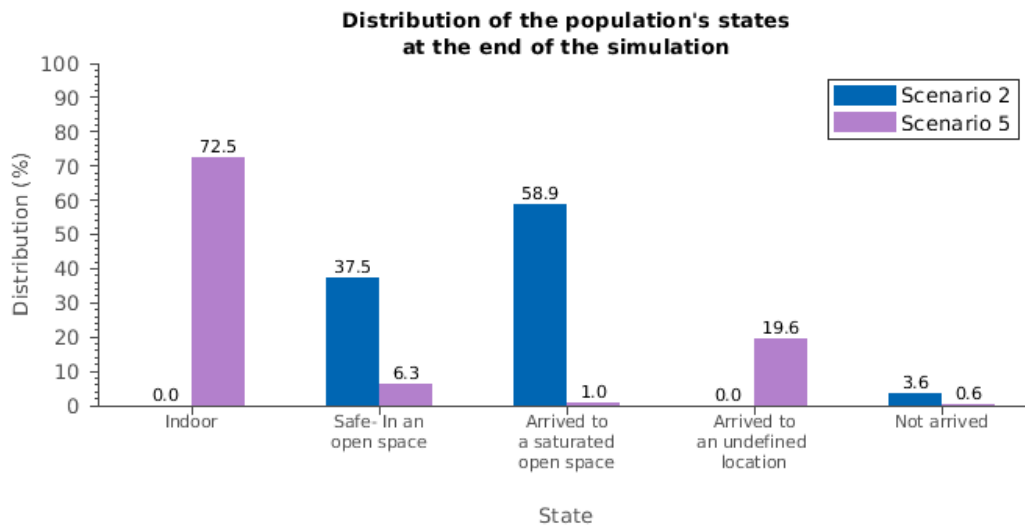


Figure 6-27: Comparison of the distribution of the population's states at the end of the simulation in Scenarios 2 (ideal behaviors) and 5 (realistic behaviors)

From Figure 6-28 we notice that the arrival times to open spaces are significantly higher in Scenario 5 than in Scenario 2. The minimum arrival time increases from 8 s in Scenario 2 to 18 s in Scenario 5, while the average arrival time increases from 198 s to 314 s in Scenario 5. This represents a 59% increase in the average time taken by a person to reach a safe area when realistic behaviors are considered.

The longer arrival times observed in Scenario 5 can be explained by two possible factors. Firstly, when realistic behaviors are considered, the evacuation delay is longer due to pre-evacuation behaviors, which results in a longer time taken to start moving towards the open space. Secondly, in Scenario 5, as all the population is located at home, all the individuals behave in groups (except people in households composed of only one member). In total, 207 198 groups were formed in Scenario 5. As people navigate in groups, the individuals' speed is reduced to the speed of the slowest group member, which increases the travel time to reach an open space. Below, we investigate further these two aspects to confirm their effects on the arrival times to open spaces.

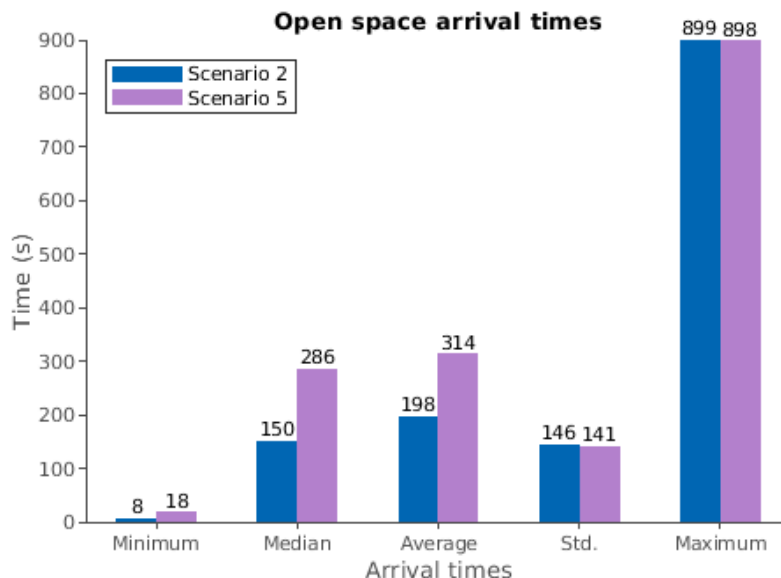


Figure 6-28: Comparison between the open spaces arrival times in Scenario 5 and Scenario 2

The time taken for a person to arrive to an open space can be divided into two parts: the time taken to evacuate (i.e. the evacuation delay) and the time taken to travel, calculated as the difference between the time of arrival and the evacuation delay. We compared the average evacuation delays and the average travel times of the people who arrived to open spaces for Scenarios 2 and 5 (Figure 6-29). We can see

that in Scenario 5, both the evacuation delay and the travel time are higher than in Scenario 2. On average, a person took 72 more seconds to evacuate when realistic behaviors were considered, and an additional 44 s for traveling towards open spaces. Although the increase in the evacuation delay can be partially explained by the pre-evacuation behaviors, the increase in the travel times can only be explained by the group behavior.

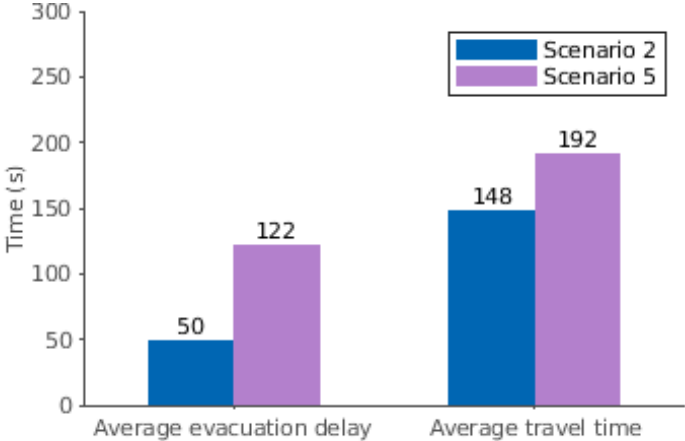


Figure 6-29: Average evacuation delays and travel times in Scenarios 2 and 5

To further illustrate the effects of the group behavior on a person’s evacuation delay and travel speed, we compared for Scenario 5 the individual evacuation delays and speeds of each person to the actual delays and speeds resulting from the group behavior. In Figure 6-30 (a), we see that the average evacuation delay of people when a person is evacuating individually is 90 s. When people behave in groups, the average evacuation delay increases to 122 s. Therefore, the group behavior results in a 30% increase of the average evacuation delay.

Furthermore, in Figure 6-30 (b) we see that for individualistic behaviors, the average natural speed of a person is 2 m/s. When group behaviors are considered, the average natural speed decreases to 1.2 m/s, which represents a 40% decrease in a person’s speed.

Therefore, the effect of group behavior on the increase of arrival times is two-fold: it increases the evacuation delays of the individuals and it increases their travel time due to the decrease of the individuals’ speeds.

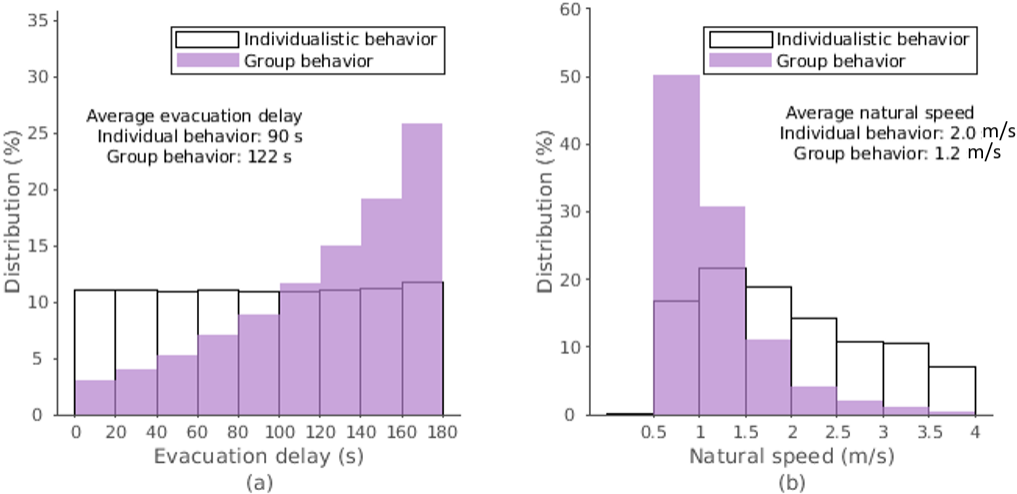


Figure 6-30: Effect of the group behavior on the evacuation delay and the speed

To conclude on the effects of realistic human behaviors on people’s arrivals to safe areas in the immediate aftermath of an earthquake, we saw that for a scenario of PGA= 0.3 g, only 6.3% of the

population would arrive to open spaces when realistic behaviors are considered. This is mainly because 72.5% of the population would remain indoors, and the majority of those who evacuate would go to an undefined location. Furthermore, the average time taken for a person to reach an open space is increased by 59% compared to the same scenario with ideal behaviors. The increase in the time to arrive to open spaces is caused by an increase in the evacuation delay and an increase in the travel time to reach an open space, which are both affected by the group behaviors.

### **6.7.2.3. What-if we consider a day scenario with realistic behaviors?**

In order to analyze the effect of the population's spatial distribution on the the arrival to safe areas in the aftermath of an earthquake, we considered a day scenario with an earthquake of PGA of 0.3 g, where people adopt realistic behaviors and all open spaces are unlocked (Scenario 6). We compare this scenario to Scenario 5, in order to identify the effect of the population's spatial distribution. The only changes between Scenario 6 and Scenario 5 is the spatial distribution of the population. In Scenario 6, 30% of the population is at home, 50% of the population is at work and 20% of the population is outdoors, while in Scenario 5 100% of the population is at home when the earthquake occurs.

Figure 6-31 shows the distribution of the population's states at the end of the simulation in Scenario 6 and Scenario 5. We see that in Scenario 6 a lower percentage of the population is indoors at the end of the simulation than in Scenario 5 (52.4% in Scenario 6 and 72.5% in Scenario 5). This can be explained by the fact that at the start of the simulation in Scenario 6, 20% of the population was already outdoors, compared to none in Scenario 5. In Scenario 6, 35% of the people who were indoors evacuated, while only 27.5% evacuated in Scenario 5. The increase in the percentage of the population who evacuates could be related to a different distribution on the damage states between residential and non-residential buildings, which would make people inside non-residential buildings more likely to evacuate. Another contributing factor could be the decreased effect of the group behaviors in Scenario 6. Only 64 813 groups were formed indoors in Scenario 6 (compared to 207 198 in Scenario 5). This is due to the fact that people at work are less likely to be in the same building as another household member, and therefore people at work decided individually if they wanted to evacuate or not. However, as the changes are not striking, the increase in the percentage of the population who evacuates for a day scenario was not further investigated.

If we compare the distribution of the people who are outdoors at the end of the simulations in the two scenarios, the most important observations are:

- the slight increase in the percentage of the population safe in open spaces in Scenario 6 (8.3%) compared to Scenario 5 (6.3%);
- the apparition of a new destination in Scenario 6, which is “arriving to home” (2.5% of the population). This behavior is not present in Scenario 5 as all the population was at home at the start of the simulation;
- the significant increase of the percentage of the population who has not arrived from less than 1% in Scenario 5 to 16.1% in Scenario 6. The target destinations of those who have not arrived in Scenario 6 are displayed in Figure 6-32: 96% were heading towards home.

Consequently, although more people undertake mobility behaviors when they are already outside at the time of the earthquake, the percentage of the population in open spaces when considering realistic behaviors remains low. This is because people have a preference for either going home or to an undefined location. This observation is not surprising, as it corresponds well to the behavioral rules defined in the model (see Chapter3 section 3.4.2). The interesting observation here is that most people who wanted to go home were not able to arrive to their destination in 15 minutes. This result could be explained by the fact that we did not impose any restriction on the choice of home as a target destination for people who are far away from home. Consequently, an agent in PEERS might be at several kilometers away from its home and still decide to go there without being able to arrive within 15 minutes.

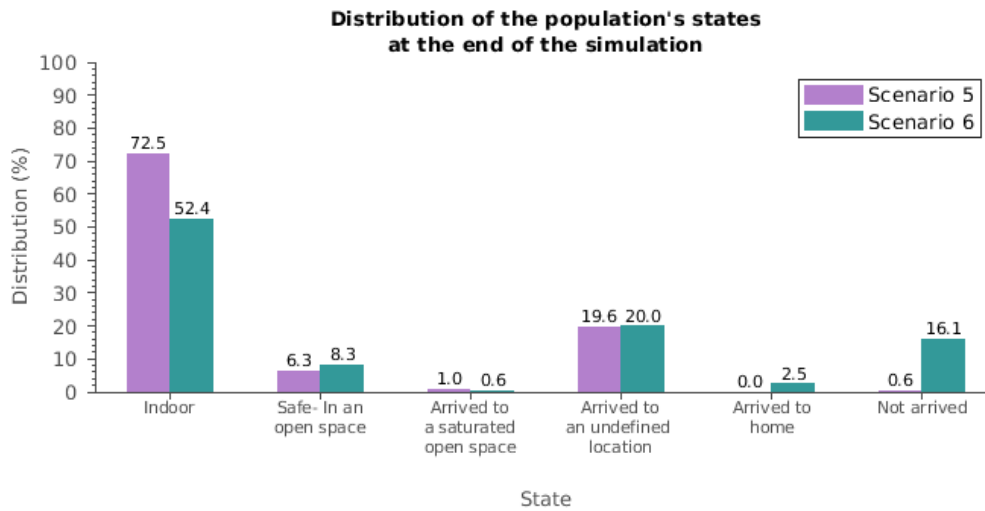


Figure 6-31: Comparison of the distribution of the population's states at the end of the simulation in Scenario 5 (night scenario) and Scenario 6 (day scenario)

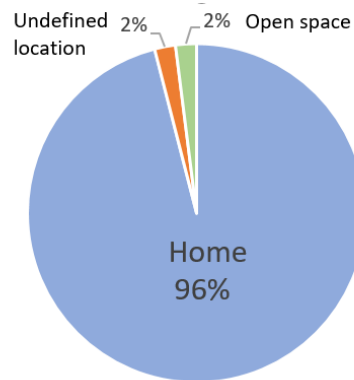


Figure 6-32: Distribution of the target destinations of the people who were still moving at the end of the simulation in Scenario 6

An analysis of the population's arrival times to open spaces, displayed in Figure 6-33, shows that in Scenario 6 the minimum, median and average arrival times are lower than those in Scenario 5. On average, a person took 87 s (around 1.5 min) less to arrive to an open space compared to a night scenario. This represents a decrease of 28% from the time taken to arrive to an open space during the night. The faster arrivals to open spaces in a day scenario can be explained by the fact that people are already outdoors at the time of the earthquake, which reduces the time people take to evacuate their buildings. This is further confirmed by the minimum arrival time of 0 s, which suggests that some people were already just outside an open space at the start of the simulation.

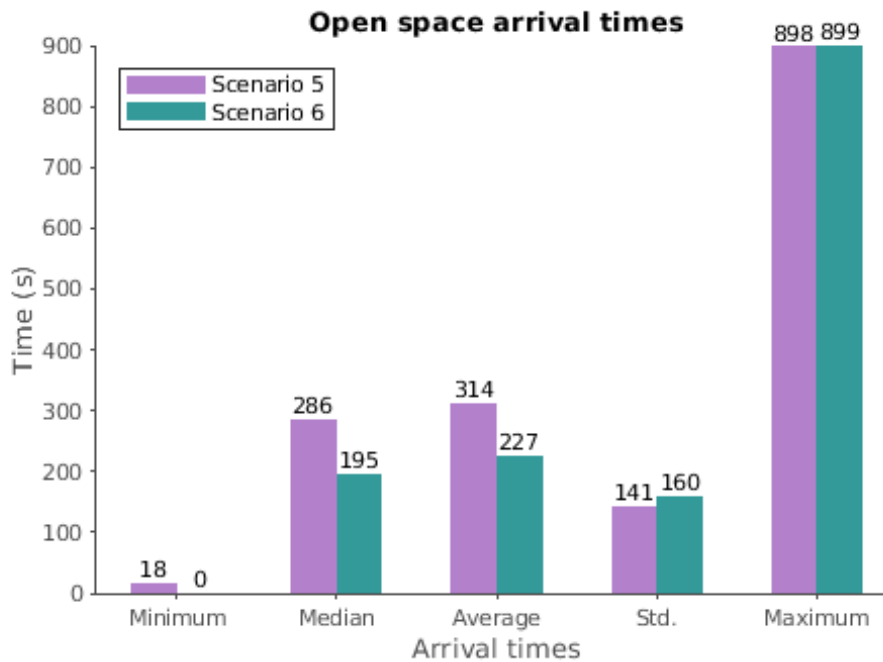


Figure 6-33: Comparison of the arrival times to open spaces between Scenario 5 and Scenario 6

In conclusion, for a day scenario where realistic behaviors are considered, some of the people who are away from home will want to join their relatives and will therefore go home. However, those who decide to go home are unlikely to arrive to their destination within 15 min when moving on foot. For the people arriving to open spaces, the time taken to reach an open space is reduced by 28% compared to a night scenario, as people who are already outdoors take less time to start undertaking mobility behaviors, and because they are less likely to behave in groups.

#### 6.7.2.4. Conclusion on the effects of more complex physical and social contexts on the population's safety

In this section we analyzed the effects on the population's safety in the immediate aftermath of an earthquake of variable PGA, of realistic behaviors and of the population's spatial distribution for a day scenario.

The change of the earthquake's PGA did not yield in changes in the number of people safe in open spaces, as the nearest-to-people open spaces were saturated for the two earthquake scenarios. The consideration of realistic behaviors yielded to a significant decrease in the percentage of safe people in night scenarios, from 37.5% in a night scenario with ideal behaviors, to 6.3% in a night scenario with realistic behaviors. When the time of the day was varied for realistic behaviors, a day scenario resulted in an increase of the percentage of the population arriving to safe areas to 8.3%.

Regarding the time taken by the individuals to reach a safe area, the increase of the earthquake's PGA resulted in a 33% increase in the time to reach safety compared to a more moderate PGA. For a moderate earthquake, the consideration of realistic behaviors resulted in arrival times delayed by 59% compared to ideal behaviors. Finally, when realistic behaviors were considered, a day scenario resulted in the decrease of 28% of the time taken to reach an open space compared to a night scenario.

## 6.8.DISCUSSION

In this chapter, we have presented the verification of the implementation of the key components of PEERS through the outputs of simulations performed at a reduced spatial scale using GAMA's interactive interface. We have also presented the challenges of performing large-scale simulations comprising around a million agents interacting in a 20 km<sup>2</sup> spatial area. Similar challenges were faced by previous studies who developed ABMs for the simulation of evacuation of large urban areas which often resulted in limiting the study area to a few districts (Bañgate, 2019) or to the city center only (Zlateski et al., 2020).

In this work, despite the challenges faced we were able to perform simulations at the scale of the city of Beirut. However, the technical limitations resulted in defining a reduced experiments plan, as the exploration of the whole parameter space could not be achieved with the current implementation of the model and the current computational resources.

The experiment plan was designed to answer two main research questions. The first one was related to the capacity of the open spaces in Beirut in providing shelter for the population in the immediate aftermath of an earthquake. This question was analyzed through 3 scenarios representing near ideal conditions with varying complexities. The first one was in an ideal case with no earthquake, the second was a moderate earthquake of PGA of 0.3 g, and finally the third one was an earthquake of 0.3 g with 5 locked open spaces. The second question was related to effects of more complex physical and social environments on the population's arrivals to safe areas. This question was analyzed by varying the earthquake's PGA, by considering realistic behaviors and by considering a day scenario. The key findings that the simulations in PEERS revealed can be summarized as follows:

### 1) Actual capacity of open spaces in Beirut

In Beirut, if all the residents were to evacuate and head to the nearest open space, only 38% of the residents could have a safe access to an open space. Although the theoretical capacity of open spaces should allow sheltering all the city's residents, the distribution of the open spaces in terms of size and location only makes it possible to use 15% of the open spaces' capacity. While locking some open spaces did not contribute to a change of this tendency at a macro-scale, the effects at a micro-scale were critical for some of the locked open spaces. This is the case of the Sanayeh garden, the Hippodrome and Horsh Beirut. Locking these open spaces resulted in an increase of the influx on the open spaces nearby, which were already saturated. Therefore, most of the people who were heading towards these locked open spaces could not be redirected to another safe area. These are important findings on Beirut's urban form that were revealed through the simulations in PEERS. It further proves that the city's dense urbanization and lack of planned open spaces have a detrimental effect on the population's safety in case of seismic crisis.

The case of Beirut is not unique; dense cities exposed to a high seismic hazard that have poor urban planning are unprepared for a major seismic event. This is the case of Istanbul in Turkey for instance, where a previous study has demonstrated the lack of evacuation areas within walking distance from areas with high population concentration (Yücel, 2018). The city's unpreparedness for a big earthquake was revealed to the public in the earthquake that occurred in Istanbul on 26 September 2019 (Magnitude 5.8), as reported by a tweet from a Turkish citizen (Figure 6-34).

From this perspective, running evacuation simulations with realistic spatial data can contribute to the assessment of the current capacities of the urban area. Such simulations can help to improve the urban planning and the city's earthquake preparedness by testing what-if scenarios, such as: what-if we demolish this old building and transform this area into an open space? These simulations can have a high positive impact if taken into account by the local stakeholders in charge of decision-making.



Figure 6-34: Tweet from a Turkish citizen just after the 26 September 2019 earthquake (M 5.8) in Istanbul, highlighting the insufficiency of open spaces. Retrieved from: <https://twitter.com/canokar/status/1177187759645216768>

2) The important effect of debris and human behaviors on the population's safety in the aftermath of an earthquake

Through the analysis of the simulations' results, we saw that the population's safety in the immediate aftermath of an earthquake does not only depend on the availability of open spaces. The average time taken by the population to reach open spaces was considerably increased by (i) the presence of debris that slow down evacuation speed and (ii) the accounting for realistic behaviors that increase the pre-evacuation delay and hereafter decrease the speed due to the group behavior.

i. The influence of debris

In order to determine the influence of the debris on the time taken to reach an open space in different seismic scenarios, we considered as a reference the average time to arrive to an open space in the scenario with no debris. In Figure 6-35, we can see that the debris resulting from the moderate earthquake resulted in a 9% increase of the arrival times. For the earthquake of PGA 0.5 g, the delay in arrival to open spaces caused by debris considerably increases to 45%, which outlines that the debris have a very important effect on the arrival of the population to safe areas.

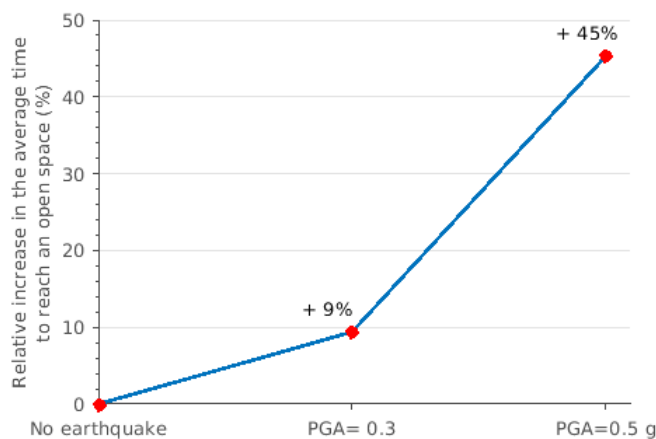


Figure 6-35 : Increase in arrival times caused by the debris in different seismic scenarios compared to the case with no earthquake

Indeed, debris hinder the evacuation when they are too high and too far from buildings. If we consider the example of the August 24, 2016 Amatrice, Italy earthquake (Magnitude 6.0), in which the most ancient building stock collapsed and masonry structures suffered from very heavy damages (Quest W.G. et al., 2016), high piles of debris were deposited on pathways between buildings as it can be seen on

Figure 6-36. Due to the height of the debris, it was not only difficult to move around in the city, but also people were trapped inside buildings and they needed to be rescued from collapsed structures (Figure 6-37). Consequently, the integration of realistic estimates of debris is primordial for the analysis of pedestrians' evacuation especially in scenarios with severe buildings damages.



Figure 6-36 : Damage and debris during the August 24, 2016 Amatrice, Italy earthquake. Source: (Bañgate, 2019)



Figure 6-37: Rescue of people trapped in debris during in the aftermath of the August 24, 2016 Amatrice earthquake. Photograph by: Alessandra Tarantino/AP

## ii. The influence of human behavior

Another important factor affecting the time taken to arrive to safe areas is the human behavior. When realistic human behaviors were considered with an earthquake of PGA of 0.3 g, the arrival times to open spaces were 59% longer than in the scenario with ideal behaviors.

The importance of the behavioral response in moderate earthquakes has been demonstrated in the case of the 11 May 2011 Lorca, Spain earthquake (M 5.2). The 9 fatalities caused during this earthquake occurred when people rushed into the streets while the ground was shaking and they were consequently hit and killed by falling non-structural elements (parapets, cornices, etc.) (Moreno et al., 2012). Hence, the fatalities were not related to building collapse or structural damages but rather to the individual responses.

This outlines that human behaviors have an essential role on the population’s safety and should not be neglected when analyzing the population’s evacuation in the immediate aftermath of an earthquake.

Finally, we compared the relative importance of the presence of debris and the human behaviors on the population’s safety by considering as a common reference the average time taken to arrive to an open space in an earthquake of 0.3 g with ideal behaviors. When a stronger earthquake was considered, i.e. more significant debris, the arrival times were increased by 33%. On the other hand, when realistic human behaviors were considered, the arrival times were increased by 59% (Figure 6-38).

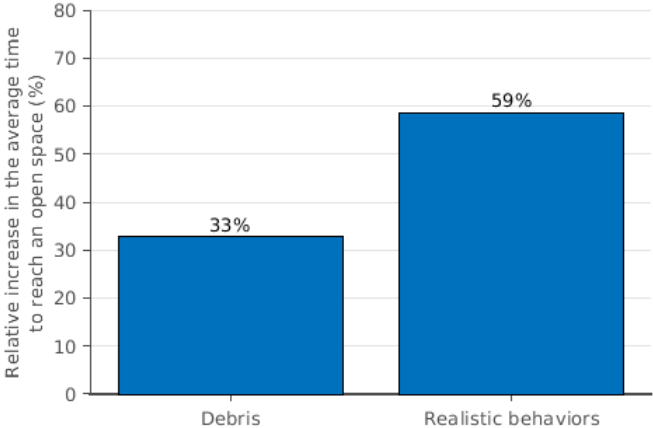


Figure 6-38: Relative effects of the debris (PGA 0.5 g) and realistic human behaviors on the increase of the average time taken to reach an open space, compared to a scenario of PGA 0.3 g and with ideal behaviors

We can see that human behaviors have a higher influence on the population’s safety in the aftermath of an earthquake than the consideration of a more pessimistic earthquake scenario (and debris). This further strengthens our point on the importance of considering realistic human behaviors when simulating earthquake evacuation.

Next chapter will provide the general conclusion in addition to an overview of the limitations of the study as well as perspectives for future work.



# Chapter 7: Conclusion and future work

This chapter is structured as follows: section 7.1 details the conclusions and summarizes the contributions of the thesis; section 7.2 presents the limitations and future works of our study; finally, section 7.3 provides the concluding remarks and long-term perspectives.

## 7.1.CONCLUSION

Earthquakes have been a subject of analysis in various disciplines. While some studies developed physical centered approaches that estimate the structural damages and infer economic and human losses, other studies took interest in what makes individuals more likely to suffer from harm as a result of an earthquake. The past 25 years have seen a rise of integrated approaches that combine both physical and social vulnerabilities into earthquake risk assessment. However, social vulnerability is in most cases considered as an “aggravating factor” without accounting for the society’s capacity to cope, adapt and overcome the effects of the earthquake. Assessed in pre-crisis conditions, such seismic risk integrated approaches do not also account for the dynamics of seismic crises, especially the change in the environment due to the generated debris and human behaviors and mobility. Lessons from past earthquakes indicate the importance of these factors on people’s exposure to hazard and risk management. This means that current integrated approaches fail to capture the full interplay between the natural and social environments during earthquakes.

In order to advance in fully integrating the social dimension into seismic risk assessment, this thesis presented an interdisciplinary seismic risk modeling approach, merging earth, social and computer sciences, while integrating both the physical and social components of earthquake risk. This interdisciplinary approach involved mobilizing concepts and methods issued from different disciplinary domains. More specifically, this thesis explored how modeling human behaviors and mobility in a modified environment caused by building damage and debris can allow to identify and rank physical and social elements at play during a seismic event. This is achieved by looking at people’s safety in the aftermath of an earthquake, with safety defined as being in an open space away from buildings and debris.

Modeling human behavior in a seismic crisis requires - at the building scale - a realistic assessment of damage and related debris, of the population distribution representing the social structure of the studied region, and a well-calibrated evacuation simulation model that includes calibrated human behavior and takes into account social interactions between individuals.

To tackle this issue, we developed PEERS, an agent-based model (ABM) for the simulation of pedestrian evacuation in the event of an earthquake. We focused on the simulation of the crisis from the occurrence of the earthquake until 15 minutes later. PEERS performs dynamic simulations of an earthquake integrating both its physical and the social aspects. The physical component is taken into account by the realistic estimation of building damage and debris formation. The social aspect is incorporated by incorporating human behaviors in reaction to the earthquake; this is represented by individuals’ evacuation and mobility decisions, and the interaction among individuals that can result in the formation of groups. One of the originalities of PEERS compared to other agent-based models for the simulation of pedestrian evacuation is that the calibration of behavioral responses in Beirut is based on survey data from the August 4, 2020 explosion at the port of Beirut. The survey data clearly outline that a great proportion of the population do not know where to take shelter in case of emergency, and that most people would try to meet up with family members. The simulations were applied to the case of Beirut, Lebanon, which is a city prone to large magnitude earthquakes. The elementary data related to site response and building properties (number of floors, age of construction, vulnerability class) needed in this thesis were already acquired through previous projects. However, the building database was incomplete. Therefore, one of the challenges in this thesis was to generate a complete building database for Beirut using open source geographic data and satellite images for measuring the height of the buildings. We contributed to, and relied on, volunteered geographic information from OpenStreetMap for the construction of a building database for Beirut. Once the building footprints were extracted, we estimated the building heights by processing high-resolution satellite images, and

qualified the vulnerability of the buildings using machine-learning tools trained on the pre-existing, but incomplete, building database. The contribution to the digitization of buildings in OpenStreetMap has a direct impact on the community as it provides an open source database that can be easily accessed for other studies interested in Beirut's buildings. Furthermore, the methodology that was developed to identify the characteristics of the building stock can also be replicated on other study areas where the information on the building's vulnerability is scarce. We further developed the approach proposed by Salameh et al. (2017) to predict mean seismic damage at the building scale. This was done by accounting for the contribution of linear and non-linear site effects in seismic damage, particularly the spectral coincidence between soils and buildings on building damages. The mean seismic damage can be predicted using simple indicators related to buildings, soil and seismic solicitation: i.e. the ratio between building and soil fundamental resonance frequencies, the amplitude of the H/V peak as a proxy for site amplification, PGA and PGV at outcropping rock. The seismic damages estimated for the two earthquake scenarios of PGA=0.3 g (which corresponds to the regulatory PGA) and PGA=0.5 g correspond to slight to moderate, and moderate to extensive damages throughout the city, respectively. Whatever the earthquake scenario, the greatest damage is concentrated in sediment areas that are prone to site effects, especially when soil and building resonance frequencies coincide. The uncertainty of +/- 3 floors when estimating the building height from satellite images on seismic damages translates into an overall lower or larger level of damage at the city level. The 0.5 g earthquake scenario shows the importance of non-linear soil behavior in reducing seismic damages for the more vulnerable buildings (class 1) while increasing seismic damages for the less vulnerable ones (class 3).

Being at the core of the interactions between the physical environment and the social component of seismic risk, estimating the debris is a key step in the process of modeling a seismic crisis. The literature is poor in estimating debris while quantifying both the debris height and extent for varying levels of building damage. In this thesis, we developed an approach that computes the volume of generated debris according to the damage level, and then distributes it around the building according to geometrical rules. For the 0.5 g scenario, the extent of debris is significant, reaches up to 7 m away from buildings. This approach was validated by comparing its performance to other approaches in the literature for cases of complete collapse.

Finally, despite the uncertainties on the population's size and the limited data about the distribution of households in Beirut, we developed an approach for estimating the population size and generated a synthetic population of individuals and households that replicates the available data. The population size, estimated to be 819 717 individuals, was found using a GIS-based approach that identified the function of buildings and estimated the number of residential apartments. For the generation of the synthetic population, in addition to generating individuals using Gen\*(Chapuis et al., 2019), an algorithm was developed to assign individuals into households (246 325 households) based on heuristic rules that correspond to available data.

The models and data allowed us to run several earthquake evacuation simulations in PEERS. We adopted a "what-if" approach to investigate (i) the capacity of the open spaces in Beirut for providing shelter for the population in the immediate aftermath of an earthquake and (ii) the effects of more complex physical and social environments on the population's arrivals to safe areas. The key findings are:

- In Beirut, the distribution of open spaces in terms of size and location cannot ensure the safety of all of the population, even in ideal conditions where the behavioral component is reduced to reaching the closest safe area only. Indeed, in this case, only 38% of the population reached a safe area within 15 min after the onset of ground shaking even though the theoretical capacity of open spaces should shelter all of the city's residents. This is explained by the distribution of the open spaces in terms of size and location within the city, as large open spaces are on the outskirts of the city. This is an important finding on Beirut's urban form that was found through the simulations in PEERS.
- Debris and human behaviors both significantly delay the arrival times to open spaces. Debris result in a slower evacuation speed. Modeling realistic behaviors increases pre-evacuation delay and decreases the speed due to the group behavior. In the case of Beirut, human behaviors have

a higher influence on the population's safety than a more pessimistic earthquake scenario with greater debris. We found that including realistic human behavior delays the arrival time to an open space by about two times compared to the delay caused only by the presence of debris. This further proves the importance of considering realistic human behaviors when simulating earthquake evacuation.

## 7.2.LIMITATIONS AND FUTURE WORK

The limitations, which can be addressed in future work, fall into three categories: modeling the consequences of the earthquake, agent behaviors, and simulations. These are detailed below.

- **EARTHQUAKE CONSEQUENCES**

Regarding earthquake consequences, the main limitations found were related to the estimation of debris and casualties, presented as follows:

**Estimation of debris.** The debris estimation model was based on an analytical approach. Although the model compared well with existing studies, the validation with observation and experimental data is better. Debris are generated uniformly around buildings; however, this does not represent the directional effect of the ground motion where more debris would be observed in the direction of the propagation of the seismic wave. Therefore, the developed model predicts the least expected debris around buildings. Nevertheless, as the impact of debris on pedestrian's safety in the aftermath of an earthquake is highly important, more effort should be done on improving debris estimations in future works. As a first step, the proposed model can be calibrated in an experimental setup, by performing experiments on a shaking table and observing the extents and heights of the generated debris. Furthermore, the experiments can be validated by observations from real events through the analysis of satellite images and street-view photography in pre/post-earthquake conditions, eventually combined with in-situ evaluation of building typologies. This would allow establishing relationships between building types and generated debris.

**Estimation of casualties.** The estimated injuries and fatalities - especially for the pessimistic scenario of  $PGA = 0.5g$  - seem low (2000 injuries, 60 fatalities). The realism of these estimates could not be assessed in the absence of earthquake casualty data on earthquakes in Lebanon. The casualty rates in buildings and in debris zones were derived from HAZUS, which is originally targeted for studies in the US. Although there are other studies that developed casualty rates in earthquakes, these casualty rates are often restricted to the probability of death for full building collapse and do not take into account other levels of injuries. Future work should focus on the analysis of casualty rates across different geographic and cultural contexts. In the absence of sufficient data, this can be done by comparing the study area to other countries with similar contexts.

- **BEHAVIOR OF AGENTS IN PEERS**

Moreover, the behavioral rules of agents in PEERS also had few limitations, mainly in the calibration of human behaviors, in the mobility of the agents and in the group behaviors, as explained below.

**Calibration of human behaviors.** The survey data used for the calibration of PEERS are based on the particular case of the Beirut port explosion. The behavioral responses should be compared to observations in earthquakes in Beirut in order to validate that the same trends would be observed.

Moreover, the survey should be improved to include close-ended questions about the individual mobility in the aftermath of an earthquake, in which the respondent picks the first destination he/she went to. By defining the possible answers and limiting the options to one choice only, a multivariate statistical analysis can be done to identify the motivations depending on the choice of target destinations.

Furthermore, as behavioral data are extremely scarce, more efforts should be done to diffuse the survey in future seismic events. The survey can be used to compile a comprehensive database on human behaviors across several cultures and for different levels of earthquake shaking. A possible approach could be through the diffusion of the questionnaire through platforms such as the USGS "Did you feel

it?<sup>9</sup>” or the EMSC “Lastquake<sup>10</sup>” platforms that collect the experiences of individuals who felt earthquakes. An extension could be added to these platforms where users can also answer the survey and indicate how they behaved.

**Mobility of agents in PEERS.** In PEERS, the mobility destination is calculated on a straight-line distance. This choice is very crude as it does not take into account the presence of obstacles on the path, such as buildings, which considerably increase the total distance traveled by the agents, nor the slope of the terrain that imposes further challenges on mobility. A more realistic representation of pedestrians’ mobility could be achieved by performing an accessibility analysis in which, for each location on the map, the nearest facility in terms of real travel distance (that takes into account obstacles) or travel time is calculated.

Furthermore, all agents in PEERS are given the ability to decide on their behavior and move towards their destination. This does not reflect reality, as young children and people with psychological or mobility disabilities might have limited capability for decision-making and autonomous mobility.

A more realistic approach could be achieved by considering a percentage of agents who have disabilities. This percentage could be calibrated by real data from the study area. These agents would have a very low probability of moving or deciding autonomously. Moreover, other agents could be given the role of “caregiver”, who assist disabled agents and young children in evacuation. Nevertheless, this approach needs to be complemented by a refined spatial distribution of the population for a day scenario, to consider age-based rules and a finer categorization of the buildings functions (i.e. children younger than 2 years old would be either at home with a family member, or at daycare with a professional caregiver).

**Group behaviors.** In the current version of PEERS, the choice of evacuation and mobility destination only depends on the group’s leader decisions and disregards other members’ needs. This is not very realistic, especially for cases where one of the group members needs to go to hospital and the group leader does not, which results in the person not receiving medical assistance. This can be improved, for instance, by considering a democratic decision-making approach in the group where the final group’s decision depends on the choices of the majority of the group members, with a higher priority given to medical needs. Nevertheless, this is a hypothetical approach that needs to be complemented by more studies on how group decision making occurs in different cultural contexts.

To stress the importance of cultural context, the choice of the group leader as being the head of the household assumes hierarchical roles in the family structure, which might not be adapted to all case studies. Similarly, in the absence of the head of the household, in the current version of PEERS the leader is assigned as a function of the group members’ age in an absolute manner. This might not reflect reality in which adults with senior parents often assume leadership positions. Therefore, more research should be done on age and leadership in family structures.

Moreover, an improvement for group behaviors is how groups deal with death and severe injuries of one of the group members. Usually people stop and wait next to a critically injured person who is severely injured and call for medical assistance, especially if that person is a family member (Bañgate, 2019). This is not taken into account in PEERS and should be improved in future versions of the model.

Finally, future versions of PEERS can also include groups formed by other social bonds such as friends and coworkers, and spontaneous groups that form during a crisis between strangers, which has been observed in previous crises.

---

9 <https://earthquake.usgs.gov/data/dyfi/>

10 <https://www.emsc-csem.org/#2>

- **SIMULATIONS IN PEERS**

Finally, two main limitations in the simulations were the validation of the simulation outputs and the limited number of experiments performed.

**Validation of the simulation outputs.** The simulation outputs of PEERS could not be adequately validated in this study, as no actual measures exist for counting the number of people in open spaces in the aftermath of a seismic event, or for the time taken for the population to reach an open space. Consequently, the validation of PEERS was restricted to the validation of the conceptual model and the validation of the data used as input of the model. Possible approaches could be the use of videos and photos available through social media or on-line after an earthquake and/or the use of dark fiber optics data to monitor the population flow and count the number of individuals grouping in a safe area.

**Limited number of experiments performed in PEERS.** Although simulations with PEERS could be performed at a large spatial scale, the execution of the simulations needed colossal computation resources that reduced the number of experiments done in this thesis. Future works can focus on the optimizing the implementation of PEERS, mainly by reducing the number of processes in the simulation's initialization, and by executing the simulation in parallel on multiple threads. Furthermore, the performance gains that might be achieved by implementing the model on a different platform (such as Unity<sup>11</sup>) can be investigated. Once the simulations can be executed at a faster speed at large scale, a richer experiment plan covering more diverse seismic scenarios can be defined. Moreover, a thorough sensitivity analysis and studying the propagation of uncertainties from the model's inputs to its outputs (e.g. using OpenMole) could improve the calibration of PEERS. Finally, optimizing the simulation can also contribute to the increase and the diversification of the simulation's outputs. For instance, spatio-temporal data on the agents' evacuation could be captured and eventually used to analyze pedestrians' trajectories.

### **7.3.CONCLUDING REMARKS AND LONG-TERM PERSPECTIVES**

Despite the several technical and methodological limitations of PEERS, the simulations gave a first estimation of the importance of human behaviors and debris on pedestrians' evacuation in the aftermath of an earthquake. We were also able to weigh the relative importance of these two factors when compared to a common reference.

The methodology for the simulation and comparison of the importance of variables can be adopted to develop a seismic risk index that integrates all of the components that interact in a seismic crisis, including the individual behaviors. These components should be identified and included in the model. After defining the rules of the interactions between these components, the dynamic simulations can be executed. Finally, through the analysis of the simulation results, the relative weight of each component can be inferred and used to calibrate the seismic risk index.

Another practical application of integrated simulations of seismic crises, could be through the development of a serious game, in which game players can take the role of a person, decide on the behaviors to adopt, and see the consequences of this behavior. The game could be used as an educational tool to increase seismic risk awareness and the knowledge of appropriate protective behaviors in case of earthquakes.

Finally, integrated seismic crises simulations can be given an operational dimension, and be used as a decision-support system. Simulations of different scenarios can help decision-makers decide on the most adapted behavioral guidelines for earthquake protection. Similarly, the simulations can be used to influence policies about the built environment such as the number, size and distribution of open spaces.

---

11 <https://unity.com/fr>



# References

- ADRC, 2005. Total Disaster Risk Management. Asian Disaster Reduction Center (ADRC).
- Agnew, D.C., 2002. 1 History of seismology, in: *International Geophysics*. Elsevier, pp. 3–11. [https://doi.org/10.1016/S0074-6142\(02\)80203-0](https://doi.org/10.1016/S0074-6142(02)80203-0)
- Aguirre, B.E., Torres, M.R., Gill, K.B., Lawrence Hotchkiss, H., 2011. Normative Collective Behavior in The Station Building Fire\*: Normative Collective Behavior in The Station Building Fire. *Social Science Quarterly* 92, 100–118. <https://doi.org/10.1111/j.1540-6237.2011.00759.x>
- Akkar, S., Sandıkkaya, M.A., Bommer, J.J., 2014. Empirical ground-motion models for point- and extended-source crustal earthquake scenarios in Europe and the Middle East. *Bull Earthquake Eng* 12, 359–387. <https://doi.org/10.1007/s10518-013-9461-4>
- Alexander, D., 2012. Models of Social Vulnerability to Disasters\*. *RCCS Annual Review*. <https://doi.org/10.4000/rccsar.412>
- Alexander, D., 2000. *Confronting catastrophe: new perspectives on natural disasters*. Oxford University Press, USA.
- Alexander, D., 1990. Behavior During Earthquakes: A Southern Italian Example. *International Journal of Mass Emergencies and Disasters* 8, 5–9.
- Alexander, D., Magni, M., 2013. Mortality in the L’Aquila (Central Italy) Earthquake of 6 April 2009. *PLoS Curr*. <https://doi.org/10.1371/50585b8e6efd1>
- Alizadeh, M., Alizadeh, E., Asadollahpour Kotenae, S., Shahabi, H., Beiranvand Pour, A., Panahi, M., Bin Ahmad, B., Saro, L., 2018. Social Vulnerability Assessment Using Artificial Neural Network (ANN) Model for Earthquake Hazard in Tabriz City, Iran. *Sustainability* 10, 3376. <https://doi.org/10.3390/su10103376>
- Allan, P., Bryant, M., Wirsching, C., Garcia, D., Teresa Rodriguez, M., 2013. The Influence of Urban Morphology on the Resilience of Cities Following an Earthquake. *Journal of Urban Design* 18, 242–262. <https://doi.org/10.1080/13574809.2013.772881>
- Althaus, C.E., 2005. A Disciplinary Perspective on the Epistemological Status of Risk. *Risk Analysis* 25, 567–588. <https://doi.org/10.1111/j.1539-6924.2005.00625.x>
- An, L., 2012. Modeling human decisions in coupled human and natural systems: Review of agent-based models. *Ecological Modelling* 229, 25–36. <https://doi.org/10.1016/j.ecolmodel.2011.07.010>
- Aouad, D., Kaloustian, N., 2021. Sustainable Beirut City Planning Post August 2020 Port of Beirut Blast: Case Study of Karantina in Medawar District. *Sustainability* 13, 6442. <https://doi.org/10.3390/su13116442>
- Arango, M.C., Lubkowski, Z.A., 2012. Seismic Hazard Assessment and Design Requirements for Beirut, Lebanon. Presented at the 15th World Conference on Earthquake Engineering, Lisboa, Portugal.
- Argyroudis, S., Selva, J., Gehl, P., Pitilakis, K., 2015. Systemic Seismic Risk Assessment of Road Networks Considering Interactions with the Built Environment: Systemic seismic risk assessment of road networks. *Computer-Aided Civil and Infrastructure Engineering* 30, 524–540. <https://doi.org/10.1111/mice.12136>
- Armaş, I., 2008. Social vulnerability and seismic risk perception. Case study: the historic center of the Bucharest Municipality/Romania. *Natural Hazards* 47, 397–410. <https://doi.org/10.1007/s11069-008-9229-3>
- Assimaki, D., Li, W., Kalos, A., 2011. A Wavelet-based Seismogram Inversion Algorithm for the In Situ Characterization of Nonlinear Soil Behavior. *Pure Appl. Geophys.* 168, 1669–1691. <https://doi.org/10.1007/s00024-010-0198-6>
- Aven, T., 2016. Risk assessment and risk management: Review of recent advances on their foundation. *European Journal of Operational Research* 253, 1–13. <https://doi.org/10.1016/j.ejor.2015.12.023>
- Bañgate, J., 2019. Multi agent modeling of seismic crisis. Université Grenoble Alpes, Grenoble, France.
- Bañgate, J., Dugdale, J., Beck, E., Adam, C., 2018. A multi-agent system approach in evaluating human spatio-temporal vulnerability to seismic risk using social attachment. Presented at the WIT Transactions on Engineering Sciences, Sevilla, Spain, pp. 47–58. <https://doi.org/10.2495/RISK180041>

- Bañgate, J., Dugdale, J., Beck, E., Adam, C., 2017. SOLACE a multi-agent model of human behaviour driven by social attachment during seismic crisis, in: 2017 4th International Conference on Information and Communication Technologies for Disaster Management (ICT-DM). Presented at the 2017 International Conference on Information and Communication Technologies for Disaster Management (ICT-DM), IEEE, Münster, pp. 1–9. <https://doi.org/10.1109/ICT-DM.2017.8275676>
- Bañgate, J.M., Dugdale, J., Beck, E., Adam, C., 2019. Review of Agent Based Modelling of Social Attachment in Crisis Situations: *International Journal of Information Systems for Crisis Response and Management* 11, 35–64. <https://doi.org/10.4018/IJISCRAM.2019010103>
- Barbat, A.H., Pujades, L.G., Lantada, N., 2006. Performance of Buildings under Earthquakes in Barcelona, Spain. *Computer-aided Civil Eng* 21, 573–593. <https://doi.org/10.1111/j.1467-8667.2006.00450.x>
- Barthelemy, J., Toint, P.L., 2013. Synthetic Population Generation Without a Sample. *Transportation Science* 47, 266–279. <https://doi.org/10.1287/trsc.1120.0408>
- Battegazzorre, E., Bottino, A., Domaneschi, M., Cimellaro, G.P., 2021. IdealCity: A hybrid approach to seismic evacuation modeling. *Advances in Engineering Software* 153, 102956. <https://doi.org/10.1016/j.advengsoft.2020.102956>
- Beck, E., Cartier, S., Colbeau-Justin, L., Azzam, C., Saikali, M., 2018. Vulnerability to earthquake of Beirut residents (Lebanon): perception, knowledge, and protection strategies. *Journal of Risk Research* 1–18. <https://doi.org/10.1080/13669877.2018.1466826>
- Beck, E., Dugdale, J., Adam, C., Gädatzis, C., Bangate, J., 2020. A methodology for co-constructing an interdisciplinary model: from model to survey, from survey to model. *ArXiv abs/2011.13604*.
- Beck, E., Dugdale, J., Van Truong, H., Adam, C., Colbeau-Justin, L., 2014. Crisis Mobility of Pedestrians: From Survey to Modelling, Lessons from Lebanon and Argentina, in: *Information Systems for Crisis Response and Management in Mediterranean Countries*. Springer International Publishing, Cham, pp. 57–70. [https://doi.org/10.1007/978-3-319-11818-5\\_6](https://doi.org/10.1007/978-3-319-11818-5_6)
- Beresnev, I.A., Wen, K.-L., 1996. Nonlinear soil response—A reality? *Bulletin of the Seismological Society of America* 86, 1964–1978.
- Bernardini, G., D’Orazio, M., Quagliarini, E., 2016. Towards a “behavioural design” approach for seismic risk reduction strategies of buildings and their environment. *Safety Science* 86, 273–294. <https://doi.org/10.1016/j.ssci.2016.03.010>
- Bernardini, G., Lovreglio, R., Quagliarini, E., 2019. Proposing behavior-oriented strategies for earthquake emergency evacuation: A behavioral data analysis from New Zealand, Italy and Japan. *Safety Science* 116, 295–309. <https://doi.org/10.1016/j.ssci.2019.03.023>
- Bianchi, F., Squazzoni, F., 2015. Agent-based models in sociology. *WIREs Computational Statistics* 7, 284–306. <https://doi.org/10.1002/wics.1356>
- Birkmann, J. (Ed.), 2013. *Measuring vulnerability to natural hazards: towards disaster resilient societies*, 2. ed. ed. United Nations Univ. Press, Tokyo.
- Birkmann, J. (Ed.), 2006. *Measuring vulnerability to natural hazards: towards disaster resilient societies*. United Nations University, Tokyo ; New York.
- Blaikie, P., Cannon, T., Davis, I., Wisner, B., 1994. *At risk. Natural hazards, people’s vulnerability and disasters*.
- Bolton, P., 2007. *Managing pedestrians during evacuations of metropolitan areas*. (No. FHWA-HOP-07-066). U.S. Department of Transportation Federal Highway Administration.
- Bonabeau, E., 2002. Agent-based modeling: Methods and techniques for simulating human systems. *Proceedings of the National Academy of Sciences* 99, 7280–7287. <https://doi.org/10.1073/pnas.082080899>
- Bonilla, L., 2005. Hysteretic and Dilatant Behavior of Cohesionless Soils and Their Effects on Nonlinear Site Response: Field Data Observations and Modeling. *The Bulletin of the Seismological Society of America* 95, 2373–2395. <https://doi.org/10.1785/0120040128>
- Bonilla, L.F., 2001. *NOAH: users manual*. Institute for Crustal Studies, University of California, Santa Barbara 38.
- Borcherdt, R.D., 1970. Effects of local geology on ground motion near San Francisco Bay. *Bulletin of the Seismological Society of America* 60, 29–61.

- Box, G.E.P., 1976. Science and Statistics. *Journal of the American Statistical Association* 71, 791–799.
- Bracha, H.S., 2004. Freeze, Flight, Fight, Fright, Faint: Adaptationist Perspectives on the Acute Stress Response Spectrum. *CNS Spectrums* 9, 679–685. <https://doi.org/10.1017/S1092852900001954>
- Brax, M., Bard, P.-Y., Duval, A.-M., Bertrand, E., Rahhal, M.-E., Jomaa, R., Cornou, C., Voisin, C., Sursock, A., 2018. Towards a microzonation of the Greater Beirut area: an instrumental approach combining earthquake and ambient vibration recordings. *Bulletin of Earthquake Engineering* 16, 5735–5767. <https://doi.org/10.1007/s10518-018-0438-1>
- Brax, M., Cornou, C., Voisin, C., Bard, P.-Y., 2014. Mapping the fundamental frequencies in the city of Beirut using ambient noise measurements. Presented at the Second European Conference on Earthquake Engineering and Seismology, Istanbul, Turkey.
- Broxton, M.J., Edwards, L.J., 2008. The Ames Stereo Pipeline: Automated 3D Surface Reconstruction from Orbital Imagery. Presented at the 39th Lunar and Planetary Science Conference, (Lunar and Planetary Science XXXIX), League City, Texas.
- Buckle, P., Mars, G., Smale, S., 2000. New approaches to assessing vulnerability and resilience. *Australian Journal of Emergency Management*, The 15, 8–14.
- Burns, T.R., Roszkowska, E., Machado Des Johansson, N., Corte, U., 2018. Paradigm Shift in Game Theory: Sociological Re-Conceptualization of Human Agency, Social Structure, and Agents' Cognitive-Normative Frameworks and Action Determination Modalities. *Social Sciences* 7. <https://doi.org/10.3390/socsci7030040>
- Burton, C., Silva, V., 2014. Integrated Risk Modeling Within The Global Earthquake Model (Gem): Test Case Application For Portugal. Presented at the Second European Conference on Earthquake Engineering and Seismology, Istanbul, Turkey. <https://doi.org/10.13140/2.1.4084.8643>
- Calvi, G.M., Pinho, R., Magenes, G., Bommer, J.J., Restrepo-Vélez, L.F., Crowley, H., 2006. Development of seismic vulnerability assessment methodologies over the past 30 years. *ISET Journal of Earthquake Technology* 43, 75–104.
- Campbell, M.J., Dennison, P.E., Butler, B.W., Page, W.G., 2019. Using crowdsourced fitness tracker data to model the relationship between slope and travel rates. *Applied Geography* 106, 93–107. <https://doi.org/10.1016/j.apgeog.2019.03.008>
- Cardona, O.D., Hurtado, J.E., 2000. Holistic seismic risk estimation of a metropolitan center. Presented at the 12th World Conference on Earthquake Engineering.
- Carreño, M.L., Cardona, O.D., Barbat, A.H., 2012. New methodology for urban seismic risk assessment from a holistic perspective. *Bulletin of Earthquake Engineering* 10, 547–565. <https://doi.org/10.1007/s10518-011-9302-2>
- Carreño, M.-L., Cardona, O.D., Barbat, A.H., 2007. Urban Seismic Risk Evaluation: A Holistic Approach. *Natural Hazards* 40, 137–172. <https://doi.org/10.1007/s11069-006-0008-8>
- Cartier, S., Beck, E., Justin, L.C., Donabedian-Demopoulos, A., 2017. Les représentations du risque sismique à Beyrouth et Bourj Hammoud. *Travaux et Jours*.
- Castro, S., Poulos, A., Herrera, J.C., de la Llera, J.C., 2019. Modeling the Impact of Earthquake-Induced Debris on Tsunami Evacuation Times of Coastal Cities. *Earthquake Spectra* 35, 137–158. <https://doi.org/10.1193/101917EQS218M>
- Caumont, D., Ivanaj, S., 2017. Chapitre 3. Comment exploiter un tableau de contingence, in: *Analyse des données*, Management Sup. Dunod, Paris, pp. 79–114.
- Chapuis, K., 2019. A brief review of synthetic population generation practices in agent-based social simulation. Presented at the Social Simulation Conference 2019, Mainz, Germany.
- Chapuis, K., Gaudou, B., Amblard, F., Thiriot, S., 2019. Gen\*: an integrated tool for realistic agent population synthesis. Presented at the Proceedings of the Social Simulation Conference 2019, Mainz, Germany.
- Cherif, S., Chourak, M., Abed, M., Pujades, L., 2017. Seismic risk in the city of Al Hoceima (north of Morocco) using the vulnerability index method, applied in Risk-UE project. *Nat Hazards* 85, 329–347. <https://doi.org/10.1007/s11069-016-2566-8>
- Chertkoff, J.M., Kushigian, R.H., 1999. Don't panic: The psychology of emergency egress and ingress. Praeger Pub Text.
- Chopra, A.K., Goel, R.K., 1999. Capacity-Demand-Diagram Methods Based on Inelastic Design Spectrum. *Earthquake Spectra* 15, 637–656. <https://doi.org/10.1193/1.1586065>

- Chu, M.L., Law, K., 2013. Computational Framework Incorporating Human Behaviors for Egress Simulations. *Journal of Computing in Civil Engineering* 27, 699–707. [https://doi.org/10.1061/\(ASCE\)CP.1943-5487.0000313](https://doi.org/10.1061/(ASCE)CP.1943-5487.0000313)
- Cimellaro, G.P., Ozzello, F., Vallero, A., Mahin, S., Shao, B., 2017. Simulating earthquake evacuation using human behavior models: Simulating earthquake evacuation using human behavior models. *Earthquake Engineering & Structural Dynamics* 46, 985–1002. <https://doi.org/10.1002/eqe.2840>
- Clark, G.N., BouDagher-Fadel, M., 2020. Insights into the Cenozoic geology of North Beirut (harbour area): biostratigraphy, sedimentology and structural history. *UCL Open Environ* 2. <https://doi.org/10.14324/111.444/ucloe.000004>
- Coburn, A., Spence, R., Pomonis, A., 1994. *Training Manual: Vulnerability and Risk Assessment* (2nd edition). UNDP Disaster Management Training Programme.
- Cocking, C., Drury, J., Reicher, S., 2009. The psychology of crowd behaviour in emergency evacuations: Results from two interview studies and implications for the Fire and Rescue Services. *The Irish Journal of Psychology* 30, 59–73. <https://doi.org/10.1080/03033910.2009.10446298>
- Crichton, D., 1999. The risk triangle. *Natural disaster management* 102.
- Crowley, Dabbeek, Despotaki, Rodrigues, Martins, Silva, Romão, Pereira, Weatherill, Danciu, 2021. *European Seismic Risk Model (ESRM20)* (No. EFEHR Technical Report 002 V1.0.1).
- Daeron, M., Klinger, Y., Tapponnier, P., Elias, A., Jacques, E., Surssock, A., 2007. 12,000-Year-Long Record of 10 to 13 Paleoearthquakes on the Yammouneh Fault, Levant Fault System, Lebanon. *Bulletin of the Seismological Society of America* 97, 749–771. <https://doi.org/10.1785/0120060106>
- Darendeli, M.B., 2001. *Development of a New Family of Normalized Modulus Reduction and Material Damping Curves*. University of Texas, Austin.
- Dash, N., 2002. *Decision-making under extreme\* uncertainty: Rethinking hazard-related perceptions and action*. Florida International University, Florida.
- Daudé, É., Taillandier, P., Caron, C., Gaudou, B., Saval, A., Chapuis, K., Tranouez, P., Drogoul, A., Rey-Coyrehourq, S., Zucker, J.-D., 2019. ESCAPE: Exploring by Simulation Cities Awareness on Population Evacuation. Presented at the 16th International Conference on Information Systems for Crisis Response and Management (ISCRAM 2019), Valencia, Spain, pp. 76–93.
- Davidson, R., 1997. EERI Annual Student Paper Award A Multidisciplinary Urban Earthquake Disaster Risk Index. *Earthquake Spectra* 13, 211–223. <https://doi.org/10.1193/1.1585942>
- Davie, M., 2006. *Beyrouth et ses Faubourgs (1840–1940): Une Integration Inachevee.*, CERMO. ed. Presses de l'Ifpo, Beirut, Lebanon.
- Davie, M.F., 1993. *A Post-War Urban Geography of Beirut*. Presented at the 1993 EURAMES Conference, Warwick.
- de Leeuw, J., 1988. Model selection in multinomial experiments, in: Dijkstra, T.K. (Ed.), *On Model Uncertainty and Its Statistical Implications*. Springer Berlin Heidelberg, Berlin, Heidelberg, pp. 118–138.
- Domaneschi, M., Cimellaro, G.P., Scutiero, G., 2019. A simplified method to assess generation of seismic debris for masonry structures. *Engineering Structures* 186, 306–320. <https://doi.org/10.1016/j.engstruct.2019.01.092>
- D'Orazio, M., Quagliarini, E., Bernardini, G., Spalazzi, L., 2014. EPES – Earthquake pedestrians' evacuation simulator: A tool for predicting earthquake pedestrians' evacuation in urban outdoor scenarios. *International Journal of Disaster Risk Reduction* 10, 153–177. <https://doi.org/10.1016/j.ijdr.2014.08.002>
- Douglas, J., 2003. Earthquake ground motion estimation using strong-motion records: a review of equations for the estimation of peak ground acceleration and response spectral ordinates. *Earth-Science Reviews* 61, 43–104. [https://doi.org/10.1016/S0012-8252\(02\)00112-5](https://doi.org/10.1016/S0012-8252(02)00112-5)
- Drury, J., 2018. The role of social identity processes in mass emergency behaviour: An integrative review. *European Review of Social Psychology* 29, 38–81. <https://doi.org/10.1080/10463283.2018.1471948>

- Drury, J., Cocking, C., Reicher, S., 2009a. Everyone for themselves? A comparative study of crowd solidarity among emergency survivors. *British Journal of Social Psychology* 48, 487–506. <https://doi.org/10.1348/014466608X357893>
- Drury, J., Cocking, C., Reicher, S., 2008. Everyone for Themselves? A Comparative Study of Crowd Solidarity Among Emergency Survivors. *The British journal of social psychology / the British Psychological Society* 48, 487–506. <https://doi.org/10.1348/014466608X357893>
- Drury, J., Cocking, C., Reicher, S.D., 2009b. The Nature of Collective Resilience: Survivor Reactions to the 2005 London Bombings. *International journal of mass emergencies and disasters* 27, 66–95.
- Dubertret, L., 1945. Géologie du Site de Beyrouth avec carte geologique 1/20,000, in: Delegation Generale de France Au Levant, Section Geologique; pp. 1–5.
- Dynes, R.R., 2003. The Lisbon earthquake in 1755: the first modern disaster. Disaster Research Center-University of Delaware, Newark, U.S.A.
- Dynes, R.R., 1999. The dialogue between Voltaire and Rousseau on the Lisbon earthquake: The emergence of a social science view. *International Journal of Mass Emergencies and Disasters* 18, 97–115.
- Ein-Dor, T., 2014. Social defense theory: How a mixture of personality traits in group contexts may promote our survival. pp. 357–372. <https://doi.org/10.1037/14250-020>
- Elias, A., Tapponnier, P., Singh, S.C., King, G.C.P., Briais, A., Daëron, M., Carton, H., Surssock, A., Jacques, E., Jomaa, R., Klinger, Y., 2007. Active thrusting offshore Mount Lebanon: Source of the tsunamigenic A.D. 551 Beirut-Tripoli earthquake. *Geology* 35, 755–758. <https://doi.org/10.1130/G23631A.1>
- Ellenblum, R., Marco, S., Agnon, A., Rockwell, T., Boas, A., 1998. Crusader castle torn apart by earthquake at dawn, 20 May 1202. *Geol* 26, 303. [https://doi.org/10.1130/0091-7613\(1998\)026<0303:CCTABE>2.3.CO;2](https://doi.org/10.1130/0091-7613(1998)026<0303:CCTABE>2.3.CO;2)
- Elnashai, A.S., Di Sarno, L., 2008. *Fundamentals of earthquake engineering*. Wiley New York.
- Erdik, M., 2017. Earthquake risk assessment. *Bulletin of Earthquake Engineering* 15, 5055–5092. <https://doi.org/10.1007/s10518-017-0235-2>
- European Centre on Prevention and Forecasting of Earthquakes (ECPFE), Earthquake Planning and Protection Organization (OASP), 2002. *Emergency evacuation of the population in case of an earthquake*.
- Faour, G., Mhaweji, M., 2014. Mapping Urban Transitions in the Greater Beirut Area Using Different Space Platforms. *Land* 3, 941–956. <https://doi.org/10.3390/land3030941>
- Fawaz, M., Peillen, I., 2003. On the Difficulties of Mapping Slums in Beirut.
- Fayjaloun, R., Dabaghi, M., Cornou, C., Causse, M., Lu, Y., Stehly, L., Voisin, C., Mariscal, A., 2021. Hybrid Simulation of Near-Fault Ground Motion for a Potential Mw 7 Earthquake in Lebanon. *Bulletin of the Seismological Society of America*. <https://doi.org/10.1785/0120210091>
- Federal Emergency Management Agency (FEMA), 2012. *Multi-hazard loss estimation methodology, earthquake model HAZUS-MH 2.1 technical manual*. Federal Emergency Management Agency, Washington, DC, United States.
- FEMA, USGS, PDC, 2017. *Hazus Estimated Annualized Earthquake Losses for the United States (No. FEMA P-366)*. Federal Emergency Management Agency.
- Ferber, J., Weiss, G., 1999. *Multi-agent systems: an introduction to distributed artificial intelligence*. Addison-Wesley Reading.
- Fernandez, J., Mattingly, S., Bendimerad, F., Cardona, O.D., 2006. *Application of Indicators in Urban and Megacities Disaster Risk Management, A Case Study of Metro Manila (EMI Topical Report No. TR-07-01)*.
- Finn, W.D.L., 1991. Geotechnical engineering aspects of microzonation. Presented at the Fourth International Conference on Seismic Zonation, Stanford, California, pp. 236–253.
- Flight Safety Foundation, 2004. Attempts to retrieve carry-on baggage increase risks during evacuation. *Cabin Crew Safety* 39.
- Fowler, M., Scott, K., 2002. *UML distilled: a brief guide to the standard object modeling language*, 2. ed., 10. print. ed, Object technology series. Addison-Wesley, Boston.

- Frankel, A., 2002. Nonlinear and Linear Site Response and Basin Effects in Seattle for the M 6.8 Nisqually, Washington, Earthquake. *Bulletin of The Seismological Society of America - BULL SEISMOL SOC AMER* 92, 2090–2109. <https://doi.org/10.1785/0120010254>
- Freeman, S.A., Associates, E., Street, P., 2004. Review of the development of the capacity spectrum method. *ISET Journal of Earthquake Technology* 41, 1–13.
- Gaillard, J.-C., Clavé, E., Vibert, O., Azhari, Dedi, Denain, J.-C., Efendi, Y., Grancher, D., Liamzon, C.C., Sari, D.R., Setiawan, R., 2008. Ethnic groups' response to the 26 December 2004 earthquake and tsunami in Aceh, Indonesia. *Nat Hazards* 47, 17–38. <https://doi.org/10.1007/s11069-007-9193-3>
- Gaire, N., Song, Z., Christensen, K.M., Sharifi, M.S., Chen, A., 2018. Exit choice behavior of pedestrians involving individuals with disabilities during building evacuations. *Transportation research record* 2672, 22–29.
- Gall, M., Nguyen, K.H., Cutter, S.L., 2015. Integrated research on disaster risk: Is it really integrated? *International Journal of Disaster Risk Reduction* 12, 255–267. <https://doi.org/10.1016/j.ijdr.2015.01.010>
- Garatwa, W., Bollin, C., 2002. Disaster risk management: Working concept. German Technical Cooperation (GTZ).
- Gavrilets, S., 2015. Collective action and the collaborative brain. *Journal of The Royal Society Interface* 12, 20141067. <https://doi.org/10.1098/rsif.2014.1067>
- Geiß, C., Schauß, A., Riedlinger, T., Dech, S., Zelaya, C., Guzmán, N., Hube, M., Jokar Arsanjani, J., Taubenböck, H., 2017. Joint use of remote sensing data and volunteered geographic information for exposure estimation: evidence from Valparaíso, Chile. *Natural Hazards* 86. <https://doi.org/10.1007/s11069-016-2663-8>
- Gladwin, H., Peacock, W., 1997. Warning and evacuation: a night for hard houses, in: Peacock, W., Morrow, B., Gladwin, H (Eds.), *Hurricane Andrew: Ethnicity Gender and Sociology of Disasters*. Routledge, London.
- Godschalk, D.R., 2003. Urban Hazard Mitigation: Creating Resilient Cities. *Natural Hazards Review* 4, 136–143. [https://doi.org/10.1061/\(ASCE\)1527-6988\(2003\)4:3\(136\)](https://doi.org/10.1061/(ASCE)1527-6988(2003)4:3(136))
- Goltz, J.D., Bourque, L.B., 2017. Earthquakes and human behavior: A sociological perspective. *International Journal of Disaster Risk Reduction* 21, 251–265. <https://doi.org/10.1016/j.ijdr.2016.12.007>
- Goltz, J.D., Park, H., Nakano, G., Yamori, K., 2020a. Earthquake ground motion and human behavior: Using DYFI data to assess behavioral response to earthquakes. *Earthquake Spectra* 875529301989995. <https://doi.org/10.1177/8755293019899958>
- Goltz, J.D., Park, H., Quitoriano, V., Wald, D.J., 2020b. Human Behavioral Response in the 2019 Ridgecrest, California, Earthquakes: Assessing Immediate Actions Based on Data from “Did You Feel It?” *Bulletin of the Seismological Society of America*. <https://doi.org/10.1785/0120200159>
- Goltz, J.D., Russel, L.A., Bourque, L.B., 1992. Initial Behavioral Response to a Rapid Onset Disaster: A Case Study of the October 1, 1987 Whittier Narrows Earthquake. *International Journal of Mass Emergencies and Disasters* 10.
- Gomez-Zapata, J., Zafriir, R., Pittore, M., Merino, Y., 2022. Towards a Sensitivity Analysis in Seismic Risk with Probabilistic Building Exposure Models: An Application in Valparaíso, Chile Using Ancillary Open-Source Data and Parametric Ground Motions. *ISPRS International Journal of Geo-Information* 11, 113. <https://doi.org/10.3390/ijgi11020113>
- Gong, J., Liu, Yaolin, Liu, Yanfang, Huang, P., Li, J., 2017. Evaluating the Evacuation and Rescue Capabilities of Urban Open Space from a Land Use Perspective: A Case Study in Wuhan, China. *ISPRS Int. J. Geo-Information* 6, 227. <https://doi.org/10.3390/ijgi6070227>
- Grünthal, G., 1998. European macroseismic scale 1998 : EMS-98, Cahiers du Centre Européen de Géodynamique et de Séismologie. MINISTERE DE LA CULTURE, DE L'ENSEIGNEMENT SUPERIEUR ET DE LA RECHERCHE, Luxembourg.
- Harajli, M., Sadek, S., Asbahian, R., 2002. Evaluation of the seismic hazard of Lebanon. *Journal of Seismology* 6, 257–277.

- Hardin, B.O., Drnevich, V.P., 1972a. Shear Modulus and Damping in Soils: Measurement and Parameter Effects (Terzaghi Lecture). *J. Soil Mech. and Found. Div.* 98, 603–624. <https://doi.org/10.1061/JSFEAQ.0001756>
- Hardin, B.O., Drnevich, V.P., 1972b. Shear Modulus and Damping in Soils: Design Equations and Curves. *J. Soil Mech. and Found. Div.* 98, 667–692. <https://doi.org/10.1061/JSFEAQ.0001760>
- Hashemi, M., Alesheikh, A.A., 2013. GIS: agent-based modeling and evaluation of an earthquake-stricken area with a case study in Tehran, Iran. *Nat Hazards* 69, 1895–1917. <https://doi.org/10.1007/s11069-013-0784-x>
- Heath, S.E., Kass, P.H., Beck, A.M., Glickman, L.T., 2001. Human and pet-related risk factors for household evacuation failure during a natural disaster. *American journal of epidemiology* 153, 659–665.
- Heide, E.A., 2004. Common misconceptions about Disasters: Panic, the “Disaster Syndrome,” and Looting, in: *The First 72 Hours: A Community Approach to Disaster Preparedness*. iUniverse Publishing, Lincoln (Nebraska).
- Helbing, D., Farkas, I., Vicsek, T., 2000. Simulating Dynamic Features of Escape Panic. *Nature* 407, 487–490. <https://doi.org/10.1038/35035023>
- Helbing, D., Farkas, I.J., Molnar, P., Vicsek, T., 2002. Simulation of Pedestrian Crowds in Normal and Evacuation Situations. *Pedestrian evacuation and dynamics* 21, 21–58.
- Helbing, D., Molnar, P., 1995. Social Force Model for Pedestrian Dynamics. *Phys. Rev. E* 51, 4282–4286. <https://doi.org/10.1103/PhysRevE.51.4282>
- Hori, M., 2011. *Introduction to computational earthquake engineering*, 2nd ed. ed. Imperial College Press, London.
- Hori, T., Zhang, J., Tatano, H., Okada, N., Likebuchi, S., 2002. Micro-zonation-based flood risk assessment in urbanized floodplain. Presented at the Proceedings of The Second Annual IIASA-DPRI Meeting “Integrated Disaster Risk Management: Megacity Vulnerability and Resilience”, IIASA, A-2361, Laxenburg, Austria.
- Horspool, N., Elwood, K., Johnston, D., Deely, J., Ardagh, M., 2020. Factors influencing casualty risk in the 14th November 2016 MW7.8 Kaikōura, New Zealand earthquake. *International Journal of Disaster Risk Reduction* 51, 101917. <https://doi.org/10.1016/j.ijdrr.2020.101917>
- Hughes, R.L., 2003. The flow of human crowds. *Annual review of fluid mechanics* 35, 169–182.
- Huijjer, C., Harajli, M., Sadek, S., 2016. Re-evaluation and updating of the seismic hazard of Lebanon. *J Seismol* 20, 233–250. <https://doi.org/10.1007/s10950-015-9522-z>
- Huijjer, C., Harajli, M., Sadek, S., 2011. UPGRADING THE SEISMIC HAZARD OF LEBANON IN LIGHT OF THE RECENT DISCOVERY OF THE OFFSHORE THRUST FAULT SYSTEM. *Lebanese Science Journal* 12, 67–82.
- Human Rights Watch, 2021. “They Killed Us from the Inside”: An Investigation into the August 4 Beirut Blast. Human Rights Watch.
- Ibrion, M., 2018. Earthquake Culture: A Significant Element in Earthquake Disaster Risk Assessment and Earthquake Disaster Risk Management, in: Svalova, V. (Ed.), *Risk Assessment*. IntechOpen, London, p. Ch. 3. <https://doi.org/10.5772/intechopen.70434>
- International Council for Science, 2008. A science plan for integrated research on disaster risk: addressing the challenge of natural and human-induced environmental hazards. ICSU, Paris.
- Iskandar, R., Allaw, K., Dugdale, J., Beck, E., Adjizian-Gérard, J., Cornou, C., Harb, J., Lacroix, P., Badaro-Saliba, N., Cartier, S., Zaarour, R., 2020. Agent-based simulation of pedestrians’ earthquake evacuation; application to Beirut, Lebanon. Presented at the 17th World Conference on Earthquake Engineering, Sendai, Japan.
- Iskandar, R., Dugdale, J., Beck, E., Cornou, C., 2021. PEERS: An integrated agent-based framework for simulating pedestrians’ earthquake evacuation. Presented at the ISCRAM 2021 Conference Proceedings – 18th International Conference on Information Systems for Crisis Response and Management, Blacksburg, VA, USA: Virginia Tech, pp. 86–96.
- Jaiswal, K.S., Wald, D., 2010a. An Empirical Model for Global Earthquake Fatality Estimation. *Earthquake Spectra* 26, 1017–1037. <https://doi.org/10.1193/1.3480331>
- Jaiswal, K.S., Wald, D.J., 2010b. Development of semi-empirical loss model within the USGS prompt assessment of global earthquake response (PAGER) system. Presented at the Proc. of the 9th

- US and 10th Canadian Conference on Earthquake Engineering: Reaching Beyond Borders, Toronto, Canada, p. 12.
- Javier Ortega, Graça Vasconcelos, Hugo Rodrigues, Mariana Correia, Paulo B. Lourenço, 2017. Traditional earthquake resistant techniques for vernacular architecture and local seismic cultures: A literature review. *Journal of cultural heritage* 5483, 1. <https://doi.org/10.1016/j.culher.2017.02.015>
- Jayakody, C., Amaratunga, D., Haigh, R., 2016. The use of Public Open Spaces for Disaster Resilient Cities. Presented at the 12th International Conference of the International Institute for Infrastructure Resilience and Reconstruction, University of Peradeniya, Kandy, Sri Lanka.
- Johnson, N.R., 1988. Fire in a crowded theater: A descriptive investigation of the emergence of panic. *International Journal of Mass Emergencies and Disasters* 6, 7–26.
- Johnson, N.R., 1987. Panic and the breakdown of social order: Popular myth, social theory, empirical evidence. *Sociological focus* 20, 171–183.
- Jon, I., Lindell, M., Prater, C., Huang, S.-K., Wu, H.-C., Johnston, D., Becker, J., Shiroshita, H., Doyle, E., Potter, S., McClure, J., Lambie, E., 2016. Behavioral Response in the Immediate Aftermath of Shaking: Earthquakes in Christchurch and Wellington, New Zealand, and Hitachi, Japan. *International Journal of Environmental Research and Public Health* 13, 1137. <https://doi.org/10.3390/ijerph13111137>
- Kaklamanos, J., Baise, L.G., Thompson, E.M., Dorfmann, L., 2015. Comparison of 1D linear, equivalent-linear, and nonlinear site response models at six KiK-net validation sites. *Soil Dynamics and Earthquake Engineering* 69, 207–219.
- Kanafani, S., 2016. Made to fall apart : an ethnography of old houses and urban renewal in Beirut. University of Manchester.
- Kästli, P., Fäh, D., 2006. Rapid estimation of macroseismic effects and shake maps combining macroseismic and instrumental data. Presented at the Proceedings of the First European Conference on Earthquake Engineering and Seismology (ECEES), Geneva, Switzerland.
- Kawase, H., 2003. Site effects on strong ground motions. *International Geophysics* 81, 1013–1030. [https://doi.org/10.1016/S0074-6142\(03\)80175-4](https://doi.org/10.1016/S0074-6142(03)80175-4)
- Kazarian, S.S., 2005. Family Functioning, Cultural Orientation, and Psychological Well-Being Among University Students in Lebanon. *The Journal of Social Psychology* 145, 141–154. <https://doi.org/10.3200/SOCP.145.2.141-154>
- Khair, K., Karakaisis, G.F., Papadimitriou, E., 2000. Seismic zonation of the Dead Sea Transform Fault area. *Annals of Geophysics* 43.
- Khan, A.A., Noji, E.K., 2016. Hajj stampede disaster, 2015: Reflections from the frontlines. *American journal of disaster medicine* 11 1, 59–68.
- Khazai, B., Bendimerad, F., 2011. Risk and Resiliency Indicators (EMI Topical Report No. TR-1 1-03).
- Khazai, B., Burton, C., Tormene, P., Power, C., Daniell, J.E., Wyss, B., 2014. Integrated Risk Modelling Toolkit and Database for Earthquake Risk Assessment. Presented at the Second European Conference on Earthquake Engineering and Seismology, Istanbul, Turkey.
- Kim, B., Hashash, Y.M., Stewart, J.P., Rathje, E.M., Harmon, J.A., Musgrove, M.I., Campbell, K.W., Silva, W.J., 2016. Relative differences between nonlinear and equivalent-linear 1-D site response analyses. *Earthquake Spectra* 32, 1845–1865.
- Koren, D., Rus, K., 2019. The Potential of Open Space for Enhancing Urban Seismic Resilience: A literature Review. *Sustainability* 11, 5942. <https://doi.org/10.3390/su11215942>
- Kramer, S.L., 1996. Geotechnical earthquake engineering. Pearson Education India.
- Kravari, K., Bassiliades, N., 2015. A Survey of Agent Platforms. *JASSS* 18, 11. <https://doi.org/10.18564/jasss.2661>
- Krayem, A., Yeretzi, A., Faour, G., Najem, S., 2021. Machine learning for buildings' characterization and power-law recovery of urban metrics. *PLoS ONE* 16, e0246096. <https://doi.org/10.1371/journal.pone.0246096>
- Kuligowski, E.D., 2011. Terror Defeated: Occupant Sensemaking, Decision-Making and Protective Action in the 2001 World Trade Center Disaster. Univ. of Colorado, Boulder, CO.
- Lagomarsino, S., Giovinazzi, S., 2006. Macroseismic and mechanical models for the vulnerability and damage assessment of current buildings. *Bulletin of Earthquake Engineering* 4, 415–443. <https://doi.org/10.1007/s10518-006-9024-z>

- Lambie, E.S., Wilson, T.M., Brogt, E., Johnston, D.M., Ardagh, M., Deely, J., Jensen, S., Feldmann-Jensen, S., 2017. Closed Circuit Television (CCTV) Earthquake Behaviour Coding Methodology: analysis of Christchurch Public Hospital video data from the 22 February Christchurch earthquake event. *Nat Hazards* 86, 1175–1192. <https://doi.org/10.1007/s11069-016-2735-9>
- Lantada, N., Irizarry, J., Barbat, A.H., Goula, X., Roca, A., Susagna, T., Pujades, L.G., 2010. Seismic hazard and risk scenarios for Barcelona, Spain, using the Risk-UE vulnerability index method. *Bulletin of Earthquake Engineering* 8, 201–229. <https://doi.org/10.1007/s10518-009-9148-z>
- Lebanese Republic Central Administration of Statistics, 2020. Labour force and household living conditions survey: (LFH LCS) 2018-2019 Lebanon. Central Administration of Statistics, Beirut, Lebanon.
- Li, S., Yu, X., Zhang, Y., Zhai, C., 2018. A numerical simulation strategy on occupant evacuation behaviors and casualty prediction in a building during earthquakes. *Physica A: Statistical Mechanics and its Applications* 490, 1238–1250. <https://doi.org/10.1016/j.physa.2017.08.058>
- Lin, K.-H.E., Chang, Y.-C., Liu, G.-Y., Chan, C.-H., Lin, T.-H., Yeh, C.-H., 2015. An interdisciplinary perspective on social and physical determinants of seismic risk. *Natural Hazards and Earth System Sciences* 15, 2173–2182. <https://doi.org/10.5194/nhess-15-2173-2015>
- Lindell, M.K., Perry, R.W., 2003. *Communicating environmental risk in multiethnic communities*. Sage publications.
- Lindell, M.K., Prater, C.S., Wu, H.C., Huang, S.-K., Johnston, D.M., Becker, J.S., Shiroshita, H., 2016. Immediate behavioural responses to earthquakes in Christchurch, New Zealand, and Hitachi, Japan. *Disasters* 40, 85–111. <https://doi.org/10.1111/disa.12133>
- Lu, X., Yang, Z., Cimellaro, G.P., Xu, Z., 2019. Pedestrian evacuation simulation under the scenario with earthquake-induced falling debris. *Safety Science* 114, 61–71. <https://doi.org/10.1016/j.ssci.2018.12.028>
- Ma, H.K., 2017. The Development of Altruism with Special Reference to Human Relationships: A 10-Stage Theory. *Frontiers in Public Health* 5.
- Ma, T., Wang, Q., Larrañaga, M.D., 2011. The utility of a panic model on simulating crowd disasters. Presented at the Fire and Evacuation Modeling Technical Conference 2011, Baltimore, Maryland.
- Mady, C., 2015. Nostalgia for a past: Beirut's shared open spaces. *On the W@terfront* 40, 7–22.
- Makhoul, N., Argyroudis, S., 2018. LOSS ESTIMATION SOFTWARE: DEVELOPMENTS, LIMITATIONS AND FUTURE NEEDS. Presented at the 16th European Conference on Earthquake Engineering, Thessaloniki.
- Maktabi, R., 1999. The Lebanese census of 1932 revisited. Who are the Lebanese? *British Journal of Middle Eastern Studies* 26, 219–241. <https://doi.org/10.1080/13530199908705684>
- Manley, M.T., 2012. *Exitus: An Agent-Based Evacuation Simulation Model For Heterogeneous Populations*. Utah State University, Utah.
- Maqsood, S.T., Schwarz, J., 2011. Estimation of Human Casualties from Earthquakes in Pakistan--An Engineering Approach. *Seismological Research Letters* 82, 32–41. <https://doi.org/10.1785/gssrl.82.1.32>
- Marre, K., 2013. Components of risk: a comparative glossary, in: *Measuring Vulnerability to Natural Hazards. Towards Disaster Resilient Societies*. pp. 569–618.
- Marulanda, M.C., Carreño, M.L., Cardona, O.D., Ordaz, M.G., Barbat, A.H., 2013. Probabilistic earthquake risk assessment using CAPRA: application to the city of Barcelona, Spain. *Natural Hazards* 69, 59–84. <https://doi.org/10.1007/s11069-013-0685-z>
- Masters, R.D., Kelly, C. (Eds.), 1992. *The collected writings of Rousseau*. University Press of New England, Hanover.
- Mawson, A.R., 2005. Understanding Mass Panic and Other Collective Responses to Threat and Disaster. *Psychiatry: Interpersonal and Biological Processes* 68, 95–113. <https://doi.org/10.1521/psyc.2005.68.2.95>
- Mayoral, J., Asimaki, D., Tepalcapa, S., Wood, C., Román-de la Sancha, A., Hutchinson, T., Franke, K., Montalva, G., 2019. Site effects in Mexico City basin: Past and present. *Soil Dynamics and Earthquake Engineering* 121, 369–382. <https://doi.org/10.1016/j.soildyn.2019.02.028>

- Mazraani, D., 2020. Urban Vacant Parcels as Opportunities to Reclaim Public Spaces in Times of Crises and Austerity. *Peace Building in Lebanon News Supplement* 11.
- McBride, S.K., Smith, H., Morgoch, M., Sumy, D., Jenkins, M., Peek, L., Bostrom, A., Baldwin, D., Reddy, E., de Groot, R., Becker, J., Johnston, D., Wood, M., 2022. Evidence-based guidelines for protective actions and earthquake early warning systems. *GEOPHYSICS* 87, WA77–WA102. <https://doi.org/10.1190/geo2021-0222.1>
- McCulloch, W.S., Pitts, W., 1943. A logical calculus of the ideas immanent in nervous activity. *The bulletin of mathematical biophysics* 5, 115–133.
- McGuire, R.K., 2008. Probabilistic seismic hazard analysis: Early history. *Earthquake Engng Struct. Dyn.* 37, 329–338. <https://doi.org/10.1002/eqe.765>
- McPherson, T., Brown, M., 2004. Estimating daytime and nighttime population distributions in U.S. Cities for emergency response activities. Presented at the 84th AMS Annual Meeting: Symposium on Planning, Nowcasting, and Forecasting in the Urban Zone, Duke University Press, Seattle WA, pp. 1–37. <https://doi.org/10.1215/9780822384625-001>
- Méjean, A., 2021. La prévention du risque sismique à Beyrouth (Liban): La prise en compte des comportements humains en géographie.
- Mikami, S., Ikeda, R., 1985. Human Responses to Disasters. *International journal of mass emergencies and disasters* 3, 107–132.
- Mileti, D.S., Cress, D.M., Darlington, J.D., 2002. Earthquake culture and corporate action, in: *Sociological Forum*. Springer, pp. 161–180.
- Minsky, M., Papert, S., 1969. An introduction to computational geometry. Cambridge tiass., HIT 479, 480.
- Misyak, J.B., Melkonyan, T., Zeitoun, H., Chater, N., 2014. Unwritten rules: virtual bargaining underpins social interaction, culture, and society. *Trends Cogn Sci* 18, 512–519. <https://doi.org/10.1016/j.tics.2014.05.010>
- Mobbs, D., Hagan, C.C., Dalgleish, T., Silston, B., Prévost, C., 2015. The ecology of human fear: survival optimization and the nervous system. *Frontiers in Neuroscience* 9.
- Moreno, F.M., Ortuño, A.S., Díaz, J.M., Martín, J.A.L., Miras, R.T., Sapena, A.H., 2012. EsLorca: una iniciativa para la educación y concienciación sobre el riesgo sísmico. *Boletín Geológico y Minero* 123.
- Mouroux, P., Le Brun, B., 2006. Risk-Ue Project: An Advanced Approach to Earthquake Risk Scenarios With Application to Different European Towns, in: *Assessing and Managing Earthquake Risk. Geotechnical, Geological And Earthquake Engineering*. Springer, Dordrecht, pp. 479–508.
- Moussaïd, M., Trauernicht, M., 2016. Patterns of cooperation during collective emergencies in the help-or-escape social dilemma. *Sci Rep* 6, 33417. <https://doi.org/10.1038/srep33417>
- Müller, K., Axhausen, K.W., 2011. Population synthesis for microsimulation: State of the art.
- Municipality of Beirut, UN Habitat, 2020. Beirut Municipality Rapid Building-level Damage Assessment, Beirut port explosion response.
- Murakami, H.O., Durkin, Michael E., 1988. Studies of occupant behavior in earthquakes review and perspectives. Presented at the Ninth World Conference on Earthquake Engineering, Tokyo, p. VII-681-VII-686.
- Myntti, C., Mabsout, M., 2014. Improving Walkability in Beirut: Lessons from the Jeanne d’Arc Street case, Sustainable Transport- Policy Brief #6. American University of Beirut.
- Nakamura, Y., 1989. A method for dynamic characteristics estimation of subsurface using microtremor on the ground surface. *Railway Technical Research Institute, Quarterly Reports* 30.
- Nemer, T., Meghraoui, M., 2006. Evidence of coseismic ruptures along the Roum fault (Lebanon): a possible source for the AD 1837 earthquake. *Journal of Structural Geology* 28, 1483–1495. <https://doi.org/10.1016/j.jsg.2006.03.038>
- Ngai, K.M., Burkle, F.M., Hsu, A., Hsu, E.B., 2009. Human Stampedes: A Systematic Review of Historical and Peer-Reviewed Sources. *Disaster Medicine and Public Health Preparedness* 3, 191–195.
- Nievas, C.I., Pilz, M., Prehn, K., Schorlemmer, D., Weatherill, G., Cotton, F., 2022. Calculating earthquake damage building by building: the case of the city of Cologne, Germany. *Bull Earthquake Eng* 20, 1519–1565. <https://doi.org/10.1007/s10518-021-01303-w>

- Nishino, T., Tanaka, T., Hokugo, A., 2012. An evaluation method for the urban post-earthquake fire risk considering multiple scenarios of fire spread and evacuation. *Fire Safety Journal* 54, 167–180. <https://doi.org/10.1016/j.firesaf.2012.06.002>
- Noji, E.K., Kelen, G.D., Armenian, H.K., Oganessian, A., Jones, N.P., Sivertson, K.T., 1990. The 1988 earthquake in Soviet Armenia: A case study. *Annals of Emergency Medicine* 19, 891–897. [https://doi.org/10.1016/S0196-0644\(05\)81563-X](https://doi.org/10.1016/S0196-0644(05)81563-X)
- Ohta, Y., Ohashi, H., 1985. Field Survey on Occupant Behavior in an Earthquake. *Int. J. Mass Emerg. Disasters* 3, 147–160.
- Okasaki, K., 2000. RADIUS—Risk Assessment Tools for Diagnosis of Urban Areas Against Seismic Disasters. United Nations International Strategy for Disaster Reduction.
- Osaragi, T., Oki, T., Tokyo Institute of Technology 2-12-1-W8-10, O-okayama, Meguro-ku, Tokyo 152-8552, Japan, 2017. Wide-Area Evacuation Simulation Incorporating Rescue and Firefighting by Local Residents. *J. Disaster Res.* 12, 296–310. <https://doi.org/10.20965/jdr.2017.p0296>
- Pai, C.-H., Tien, Y.-M., Teng, T.-L., 2007. A study of the human-fatality rate in near-fault regions using the Victim Attribute Database. *Natural Hazards* 42, 19–35.
- Palm, R., 1998. Urban earthquake hazards: The impacts of culture on perceived risk and response in the USA and Japan. *Applied Geography* 35–46.
- Pan, X., Han, C.S., Dauber, K., Law, K.H., 2007. A multi-agent based framework for the simulation of human and social behaviors during emergency evacuations. *AI & SOCIETY* 22, 113–132. <https://doi.org/10.1007/s00146-007-0126-1>
- Peek-Asa, C., 1998. Fatal and hospitalized injuries resulting from the 1994 Northridge earthquake. *International Journal of Epidemiology* 27, 459–465. <https://doi.org/10.1093/ije/27.3.459>
- Pico, L., Amat, J.-P., 2006. Temps urbain, temps sismique et ruptures : le cas de Beyrouth. Presented at the Interactions Nature-Société, analyse et modèles, La Baule.
- Pilger, C., Gaebler, P., Hupe, P., Kalia, A.C., Schneider, F.M., Steinberg, A., Sudhaus, H., Ceranna, L., 2021. Yield estimation of the 2020 Beirut explosion using open access waveform and remote sensing data. *Sci Rep* 11, 14144. <https://doi.org/10.1038/s41598-021-93690-y>
- Pitilakis, K., Gazepis, C., Anastasiadis, A., 2004. Design Response Spectra and Soil Classification for Seismic Code Provisions. Presented at the 13th World Conference on Earthquake Engineering, Vancouver, B.C., Canada.
- Porter, K., 2009. Cracking an Open Safe: HAZUS Vulnerability Functions in Terms of Structure-Independent Spectral Acceleration. *Earthquake Spectra* 25, 361–378. <https://doi.org/10.1193/1.3106680>
- Posel, D.R., 2001. Who are the heads of household, what do they do, and is the concept of headship useful? An analysis of headship in South Africa. *Development Southern Africa* 18, 651–670. <https://doi.org/10.1080/03768350120097487>
- Poulton, M.M., 2001. Computational neural networks for geophysical data processing. Elsevier.
- Prati, G., Catufi, V., Pietrantonì, L., 2012. Emotional and behavioural reactions to tremors of the Umbria-Marche earthquake. *Disasters* 36, 439–451. <https://doi.org/10.1111/j.1467-7717.2011.01264.x>
- Prati, G., Saccinto, E., Pietrantonì, L., Pérez-Testor, C., 2013. The 2012 Northern Italy Earthquakes: modelling human behaviour. *Natural Hazards* 69, 99–113. <https://doi.org/10.1007/s11069-013-0688-9>
- Preciado, A., Ramirez-Gaytan, A., Salido Ruiz, R., Caro Becerra, J.L., Lujan-Godinez, R., 2015. Earthquake risk assessment methods of unreinforced masonry structures: Hazard and vulnerability. *Earthquakes and Structures* 9, 719–733. <https://doi.org/10.12989/eas.2015.9.4.719>
- Prédhumeau, M., 2021. Modélisation et simulation de comportements piétons réalistes en espace partagé avec un véhicule autonome (Theses). Université Grenoble Alpes [2020-....].
- Proulx, G., 1995. Evacuation time and movement in apartment buildings. *Fire Safety Journal* 24, 229–246. [https://doi.org/10.1016/0379-7112\(95\)00023-M](https://doi.org/10.1016/0379-7112(95)00023-M)
- Puglia, R., Pacor, F., Gallipoli, M., Bindi, D., Mucciarelli, M., 2011. Proposal for a soil classification based on parameters alternative or complementary to Vs ,30. *Bulletin of Earthquake Engineering - BULL EARTHQ ENG* 9. <https://doi.org/10.1007/s10518-011-9274-2>

- Quagliarini, E., Bernardini, G., Wazinski, C., Spalazzi, L., D’Orazio, M., 2016. Urban scenarios modifications due to the earthquake: ruins formation criteria and interactions with pedestrians’ evacuation. *Bulletin of Earthquake Engineering* 14, 1071–1101. <https://doi.org/10.1007/s10518-016-9872-0>
- Quarantelli, E.L., 1991. Disaster response: generic or agent-specific?, in: Kreimer, A., Munasinghe, M. (Eds.), *Managing Natural Disasters and the Environment*. The World Bank, Washington DC, United States, pp. 97–105.
- Quest W.G., Raffaele Azzaro, Andrea Tertulliani, Filippo Bernardini, Romano Camassi, Sergio Del Mese, Emanuela Ercolani, Laura Graziani, Mario Locati, Alessandra Maramai, Vera Pessina, Antonio Rossi, Andrea Rovida, Paola Albini, Luca Arcoraci, Michele Berardi, Christian Bignami, Beatriz Brizuela, Corrado Castellano, Viviana Castelli, Salvatore D’Amico, Vera D’Amico, Antonio Fodarella, Ilaria Leschiutta, Alessandro Piscini, Manuela Sbarra, 2016. The 24 August 2016 Amatrice earthquake: macroseismic survey in the damage area and EMS intensity assessment. *Annals of Geophysics* 59, 13. <https://doi.org/10.4401/ag-7203>
- Rao, A.S., Georgeff, M.P., 1995. BDI Agents: From Theory to Practice. *ICMAS 95*, 312–319.
- Rapaport, C., Ashkenazi, I., 2020. Drop down or flee out? *International Journal of Disaster Resilience in the Built Environment* 10, 52–64. <https://doi.org/10.1108/IJDRBE-09-2018-0040>
- Rashed, T., Weeks, J., 2002. Assessing vulnerability to earthquake hazards through spatial multicriteria analysis of urban areas. *International Journal of Geographical Information Science* 17, 547–576. <https://doi.org/10.1080/1365881031000114071>
- Ravari, Z.A., Ghazi, I., Kahani, M., 2016. Study the vulnerability and blocking of streets after earthquake (case study: Kerman Shariati and Shahid Beheshti Streets and Jomhuri Boulevard). *Int J Health Syst Disaster Manage* 4, 25–30. <https://doi.org/10.4103/2347-9019.175673>
- Regnier, J., Cadet, H., Bonilla, L.F., Bertrand, É., Semblat, J.F., 2013. Assessing Nonlinear Behavior of Soils in Seismic Site Response: Statistical Analysis on KiK-net Strong-Motion Data. *Bulletin of the Seismological Society of America* 103, 1750–1770.
- Riboldi, A., 2014. Pedestrian dynamics: modelling and calibration of a 2-dimensional cellular automata model. Politecnico di Milano.
- Riedel, I., Guéguen, P., 2018. Modeling of damage-related earthquake losses in a moderate seismic-prone country and cost–benefit evaluation of retrofit investments: application to France. *Nat Hazards* 90, 639–662. <https://doi.org/10.1007/s11069-017-3061-6>
- Rojo, M.B., Beck, E., Lutoff, C., 2017. The street as an area of human exposure in an earthquake aftermath: the case of Lorca, Spain, 2011. *Natural Hazards and Earth System Sciences* 17, 581–594. <https://doi.org/10.5194/nhess-17-581-2017>
- Rousseau, J.-J., 1756. *Lettre à Voltaire sur la Providence*.
- Sadek, S., Dabaghi, M., O’Donnell, T.M., Zimmaro, P., Hashash, Y.M.A., Stewart, J.P., 2022. Impacts of 2020 Beirut Explosion on Port Infrastructure and Nearby Buildings. *Nat. Hazards Rev.* 23, 04022008. [https://doi.org/10.1061/\(ASCE\)NH.1527-6996.0000550](https://doi.org/10.1061/(ASCE)NH.1527-6996.0000550)
- Salameh, C., 2016. Ambient vibrations, spectral content and seismic damages : new approach adapted to the urban scale. Application on Beirut (Theses). Université Grenoble Alpes.
- Salameh, C., Bard, P.-Y., Guillier, B., Harb, J., Cornou, C., Gérard, J., Almakari, M., 2017. Using ambient vibration measurements for risk assessment at an urban scale: from numerical proof of concept to Beirut case study (Lebanon). *Earth, Planets and Space* 69, 1–17. <https://doi.org/10.1186/s40623-017-0641-3>
- Salameh, C., Guillier, B., Harb, J., Cornou, C., Bard, P.-Y., Voisin, C., Mariscal, A., 2016. Seismic response of Beirut (Lebanon) buildings: instrumental results from ambient vibrations. *Bull Earthquake Eng* 14, 2705–2730. <https://doi.org/10.1007/s10518-016-9920-9>
- Salgado-Gálvez, M.A., Zuloaga Romero, D., Velásquez, C.A., Carreño, M.L., Cardona, O.-D., Barbat, A.H., 2016. Urban seismic risk index for Medellín, Colombia, based on probabilistic loss and casualties estimations. *Natural Hazards* 80, 1995–2021. <https://doi.org/10.1007/s11069-015-2056-4>
- Salloum, N., Jongmans, D., Cornou, C., Youssef Abdel Massih, D., Hage Chehade, F., Voisin, C., Mariscal, A., 2014. The shear wave velocity structure of the heterogeneous alluvial plain of Beirut (Lebanon): combined analysis of geophysical and geotechnical data. *Geophysical Journal International* 199, 894–913. <https://doi.org/10.1093/gji/ggu294>

- Sanchez-Sesma, F.J., 1987. Site effects on strong ground motion. *Soil Dynamics and Earthquake Engineering* 6, 124–132. [https://doi.org/10.1016/0267-7261\(87\)90022-4](https://doi.org/10.1016/0267-7261(87)90022-4)
- Santarelli, S., Bernardini, G., Quagliarini, E., 2018. Earthquake building debris estimation in historic city centres\_ From real world data to experimental-based criteria. *International Journal of Disaster Risk Reduction* 31, 281–291.
- Santos-Reyes, J., Gouzeva, T., 2020. Mexico city’s residents emotional and behavioural reactions to the 19 September 2017 earthquake. *Environmental Research* 186, 109482. <https://doi.org/10.1016/j.envres.2020.109482>
- Sawai, M., 2012. Who is vulnerable during tsunamis? Experiences from the Great East Japan Earthquake 2011 and the Indian Ocean Tsunami 2004. United Nations ESCAP.
- Schmidt, N.B., Richey, J.A., Zvolensky, M.J., Maner, J.K., 2008. Exploring human freeze responses to a threat stressor. *J Behav Ther Exp Psychiatry* 39, 292–304. <https://doi.org/10.1016/j.jbtep.2007.08.002>
- Schnabel, P.B., Lysmer, J., Seed, B., 1972. A computer program for earthquake analysis of horizontally layered sites (No. EERC 72-12). Earthquake Engineering Research Center, University of California, Berkely.
- Schneiderbauer, S., Ehrlich, D., 2004. Risk, hazard and people’s vulnerability to natural hazards. A review of definitions, concepts and data (No. EUR 21410 EN). European Commission Joint Research Centre.
- Shapira, S., Aharonson-Daniel, L., Shohet, I.M., Peek-Asa, C., Bar-Dayyan, Y., 2015. Integrating epidemiological and engineering approaches in the assessment of human casualties in earthquakes. *Natural Hazards* 78, 1447–1462. <https://doi.org/10.1007/s11069-015-1780-0>
- Shapira, S., Novack, L., Bar-Dayyan, Y., Aharonson-Daniel, L., 2016. An Integrated and Interdisciplinary Model for Predicting the Risk of Injury and Death in Future Earthquakes. *PLOS ONE* 11, e0151111. <https://doi.org/10.1371/journal.pone.0151111>
- Shrestha, S.R., Sliuzas, R., Kuffer, M., 2018. Open spaces and risk perception in post-earthquake Kathmandu city. *Applied Geography* 93, 81–91. <https://doi.org/10.1016/j.apgeog.2018.02.016>
- Silva, V., Crowley, H., Pagani, M., Pinho, R., Monelli, D., 2012. Development and Application of OpenQuake, an Open Source Software for Seismic Risk Assessment. Presented at the 15th World Conference on Earthquake Engineering, 15WCEE, Lisboa, Portugal.
- Slovic, P., Weber, E., 2002. Perception of Risk Posed by Extreme Events, *Science*.
- So, E., Spence, R., 2013. Estimating shaking-induced casualties and building damage for global earthquake events: a proposed modelling approach. *Bull Earthquake Eng* 11, 347–363. <https://doi.org/10.1007/s10518-012-9373-8>
- Solberg, C., Joffe, H., Rossetto, T., 2008. How people behave in anticipation of and during earthquakes: A review of social science literature on what drives this behaviour. Presented at the The 14th World Conference on Earthquake Engineering, Beijing, China.
- Spence, R., Bommer, J., Del Re, D., Bird, J., Aydinoglu, N., Tabuchi, S., 2003. Comparing loss estimation with observed damage: a study of the 1999 Kocaeli earthquake in Turkey. *Bulletin of Earthquake Engineering* 1, 83–113.
- Strauss, A., 1944. The literature on panic. *The Journal of Abnormal and Social Psychology* 39, 317–328.
- Sun, L., Erath, A., 2015. A Bayesian network approach for population synthesis. *Transportation Research Part C: Emerging Technologies* 61, 49–62. <https://doi.org/10.1016/j.trc.2015.10.010>
- Sun, L., Erath, A., Cai, M., 2018. A hierarchical mixture modeling framework for population synthesis. *Transportation Research Part B: Methodological* 114, 199–212. <https://doi.org/10.1016/j.trb.2018.06.002>
- Taillandier, P., Gaudou, B., Grignard, A., Huynh, Q.-N., Marilleau, N., Caillou, P., Philippon, D., Drogoul, A., 2018. Building, composing and experimenting complex spatial models with the GAMA platform. *GeoInformatica* 23, 299–322. <https://doi.org/10.1007/s10707-018-00339-6>
- Taillefer, N., Arroucau, P., Leone, F., Defossez, S., Clément, J., Déroche, M.-S., Giry, C., Lancieri, M., Quistin, P., 2021. Association Française du Génie Parasismique: rapport de la mission du séisme du Teil du 11 novembre 2019 (Ardèche).

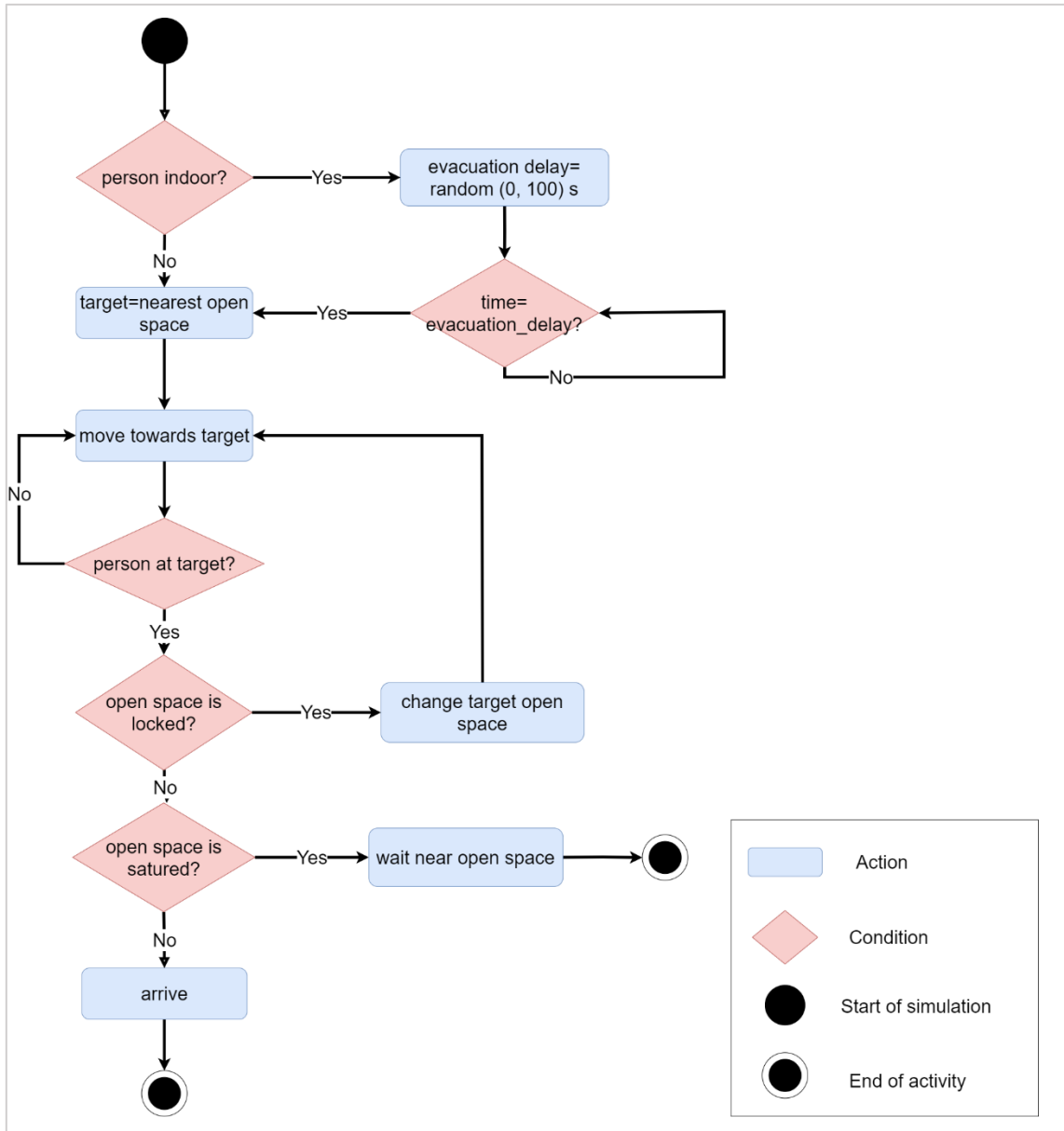
- Takewaki, I., 1998. Remarkable response amplification of building frames due to resonance with the surface ground. *Soil Dynamics and Earthquake Engineering* 17, 211–218. [https://doi.org/10.1016/S0267-7261\(98\)00006-2](https://doi.org/10.1016/S0267-7261(98)00006-2)
- Tate, E., 2012. Social vulnerability indices: a comparative assessment using uncertainty and sensitivity analysis. *Natural Hazards* 63, 325–347. <https://doi.org/10.1007/s11069-012-0152-2>
- Taylan Susan, A., 2015. Factors influencing homeowners' seismic risk mitigation behavior: A case study in Zeytinburnu district of Istanbul. *International Journal of Disaster Risk Reduction* 13, 414–426. <https://doi.org/10.1016/j.ijdrr.2015.08.006>
- Thywissen, K., 2006. Components of risk: a comparative glossary. UNU-EHS.
- Tobler, W., 1993. Three presentations on geographical analysis and modeling 26.
- Torrens, P.M., 2014. High-resolution space–time processes for agents at the built–human interface of urban earthquakes. *International Journal of Geographical Information Science* 28, 964–986. <https://doi.org/10.1080/13658816.2013.835816>
- Triggs, B., McLauchlan, P.F., Hartley, R.I., Fitzgibbon, A.W., 2000. Bundle Adjustment — A Modern Synthesis. *Vision Algorithms: Theory and Practice, Lecture Notes in Computer Science* 1883, 298–372. [https://doi.org/10.1007/3-540-44480-7\\_21](https://doi.org/10.1007/3-540-44480-7_21)
- Turner, Billie L., Kasperson, R.E., Matson, P.A., McCarthy, J.J., Corell, R.W., Christensen, L., Eckley, N., Kasperson, J.X., Luers, A., Martello, M.L., 2003. A framework for vulnerability analysis in sustainability science. *Proceedings of the national academy of sciences* 100, 8074–8079.
- Turner, B. L., Kasperson, R.E., Matson, P.A., McCarthy, J.J., Corell, R.W., Christensen, L., Eckley, N., Kasperson, J.X., Luers, A., Martello, M.L., Polsky, C., Pulsipher, A., Schiller, A., 2003. A framework for vulnerability analysis in sustainability science. *Proceedings of the National Academy of Sciences* 100, 8074–8079. <https://doi.org/10.1073/pnas.1231335100>
- Turner, R.H., Killian, L.M., 1987. *Collective behavior*, 3rd ed. ed. Prentice-Hall, Inc.
- UNDRO, 1980. *Natural Disasters and Vulnerability Analysis (Report of Expert Group Meeting- 9-12 July 1979)*.
- UNISDR, 2015. *Science is used for disaster risk reduction. UNISDR Science and Technical Advisory Group Report 2015*, Geneva: United Nations Office for Disaster Risk Reduction.
- UN/ISDR (United Nations International Strategy for Disaster Reduction), 2004. *Glossary. Basic Terms of Disaster Risk Reduction*. United Nations.
- United Nations, 2015. *Proposed Updated Terminology on Disaster Risk Reduction: A Technical Review*. The United Nations Office for Disaster Risk Reduction.
- United Nations, 2005. *Report of the World Conference on Disaster Reduction*. Kove, Hyogo, Japan.
- Verdeil, E., Dewailly, B., 2019. The Population of Lebanon: the Enigma, in: *Atlas of Lebanon: New Challenges*.
- Verdeil, E., Faour, G., Velut, S., 2006. Population et peuplement, in: *Atlas Du Liban*. Presses de l'Ifpo, Beyrouth.
- Verdière, N., Lanza, V., Charrier, R., Provitolo, D., Dubos-Paillard, E., Bertelle, C., Alaoui, A., 2014. Mathematical modeling of human behaviors during catastrophic events. Presented at the 4th International Conference on Complex Systems and Applications (ICCSA2014), Le Havre, France, pp. 67–74.
- Villagra, P., Rojas, C., Ohno, R., Xue, M., Gómez, K., 2014. A GIS-base exploration of the relationships between open space systems and urban form for the adaptive capacity of cities after an earthquake: The cases of two Chilean cities. *Applied Geography* 48, 64–78. <https://doi.org/10.1016/j.apgeog.2014.01.010>
- Wald, D., Jaiswal, K.S., Marano, K., Earle, P., Allen, T., 2011. Advancements in Casualty Modelling Facilitated by the USGS Prompt Assessment of Global Earthquakes for Response (PAGER) System, in: Spence, R., So, E., Scawthorn, C. (Eds.), *Human Casualties in Earthquakes: Progress in Modelling and Mitigation*. Springer Netherlands, Dordrecht, pp. 221–230. [https://doi.org/10.1007/978-90-481-9455-1\\_15](https://doi.org/10.1007/978-90-481-9455-1_15)
- Wald, D.J., Quitoriano, V., Heaton, T.H., Kanamori, H., 1999a. Relationships between peak ground acceleration, peak ground velocity, and modified Mercalli intensity in California. *Earthquake spectra* 15, 557–564.

- Wald, D.J., Quitoriano, V., Heaton, T.H., Kanamori, H., 1999b. Relationships between Peak Ground Acceleration, Peak Ground Velocity, and Modified Mercalli Intensity in California. *Earthquake Spectra* 15, 557–564. <https://doi.org/10.1193/1.1586058>
- Walley, C.D., 1988. A braided strike-slip model for the northern continuation of the Dead Sea Fault and its implications for Levantine tectonics. *Tectonophysics* 145, 63–72. [https://doi.org/10.1016/0040-1951\(88\)90316-2](https://doi.org/10.1016/0040-1951(88)90316-2)
- Wildavsky, A., Dake, K., 1990. Theories of risk perception: Who fears what and why? *Daedalus* 119, 41–60.
- Wisner, B., 2004. Assessment of capability and vulnerability, in: Bankoff, G., Georg, F., Hilhorst, D. (Eds.), *Mapping Vulnerability: Disasters, Development and People*. Earthscan, London, pp. 183–193.
- Wolfram, S., 1983. Statistical mechanics of cellular automata. *Rev. Mod. Phys.* 55, 601–644. <https://doi.org/10.1103/RevModPhys.55.601>
- Wood, M.M., Mileti, D.S., Bean, H., Liu, B.F., Sutton, J., Madden, S., 2018. Milling and Public Warnings. *Environment and Behavior* 50, 535–566. <https://doi.org/10.1177/0013916517709561>
- Wooldridge, M., Jennings, N.R., 1995. Intelligent agents: theory and practice. *The Knowledge Engineering Review* 10, 115–152. <https://doi.org/10.1017/S0269888900008122>
- Wyss, M., 2005. Human losses expected in Himalayan earthquakes. *Natural Hazards* 34, 305–314.
- Xiao, M.-L., Chen, Y., Yan, M.-J., Ye, L.-Y., Liu, B.-Y., 2016. Simulation of household evacuation in the 2014 Ludian earthquake. *Bulletin of Earthquake Engineering* 14, 1757–1769. <https://doi.org/10.1007/s10518-016-9887-6>
- Yameogo, B.F., Gastineau, P., Hankach, P., VANDANJON, P.O., 2020. Comparing Methods for Generating a Two-Layered Synthetic Population. *Transportation Research Record* 2675, 136–147. <https://doi.org/10.1177/0361198120964734>
- Yassin, N., 2012. Beirut. *Cities* 29, 64–73. <https://doi.org/10.1016/j.cities.2011.02.001>
- Yücel, G., 2018. Earthquake and Evacuation Area Assessment for Istanbul Aviclar District. *Disaster science and engineering* 5, 65–79.
- Zheng, X., Zhong, T., Liu, M., 2009. Modeling crowd evacuation of a building based on seven methodological approaches. *Building and Environment* 44, 437–445. <https://doi.org/10.1016/j.buildenv.2008.04.002>
- Zhou, J., Li, S., Nie, G., Fan, X., Tan, J., Li, H., Pang, X., 2018. Developing a database for pedestrians' earthquake emergency evacuation in indoor scenarios. *PLOS ONE* 13, e0197964. <https://doi.org/10.1371/journal.pone.0197964>
- Zhu, Y., Ferreira, J., 2014. Synthetic Population Generation at Disaggregated Spatial Scales for Land Use and Transportation Microsimulation. *Transportation Research Record* 2429, 168–177. <https://doi.org/10.3141/2429-18>
- Zia, K., Riener, A., Farahi, K., Ferscha, A., 2013. An Agent-Based Parallel Geo-Simulation of Urban Mobility during City-scale Evacuation. *Simulation* 89, 1184–1214. <https://doi.org/10.1177/0037549713485468>
- Zlateski, A., Lucesoli, M., Bernardini, G., Ferreira, T.M., 2020. Integrating human behaviour and building vulnerability for the assessment and mitigation of seismic risk in historic centres: Proposal of a holistic human-centred simulation-based approach. *International Journal of Disaster Risk Reduction* 43, 101392. <https://doi.org/10.1016/j.ijdrr.2019.101392>



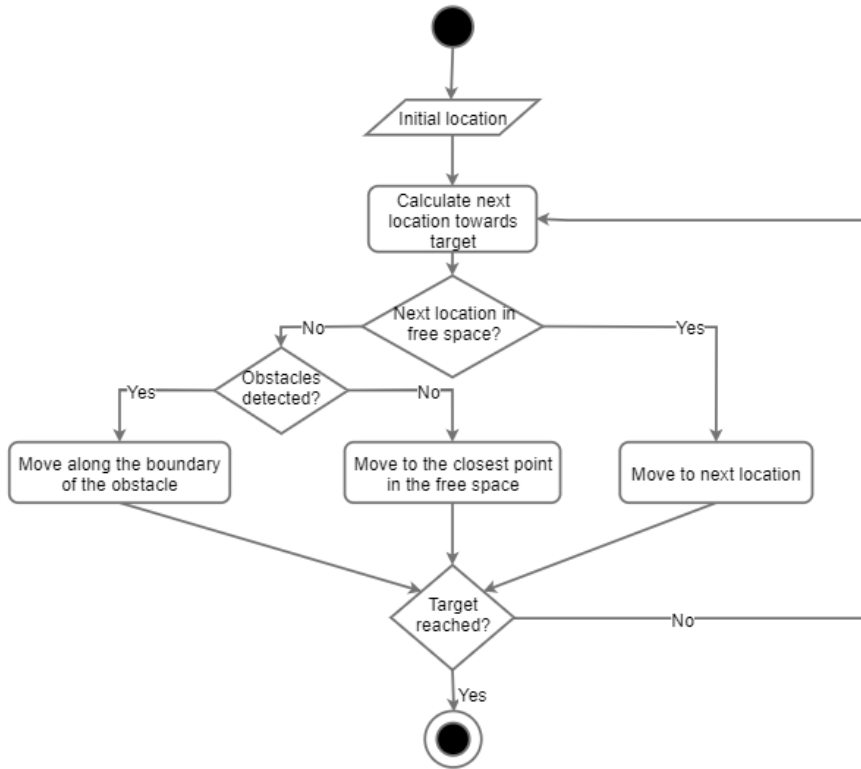
# Appendix A

Activity diagram for a person agent when ideal behaviors are considered



# Appendix B

Flowchart of the motion in the free space and the movement around obstacles



# Appendix C

## Distribution of the characteristics of the dataset for the simulation of the structural responses

### C-1 Soil profile parameters

The soil profile database consists of 887 real soil profiles consisting in surface-to-downhole measurements where S and P wave velocity profiles (VS and VP respectively) have been systematically derived at each site. The soil database has been collected from the following:

- 614 soil profiles from KIKNET (Japanese sites)
- 251 soil profiles from BOORE (Californian sites)
- 22 soil profiles from NERIES (European sites)

Each soil profile is then defined by the number of layers, the thickness, VP, VS, the density for each layer based on the format:

- Number of layers including half-space
- Thickness (m); VP (m/s); VS (m/s); Density (Kg/m<sup>3</sup>) of each layer

This distribution of Vs<sub>30</sub> and f<sub>0</sub> for the different soil profiles is presented in Figure A-1. The majority of sites are soft, but with high natural frequency. 299 profiles contain one or more LVZ (low velocity zone: zone where the shear wave velocity is lower than the one of the layer above). 298 profiles have natural frequencies ranging between 5 and 15 Hz, 522 present low natural frequencies (less than 5 Hz).

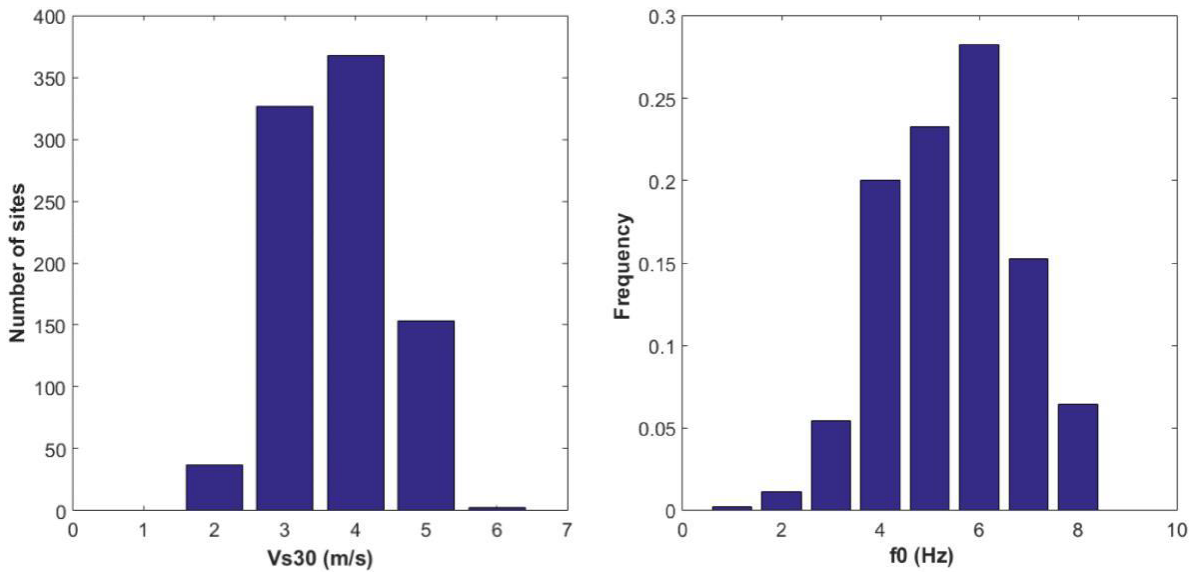


Figure C-1: Distribution of Vs<sub>30</sub> on the left and f<sub>0</sub> on the right.

## C2- Seismic signals

60 seismic signals that are a series of realistic, synthetic accelerograms generated with the Sabetta and Pugliese (Sabetta and Pugliese, 1996) approach. The generated magnitudes vary between 3 and 7, with distances from 10 to 100 km, and peak ground accelerations (PGA) from 0.02 to 8.6 m/s<sup>2</sup>. Table C-2 contains the different parameters for the synthetic seismic signals.

Table C-2: Parameters of the synthetic signals

Signal	Magnitude	Distance (km)	PGA (m/s <sup>2</sup> )	Signal	Magnitude	Distance (km)	PGA (m/s <sup>2</sup> )	Signal	Magnitude	Distance (km)	PGA (m/s <sup>2</sup> )
M3_R10_1	3	10	0.11	M5_R25_3	5	25	0.27314	M6_R25_2	6	25	0.49361
M3_R10_2	3	10	0.108	M5_R50_1	5	50	0.17931	M6_R25_3	6	25	0.6886
M3_R10_3	3	10	0.122	M5_R50_2	5	50	0.14757	M7_R10_1	7	10	4.28
M4_R10_1	4	10	0.31836	M5_R50_3	5	50	0.16889	M7_R10_2	7	10	4.0324
M4_R10_2	4	10	0.29552	M6_R05_1	6	5	3.02	M7_R10_3	7	10	3.6485
M4_R10_3	4	10	0.32781	M6_R05_2	6	5	2.5	M7_R15_1	7	15	3.01
M4_R25_1	4	25	0.11011	M6_R05_3	6	5	2.86	M7_R15_2	7	15	2.96
M4_R25_2	4	25	0.12485	M6_R10_1	6	10	1.6733	M7_R15_3	7	15	2.62
M4_R25_3	4	25	0.12006	M6_R10_2	6	10	1.2669	M7_R20_1	7	20	2.22
M5_R10_1	5	10	0.894	M6_R10_3	6	10	1.5712	M7_R20_2	7	20	2.28
M5_R10_2	5	10	0.71368	M6_R02_1	6	2	4.05	M7_R20_3	7	20	1.8
M5_R10_3	5	10	0.75199	M6_R02_2	6	2	3.5	M7_R25_1	7	25	1.6447
M5_R25_1	5	25	0.42339	M6_R02_3	6	2	3.85	M7_R25_2	7	25	1.8023
M5_R25_2	5	25	0.32388	M6_R25_1	6	25	0.87196	M7_R25_3	7	25	1.4558

### C3- Single degree of freedom oscillators

141 SDOF are considered: they cover a wide range of elastic limit, ductility capacity coefficient, and fundamental periods. The oscillators are grouped into 5 typologies: 51 buildings in Masonry, 9 in Non-designed Reinforced Concrete, 27 in Low Ductility Reinforced Concrete, 27 in Medium Ductility Reinforced Concrete and 27 in High Ductility Reinforced Concrete. The ductility capacity that refers to the ability of a material to deform plastically without breaking is given by the ratio between the ductility limit ( $du$ ) and the yield limit ( $dy$ ) based on:  $\mu=du/dy$ .

The distribution of the yielding displacement  $dy$  (in meters) with respect to the period (in seconds) is shown in Fig. C3 considering the 141 structures: Figure C3 a) represents a classification in terms of 2 categories: 51 Masonry and 90 Reinforced concrete; Figure C3 b) represents a classification in terms of the five major categories. Figure C3 c) and d) display the variation of the ductility capacity or  $du/dy$  in function of the period with respect to the 2 main categories and the five typology classes respectively.

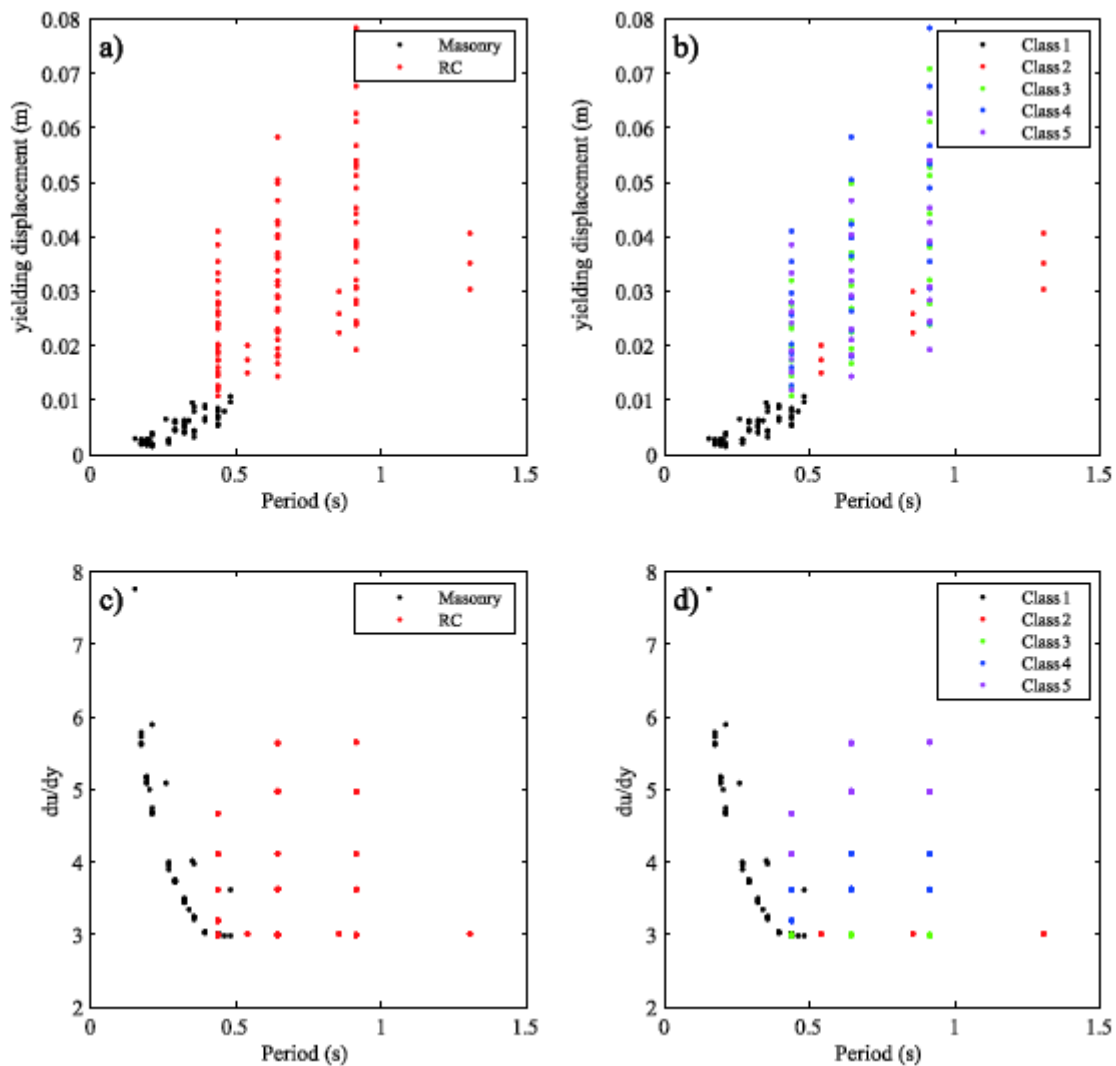


Figure C-3 : Distribution of the 141 structures taken from Lagomarsino and Giovinazzi (2006): yielding displacement  $dy$  (m) as function of the period (s) with respect to a) 2 main categories Masonry and RC and b) the 5 typology classes;  $du/dy$  in function of the period (s) with respect to c) 2 main categories Masonry and RC and d) the 5 typology classes.

# Appendix D

## Population distribution for day and night scenarios

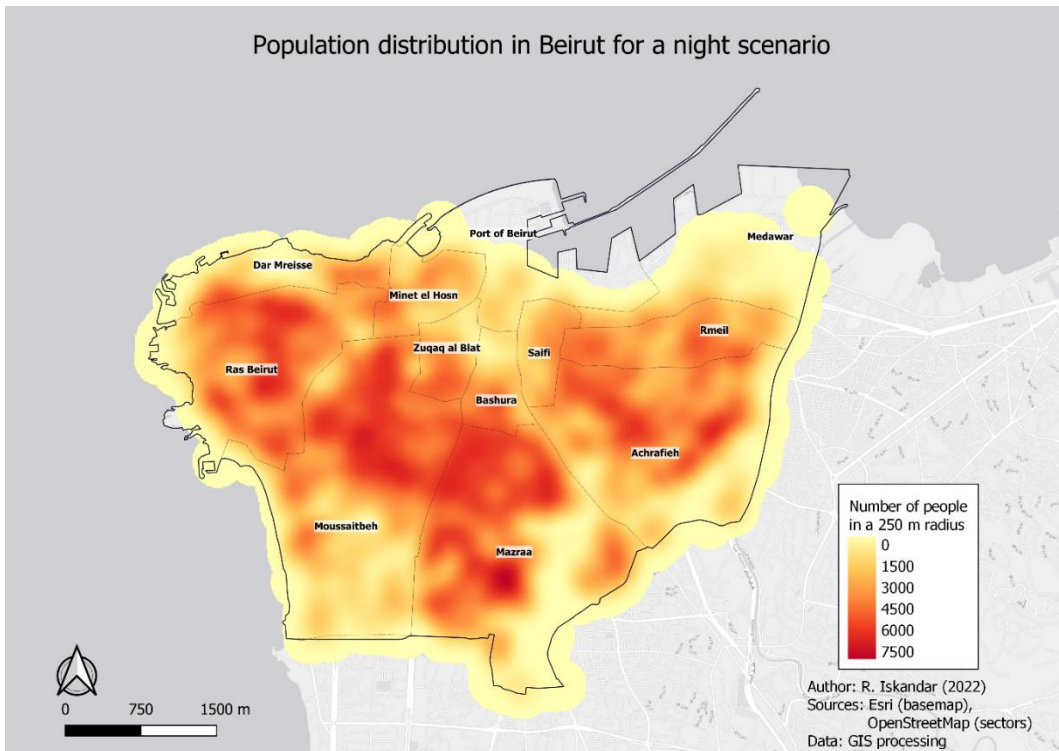


Figure D1: Distribution of the population in Beirut for a night scenario. This map was obtained using a heatmap processing in QGIS on a radius of 250 m.

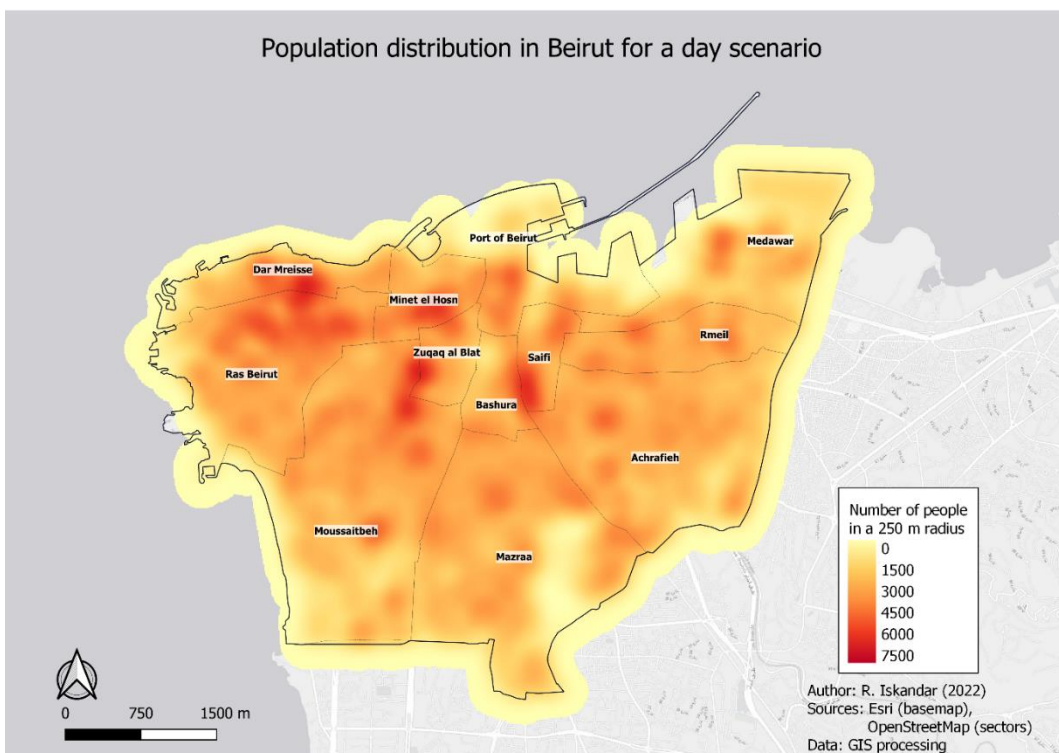


Figure D2: Distribution of the population in Beirut for a day scenario. This map was obtained using a heatmap processing in QGIS on a radius of 250 m.

# Appendix E

## Questionnaire on the behaviors in the response to the August 4 Beirut port explosion

<input type="checkbox"/> What city were you in when the explosions occurred? * <input checked="" type="radio"/> In Beirut ; <input type="radio"/> Outside of Beirut ;
<input type="checkbox"/> Specify the district * <input checked="" type="radio"/>
<input type="checkbox"/> Specify the city * <input checked="" type="radio"/>
<input type="checkbox"/> Where have you been ? * <input checked="" type="radio"/> At home ; <input type="radio"/> At work ; <input type="radio"/> At friends'/ family ; <input type="radio"/> In a public building (library, store, restaurant, hospital, swimming pool, etc.) ; <input type="radio"/> In a park, a square or a field ; <input type="radio"/> On the road ; <input type="radio"/> Other ;
<input type="checkbox"/> Were you alone or with other people? * <input checked="" type="radio"/> Alone ; <input type="radio"/> With other people ;
<input type="checkbox"/> Were you with dependent people: children, elderly or disabled? * <input checked="" type="radio"/> With children ; <input type="radio"/> With elderly people ; <input type="radio"/> With disabled people ; <input type="radio"/> No ;
<input type="checkbox"/> Specify the age of each child * <input checked="" type="radio"/>
<input type="checkbox"/> Did you feel the first explosion? * <input checked="" type="radio"/> Yes ; <input type="radio"/> No ;
<input type="checkbox"/> What environmental clues have you felt? <input checked="" type="radio"/> I saw the fire at the port or the fumes ; <input type="radio"/> I heard the sound of the explosion ; <input type="radio"/> I felt the vibrations on the ground ; <input type="radio"/> There was damage (debris) around me ; <input type="radio"/> Other ;
<input type="checkbox"/> Before you knew it was an explosion, what did you think was the origin of this event? <input checked="" type="radio"/>
<input type="checkbox"/> Did you think it was an earthquake? * <input checked="" type="radio"/> Yes ; <input type="radio"/> No ;
<input type="checkbox"/> How did you react after the first explosion? <input checked="" type="radio"/> I ignored the blast and continued with what I was doing ; <input type="radio"/> I went to the windows (balconies) to observe the event ; <input type="radio"/> I documented the event with my smartphone (photos, videos ...) ; <input type="radio"/> I took shelter under a piece of furniture / a door ; <input type="radio"/> I didn't have time to react ; <input type="radio"/> I searched for information on the origin of what I felt ; <input type="radio"/> I contacted my relatives ; <input type="radio"/> I walked / ran to the exit (if you were in a building) ; <input type="radio"/> I entered a building (if you were outside) ; <input type="radio"/> Other ;
<input type="checkbox"/> Specify the source (s) of information <input checked="" type="radio"/>
<input type="checkbox"/> Did you feel the second explosion? * <input checked="" type="radio"/> Yes ; <input type="radio"/> No ;
<input type="checkbox"/> What environmental clues have you felt? <input checked="" type="radio"/> I saw the fire at the port or the fumes ; <input type="radio"/> I heard the sound of the explosion ; <input type="radio"/> I felt the vibrations on the ground ; <input type="radio"/> There was damage (debris) around me ; <input type="radio"/> Other ;
<input type="checkbox"/> Before you knew it was an explosion, what did you think was the origin of this event? <input checked="" type="radio"/>
<input type="checkbox"/> Did you think it was an earthquake? * <input checked="" type="radio"/> Yes ; <input type="radio"/> No ;
<input type="checkbox"/> What source (s) of information did you use to look for information on the origin of the event? <input checked="" type="radio"/> Television ; <input type="radio"/> Radio ; <input type="radio"/> Social networks (Twitter, Instagram, Facebook ...) ; <input type="radio"/> Phone calls / messages (or WhatsApp) ; <input type="radio"/> People near me ; <input type="radio"/> Other ;

<input type="checkbox"/>	Did you use social media ? If yes, specify for what reason (s)
<input checked="" type="radio"/>	No ; Yes, to share an alert ; Yes, to share information ; Yes, to describe the event ; Yes, to share my experience ; Yes, to express my emotions ; Yeah, to confirm what I felt ; Yes, for other reasons. Specify ;
<input type="checkbox"/>	Have you experienced any interruption in communication services?
<input checked="" type="radio"/>	Yes, telephone lines interruption ; Yes, internet network interruption ; No ;
<input type="checkbox"/>	Were you in a building at the time of the second explosion? *
<input checked="" type="radio"/>	Yes ; No ;
<input type="checkbox"/>	Was the building you were in damaged?
<input checked="" type="radio"/>	Yes, low damage ; Yes, moderate damage ; Yes, strong damage ; Yes, totally destroyed ; No ;
<input type="checkbox"/>	What did you do at the time of the explosion?
<input checked="" type="radio"/>	I took shelter under a piece of furniture / a door ; I walked / ran to the exit ; I protected / helped someone ; I didn't do anything, I stayed there ; I didn't have time to react ; Other ;
<input type="checkbox"/>	Did you get out of the building you were in? *
<input checked="" type="radio"/>	Yes ; No ;
<input type="checkbox"/>	What were your reasons for staying?
<input checked="" type="radio"/>	The place I was in was not damaged ; I was not / no one near me was injured ; I wanted to protect my home from possible burglaries ; I felt safer inside than outside the building ; Other ;
<input type="checkbox"/>	Did you wait for everyone in the household before evacuating?
<input checked="" type="radio"/>	Yes ; No ; I was alone ;
<input type="checkbox"/>	What clues triggered your exit?
<input checked="" type="radio"/>	Noises ; Falling objects, broken glass ; Oscillation of objects (portraits on the walls, chandelier, etc.) ; Sirens, alarms ; People screaming ; Seeing other people going outside ; Seeing injured or dead people ; Evacuation order ; Other ;
<input type="checkbox"/>	How long has passed before your exit?
<input checked="" type="radio"/>	A few seconds ; A few minutes ; Less than an hour ; A few hours ; I do not remember ;
<input type="checkbox"/>	What delayed your exit from the building?
<input checked="" type="radio"/>	I looked for people ; I was injured ; I helped injured people in the building ; I cut off the gas / electricity ; I prepared an emergency kit (water, food, torch ...) ; I took personal belongings ; I documented the event with my smartphone (photos, videos ...) ; The fear ; Uncertainty ; Fascination ; The feeling that it was not necessary to leave the building ; Other ;
<input type="checkbox"/>	What did you do at the time of the explosion ?
<input checked="" type="radio"/>	I didn't do anything / I continued what I was doing ; I stayed still ; I protected / helped someone ; I entered a building ; I moved away from the buildings ; Other ;
<input type="checkbox"/>	Other observations / comments regarding your experience of the explosions:
<input type="checkbox"/>	When you were outside, what did you do?
<input checked="" type="radio"/>	I tried to reach my children ; I tried to join my husband / wife ; I tried to join my parents ; I helped people I didn't know ; I followed someone ; I moved away from the buildings ; I went to a safe area (Safe area: space away from buildings in which you are protected in the event of emergencies: fires, eart Other ;
<input type="checkbox"/>	Where did you go?
<input checked="" type="radio"/>	
<input type="checkbox"/>	For what reason (s) did you choose this place?
<input checked="" type="radio"/>	
<input type="checkbox"/>	What mean(s) of transport did you use for your travels?
<input checked="" type="radio"/>	Walk ; Car ; Service, taxi, bus ... ; Motorcycle / scooter ; Other ;

<input type="checkbox"/>	For what reason (s) did you choose this (these) mean(s) of transport?
●	
<input type="checkbox"/>	Generally, do you know where the safe area is near you? *
<input type="checkbox"/>	Safe area: space away from buildings in which you are protected in the event of emergencies: fires, earthquakes, explosions, etc.
●	Yes, I know the safe zone near my work ; Yes, I know the safe zone near my home ; Yes, I know the safe zone near my work and home ; No I do not know ;
<input type="checkbox"/>	In which city do you live ? (Specify casa) *
●	
<input type="checkbox"/>	What is your age ? *
●	Under 18 ; 18-24 ; 25-39 ; 40-64 ; 65 and over ;
<input type="checkbox"/>	What is your gender? *
●	Male ; Female ; I prefer not to answer ;
<input type="checkbox"/>	What is your educational level? *
●	Never went to school ; Primary / Complementary level ; Secondary level ; Higher level (after the baccalaureate) ; I prefer not to answer ;
<input type="checkbox"/>	How many people do you normally live with? *
●	Children 10 and under ; Children aged 11 and over ; Husband / wife or partner ; Parents ; Parents or dependent relatives ; Othe. 0 ; 1 ; 2 ; 3 ; 4 ; 5 ;
<input type="checkbox"/>	Do you look after an elderly or disabled person who does not live with you? *
●	Yes ; No ;
<input type="checkbox"/>	Do you suffer from a disability affecting your mobility? *
●	Yes ; No ; I prefer not to answer ;
<input type="checkbox"/>	Other comment / remark:

# Appendix F

## PEERS simulations outputs

Table F-1: PEERS simulations outputs

Output	Target level	Frequency of save	Data
Attribute table of person agents	File containing the attributes of each person	Every 100 cycles	Name/Age/Gender/location/initial location/evacuation delay The initial place (at home, at work, outdoors) Target destination Injury status Safety status
Aggregated population data	Population (aggregated persons)	Every cycle	Number of people indoor Number of people who have not arrived Number of safe people Number of people who arrived at their destination Number of people outside of a saturated open space Number of people with moderate injuries Number of people with severe injuries Number of people deceased
Arrivals data	By destination type: Open space, Hospital, Home and Undefined location	Everytime a person arrives	Name of the person who arrived Initial location Arrival location Time of arrival
Attribute table of group agents	For each Group	Every 100 cycles	Group size Group leader Group members Group destination Group target location Injury levels of the group members
Attribute table of open space agents	For each open space	Every 100 cycles	Minimum, maximum and average arrival times Number of occupants Percent occupied Percent of the population received by the open space Is fully occupied or no Is locked or no

# Appendix G

## Open space occupancy changes at the scale of Beirut when some of the open spaces were closed

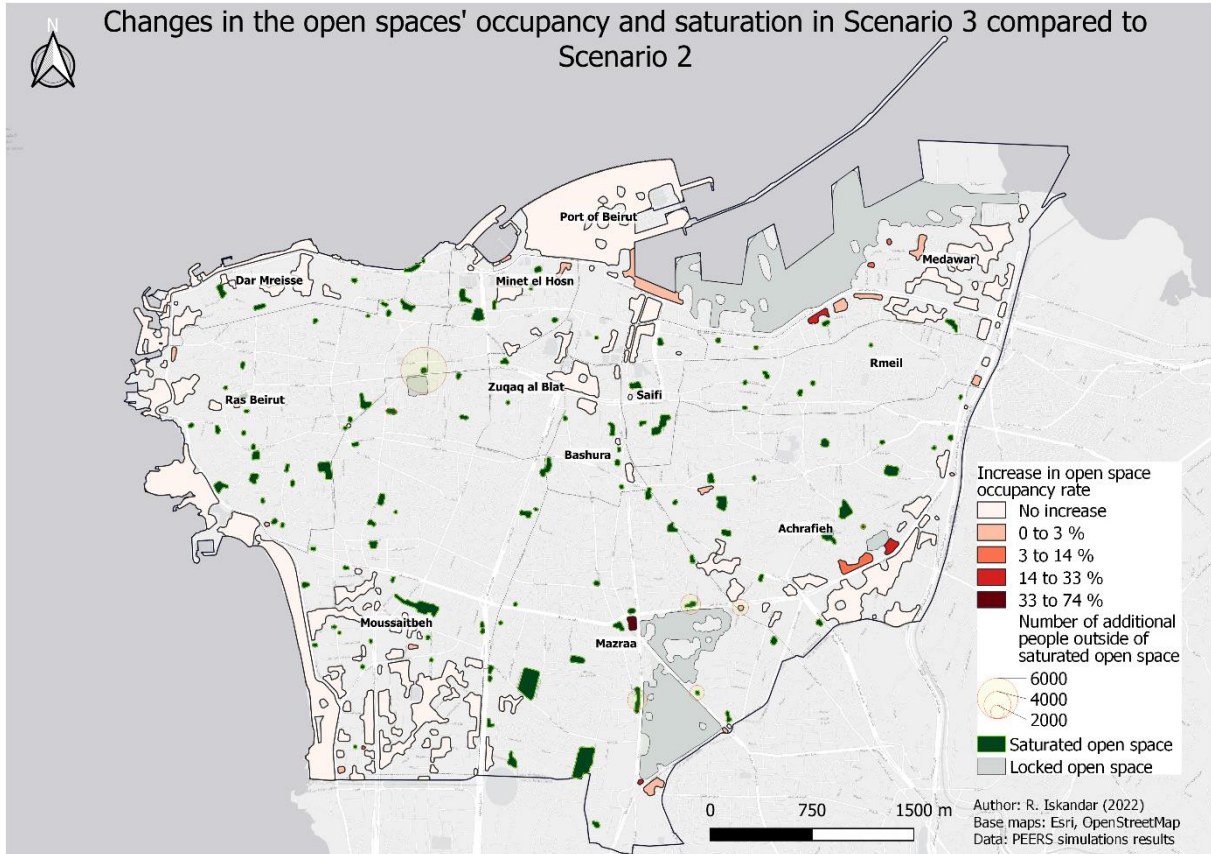


Figure G-1: Map of the changes in open spaces' occupancies and number of people outside of saturated open spaces between Scenarios 3 and 2